Crystallization of Lithium Disilicate Glass Using Variable Frequency Microwave Processing

Morsi Mohamed Mahmoud

Dissertation submitted to the faculty of the Virginia Polytechnic Institute and State University in partial fulfillment of the requirements for the degree of

Doctor of Philosophy In
Materials Science and Engineering

Dr. David E. Clark, Chair
Dr. Carlos Suchicital
Dr. Dwight Viehland
Dr. Gary R. Pickrell
Dr. Guo-Quan Lu

April 24, 2007
Blacksburg, Virginia

Keywords: Crystallization, Glass-ceramic, Lithium disilicate glass, Variable frequency microwave processing, Microwave-material interactions

Crystallization of Lithium Disilicate Glass Using Variable Frequency Microwave Processing

Morsi Mohamed Mahmoud

ABSTRACT

The lithium disilicate (LS_2) glass system provides the basis for a large number of useful glass-ceramic products. Microwave processing of materials such as glass-ceramics offers unique benefits over conventional processing techniques. Variable frequency microwave (VFM) processing is an advanced processing technique developed to overcome the hot spot and the arcing problems in microwave processing. In general, two main questions are addressed in this dissertation:

1- How does microwave energy couple with a ceramic material to create heat? and,
2- Is there a "microwave effect" and if so what are the possible explanations for the existence of that effect?

The results of the present study show that VFM processing was successfully used to crystallize LS_2 glass at a frequency other than 2.45 GHz and without the aid of other forms of energy (hybrid heating). Crystallization of LS_2 glass using VFM heating occurred in a significantly shorter time and at a lower temperature as compared to conventional heating.

Furthermore, the crystallization mechanism of LS_2 glass in VFM heating was not exactly the same as in conventional heating. Although LS_2 crystal phase (Orthorhombic Ccc2) was developed in the VFM crystallized samples as well as in the conventionally crystallized samples as x-ray diffraction (XRD) confirmed, the structural units of SiO_4

tetrahedra (Q species) in the VFM crystallized samples were slightly different than the ones in conventionally crystallized samples as the Raman spectroscopy revealed.

Moreover, the observed reduction in the crystallization time and apparent temperature in addition to the different crystallization mechanism observed in the VFM process both provided experimental evidence to support the presence of the microwave effect in the LS_2 crystallization process.

Also, the molecular orbital model was successfully used to predict the microwave absorption in LS_2 glass and glass-ceramic. This model was consistent with experiments and indicated that microwave-material interactions were highly dependent on the structure of the material.

Finally, a correlation between the Fourier transform infrared reflectance spectroscopy (FTIRRS) peak intensities and the volume fraction of crystals in partially crystallized LS_2 glass samples was established.

Dedication

I would like to dedicate this dissertation to my parents (Mohamed and Sadika), my wife (Faten), and my kids (Rowan, Nada and Abdel-Rahman).

Acknowledgements

I would like to thank my advisor and my mentor, Dr. David Clark, for his guidance, help and knowledgeable advising throughout my PhD degree. I really appreciate his concern about the quality of the work, my academic goals, and my personal life. I would also like to thank Ms. Diane Folz for guidance with laboratory work, continuous help, and opportunities she provided during my study at Virginia Tech. Thanks to all the members of my committee for their input and helpful consultation. I thank also my colleagues Carlos Folgar and David Berry for useful discussions, advice and laboratory support. Thanks also to Dr. Zak Fathi, Dr. Iftikhar Ahmad, and Mr. Keith Hicks at Lambda technologies for the kind help and for allowing me to work at their facility and giving me useful microwave processing advices. I am also indebted to Steve McCartney of Virginia Tech for help with using the SEM. I gratefully acknowledge and thank the Egyptian government scholarship program for funding me for 4 years during my PhD degree. I would also like to thank my parents, Mohamed and Sadika, for all of their patient, support and encouragement over the years. I would like to thank my wife, Faten for boundless patience, support, and understanding throughout this project. Finally, I would like to thank my kids, Rowan, Nada, and the newborn Abdel-Rahman for the joy they brought to my life.

Table of Contents

List of Figures

List of Tables

List of Equations

1. Introduction

1.1 Lithium disilicate glass and glass-ceramics

Glass-ceramics are polycrystalline materials formed by the controlled nucleation and crystallization of special formulated glasses[1]. The amorphous glass article is first formed and then thermally converted via heat treatment to a crystalline material, called a "glass-ceramic." These glass-ceramic materials go back to their discovery by S.D. Stookey in the 1950s [2].

Because lithium disilicate (LS_2) glass-ceramic was the first material that Stookey(1959) developed[3], extensive fundamental studies have documented LS_2 glass[4-13]. The structure of LS_2 glass and its corresponding crystal are well known and have been studied for a number of years[14-16]. LS_2 glass supplies a good glass forming system and crystallizes via homogenous nucleation. LS_2 glass-ceramic contains two solid phases with the same chemical composition: the amorphous phase and the crystalline phase.

The lithium disilicate crystal phase ($Li_2Si_2O_5$) melts congruently at 1033^oC and has a stoichiometric composition as shown in Figure 1.1. The structure of orthorhombic LS_2 crystals (as shown in Figure 1.2) involves corrugated sheets of $(Si_2O_5)^{-2}$ on the (010) plane that gives excellent mechanical properties for the glass-ceramic material[17]. The LS_2 glass system provides the basis for a large number of glass-ceramic products, such as cookware, radomes, ceramic composites, stovetops, and dental crowns.

The crystallization kinetics of LS_2 glass system have been studied by different techniques such as the microscopic method, the differential thermal analysis (DTA) method, and modeling for many years[10, 18-25]. The nucleation and crystal growth rate

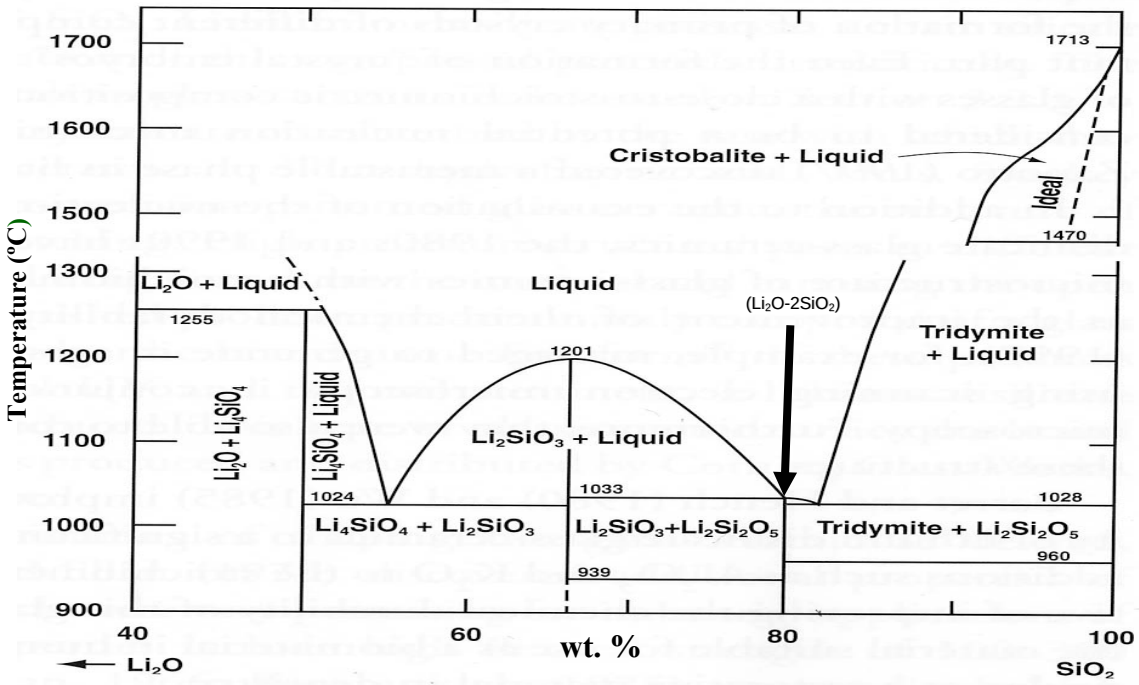

Figure 1.1: Phase diagram of Li_2O-SiO_2 [17]. Reprinted with the permission of The American Ceramic Society, www.ceramics.org, [copyright 2002]. All rights reserved.

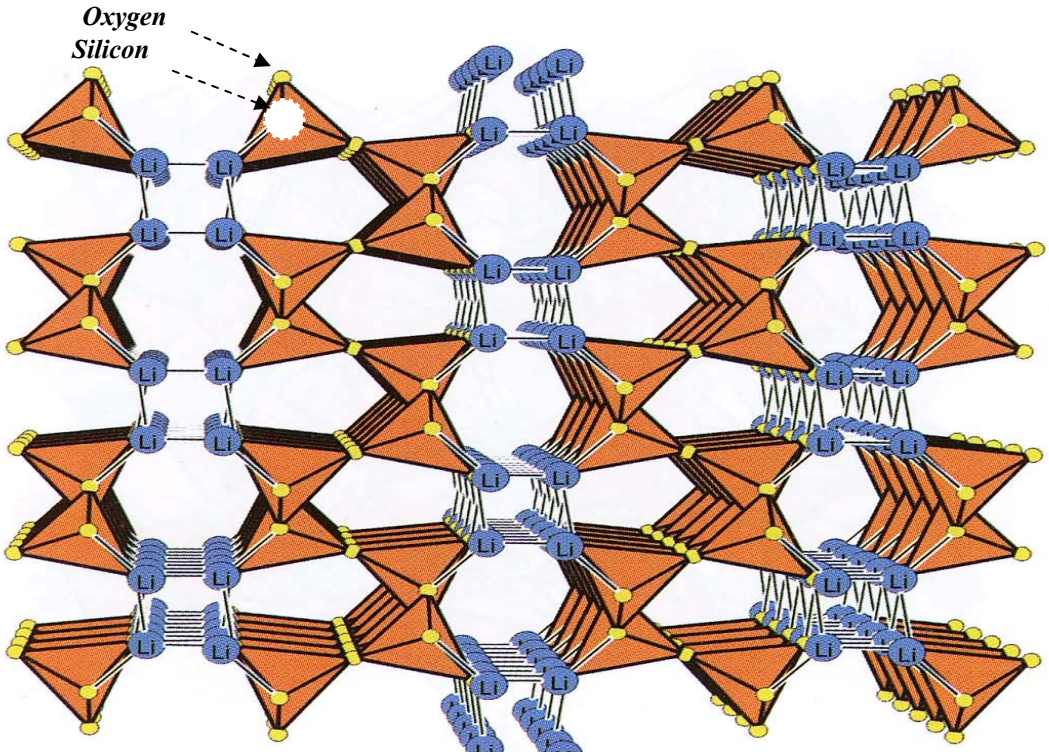

Figure 1.2: Layer structure of lithium disilicate crystal phase($Li_2Si_2O_5$)[17]. Note: Silicon atoms are hidden in the tetrahedral structure, an example is marked above. Reprinted with the permission of The American Ceramic Society, www.ceramics.org, [copyright 2002]. All rights reserved.

curves are separate on the temperature axis, so the growth component of crystallization is easily distinguished from the nucleation stage. The glass formation and crystallization behavior in binary lithium silicate glasses have been studied in detail with special emphasis on the stoichiometric composition LiO_2-$2SiO_2$[10, 11, 16, 19, 26-29].

It has been shown that lithium disilicate glass could be crystallized into glass-ceramic by using 2.45 GHz (the most common used fixed frequency) microwave energy[30, 31]. Although it was possible to crystallize LS_2 glass at 2.45 GHz, a hybrid heating process was required. To date, the use of frequencies other than 2.45 GHz has not been explored. Four major reasons to study the crystallization of LS_2 glass by variable frequency microwave (VFM) processing are as follows:

- First, LS_2 glass system has been extensively studied and well-documented with respect to conventional heating, so the comparison with microwave heating is valid. Furthermore, it provides the basis for a large number of successful glass-ceramics products, such as the new generation of dental crowns.
- Second, the crystal phase of LS_2 is compositionally identical to the parent glass, so microwave interaction due to compositional variations can be eliminated as a variable in this study.
- Third, the dielectric loss values for LS_2 glassy phase are higher than the corresponding crystal phase, which means that the LS_2 glass could be heated directly (without the aid of other energy forms) in a microwave field. When it is crystallized, LS_2 will have almost no absorption (self-terminating process). Thus, microwave absorption can be varied over a wide range by changing the crystallization percentage.
- Finally, LS_2 is an ideal system to study microwave-material interactions because it

provides a wide range of atomic and microstructural features without compositional changes. This will allow the development of a better fundamental understanding of how microwave energy interacts with materials.

1.2 Conventional heating versus microwave heating

Microwave heating is fundamentally different from conventional heating. Conventional ovens heat only the materials surface through radiation and convection. In this process, heat is conducted from the hot surface to the cool interior until a uniform temperature is reached throughout. Thus, it takes time for the interior of the material to become hot. Heat is conducted to the interior from the surface through phonon conductivity while at elevated temperatures (>600^{o}C) at this temperature the materials emit high frequency electromagnetic radiation (photon conductivity). This overall thermal conductivity is a combination of phonons and photons. To conventionally heat materials, especially poor thermal conductors (most ceramics and glasses), slow heating is recommended to ensure that extreme thermal gradients will not introduce a lot of thermal stress that could cause these brittle materials to crack.

However, the same materials (most ceramics and glasses) can be heated much more rapidly in a microwave oven, since the microwave energy heats the material volumetrically rather than from the surface to the interior[32]. Temperature gradients still exist within a microwave-heated body, but they are typically “inverted” (surface cooler than interior) as in Figure 1.3. These gradients originate from surface heat lost through convection and radiation. Microwave fields penetrate a significant distance (from several microns to meters) into materials and can therefore be absorbed throughout[33, 34]. For example, at 2.45 GHz, brass and graphite have microwave penetration depths of 2.6 and

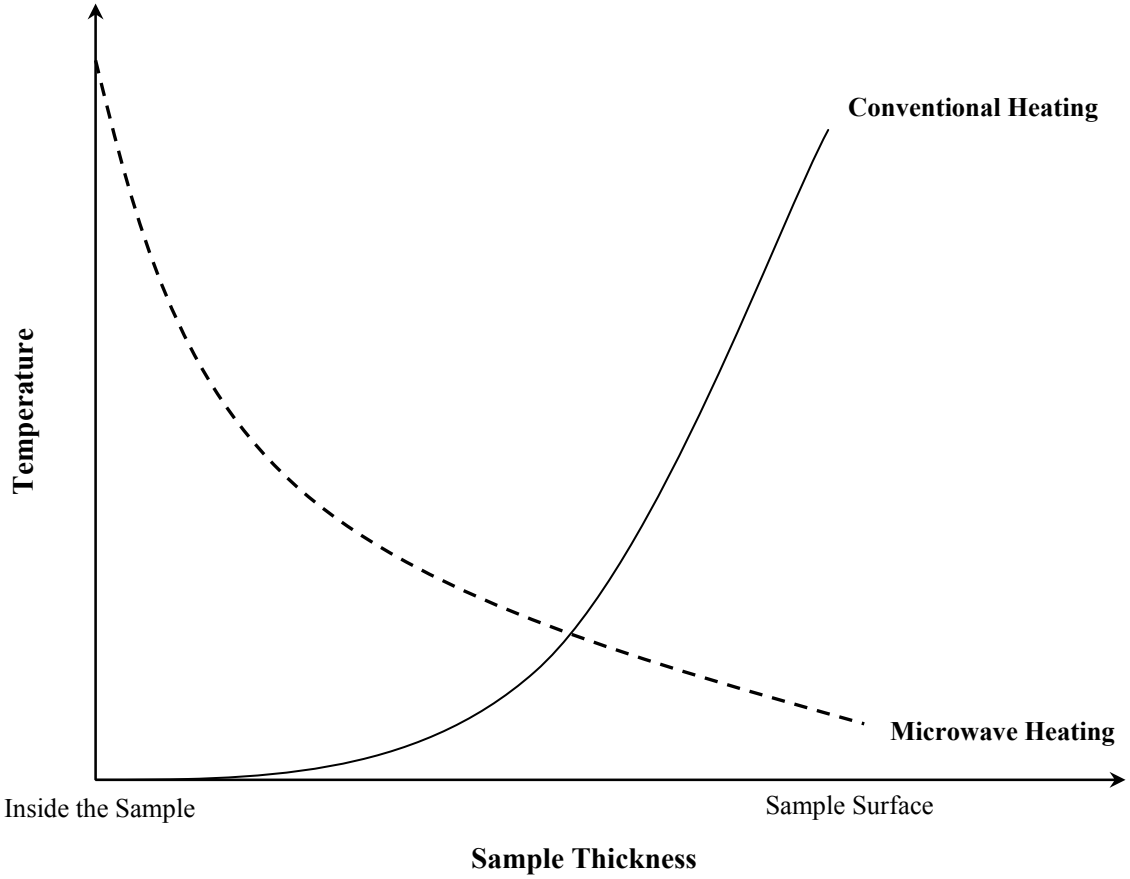

Figure 1.3: Schematic heating profiles for given material by conventional heating and by microwave heating.

38 μm, respectively, while cured epoxy and alumina (Al_2O_3) have penetration depths of 0.73 and 187 m, respectively[35].

The development of microwave technology goes back to World War II, when it was discovered that microwave energy could dry ceramic materials[36]. However, serious efforts to process ceramics with microwave energy were not reported in the literature until the late 1960s and early 1970s[37]. In recent years, many researchers have studied high-temperature processing of ceramics such as drying, sintering, joining, and melting[38-52]. The primary motivation for their efforts was the unique benefits that microwave heating might provide over conventional heating. These anticipated benefits include more precise and controlled volumetric heating, faster ramp-up to temperature, lower energy consumption, and enhanced quality and properties of the processed materials.

In many cases, microwave processing can be more efficient than conventional thermal processing because the microwave energy can be directly coupled with the material at the molecular level. This coupling or interaction results in the conversion of electromagnetic energy into heat within the material due to intermolecular friction. The absorption of microwave energy within the material depends on the incident microwave frequency, the distribution of the electric field within the material, and the dielectric properties of the material [53].

Variable frequency microwave (VFM) processing provides a new process that has been developed to reduce hot spots and arcing problems in fixed frequency microwaves (FFM). These problems arise from the uneven distribution of the electric field in FFM processing. VFM dramatically reduces production time and cost while offering the

potential to significantly improve product quality.

Variable frequency microwave heating is achieved by a method similar to that used with a fixed frequency microwave heating source. However, a VFM source will sweep through a range of radiation frequencies over set period of time. Moreover, the name VFM is derived from the variation of a source frequency over time. There are four controllable parameters that characterize VFM processing: central frequency, bandwidth, sweep-rate, and forward power. Central frequency can be adjusted to increase the coupling efficiency with the material being processed. The combination of bandwidth and sweep rate around the selected central frequency provides the necessary distribution of microwave energy to carry out uniform heating. The microwave forward power determines the heating ramp rate and can be varied depending on the desired heating-profile[54].

Microwave processing makes it possible to achieve relatively uniform heating in both small and large shapes. Moreover, the thermal stresses accompanying the conventional thermal processing appear to be of a lesser magnitude when the materials are processed with microwave energy[36]. As it turns out, researchers working with different processes and materials have observed evidence for unpredicted enhanced kinetic rates, different reaction pathways, and/or different reaction products in microwave processes when compared with conventional processing at the "same temperature." This phenomenon is referred to as a "microwave effect" and has been reported by numerous researchers [23, 25, 26, 30-43]. Janney et al[55] reported a reduction in the activation energy in the sintering process of alumina by microwave energy at 28 GHz. This reduction is suggested to be a possible explanation for the occurrence of the microwave

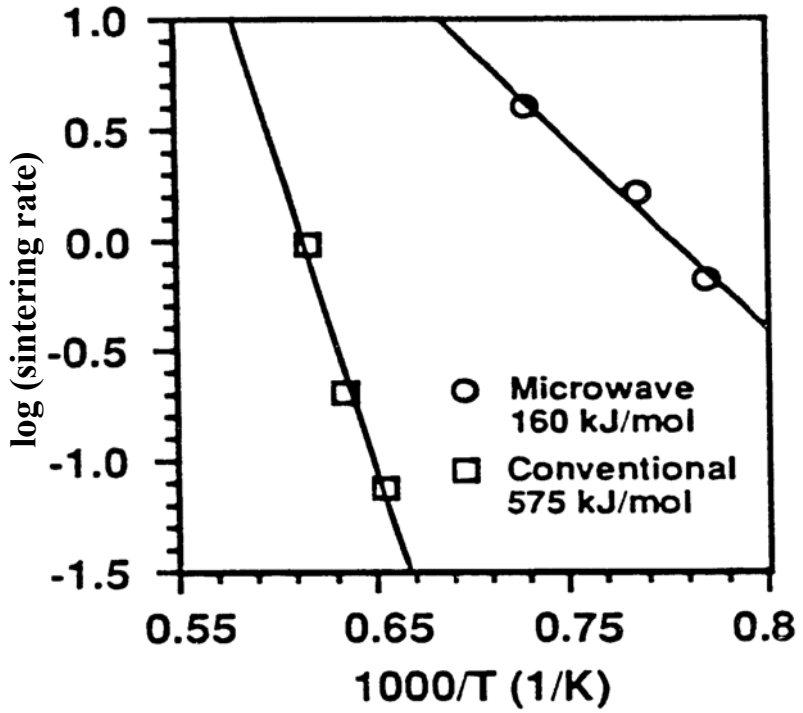

Figure 1.4a: Activation energy calculation for sintering of high-purity Al_2O_3 by microwave heating (28 GHz) and conventional heating[55]. Reprinted with the permission of MRS E-proceeding, [copyright 1991]. All rights reserved.

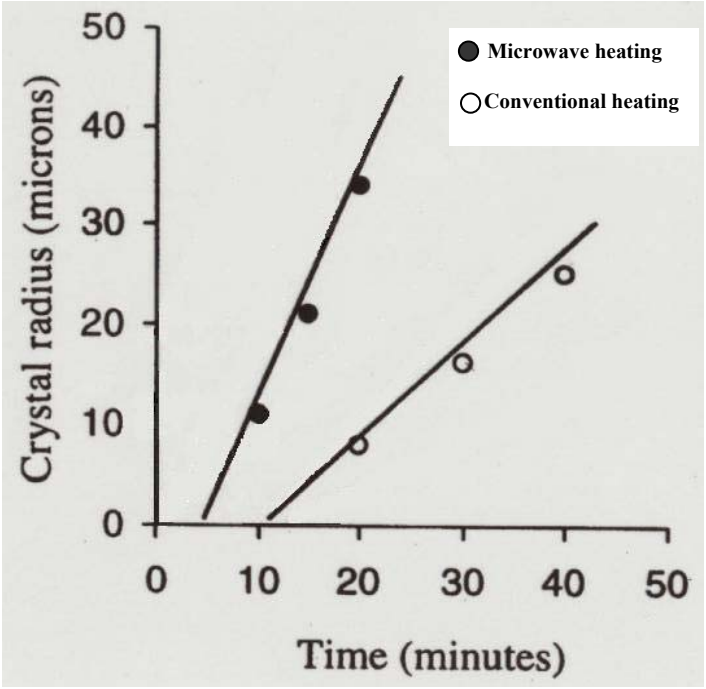

Figure 1.4b: Crystal size versus processing time for conventional and microwave (2.45 GHz) crystallization of LS_2 glass at 583°C[30]. Reprinted with the permission of The American Ceramic Society, www.ceramics.org, [copyright 2000]. All rights reserved.

effect (Figure 1.4a)[55]. Figure 1.4b shows kinetic data for LS_2 glass by conventional and microwave heating at 583^{o}C[30]. From this Figure, it is apparent that microwave heating of LS_2 glass is characterized by a higher crystal growth rate as compared to conventional heating.

Some controversy exists regarding the interpretation of the experimental results (microwave effect) because of the difficulties associated with temperature measurements[35, 56, 57]. Temperature measurement in a microwave environment is a nontrivial task. In a microwave field, thermocouples must be dielectrically shielded, thereby decreasing their thermal sensitivity. Inverted thermal gradients may exist in the material being microwave heated, so a thermocouple contacting the surface may not accurately measure bulk temperature. Because diffusion is usually thought of as a thermally activated process, accurate diffusion characterization requires accurate temperature measurement, as seen in Equation 1.1,

$$D=Do \exp(-Q/(kT)) \quad (1.1)$$

where Q is the activation energy for diffusion, Do is the diffusion coefficient and kT is the thermal energy. On the other hand, the diffusion process was shown to be greatly affected under the influence of an applied electric field, as will be discussed later (Section 5.11) where, it is proposed to add another term in Equation 1.1 that represents the electric field effect on the diffusion process (Equation 5.2.)

1.3 Statement of the work

In the following section a summary about the motivation, goals, experimental work and the results of the present study will be given. Technological progress is difficult to achieve without new processing techniques for materials, such as microwave

processing. VFM processing permits more uniform heating and precise control of microwave energy over the fixed frequency microwave (FFM) technique.

Microwave processing of materials, such as glass-ceramics, has a significant technological importance. Glass-ceramics have a better and unique combination of properties over glasses and traditional ceramics[2]. Glass-ceramics have an extremely favourable combination of mechanical, thermal, chemical, electrical, and physical properties due to their uniform, fine-grain randomly oriented polycrystalline microstructures. LS_2 glass was selected in the present study so that microwave-materials interactions and the microwave effect could be further studied.

The goals of this study were as follows:

- To determine under what conditions, other than 2.45 GHz, VFM processing could crystallize LS_2 glass.
- To provide clear experimental evidence of the non-thermal effects of microwave processing ("microwave effect") on the crystallization process of LS_2 glass.
- To compare the crystallization mechanism and the microstructural features of the VFM crystallized samples and the conventionally crystallized samples.
- To provide a better fundamental understanding of how microwave energy interacts with materials (microwave-material interactions) in general and particularly with LS_2 glass and glass-ceramic by using the molecular orbital model for microwave absorption of materials.
- To establish a correlation between the volume fraction of crystals in LS_2 glass-ceramic samples and their peak intensities obtained by Fourier transform infrared reflectance spectroscopy (FTIRRS).

Most ceramic materials have low dielectric loss and hence do not heat easily at room temperature by FFM at 2.45 GHz. Hybrid heating was developed to process those types of materials. In hybrid heating, the material is heated first by any form of energy other than microwave, such as infrared radiation, until the material reaches its critical temperature (T_{cri}). The critical temperature is defined as the temperature at which the material can be heated by microwave energy alone. In this study, the LS_2 glassy phase had a much higher dielectric loss than the corresponding crystalline phase; thus, VFM was used to crystallize LS_2 glass without the aid of any hybrid heating at a central frequency of 6.425 GHz with a band width of 1.15 GHz and a sweep time of 0.1 second[58, 59]. This goal of crystallizing LS_2 glass by VFM was designed and achieved based on the dielectric properties and the microwave cavity characterization (microwave reflected power) of the LS_2 glass.

In the VFM crystallization process, a unique LS_2 casket was successfully developed to overcome sample cracking due to the thermal shock of the LS_2 glass samples. In this casket, LS_2 glass frit was used as an insulating refractory media around the bulk LS_2 glass sample. The frit was also used to prevent contamination, to minimize the number of variables (same chemical composition) and to simplify the process for studying microwave-materials interactions.

LS_2 glass was fully crystallized by VFM processing in a significantly shorter time and lower temperature (~600^{o}C for 2 minutes) as compared to conventional heating (595^{o}C for 60 minutes). The reported reduction in time and temperature of the process in this study was also reported by many workers for other materials[32, 59-68]. These reductions are thought to be due, at least in part, to enhanced diffusion and kinetics in the

presence of microwave energy (the so called "microwave effect"). However, experimental evidence to date has not provided the clear data necessary to substantiate this claim. Because temperature measurement in a microwave field is not an easy task, some researchers argue that the observed differences are not due to the microwave effect but rather are purely thermal and misreported[35]. In the present work, crystallization of LS_2 glass was selected especially to study the legitimacy of the microwave effect. Because the crystal growth rate of any glass crystallization process reaches a maximum at T_c (the maximum crystal growth temperature), the crystal growth rate is always lower than the one at T_c , regardless whether the given temperature is higher or lower than T_c. Experimental evidence of the microwave effect on the crystallization process of LS_2 glass was established by characterizing the VFM crystallized samples using x-ray diffraction (XRD), optical microscopy, scanning electron microscopy (SEM), Fourier transform infrared reflectance spectroscopy (FTIRRS) and Raman spectroscopy.

This study compared the crystallization mechanism and the microstructural uniformity of LS_2 glass-ceramic samples crystallized by the VFM process and conventional heating. The well known polymorphic crystallization of LS_2 glass (i.e. the glassy phase and the crystalline phase have the same chemical composition) was observed in samples crystallized either by conventional or VFM heating. Both samples developed the same LS_2 crystalline phase (Orthorhombic Ccc2) as confirmed using XRD. On the other hand, the structural environment around the SiO_4 tetrahedra (Q species) of the LS_2 crystalline phase developed in the VFM crystallized sample were slightly different than the ones observed in the conventionally crystallized sample as the Raman spectroscopy revealed. The amount of Q^4 species (degree of polymerization) in the VFM

crystallized samples was slightly higher than those observed in the conventionally crystallized sample. So the crystallization mechanism(s) in both samples crystallized either by conventional or VFM heating was not exactly the same. This different crystallization mechanism observed in the VFM crystallized samples is believed to be due to the microwave effect.

Moreover, the aspect ratio of LS_2 crystals and the microstructural features in both samples crystallized either by conventional or VFM heating were studied using optical microscopy and SEM. The typical LS_2 ellipsoidal crystal shape was observed in both samples with a maximum aspect ratio of 1.6. The microstructural uniformity in both types of samples looked the same with a larger crystal size and population in the center of the samples rather than the edges. It is believed that the nucleation procedure applied in this study promotes more nuclei in the sample center than the edges.

Understanding microwave-material interactions is a very important goal in this study especially the physical mechanism by which microwave energy heats materials has not been well-established. It is believed that the interactions between microwaves and materials are controlled by polarization mechanisms (electronic polarization, atomic polarization, ionic polarization, interfacial polarization and finally dipole polarization and rotation) and conduction mechanisms (electronic or ionic conduction as well as space charge due to that conduction)[32, 69]. Dipole polarization and rotation is a very important and effective mechanism in dielectric materials, as these dipoles are believed to couple well with the microwave energy. However, most of the molecular vibrations and rotation frequencies in the infrared range are orders of magnitude higher than the microwave frequency, so how microwaves interact and heat materials is still a matter of

investigation. A molecular orbital model for absorption of microwave energy by materials developed by West and Clark[70, 71] has been used to predict the microwave absorption of LS_2 glass and glass-ceramics. This model combines the quantum molecular orbital theory with the theory of coupled oscillators to predict the microwave absorption mechanism based on degenerate states in the infrared spectra of the material. MOPAC (Molecular Orbital PACkage) that provides an interface to semi-empirical quantum molecular orbital model (PM3) has been used to calculate the microwave absorption spectra of LS_2 glass and glass-ceramics via CAChe Worksystem (Computer Aided Chemistry) software. This goal of predicting the microwave absorption in LS_2 glass and glass-ceramics will provide a fundamental understanding of how microwave energy interacts with LS_2 glass, glass-ceramics, and materials (in general), so the microwave processing technology can be better understood.

Finally, as a minor objective, a novel approach to estimate the volume fraction of crystals in the partially crystallized LS_2 glass samples by FTIRRS has been established in the present work. A correlation between the crystallization volume fraction of partially crystallized LS_2 glass and the peak intensities of the FTIRRS of same materials has been established. These samples were partially crystallized conventionally at two different crystallization temperatures (583^oC and 595^oC) at different times. These two temperatures were selected as they are just below the onset of the crystal growth process (600^oC) which is determined by the thermal analysis of LS_2 glass. This allowed for a careful and slow monitoring of the crystallization process. The crystallization volume fraction of the partially crystallized LS_2 glass was measured via stereology techniques using the point count method.

A summary of the experimental work is as follows:

Sixty rods of LS_2 glass samples were prepared from commercial glass frit to ensure better batch homogeneity. The glass frit was obtained from Specialty Glass Inc., Florida. The frit was melted in a covered Pt crucible at 1400^{o}C for 4 hours in an electric furnace and then quenched at room temperature in a cylindrical graphite mold. The quenched glass samples were annealed at 400^{o}C for 24 hours and then furnace-cooled to room temperature. Differential scanning calorimetry (DSC) measurements were then performed on the glass samples to determine the maximum nucleation (T_n) and crystallization temperatures (T_c). All the glass samples were nucleated homogenously in air by conventional heating in an electric box furnace for 2 hours to ensure a sufficient number of nucleation sites. Consequently, variable frequency microwave processing was used in that study to crystallize the nucleated glass by microwave energy while an electric furnace was used to crystallize the nucleated glass conventionally. Also, characterization of the prepared glass-ceramic samples was conducted by using XRD, optical microscopy, SEM, FTIRRS and Raman spectroscopy, and finally by density measurement. Measurements of the complex dielectric constant of LS_2 glass, nucleated glass and glass-ceramic samples between room temperature and 600°C at 2.46 GHz in air were performed using the cavity perturbation technique. Finally, the molecular orbital model for microwave absorption by materials was used to predict the microwave absorption of LS_2 glass and glass-ceramic materials by using CAChe software.

2. Glass-ceramics science

2.1 General

Glass-ceramics are an important class of materials that have been commercially quite successful[72]and have an immense technological significance. This technological significance can be summarized as follows[2]:

- A uniform chemical composition of glass-ceramics can easily be achieved since the parent glass can be obtained in a homogeneous state. This process lends a very fine-grain microstructure with almost no porosity, so most glass-ceramics have high mechanical strength and good electrical insulation**.**
- A wide practical application of glass-ceramics can be obtained by the variation of the chemical composition of the parent glass and the heat-treatment. Thus, the physical properties of glass-ceramics can be varied.
- Easier, faster and wide techniques used for shaping glass parent such as pressing, blowing or drawing techniques offers certain advantages over the techniques available for shaping conventional ceramics.
- The control of the shape and dimensions of the glass-ceramics products can be achieved without too much difficulty. While in conventional ceramic materials, a relatively large shrinkage (by volume) occur during drying and firing processes and so this change in dimensions may be accompanied by distortion.
- The glass-ceramics process has allowed new processes to be applied. The glass-ceramic-to-metal seal process has many advantages over the process available for conventional ceramics which will be very complicated. The parent glass can be easily bonded to metals in its molten state (molten glass wet other materials).

As early as the eighteenth century, the idea of fabricating polycrystalline materials by first forming glass and then nucleating and crystallizing it to form a highly crystalline material was proposed by Reaumur, a French chemist. He was unable to achieve control of the crystallization process that is necessary for the production of true glass-ceramics. However, a breakthrough was made in the 1950's by S.D. Stookey when the theory of glass phase separation was advanced[2]. Since the introduction of pyroceram (Trade name of glass-ceramics in U.S.A) in 1961 by the Corning Glass Works, the concept has been extended to dozens of compositions and applications.

As the name implies, glass-ceramics combine the nature of crystalline traditional ceramics with glass. The result is a product with especially attractive properties[73]. Glass-ceramics are prepared by crystallization of special glasses or melts of various compositions throughout the bulk of the pre-shaped glass article. This is accomplished by initially forming a glass then heat-treating it at a certain temperature to encourage the nucleation of exceptionally small and numerous crystals. These crystals are then allowed to grow at high temperature until as much as 90% of the article has crystallized[74]. In many cases, special nucleating agents are introduced into the glass to enhance the nucleation process.

Over the last few decades, glass-ceramics have gradually become established in a wide variety of technical and domestic applications. The interest in these materials is unusually great. This can be explained by the fact that glass-ceramics possess an extremely favorable combination of mechanical, thermal, chemical, electrical, and physical properties. The properties of these materials are superior to those of the majority of conventional glass or traditional ceramics materials[1].

The glass-ceramic manufacturing process has distinct advantages over other methods of making ceramics. The first stage in the glass-ceramic process is to produce a glass; subsequently, the glass is converted into a fine-grained ceramic by a controlled crystallization heat treatment. Thus, in the first stage, the well-established glass technology can be used to manufacture articles by a variety of forming techniques including blowing, casting, pressing and rolling. This provides a low-cost, high volume, rapid, and continuous manufacturing route to complex geometries that are often expensive to achieve by conventional ceramic processes such as powder pressing and sintering.

Glass-ceramics have many other advantages. Their uniform, fine-grain randomly oriented polycrystalline microstructures allow high reproducibility of properties. Usually the conversion of glass into a glass-ceramic involves only minor overall changes in volume with low or zero porosity, which is important for high strength and good electrical properties. The small dimensional changes during the manufacturing process are also valuable for many applications. The constituents of most glass-ceramics are, generally, inexpensive, being derived from relatively low-cost batch materials. Processing temperatures (300-1000^{o}C) are usually lower than those needed to process engineering ceramics such as alumina or silicon carbide. Because a wide range of formulations can be used, physical properties can often be tailored to suit particular applications[75].

The properties of glass-ceramics mainly depend upon their bulk chemical composition, phase assemblage, and microstructure. The bulk chemical composition controls glass formation and workability as well as the tendency toward internal

nucleation and crystallization in general. The phase assemblage, i.e., the type and proportion of crystalline and residual amorphous phases, generally controls the physical and mechanical properties like density and coefficient of thermal expansion, as well as chemical durability[76]. The phase assemblage, of course, is controlled largely by the bulk composition, but it is also a function of thermal history, i.e., the specific heat-treatment to which the glass has been subjected during crystallization. The microstructure of the resultant glass-ceramic is mainly regulated by the type and amount of the nucleation catalyst (if used) and by the crystallization parameters. It mainly affects the chemical, mechanical and thermal properties of the glass-ceramics. A typical temperature versus time cycle for producing a glass-ceramic is shown in Figure 2.1.

2.2. Fundamentals of glass-ceramic materials

2.2.1 The nature of glass

Certain liquids have the ability to slowly adjust their structure upon cooling and to continually stiffen to the solid state without crystallizing. These frozen liquids are called "glasses". Upon reheating, they slowly and continuously decrease in viscosity and revert to their former mobile state without any defined melting point. Thus they can be shaped in the plastic state by high-speed manufacturing techniques such as pressing, rolling, centrifugal spinning, blowing and drawing, and can be reworked by traditional flame sagging and fire-polishing techniques.

Inorganic glasses can be made from many compositions in the broad areas of silicates, phosphates, aluminates, borates, halides and chalcogenides. Silicate glasses are by far the most commercially important because they have excellent transparency and good chemical durability, and they can be made from inexpensive natural ingredients.

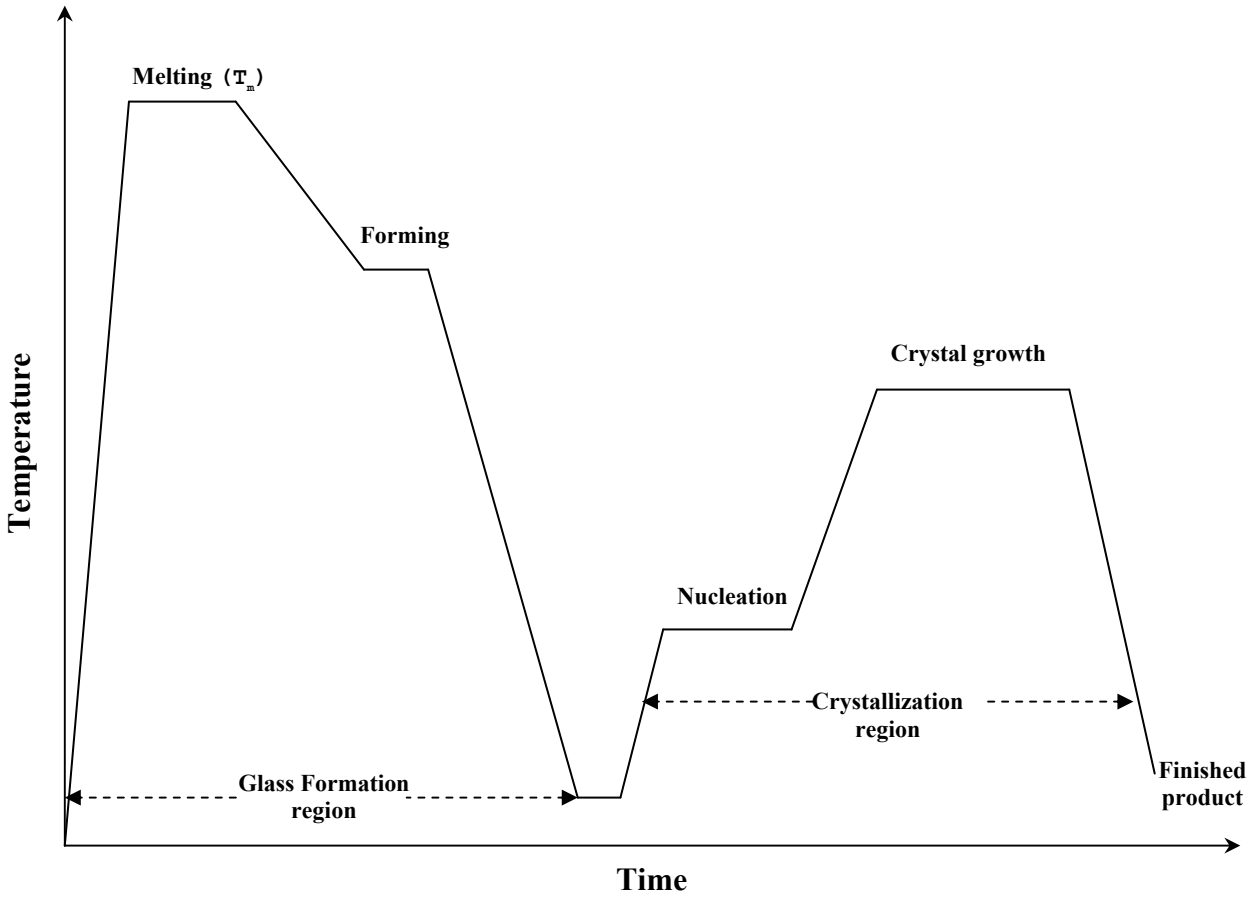

Figure 2.1: Typical thermal history for producing a glass-ceramic by controlled nucleation and growth of crystalline grains.

However, the disadvantage of glass as a versatile ceramic material is its brittleness, which makes it susceptible to mechanical failure[77].

The properties of glass, including devitrification, are mainly dependent on its structure. Thus, it is useful to consider briefly the glass structure. As in crystalline silicate, the SiO_4 tetrahedron is the basic unit in silicate glasses. According to Zachariasen[78], the SiO_4 tetrahedra are irregularly linked together in a three dimensional network. Figure 2.2a represents a random three-dimensional silica glass network, and Figure 2.2b shows the same composition after crystallization to the quartz structure[79]. The large increase in the viscosity of glass forming melts on cooling can be attributed to the formation of such irregular infinite three-dimensional network.

According to their role in the glass structure, cations can be classified into three groups:

1- Network formers, such as Si, B, P, Ge, and As, having oxygen coordination numbers of 3 or 4 and tend to produce the basic cross-linked polymeric glass structure.

2- Network modifiers, such as Na, K, Ca, and Ba, having coordination number of 6 or more and generally tend to reduce the degree of polymerization and viscosity.

3- Intermediate oxides with cations, such as Al, Zn, Mg, Pb, and Be having intermediate coordination of 4 to 6 and act either as network formers or modifiers, depending upon the glass composition.

2.2.2 Crystallization of glass

Crystallization is the process by which the well ordered or regular periodic crystalline structure is generated from the poorly ordered or random liquid structure of glass. It is generally considered as consisting of two independent processes[80]. These

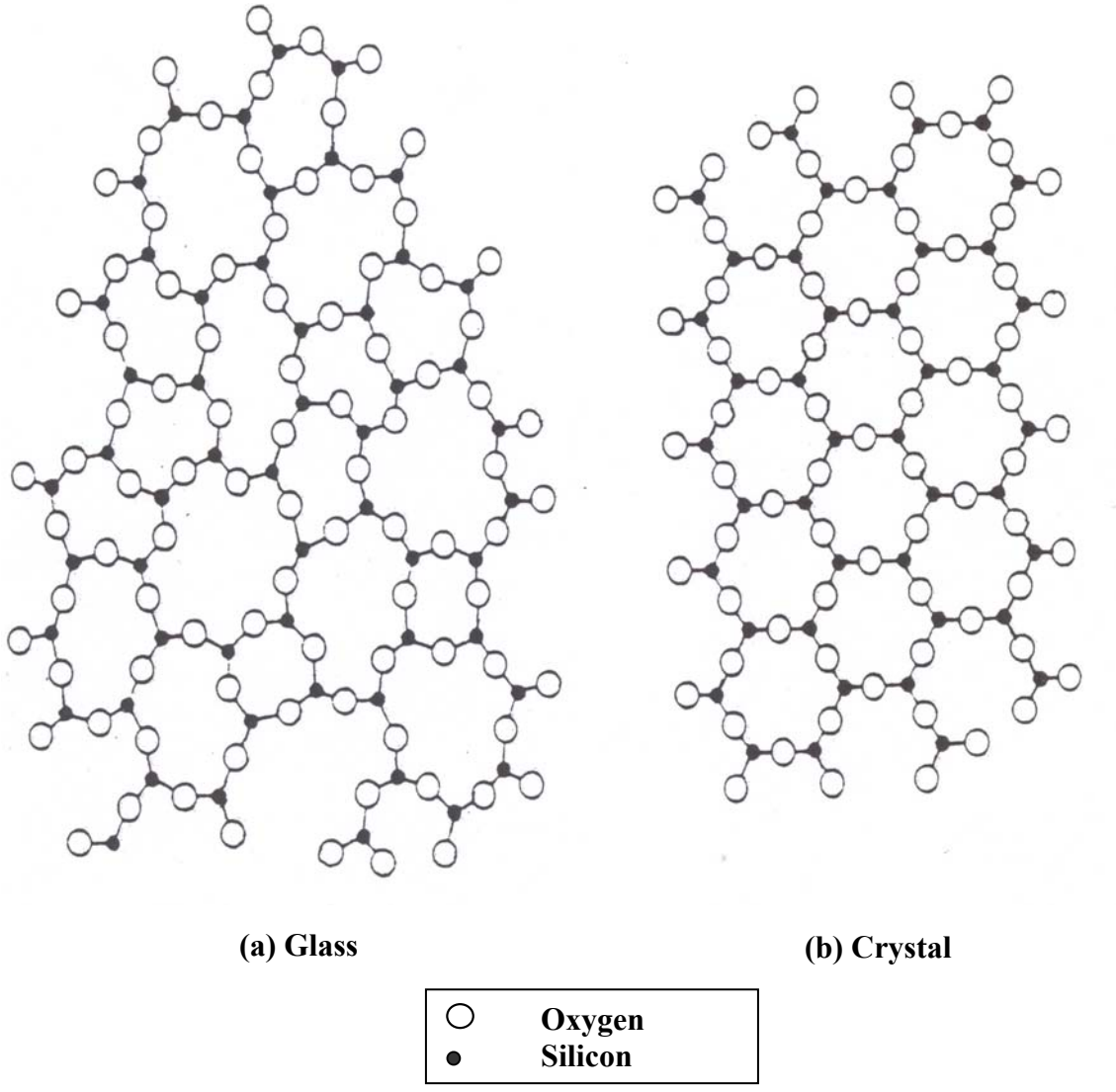

Figure 2.2: Schematic representation of

a. **The irregular network structure of SiO_2 glass before being crystallized.**
b. **The regular periodic crystalline structure of quartz[17].** Reprinted with the permission of The American Ceramic Society, www.ceramics.org, [copyright 2002].

are the nucleation, formation of crystallization centers, and the growth of crystals on these formed centers.

a. Nucleation

For crystallization to begin, crystal nuclei must be present. Nucleation involves the initiation of regions of longer-range atomic order, known as embryos. They are normally present in molten materials or in the super-cooled liquid[2]. When these embryos attain a critical minimum size capable of developing spontaneously into gross particles of the stable phase, they are known as nuclei. On heating a glass article, the main bulk of the material would crystallize internally and uniformly upon these tiny nuclei instead of crystallization from the surface of the article (Figure 2.3). Starting from these nuclei, the main crystalline phase would grow until it impinges on neighboring silicate crystals, creating a crystalline material with small amounts of residual glass.

Without the internal nucleation process, as a precursor to crystallization, devitrification is initiated at lower energy surface sites. The result is a popsicle-like structure (Figure 2.3a), where the surface oriented crystals meet in a plane of weakness. Flow of the un-crystallized core glass in response to change in bulk density during crystallization commonly forces the original shape to undergo certain distortions. On the other hand, because of efficient internal nucleation and growth in a viscous glassy medium, an exceptionally uniform and fine-grained microstructure that simply can not be found in conventional ceramics or natural rocks can be produced. Very fine, randomly oriented crystals characterize the microstructures of these super-reliable glass-ceramics (Figure 2.3b) with some residual glass matrix (up to 5%). Nucleation may take place either homogeneously, i.e., freely in the volume of the original glass phase, or

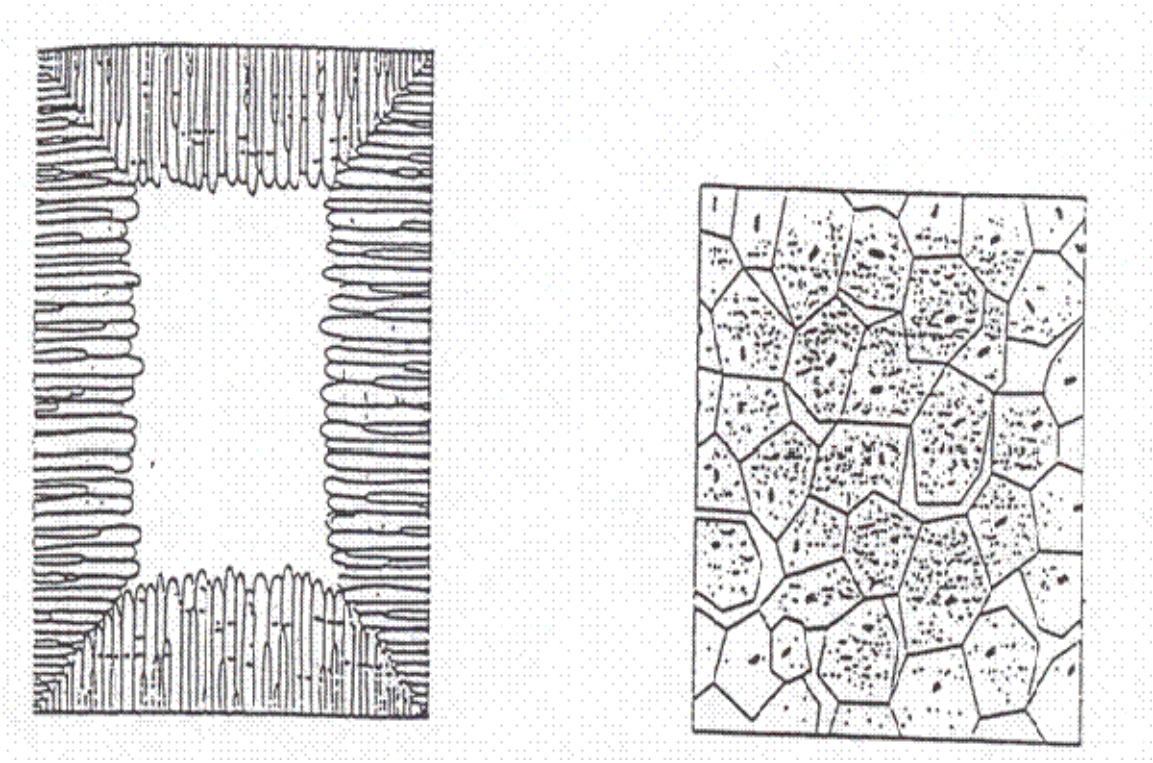

Figure 2.3: Schematic representation showing:
a. Crystallization of glass, without internal nucleation, from the surface.
b. Internal crystallization of glass showing a glass-ceramic microstructure[81].

heterogeneously on surfaces of the container, foreign particles or on the structural imperfection[82]. In homogeneous nucleation, the composition of the primary nuclei does not differ from that of the main crystalline phase, whereas, in heterogeneous nucleation the crystallization of the glass is induced by introducing foreign nuclei. The nucleating agent, which is generally a metal, oxide or fluoride, is incorporated in the batch and becomes an integral part of the glass during melting.

A generalized mechanism by which nucleating agents induce crystallization can not be developed, since the role of the nucleating agents in catalyzing the formation of nuclei and the major crystalline phases undoubtedly differs from one nucleating agent to another. However, it is safe to say that the nucleating agent introduces sites of lower thermodynamic stability in the glass[83].

Figure 2.4 illustrates some of the paths traversed on going from the homogeneous glass, through heat-treatment, to crystallization of the major phase(s)[84]. The direct transformation of homogeneous glass into the major crystalline phases (path 1) with the appearance of intermediate metastable phase was reported in LS_2 glass[85]. Other researchers reported the absence of this metastable phase[15, 16, 19, 27, 28, 86]. The polymorphic crystallization of LS_2 glass (the glassy and the crystalline phases have the same chemical composition) was well known for a number of years.

Path 6-5 (Figure 2.4) probably represents the best-understood sequence for the case in which the colloidal metallic crystals are added[3]. Small amounts of metals such as Ag, Au, Pt or Cu, are at first incorporated in the glass. By exposure to certain radiation followed by heat-treatment, colloidal particles of the metal form by a diffusion controlled mechanism, and act as nuclei for the epitaxial growths of the major phase.

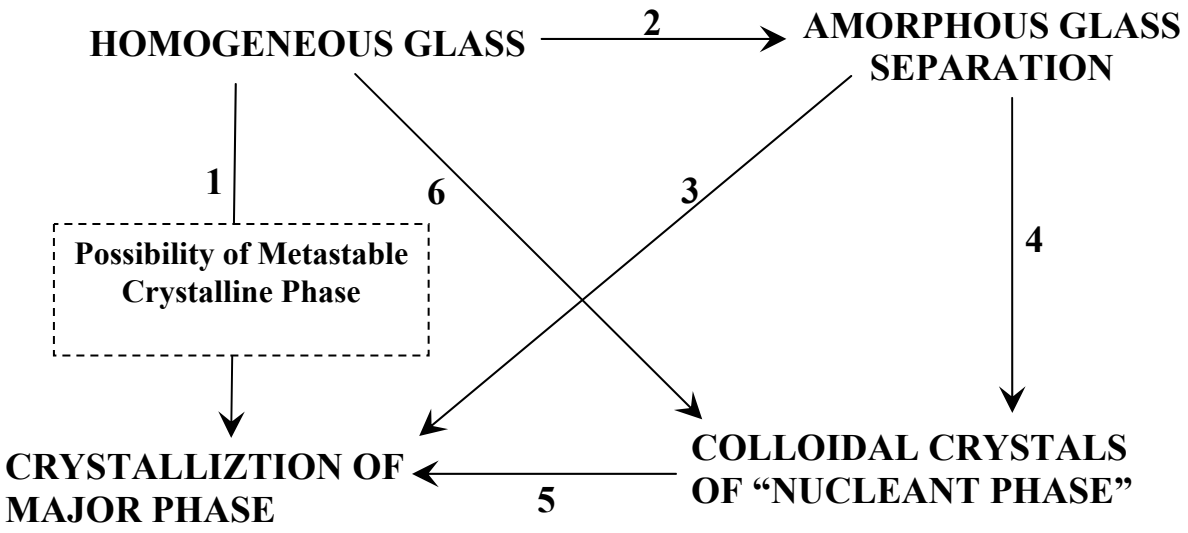

Figure 2.4: Reaction paths between the initial glass and the final glass-ceramics. Path 1 is the accepted one for LS_2 glass transformation into LS_2 glass-ceramics.

Fluorides may belong to this path[87]. Fluoride ions can be accommodated in the glass thus producing fine crystalline precipitates that can serve as nuclei.

It was shown by many authors[88-95] that for TiO_2, nucleated systems glass-in-glass phase separation (path 2-3) is at least a common event in the nucleation sequence and that one of the important functions of nucleating agents is to promote such glass-in-glass phase separation.

Structurally, glass-in-glass phase separation can take place when incompatible tetrahedral of triangular groups are introduced in the tetrahedral silicate network[96-98]. For example, a network-forming ion which forms tetrahedral or triangular groups, different in size from the silicate tetrahedra, can cause considerable distortion of the ≡Si-O-Si≡ bonds and ultimately leads to phase separation. Distortion may also occur through the effect of ions with different charges in the silicate network or from ions which change their coordination number with temperature.

Oxides commonly used to promote phase separation in glass systems are those of metals, with a strong metal oxygen bond such a TiO_2, ZrO_2, V_2O_5, Cr_2O_3, P_2O_5[2, 99]. Because of their oxygen coordination requirements, each of these oxides will compete with silica for oxygen coordination in the glass melt. Octahedral coordination of oxygen around these metal cations will be incompatible with the tetrahedra coordination requirements of silica. Consequently, there is repulsion between the two oxide groups in the glass and liquid-liquid immiscibility results.

Several explanations were given for the mechanism of nucleation through glass-in-glass separation. It has been suggested that the interfacial energy between two glassy phases is less than that between a glass and a crystalline phase, thereby reducing the

barrier to nucleation[3, 100]. It has been also pointed out that the composition of one of the amorphous phases may be more closely similar to that of the crystalline phase than the original monolithic homogeneous glass. This could lead to easier nucleation by reducing the activation energy[88, 89].

Path 2-4-5, (Fig.2.4) is also a very common nucleation sequence observed by many workers[101-108]. In this case, the amorphous phase separation is followed by the precipitation of small particles of a metastable crystalline phase which, in turn, is followed by crystallization of the major phase(s).

a.1. The nucleation rate

Nucleation happens because the atoms are constantly vibrating and moving around as a result of the thermal energy. If every atomic vibration allowed the atom to join to a nucleus, the nucleation rate (I) per unit volume per second would simply be represented by Equation 2.1[2]

$$\mathbf{I = n\,\nu} \qquad \mathbf{(2.1)}$$

where n is the number of atoms (per unit volume) and ν is the atomic vibration frequency (per second).There are two barriers for nucleation process to occur: a kinetic barrier and a thermodynamic barrier. The kinetic barrier, ΔE" is the activation energy required for an atom to cross the liquid-nucleus interface. This involves the breaking of bonds with its nearest neighbors and perhaps some reorientation into the more ordered structure within the surface of the nucleus (barrier to diffusive motion over small distances including reorientation). The thermodynamic barrier" W^*, is the net free energy change of the system after a nucleus has formed. The nucleation rate could be expressed by [2]

$$\mathbf{I = n\,\nu \exp(-NW^*/RT).\exp(-\Delta E/RT)} \qquad \mathbf{(2.2)}$$

where N is Avogadro's number, R is the gas constant and T is the absolute temperature. The net change in energy, W^*, is given by Equation 2.3[2]

$$W^* = 16\ \Pi\ \sigma^3 / 3(\Delta G)^2 \qquad (2.3)$$

where σ is the surface energy of the nucleus interface (per unit area) and ΔG is the change in the free energy in transforming a unit volume of a liquid to a unit volume of a crystal. From thermodynamics, ΔG can be expressed as in Equation 2.4 as follows[2]:

$$\Delta G = \Delta T\ \Delta H_f / T_m \qquad (2.4)$$

Where ΔH_f is the heat of fusion, T_m is the melting temperature and $\Delta T = (T - T_m)$. As a result, the nucleation rate could be expressed by Equation 2.5 and with the curve shown in Figure 2.5[2].

$$I = n\ \nu \exp\left[(-N/RT)\ (16\ \Pi\ \sigma^3 / 3\ \Delta H_f^2)\ (T_m / \Delta T)^2\right] \exp(-\Delta E/RT) \qquad (2.5)$$

When ΔT = zero, (i.e. $T = T_m$), the first term will be equal zero (thermodynamically controlled). As T decreases, the term exp (-ΔE/RT) will approach zero (kinetically controlled). In Figure 2.5, the nucleation rate reaches maximum somewhere below T_m while it will reach zero at both the high and the low temperature ends. Below T_m, the metastable zone of undercooling, there are too few nuclei that can not be detected by any measuring device[109].

b. Crystal growth

After nucleation, the nucleated glasses must be heated to higher temperatures for crystal growth to proceed, in a reasonable time. This step also represents a complex process for a number of reasons. First, a number of phases may crystallize simultaneously. Commonly, the composition of the crystals differs from the composition of the original glass. This means that the crystal-glass interface is continuously changing

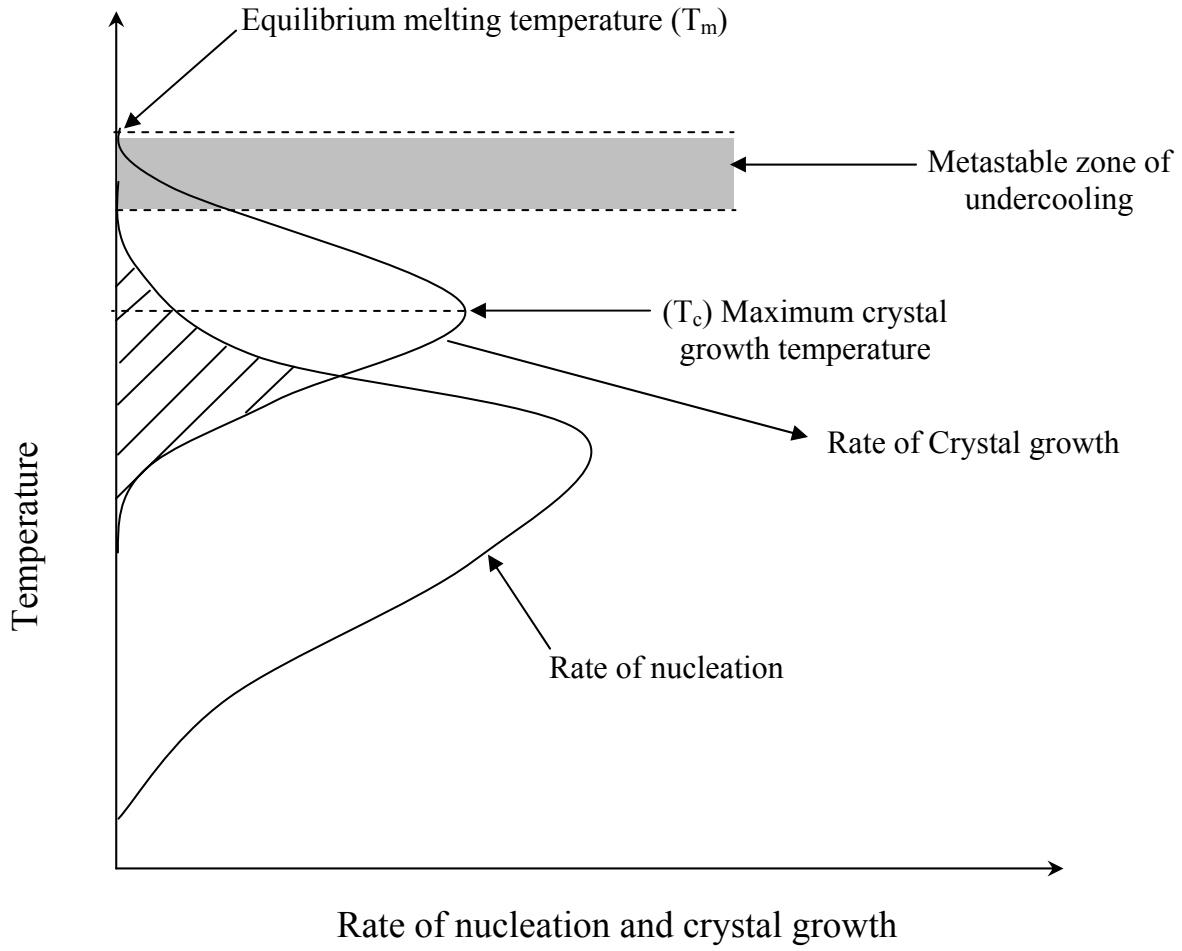

Figure 2.5: Variation of the nucleation rate, I, and the crystal growth rate, U, with temperature, T.

in composition. In addition, portions of the primary crystal phase may start transformation by solid state reaction into a new structural type[84]. Some additives can markedly promote crystallization rates in glass, while others may inhibit crystal growth. This effect may be specific to particular crystal surfaces. For example, low concentrations of various transition metal ions such as iron, zinc and vanadium in alkaline earth aluminosilicate glasses, were found to increase the rate of crystal growth[110]. Chromium ions, on the other hand, were found to decrease the rate of crystal growth[111].

From a practical standpoint, it is important that the rate of crystal growth be "just right"[84]. If it is very slow, there is the danger of deformation of the sample under its own weight before sufficient crystals form to retard flow. Conversely, if it is too fast, the heat evolved during crystallization may not be dissipated to the surroundings fast enough to avoid detrimental thermal gradients that may result in stresses sufficient to break the sample.

b.1. The crystal growth rate

In general, the rate of advance of a solid-liquid interface (crystal growth) can be described as a function of temperature by[112, 113]

$$U = (f\,D/a_o)\,[1-\exp(-\Delta G/RT)] \qquad (2.6)$$

where U is the growth rate, f is a site factor (fraction of sites at the interface where atoms can be preferentially added or removed), D is the diffusion coefficient for molecular transport across a solid liquid interface, a_o is a jump distance, and ΔG is the difference in Gibbs free energy between the solid and liquid phase. The diffusion coefficient in Equation 2.6 can be expressed as a function of viscosity, η, using the Stokes-Einstein

relation in Equation 2.7[112]:

$$\mathbf{D=kT/\ (3a_o\ \pi\ \eta)} \qquad \mathbf{(2.7)}$$

Where **η** is the viscosity and K is Boltzman constant.

Then Equation 2.6 can be expressed as

$$\mathbf{U= (f\ kT/\ (3(a_o)\ 2\ \pi\ \eta))\ [1\text{-}exp\ (-\Delta G/RT)]} \qquad \mathbf{(2.8)}$$

From Equation 2.8, it can be seen that the crystal growth rate (U) in any glass system is controlled primarily by two factors. The first one is the thermodynamic factor or barrier and is represented as [1- exp (-ΔG/RT)], and the second one is purely kinetic, i.e., related to the motion or mobility of the ions or group of ions present in this glass, and is represented as (f KT/ $(3(a_o)^2\pi\ \eta)$). At temperatures higher than the melting point ($T > T_m$), the change in the free energy (ΔG) is positive, hence the term [1- exp (-ΔG/RT)] will be a negative number leading to a negative value of U. This is in agreement with the fact that the crystals start to dissolve at temperatures higher than the melting point. While at $T=T_m$, ΔG= 0, which will yield U= 0. This is essentially in agreement with the definition of the melting point. As the temperature T is lowered below T_m, the thermodynamic factor [1-exp (-ΔG/RT)] has a significant influence on crystal growth rate. At that region, because the viscosity is low, the thermodynamic factor will mainly control the crystal growth rate because of the higher driving force of ΔG is negative. When the system is at a temperature far from equilibrium ($T \leq T_m$), the term [1-exp (-ΔG/RT)] approaches unity and the crystal growth rate is mostly governed by kinetic factors (viscosity and diffusivity). The conflicting changes in the crystal growth rate are due to changes in the thermodynamic and kinetic factors, resulting in a maximum in the temperature dependence of the crystal growth rate. As a result, the crystal growth rate curve is a

skewed bell-shaped, reaching a maximum at T_c (somewhere below T_m) and reaching zero at both the high and low temperature ends. In Figure 2.5, both I and U are plotted together against temperature.

This Figure and the earlier discussions about nucleation and crystal growth represent the kinetic theory of glass formation. The kinetic theory of glass formation addresses the question: How fast must the material be cooled to avoid detectable crystallization? This fundamental concept and especially the one related to the crystal growth rate will be used in the present study to establish the existence of the microwave effect in the crystallization process of LS_2 glass by VFM processing.

2.2.3 Crystallization parameters

a. Base glass composition

Numerous researchers showed that there are many thousands of chemical and mineral compositions that could be formed into glasses and subsequently crystallized. In spite of this proliferation of compositions, relatively few have appeared in marketable products. However, the majority of glass-ceramics are alkali and/or alkaline earth aluminosilicates[1, 2]. Lithium aluminosilicates [β-spodumene solid solution (Li_2O-Al_2O_3-$(SiO_2)_{4-10}$] have low expansion coefficients and good chemical durability. Sodium aluminosilicates or barium sodium aluminosilicates have high expansion and can be strengthened by surface compression techniques such as the application of a low expansion glass. Moreover, magnesium aluminosilicates (e.g. cordierite $2MgO.\ 2Al_2O_3.\ 5SiO_2$ and Mg stuffed β-quartz [$MgO.\ Al_2O_3.\ (SiO_2)_{2-5}$] have low expansion and can have very high strengths. Glass-ceramics based on the CaO-MgO-Al_2O_3-SiO_2 system utilizing natural rocks have also received much attention. The outstanding strength, excellent

abrasion, and chemical resistance are the most valuable features of such pyroxenic (Ca, Na) (Mg, Fe^{2+} Fe^{3+}, Al) (Si, $Al)_2O_6$ glass-ceramics[1, 114-120].

b. Nucleating agents

Nucleating agents (i.e. heterogeneous nucleation) are widely used in most of glass-ceramic production processes. Their effect is so extensive that it could be safely said that a large number of glass-ceramic products is produced with nucleating agents. Changing the nucleating agents, its concentration and/or mixing it with another agent greatly change the appearance, crystalline phases and crystal size in the resultant glass-ceramics[2, 73, 107]. LS_2 glass was selected especially in the present study because it is characterized by its homogenous nucleation and does not require any nucleating agents. The homogenously nucleated LS_2 glass by conventional heating was proposed to be crystallized by VFM processing in this study in order to minimize the number of factors and to simplify the case when the effect of VFM on the crystallization process was investigated. That will also help to understand and to study the microwave effect on LS_2 glass as well as the microwave material interaction.

c. Heat-treatment

The nucleation and crystallization processes, which are necessary for the transformation of glass into glass-ceramic, are brought about by heat-treatment. The rates of nucleation and crystal growth can then be controlled during the heat treatment process. The rate of maximum nucleation is often important in the heat treatment process[80].

The nucleation and growth rate curves are not always completely separated, and the amount of overlap will depend upon the particular system concerned. If the curves are significantly overlapped, e.g. Fig. 2.6a, only partial control is possible. In this case, as

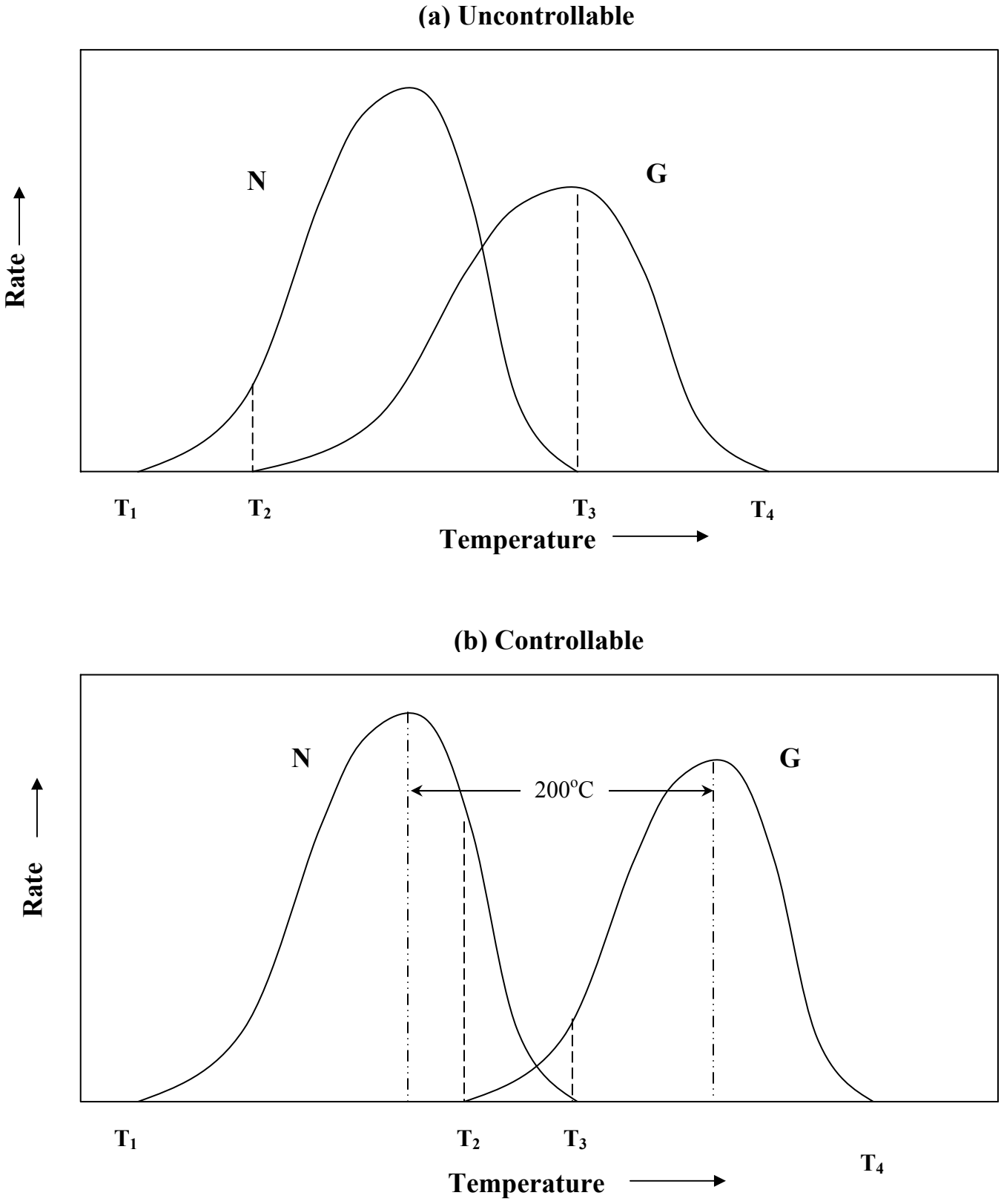

Figure 2.6: Nucleation and crystallization rates curve.
This represents the LS_2 glass system. The peak height (rate) of either N or G in the Figure is just to help the eye.

soon as nuclei form between T_2 and T_3 comparatively few crystals can grow with a wide range of crystal size. On the other hand, when the overlap of the two curves is minimum, e.g. Fig. 2.6b, complete control is possible. Therefore, by holding the glass at a temperature between T_1 and T_2, it is possible to control the number of nuclei. After the required numbers of nuclei are formed, the glass is heated in the range T_3 to T_4 where crystal growth takes place.

In well controlled (good) glass-ceramic systems, there is generally considerable separation between the two curves, and it is obvious that the exact temperatures chosen for preparation will depend upon these requirements. For example, if a large crystal size is required, a moderate rate of nucleation combined with a high crystallization rate is necessary, while for small crystal sizes the maximum nucleation rate combined with a moderate crystal growth rate should be chosen. If the shortest possible heat-treatment time is desired and no other conditions required, then maximum rates in both steps are suitable. Generally, a lower temperature holding stage is necessary in the heat-treatment cycle to serve to "nucleate" the glass after which crystals can grow during a subsequent higher temperature stage on the formed nuclei.

Lithium disilicate glass is considered a good glass-ceramic system. The difference between the maximum nucleation temperature and the maximum crystallization temperature in LS_2 is around 200^{o}C based on the thermal analysis done in this study. That difference will allow us to control the heart treatment process as in Fig. 2.6b.

3. Microwave Processing of Materials

3.1 History of microwave processing

During World War II, microwaves were first used in radar applications. In 1946, an engineer named Dr. Percy LeBaron Spencer discovered the potential of using microwaves for heating with the use of a vacuum tube known as the magnetron. Raytheon introduced the first microwave oven to the marketplace in 1952[35]. Nowadays, the home model microwave oven (2.45 GHz) has become a very common household appliance. Meanwhile, there are many applications for microwave energy to be discovered in other areas. Although microwave processing has been established in a considerable number of applications, it has not yet been established in most materials manufacturing processes as a serious alternative to conventional processing. In many cases, microwave material-processing technology has numerous advantages as compared to traditional materials processing techniques[121-124]. While microwave processing of materials is a relatively new technology, it provides a powerful and significantly different tool to process materials. Microwave processing can also improve the performance of existing materials and is an attractive alternative to conventional heating methods. It provides benefits that are not easily obtainable by other available techniques. Furthermore, microwave processing can lead to improved quality and product properties, reduced processing time, energy consumption and labor savings. It offers a number of advantages such as rapid heating, selective heating, and self-limiting reactions.

Microwaves are defined as electromagnetic waves in the frequency band from 300 MHz to 300 GHz[125]. It has been used in the processing of rubber, polymers, ceramics, composites, minerals, soils, wastes, chemicals, and powders[35]. Nowadays,

the use of microwave processing is quite extended in some industrial and medical sectors. Industrial microwave processing is usually accomplished at the frequencies set aside for industrial use—915 MHz, 2.45 GHz, 5.8 GHz and 24.124 GHz[125]. However, placing a sample in a microwave oven and expecting it to heat efficiently will seldom lead to a significant success. This is due to the complexity of microwave interactions with materials.

In microwave processing, energy is supplied by the electromagnetic field to the sample bulk. Therefore, the electric field generated within the volume of the material might induce ionic motion or molecular dipoles. The resistance of these induced motions causes losses which will cause attenuation in the electric field and volumetric heating of the material[36].

3.2 Variable frequency microwave processing

Although direct heating by microwaves can offer advantages over conventional heating, the mechanism of energy transfer in microwave heating has also resulted in several processing challenges. Fixed frequency microwave (FFM) processing was the first type of microwave processing used by researchers after Dr. LeBaron's discovery[35]. FFM allows for quicker heating than that offered by conventional processing due to its penetrating radiation into the sample. However, it has many limitations due to its static heating properties. FFM heating often results in localized heating because of the local spatial fluctuations in the electromagnetic field. This causes non-uniform power distribution within microwave cavities that will lead to uneven heating and potentially poor product quality[126]. FFM processing technology suffers from hot spots problems that could yield variable product quality. A major problem with

FFM is arcing, which occurs when a metallic material is placed inside one of these systems. It has been found that bulk materials with metallic properties cannot be adequately penetrated at normal microwave processing condition (reflectors). It has been noted that insulators with low dielectric loss factors are difficult to heat due to minimal absorption. In addition, there is a power threshold where benefits of FFM heating no longer exist. With these limitations, researchers have searched for another alternative that utilized the microwave processing capabilities[127-129].

Reduction in the effects of hot spots and improvement in the field uniformity in microwave cavities were developed by several techniques. Some techniques depend on the modification of the electric field in the cavity. Most domestic microwave ovens are equipped with turntables that rotate during operation. The purpose of this turntable is to reduce the effect of multiple hot spots. This is accomplished by exposing the material through areas of high and low power. Thus, uniformity of heating can be achieved. Another technique used was mode stirrers. These are fans that rotate within the cavity to distribute continuously the electromagnetic field.

Recently, a new process called the variable frequency microwave (VFM) technique for material processing has been developed to eliminate the inherent problem in FFM processing, namely arcing and hot spots. Variable frequency microwave (VFM) technique is an emerging technology that overcomes the inherent difficulties of hot spots and arcing experienced in fixed frequency microwave (FFM) technique. VFM was developed for the purpose of processing many of today's advanced materials including polymers, composites and fiber-reinforced materials. It is a rapid and controlled approach to more uniform heating[130]. By sweeping through a bandwidth of frequencies, the

VFM method creates multiple hot spots within the processing cavity that lead to time-averaged uniform heating[131]. The technique works by sweeping through a bandwidth of frequencies that are cycled through consecutively and then are launched into a cavity, resulting in different standing waves with many resonant modes. Figure 3.1 gives the electric field distribution in FFM and VFM as well as the advantages of VFM over FFM. By sweeping through thousands of frequencies, thousands of possible cavity modes are excited. This will lead to different distributions of hotspots within the cavity. In succession, the heating patterns associated with the different resonance modes begin to overlap resulting in a time-averaged uniformity[127, 131-140].

The name VFM is derived from the variation of the source frequency over time[130]. There are four controllable parameters that characterize VFM processing: central frequency, bandwidth, sweep-rate and forward power[132]. The central frequency can be adjusted to increase the coupling efficiency with the material being processed. The combination of bandwidth and sweep rate around the selected central frequency provides the necessary distribution of microwave energy to carry out uniform heating. Finally, the microwave forward power determines the heating ramp rate and can be varied depending on the heating profile[54]. The absorption of the microwave energy within the material depends on the incident microwave frequency, the dielectric constant of the material, dielectric loss of the material and the distribution of the electric field within the material[53, 57, 70, 125].

Variable frequency microwave processing provides a new process that can significantly reduce production time and cost while offering the potential to improve product quality as well. Variable frequency microwave heating is achieved by a method

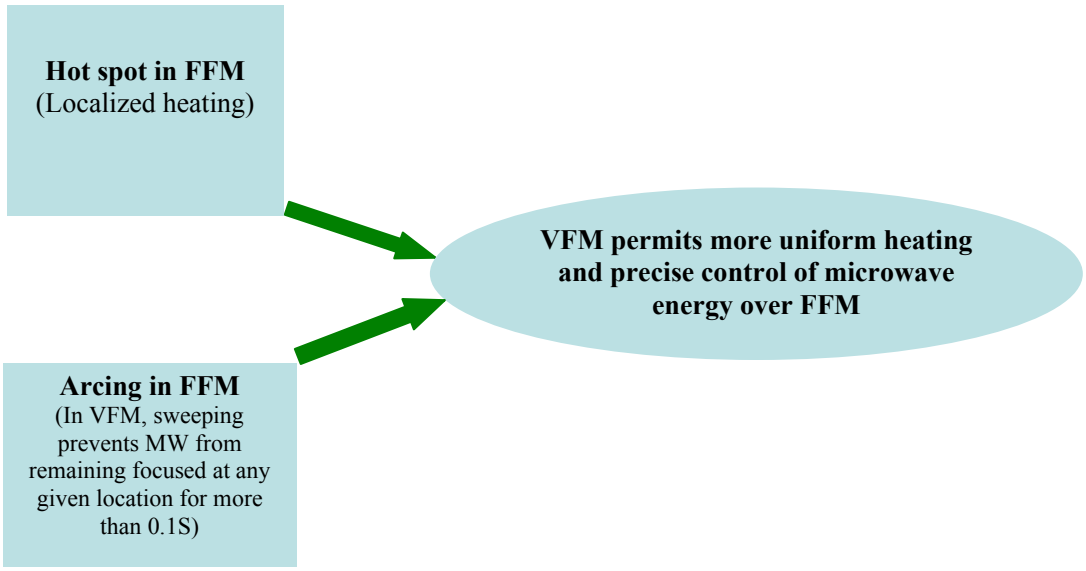

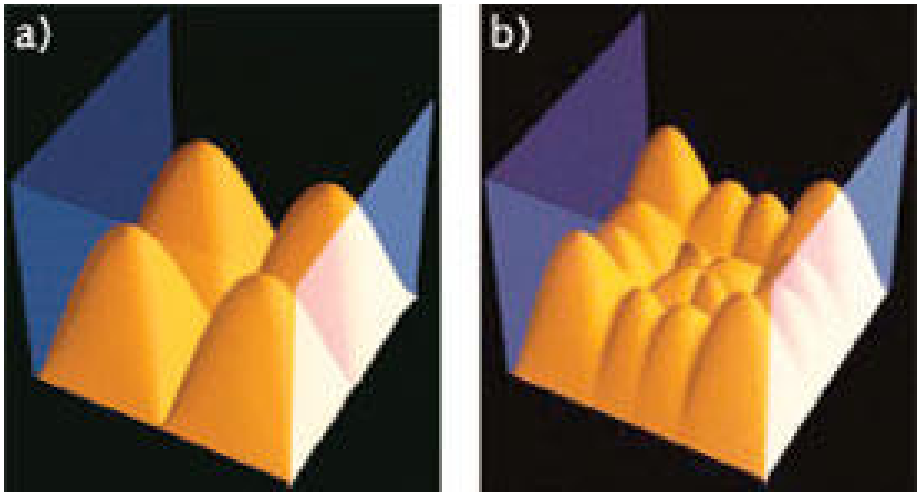

a) Electric field distribution in FFM **b) Electric field distribution in VFM**

Figure 3.1: Distribution the electric field (E) in FFM and VFM as well as the advantages of VFM over FFM[141].

similar to that used with a fixed frequency microwave heating source. However, a VFM source will sweep through a range of radiation frequencies over a set period of time[130].

3.3 Basics of microwave processing science

A basic understanding of microwaves and their interaction with materials is required to gain the advantages and to know the limitations of microwave processing. Although there is a wide range of materials that can be processed using microwaves, there are fundamental characteristics and properties that make some materials particularly conducive to microwave processing and others not. The fundamental understanding of microwave processing is very important in order to develop a given process into production. Also, the fundamental approach is required for the development of process cycles, equipment, and controls. For example, repeatability of a measurement is challenging in microwave processing since the results can be affected by many factors, such as moisture content, changes in dielectric properties during processing, electromagnetic interference with temperature measurements devices, sample size and geometry, and finally the position of the sample in the cavity.

Microwave energy is located between radio wave frequencies (RF) and infrared (IR) frequencies in the electromagnetic (EM) spectrum (Figure 3.2). Microwave energy can be reflected, transmitted and/or absorbed, depending on the type of the material. When microwave energy is absorbed by materials (absorber), it is converted into heat within the material with an increase in the material temperature. Many types of materials, such as gases, liquids, and solids, can interact with microwaves and heated. Gases can be excited by microwaves to form plasmas, under certain conditions, that can be used in material processing[142]. Most liquids can heat easily by microwaves, hence microwaves

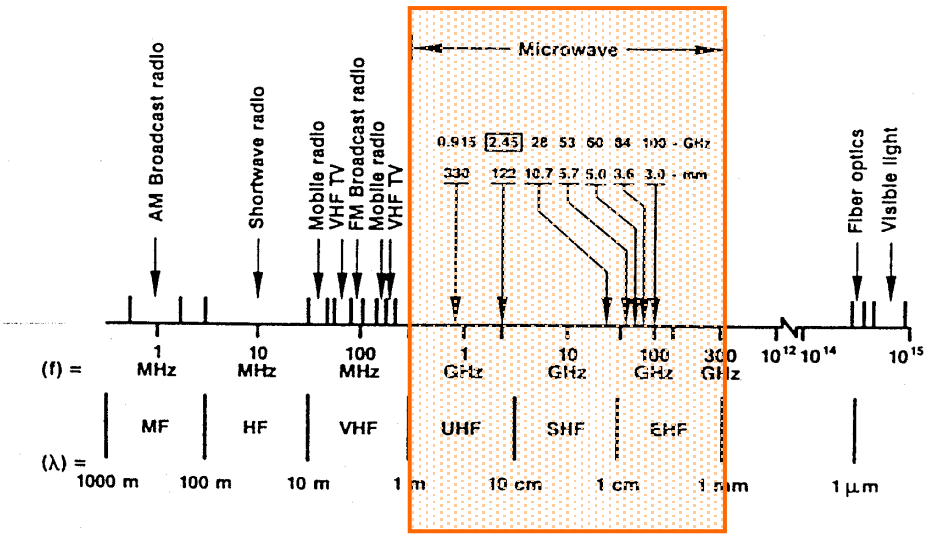

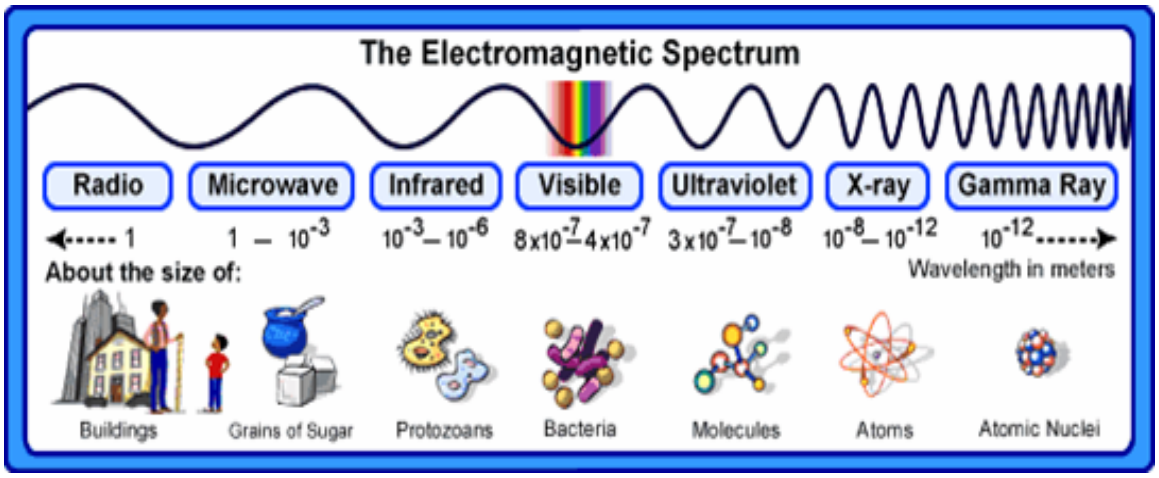

Figure 3.2: The electromagnetic (EM) spectrum and the microwave range[32]. Reprinted with the permission of The American Ceramic Society, www.ceramics.org, [copyright 2005]. All rights reserved.

have been used extensively in chemical synthesis[143].

Because water is a good absorber at 2.45 GHz, microwave ovens were designed primarily to process foods at this frequency. On the other hand, most of ceramics materials do not absorb 2.45 GHz microwave energy at room temperature[32]. As a result, a hybrid heating method was developed to overcome that problem in ceramics. In the hybrid heating process, another material, which is a good microwave absorber, is introduced into the system to first heat and couple with the microwave energy. The ceramic material is heated to its critical temperature (T_{cri}) by the conventional heating resulting from that other material. After that, the microwave absorption becomes sufficient to cause self-heating. In general, microwave absorption in ceramics may be increased by several techniques. The addition of another absorbing material (silicon carbide (SiC), carbon(C), or organic binders), altering the ceramics microstructures and defect structures, changing their form (bulk vs. powder), or changing the frequency of the incident radiation are useful techniques that successfully increase microwave absorption. VFM processing has a unique advantage over FFM by which ceramics can be heated by microwave at room temperature by using the suitable frequency range in which that material will absorb microwave without the aid of any sort of hybrid heating.

While microwave processing of ceramic materials was first recognized in the 1950s, it had been investigated by few researchers on a limited basis by the 1960s[46, 144]. In 1975, Sutton observed that microwaves can heat high alumina materials and not only removing water[145]. In this process, a temperature around 1400°C was achieved. At 2.45GHz, the high alumina ceramic material was a good microwave absorber. Meanwhile, many ceramic materials are transparent to microwave energy at this

frequency. Unfortunately, the low cost of fossil fuels limited the implementation of microwave energy for industrial applications at that time[32]. Nowadays, microwave energy has been used for processing full-scale ceramic products. Microwave processing is faster and more cost effective. It is also capable of producing products with equal or better performance when compared with products resulting from conventional heating.

Microwave energy can be absorbed in ceramics either by polarization or conduction losses. Polarization involves short-range displacement of charge. The formation and the rotation of the electric dipoles (or magnetic dipoles, if present) with the alternating electric field causes ceramics to heat. On the other hand, conduction requires long-range (compared to rotation) transport of charge. Both types of losses give rise to absorption at certain frequency ranges, as shown in Figure 3.3. In this Figure, the absorption losses (also referred to as dielectric losses), ε'', are due to both the ionic conduction, dominant at low frequencies, and rotation of permanent dipoles at higher frequencies.

The ionic conduction losses are due to the ohmic losses that occur when ions move through the lattice and collide with each other. Ionic conduction decreases with increasing frequency because the time allowed for transport in the direction of the field decreases with increasing frequency. On the other hand, increasing the temperature will increase the kinetic energy of the dipoles, making it easier for them to couple to the alternating field. As a result, a shift in the absorption curves to higher frequencies will take place.

Ionic conduction losses are important in materials such as silicate glasses[69]. At low frequencies, ions move by jumping between vacant sites or interstitial positions in

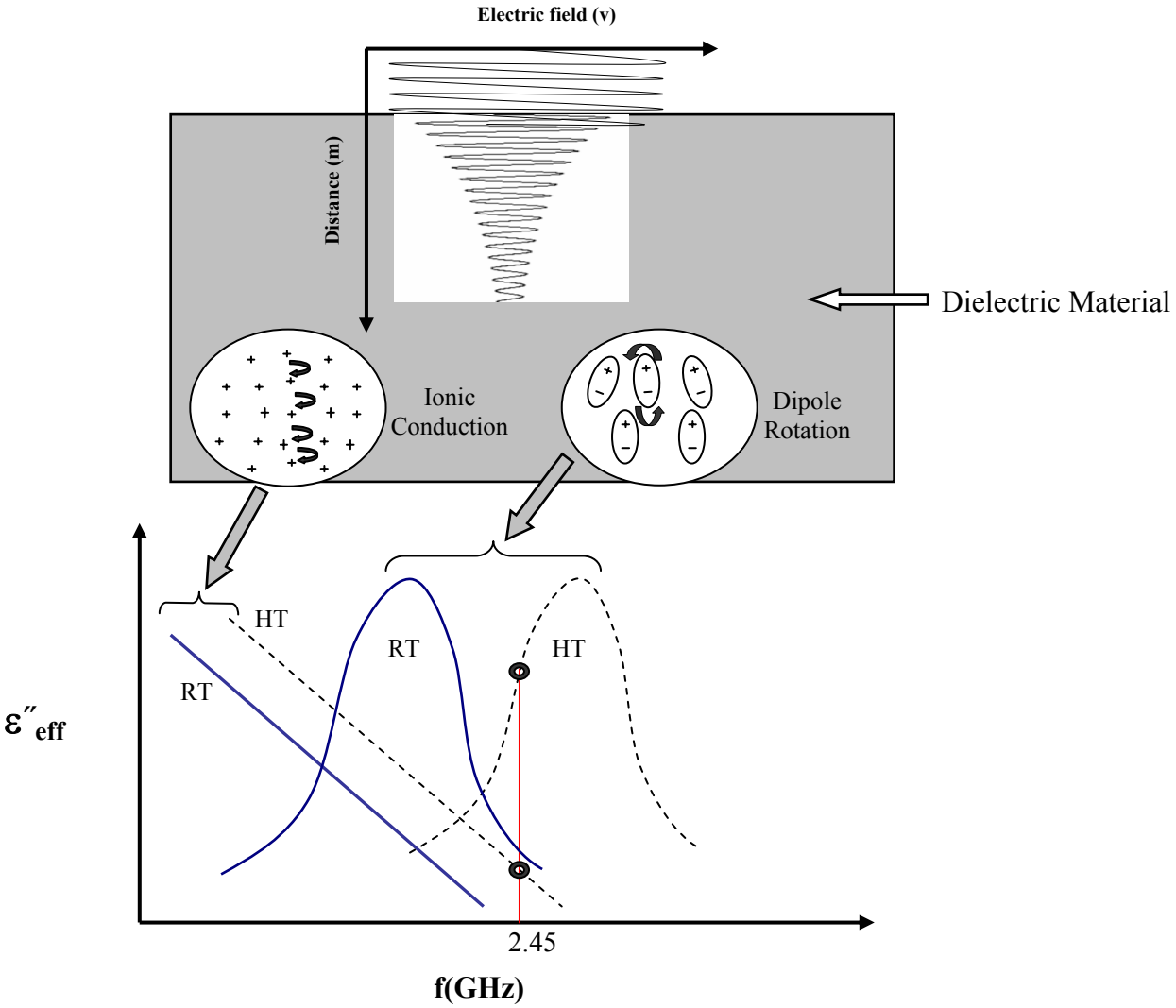

Figure 3.3: The absorption mechanisms that can contribute to ε''_{eff} [32].
Note that a material may be poorly absorbing microwave energy at room temperature and 2.45GHz but highly absorbing at high temperature.
Terms: x ≡ distance; A ≡ amplitude of the electric field; ε''_{eff} ≡ effective dielectric loss; f ≡ frequency; RT ≡ room temperature; HT ≡ high temperature. Reprinted with the permission of The American Ceramic Society, www.ceramics.org, [copyright 2005]. All rights reserved.

the network, giving rise to space charge effects. At higher frequencies, vibration losses, such as those from vibration of alkali ions in a silicate lattice (Li^+ ion in LS_2 glass), become important. Because ionic mobility is an activated process, the conductivity increases rapidly with temperature.

In addition to dipole rotation, other widely recognized polarization processes include interfacial, atomic or ionic and electronic polarization[146]. Because several processes can contribute to the losses, and it is not easy to differentiate experimentally between the losses mechanisms, losses typically are reported as effective losses, ε''_{eff}. To characterize the response of ceramics to the electromagnetic spectrum, measurements should be made over a broad range of frequencies. The frequency dependence of the polarization mechanisms in materials will vary considerably over the EM spectrum, (Figure 3.4). Because of the frequency dependence of polarization, most of the ceramics cannot heat easily at room temperature. If a material does not heat efficiently in a certain frequency range due to the absence of an absorption mechanism in that range (for example 2.45 GHz), a change either in the frequency of the radiation (VFM) or the composition of the material, or the use of hybrid heating can cause it to heat. On the other hand, ceramics can be designed to be microwave safe, such as with microwave cookware. These materials have very small or negligible absorption to heat at 2.45 GHz. Since the frequency dependence of polarization is of interest, it is important to classify the different types of polarization as shown in Figure 3.4. The polarization process can involve rapidly forming diploes and in some cases involve slowly forming dipoles.

Electronic polarization is a result of the displacement of the electrons in the atoms relative to the positively charged nuclei. This process requires 10^{-15} seconds and

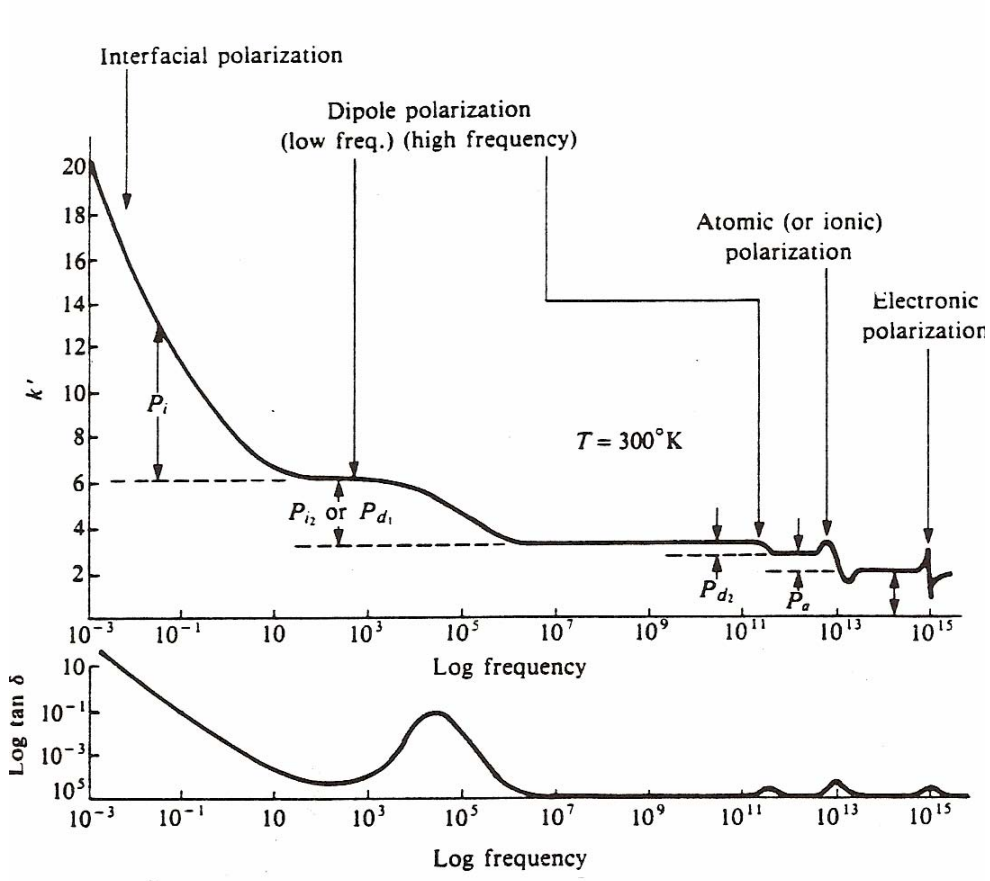

a.

b.

Figure 3.4: Frequency dependence of the polarization mechanisms in dielectrics: (a) contribution to the charging constant (representative values of ε′); (b) contribution to the loss angle (representative of ε″)[32]. Reprinted with the permission of The American Ceramic Society, www.ceramics.org, [copyright 2005]. All rights reserved.

corresponds approximately to the frequency of the ultraviolet light. This process gives rise to a resonance peak in the optical range. The refractive index of a given material is strangely dependent on that polarization[33, 146].

A relatively small atomic polarization arises from the displacement of atoms relative to one another within the molecule, a process requiring about 10^{-12} to 10^{-14} seconds and corresponding to the frequency of the infrared light. In ionic crystals, a similar but usually larger polarization arises from the displacement of oppositely charged ions, a process requiring about 10^{-12} seconds, and corresponding to the frequency of the far infrared region. A resonance absorption occurs at a frequency characteristic of the bond strength between the ions[33, 146].

Orientation polarization, also referred to as dipolar polarization, involves the perturbation of the thermal motion of ionic or molecular diploes, producing a net dipolar orientation under the effect of an applied field. This type is the most important polarization mechanism in the microwave frequency range. The time required for the dipole polarization depends upon the frictional resistance of the medium relative to the change of molecular orientation. This type of polarization results in relaxation type absorption. For gases, the time required for that process is in the range of 10^{-12} seconds, corresponding to the far infrared region. In liquids with small molecules and low viscosity, the time required is about 10^{-11} seconds while the in liquids with larger molecules it is about 10^{-6}, corresponding to the radio frequency range. In very viscous liquids, glasses and solids with high internal friction resistance, the time required for that polarization can extend to seconds, minutes, or longer[33, 146].

The dipolar polarization mechanism can be categorized into two types. First,

molecules with permanent dipole may be rotated against an elastic restoring force about its equilibrium position. The time required for the oscillation of these permanent dipoles is about 10^{-10}-10^{-12} at room temperature. This is sometimes referred as "deformation polarization".

The second mechanism of dipolar polarization involves the rotation of diploes between their equilibrium positions. This mechanism is of special interest in glass and ceramics materials. The interstitial cations give rise to losses that depend on the bond strength of those cations. The required time in this type depends on the structure of the inorganic glass and the binding energy of the alkali ions (such as: Li^+ ion in LS_2 glass) in that glass. Because this mechanism involves the same mobile cations that contribute to the dc conductivity, it is also referred to as "migration loss" [33, 146].

The last type of polarization is the interfacial polarization that arises from the accumulation of charge at the interfaces between phases. It arises only when two phases with different dielectric constant and conductivity. Impurities or second phases usually make a physical barrier to conduction and lead to charge that will build up at the interface of heterogeneous materials. The charge pile up at the different barriers leads to localized polarization of the material[33, 146]. At room temperature, that polarization is expected to have a minimum effect on LS_2 glass because (like any glass) it does not have grain boundaries and does have a homogenous single glassy phase. At higher temperature, i.e. during the crystallization process, when LS_2 crystal phase starts to appear and grow within the glassy phase (partially crystallized sample case) that mechanism will become more important because there is large difference in the dielectric properties between those two phases as discussed later in the results section.

While many researchers have reported the "microwave effect", which are enhanced rates, different reaction pathways and different reaction products, they have been unable to provide a clear scientific explanation for this behavior[32].

In a given ceramic material, the absorption of microwave energy depends on the rate of microwave energy absorption as expressed in terms of power per unit volume as[32]:

$$\mathbf{P_a = \omega\, \varepsilon_o\, \varepsilon''_{eff}\, E^2_{rms} + \omega\, \mu_o\, \mu''_{eff}\, H^2_{rms}} \qquad (\text{watts/m}^3) \qquad \mathbf{(3.1)}$$

where, in general this Equation refers to electric and magnetic losses, respectively. The magnetic losses are usually negligible and only the electric losses contribute to the absorbed power.

ω = angular frequency = $2\pi f$ (f = operating frequency in hertz);

ε_o = permittivity of free space = 8.85×10^{-12} farads/m;

E_{rms} = root mean square of the internal electric field (volts/m), and;

ε''_{eff} = effective relative dielectric loss (dissipation) factor (unitless).

The effective dielectric loss can be expressed as[32]:

$$\mathbf{\varepsilon''_{eff} = \varepsilon''_c + \varepsilon''_s + \varepsilon''_d + \varepsilon''_i + \varepsilon''_e} \qquad \mathbf{(3.2)}$$

where, ε''_c is the loss due to dc conductivity (negligible at microwave frequencies for most ceramics), as shown in Figure 3.3. The rest represent dielectric losses due to polarization mechanisms, where ε''_s = space charge or interfacial; ε''_d = dipolar; ε''_i = ionic, and ε''_e = electronic. In ionic ceramic materials, ε''_s and ε''_d are the most essential.

Because these polarization losses are a function of frequency and temperature, it is measured in order to predict if the ceramic material will heat or not, at a specified frequency. Sometimes, ε''_{eff} is replaced by $\tan\delta\varepsilon'$, where δ is the loss angle, $\tan\delta$ is the dissipation factor and ε' is the dielectric constant. Ceramics that have loss factors

between the limits $10^{-2} < \varepsilon''_{eff} < 5$ would heat using microwave heating. Others with $\varepsilon''_{eff} < 10^{-2}$ would be difficult to heat. On the other hand, those with $\varepsilon''_{eff} > 5$ would be heated mostly on surface and not the bulk[32].

The rate of temperature rise ($\Delta T/\Delta t$) in ceramic materials by microwave energy is given by[147]:

$$\frac{\Delta T}{\Delta t} = \frac{P_a}{\rho(C_p)} \qquad (°C/sec) \qquad \textbf{(3.3)}$$

where, ρ = density of the ceramic (kg/m^3),

C_p = specific heat (kJ/kg-°C).

As can be seen from Equations 3.1 and 3.3, the dielectric properties and the internal electric field are important factors to determine the power absorbed and heating possibility of the ceramic material. On the other hand, it is not trivial to determine the internal electric field. It changes from point to point within the material. The internal field is less than the external field. It is controlled by the dielectric constant, ε', as shown by[39],

$$E_{\text{int}} = \left[1 - \frac{N(\varepsilon' - 1)}{1 + N(\varepsilon' - 1)}\right] E_{ext} \qquad (V/m) \qquad \textbf{(3.4)}$$

where N is a depolarization factor that depends on shape or geometry. Thus, high values of ε' reduce the internal field and the rate of microwave heating. The internal electric field for a given point within the material can be calculated by measuring $\Delta T/\Delta t$, C_p and ε''_{eff} by [125]

$$E_{\text{int}}(rms) = \left(\frac{\rho C_p \, \Delta T / \Delta t}{\omega \varepsilon''_{eff}}\right)^{\frac{1}{2}} \qquad (V/m) \qquad \textbf{(3.5)}$$

So, the E_{ext} (rms) can be calculated using Equation 3.4. The external electric field is not uniform in most multimode microwave cavities. So, the internal electric field will not be uniform as well. As a result, home microwave ovens require turntables or mode stirrers. Their main function is to improve the electric field uniformity. In addition, the electric field uniformity can be improved by increasing the size of the oven cavity. The cavity should be much larger than the wavelength of the microwaves.

The dielectric properties control the quantitative relationships of absorbed power per unit volume (P_a) and depth of penetration (D_p). D_p is defined as the distance from the surface into the material at which P_a drops to e^{-1} (~37%) of the surface value, Equation 3.6[125]

$$D_P = \frac{\lambda_o}{2\pi(2\varepsilon')^{1/2}}\left[\left(1+\left(\varepsilon''_{eff}/\varepsilon'\right)^2\right)^{\frac{1}{2}}-1\right]^{-1/2} \quad \text{(cm)} \qquad \textbf{(3.6)}$$

where, λ_o = free space wavelength of the microwave radiation.

The depth of penetration is very important to determine if the ceramic material will heat effectively or not by microwaves. In some materials, the magnetic dipoles may be able to couple with the magnetic component of the electromagnetic field and provide an additional heating mechanism as shown later. Similar to the dielectric properties, the magnetic permeability, μ′, and loss, μ″, must be considered. Relatively few studies[63, 148] on microwave processing of magnetic materials were reported and this area appears sufficiently promising for further investigation.

The dielectric properties of most materials as a function of temperature are very important in microwave processing. These properties depend on temperature and frequency. Many ceramics exhibit an increase in ε''_{eff} with increasing temperature. Since

P_a is directly proportional to ε''_{eff}, there is a corresponding increase in the power absorbed and the heating rate of the ceramic as the temperature is increased. The reason for this abrupt change in ε''_{eff} is due to easier dipole rotation that allows the peak shown in Figure 3.4 to move closer to the microwave frequency being used. The temperature where the abrupt change in ε''_{eff} occurs is referred to as the critical temperature (T_{cri}). Below T_{cri}, an external energy source is required to heat the ceramic if FFM is being used whereas in VFM this external source can be avoided. Above T_{cri}, the sample becomes self-heating in the microwave field. There is no Equation relating T_{cri} to fundamental material values, thus the critical temperature values must be measured. For all calculations and measurements, it is important to identify specifically the material characteristics (i.e., composition, phase, form) and assumed or measured process parameters (i.e., temperature, pressure, and atmosphere). For example, 99% alumina differs from 96% alumina and α-SiC differs from β-SiC.

A potential consequence of the rapid increase in ε'' with temperature ($d\varepsilon''/dT$) in FFM will develop localized hot spots. The development of hot spots usually is referred to as “thermal runaway” (unstable accelerated heating). VFM has been developed mainly to minimize and decrease this phenomenon in microwave processing of materials.

4. Materials and Experimental Procedure

This chapter describes the procedure and experimental arrangements for the crystallization of lithium disilicate (LS_2) glass into a glass-ceramic material by conventional heating and by microwave energy as well. Melting of the glass batches, conversion of glass into glass-ceramics by both techniques, full characterization of the materials, and measurements for some properties of the obtained glass-ceramics materials will be described.

4.1. Glass preparation

LS_2 glass frit was the main starting material used for producing glass and glass-ceramic materials in this study. Since uniform mixing of the batch materials is very important to facilitate the melting process and to ensure more homogeneity in any glass preparation process, LS_2 glass frit (325 mesh-SP1714 Glass Powder-Lot # 06179112-P.O. #N18261) from Specialty Glass, Inc., Florida was used to prepare LS_2 glass samples.

LS_2 glass frit was melted in a covered platinum crucible to minimize the contamination or the reaction between the frit and the crucible body. Each batch was melted at 1400^{o}C in an electric furnace (DELTECH, Inc.), and the melt was held at the maximum temperature for 4 hours with occasional stirring to ensure complete homogenization. Figure 4.1 illustrates the melting scheme used to prepare LS_2 glass. The temperature was raised slowly and gradually to 200^{o}C and held there for 30 minutes to remove any moisture in the frit. Because LS_2 crystalline phase was found to melt congruently at 1033^{o}C as shown before in Figure 1.1[17], the temperature was raised again slowly and gradually to 1100^{o}C and held there for 1 hour. This melting regime was

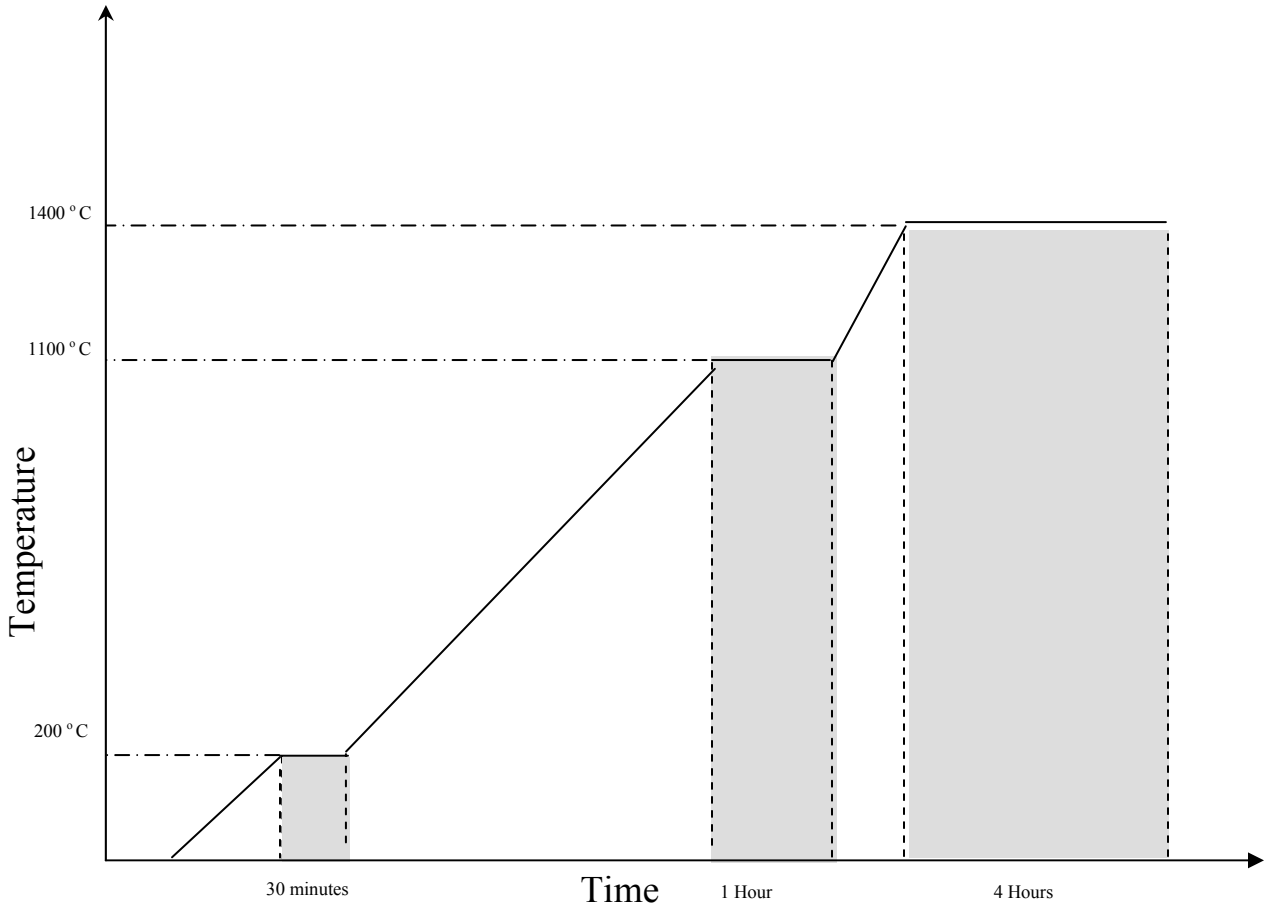

Figure 4.1: Melting regime for LS_2 glass frit.

successful in preventing spattering or splashing of the batch during melting. The temperature was raised again up to 1400^{o}C where the viscosity of the melt was low enough so that the melt could be easily poured into a mold. This regime of melting was found sufficient to yield bubble-free fluid homogeneous melts.

After completion of the melting process, the melts were cast at room temperature into a hot graphite mold (400^{o}C) to make rods (~60 mm long and ~15 mm diameter), and the samples were rapidly transferred to a box furnace (Thermolyne-Model 1400) adjusted to 400^{o}C for annealing for 10 hours, to give strain-free glass samples. After that the furnace was shut down and allowed to slowly cool to room temperature with the samples inside it before opening.

Glass specimens were cut into ~ 1 cm thick disks using a low-speed (100 rpm) diamond saw (Buehler ISOMET™ 1000 Precision Saw). Those glass disks were cleaned by ultrasonic waves for about 2 minutes to remove all the cutting oil traces and then washed with acetone before being dried at 150^{o}C at conventional hot air drier. The dried samples were stored in a desiccator with calcium oxide to keep them in a dry environment.

4.2. Thermal analysis

Differential scanning calorimetry analysis (DSC) was helpful in determining the range as well as the temperature of glass crystallization and consequently the proper heat-treatment schedule to be applied to the studied glasses. An endothermic reaction was an indication of the nucleation process in the glass and/or the melting of the glass. Thermodynamically, these two processes needed external energy to accomplish the nucleation or the melting processes. On the other hand, in most of the cases, an

exothermic reaction indicated the crystallization process. The peak height of the exotherm was proportional to the heat evolved during crystallization[18]. A more accurate assessment of this was given, however, by the peak area. The major features found in a typical DSC trace for a glass that readily crystallized during heating were the glass transition temperature (T_g), the nucleation temperature (T_n), and the crystallization temperature (T_c).

The NETZSCH model STA 449 C Jupiter® simultaneous thermal analyzer was used to identify the nucleation and crystal growth temperature for the glass. The temperature range was from room temperature to 1100°C in air with a heating rate of 10 degree C/min in Pt/Rh crucibles.

4.3. Heat treatment

The glass samples should be subjected to a controlled heat treatment schedule in order to promote the process of crystallization and the conversion of the glass into a glass-ceramic. For this purpose, a two stage heat-treatment regime (Figure 4.2) was generally implemented in the present study. This regime first included the nucleation step, which was done for all the glass samples by conventional heating in an electric furnace, followed by the crystallization step by the two different techniques: conventional heating and microwave energy. In such a two-stage heat-treatment, the low-and-high temperatures are designated as the nucleation and the crystallization treatments respectively. The choice of these heat-treatment temperatures was guided by the results of the DSC traces.

a. Nucleation stage

To ensure adequate homogenous nucleation, the glass specimens were heated

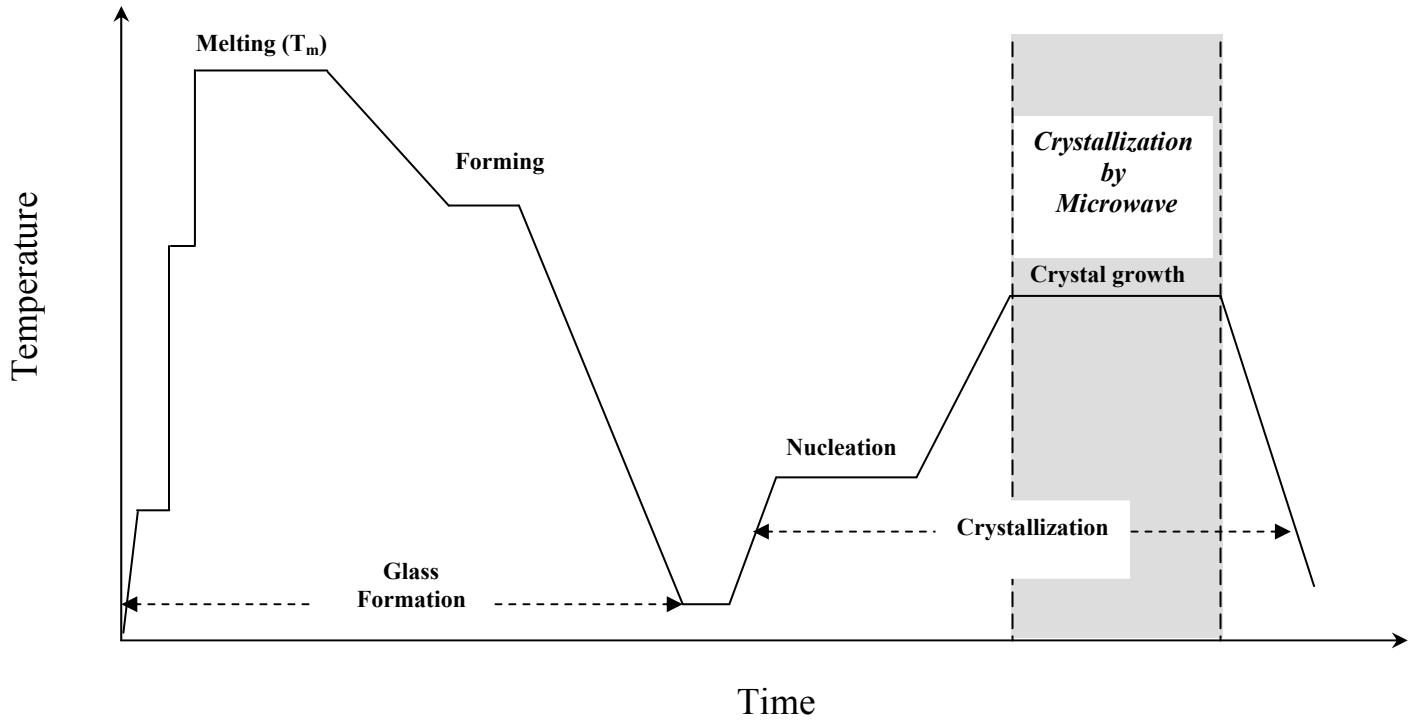

Figure 4.2: Typical two stage heat treatment for producing a glass-ceramic by controlled nucleation and crystal growth.

conventionally to the nucleation temperature (480^{o}C, 2 hours ramp) in an electric furnace (CM furnace-Model 1700) and held for a certain period of time (2 hours) followed by furnace cooling to room temperature. After such nucleation, the nucleated glass disks were crystallized by either conventional or microwave heating.

b. Crystallization stage

The nucleated glass samples were heated to the crystallization temperature in order to grow those formed nuclei to crystals and hence to convert the glass into a glass ceramic material.

The conventional crystallization was done in an electric furnace (CM furnace-Model 1700) with a 10 minute ramp to reach the desired crystallization temperature. Based on calculations, it is believed that this 10 minutes ramp time is sufficient to make the heat-treated bulk glass sample in equilibrium with the furnace temperature. Microwave crystallization of the nucleated disks was performed using a Microcure-Model 2100 (Lambda Technologies) with a frequency sweep range of 2–8 GHz, operating at a nominal power of 250W. A central frequency of 6.425 GHz with a band width of 1.15 GHz and a sweep time of 0.1 second were used to crystallize the glass samples. A 10 minute ramp to the desired temperature was used in the microwave crystallization process to simulate the conditions used for conventional crystallization. The temperature was monitored in the Microcure system by an infrared (IR) sensor and also by a regular type K thermocouple that was connected to a RayTeck T30 temperature controller (monitoring system for closed loop feedback). A schematic of the conventional crystallization and the VFM crystallization setups is shown in Figure 4.3.

In order to study the early stages of crystallization of LS_2 glass that was

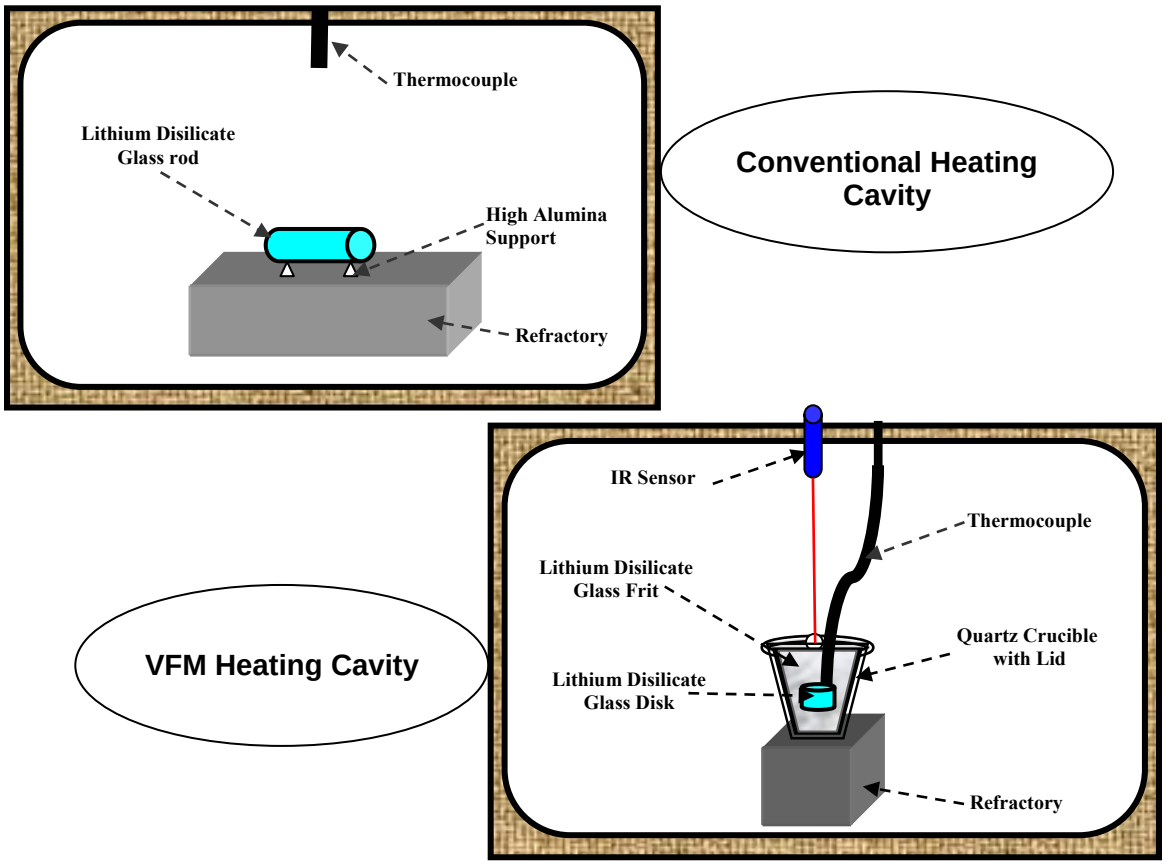

Figure 4.3: Schematic diagram of the conventional crystallization setup and for the variable frequency microwave (VFM) crystallization setup heating processes.

Table 4.1: Crystallization temperatures and time used to in that study.

Temperatures (^{o}C)	Time (minutes)													
	15	20	30	40	50	60	70	80	90	100	110	120	130	140
567^{o}C	●	●	●	●	●	●	●	●	●	●	●	●	●	●
583^{o}C	●	●	●	●		●	●							
595^{o}C	●	●	●	●		●								

crystallized by both conventional heat treatment and also by microwave energy, three crystallization temperatures (567^{o}C, 583^{o}C, and 595^{o}C) were chosen according to the thermal analysis data (DSC) with different soaking times as shown in Table 4.1.

4.4. Surface preparation

The glass, nucleated glass, and glass-ceramics samples were ground and polished so that the samples surface could be analyzed by optical microscopy, Raman spectroscopy, and FTIRRS techniques. The samples were first ground with 180 grit SiC paper to remove surface crystallization and to ensure complete flatness of the surface, then polished gradually starting from 400 to 600 grit SiC paper and finally ending with 0.25μ diamond compound on Nylon cloth. An automated Buehler machine (ECOMET® 6 Grinder/Polisher) was used to grind and polish all the samples. A fine polished surface was obtained after that procedure which is essential in studying the samples by FTIRRS, Raman spectroscopy, and optical microscopy.

4.5. Characterization techniques

4.5.1. X-ray diffraction (XRD)

Due to the very fine-grained microstructures of the obtained glass-ceramic samples, identification of the crystalline phases developed by crystallizing the glass was mainly conducted by x-ray diffraction analysis of the powdered crystalline samples. A mortar and pestle were used to grind the glass and glass-ceramic samples into a fine powder that were tested by XRD. The x-ray patterns were obtained using a Scintag x-ray diffraction spectrometer (XDS 2000). A Cu tube voltage of 45 kv and currents of 40 mA were applied. A scanning speed of 2 degrees (θ)/min was used for the analyses. The reference data for the interpretation of x-ray diffraction patterns were obtained from the

ASTM x-ray diffraction file index and from several other publications[18, 149-158].

4.5.2. Microscopy

a. Optical microscope

Probably the most nearly indispensable tool in crystallization research is the optical microscope. For this, the polished surface samples (glass or glass-ceramic samples) were etched with 2% HF (Hydrofluoric) acid for 2 minutes, washed with distilled water and then acetone before being dried. The microstructure of these samples was examined optically using a polarizing research microscope with Nomarski optics.

b. Scanning electron microscope (SEM)

Several selected heat-treated glass samples with their corresponding as-cast glasses were examined on fresh fractured surfaces and also on the polished surfaces. A scanning electron microscope (Model LEO 1550 Gemini Field Emission) with EDX (Energy Dispersive X-ray analysis) unit attached was used with accelerating voltage up to 30 K.V. and magnification from 20 x up to 900,000 x. The freshly polished surfaces were first etched for 2 minutes in 2% HF. Then, thoroughly rinsed with distilled water, dried, and coated with a thin film of evaporated gold or carbon. The coating helped to reduce the effect of sample charging in the electron beam.

4.5.3. Stereology

Stereology is the methodology to obtain quantitative estimates of geometric properties of features in three-dimensional structures from measurements that are made on two-dimensional images[159]. Since the features in the 2D image arise from the intersection of the plane with the 3D structure, it is logical to expect that measurements of the feature traces that are seen there (lower in dimension) can be utilized to obtain

information about the features that are present in 3D. In the most common type of imaging used in microscopy, the image represents a section plane through the structure. For an opaque specimen such as most materials (metals, ceramics, polymers, and composites) viewed in the light microscope, this is a cut and polished surface that is essentially planar, perhaps with minor (and ignored) relief produced by polishing and etching that reveals the structure.

The classical rules of stereology are a set of relationships that connect the various measures obtained with the different probes with the structural parameters. The most fundamental (and the oldest) rule is that the volume fraction of a phase within the structure is measured by the area fraction on the image, or $V_V = A_A$[159]. Of course, this does not imply that every image has exactly the same area fraction as the volume fraction of the entire sample. A statistical representation of the data is required to represent any type of measurement.

The connection between expected values of counts for a given probe/event combination and a geometric property of the three-dimensional structure is obtained by applying the appropriate fundamental relationship of stereology. These Equations have the status of expected value theorems. The simplest of these relations is shown in Equation 4.1[159],

$$\mathbf{\langle P_P \rangle = V_V} \qquad \mathbf{(4.1)}$$

where V_V is the volume fraction occupied by the phase being counted (volume per unit volume, a dimensionless ratio). It is the general stereological term used for any identifiable region or class of objects, including voids. The brackets around $\langle P_P \rangle$ signify the expected value for this normalized count, in this case, the point fraction. This

Equation may be read: “The expected value of the fraction of the population of points that exist in the volume of the structure under study that lie in the phase of interest is equal to the fraction of the volume of the structure occupied by that phase”[159].

a. Volume fraction from the point count

Point probes sense the volume of three-dimensional features. The most commonly measured property of three-dimensional feature sets is their volume, usually reported as the volume fraction, V_V, of the phase. This property may be estimated using either: plane, line, or point probes; the simplest and most commonly used measurement relies on point probes[159]. The population of points to be sampled by these probes is the set of points contained within the volume of the specimen in three dimensions. Point probes are normally generated by first sectioning the sample with a plane and generating a grid of points on the plane section. For example, as in the two dimensional structure described in the Figure 4.4, the event of interest is “point hits the β phase” where “β phase” is taken to mean the set of features at the focus of the analysis. These points are simply counted. The stereological relation that connects this point count with the volume of the structure is shown in Equation 4.1[159].

Visualize a specimen composed of two phases α and β. This structure is revealed by sectioning it with planes and examining fields on these sections, as shown in Figure 4.4. The population of points in the three-dimensional specimen is probed by the (20 * 20) grid of points superimposed on this structure (400 points count). For the field shown in Figure 4.4, this estimate is (80/400)*100= 20 %.

It is important to consider the precision of the measurement using the point count technique for a given sample. Precision can be increased in two ways:

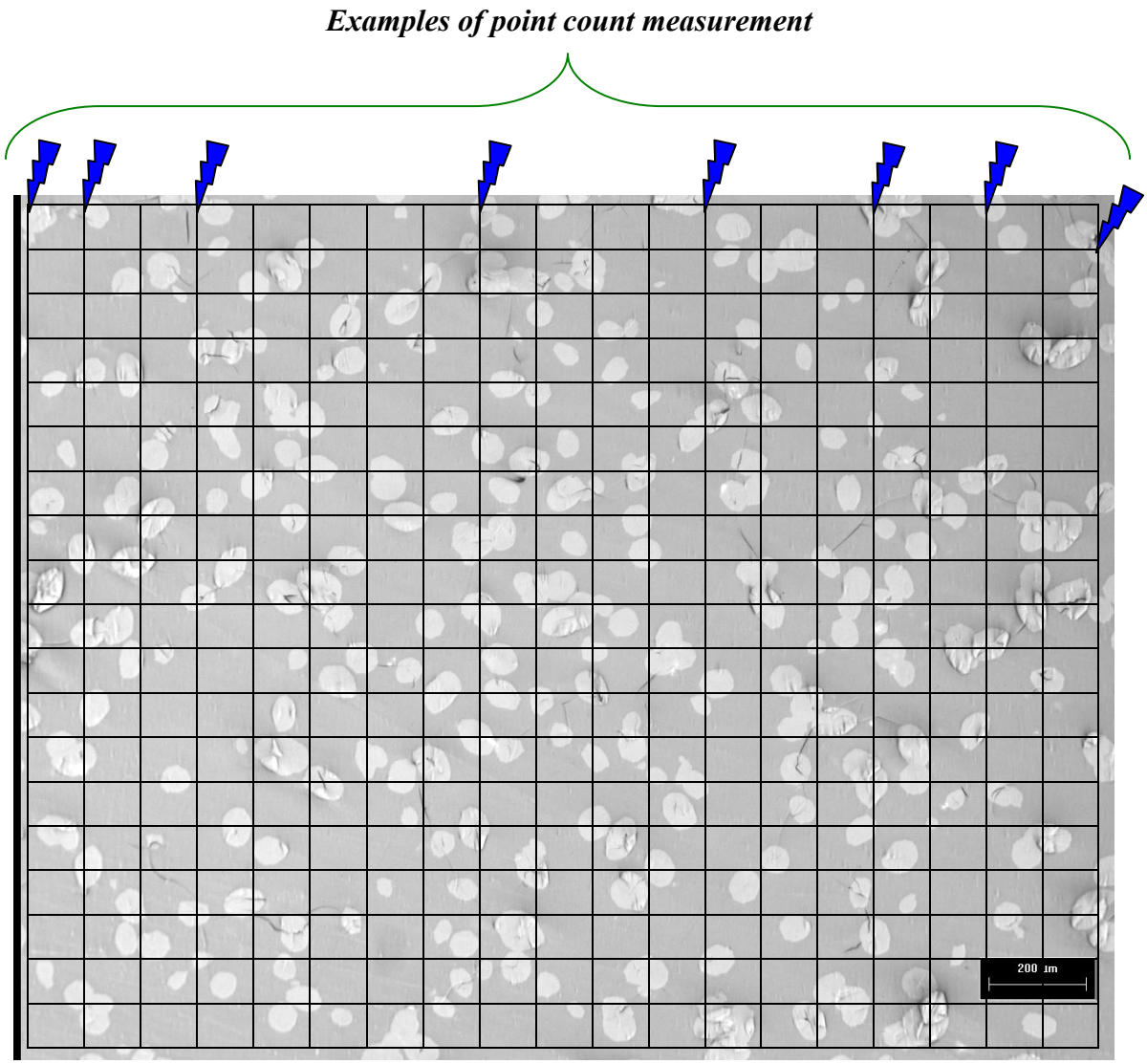

Figure 4.4: Measurement of the volume fraction V_V of a phase in three dimensions.

α phase :Gray
ß phase : White

1. Increasing the number of randomly selected fields measured in a given sample.

2. Decreasing the standard deviation of a given sample by increasing the number of points within the grid and to cover the sample field by the suitable grid area as well. So the area of the grid, the number of points within that grid, and the number of representative fields in a given sample determine the precision of the measurement.

In order to obtain an estimate of the volume fraction of β phase in the three-dimensional structure represented by the plane section in Figure 4.4, it is necessary to repeat this measurement on a number of fields that are chosen to represent the population of points in three dimensions and statistically represent the result for a given sample. Also, increasing the number of points in the grid being used and to cover most of the sample area by the grid will increase the accuracy of the measurement.

In this study, for a given sample, five (5) randomly selected fields were used to calculate the volume fraction. In each field, measurements were done by the 400 grid (20*20) for each field. The final crystallization volume fraction for the given sample is reported with its standard deviation.

4.5.4. Infrared and Raman spectroscopy

The vibrational frequencies of a molecule can be determined by two fundamental different spectroscopic techniques:

a- Infrared spectroscopy, first systematically used by W.Coblentz in 1905[160].

b- Raman spectroscopy, which was theoretically predicated in 1923 by A.Smekal and experimentally observed in 1928 by C.V.Raman and K.S.Krishana[160].

Both techniques depend on the interaction of electromagnetic radiation with matter, but the physical causes are fundamentally different. In many molecules, it is possible to

observe vibrations of different symmetry by different spectroscopic techniques. The complete picture is often only obtained by combining the two techniques. The main differences between the Infrared and Raman are summarized in Table 4.2 and Figure 4.5[161].

a. Fourier transform infrared reflectance spectroscopy (FTIRRS)

Spectroscopic methods occupy a special place in the group of methods which enables the researchers in the examination of a glass structure. Fourier transform infrared spectroscopy (FTIR) has been widely applied to the interpretation of the structural modifications occurring in glasses when subjected to a thermal treatment. It has been shown that the silicate glass structure varies with the heat treatment temperature and several properties are affected by this variation. The position and the shifting of the peaks in the FTIR spectra were used to evaluate the changes in glass properties and structure. The frequency of the IR-absorption peaks is sensitive to the nature and the type of the bonds.

The IR spectra of the polished samples surfaces were obtained by FTIRRS technique using FTIR Nicolet Avatar 330 instrument with a smart stage (SpeculATR) in specular reflectance mode with 45° angle of incidence beam and 7 mm sample mask in the range of 4000–400 cm^{-1} with an average of 32 scans.

a.1 Background

High information content, mature technology and wide applicability have made vibrational spectroscopy one of the most important methods for structure determination. The vibrational spectrum of a molecule is considered to be a unique physical property and is characteristic of the molecule. Vibrational spectroscopy has been employed over

Table 4.2: Comparison between Infrared and Raman spectroscopy.

Parameter	*IR Spectroscopy*	*Raman Spectroscopy*
Interaction	Absorption, Reflection or Transmission	Scattering
Excitation of vibrations by	Polychromatic infrared radiation	Monochromatic radiation usually in the visible range(laser)
Frequency Measurement	Absolute	Relative to the excitation
Requirement for the activity of a vibration	Change of the dipole moment	Change of the polarizability
Representation of the spectrum	Absorption logarithmic (Downwards)	Intensity Linear (Upwards)
Preferred technique for	Routine analysis, gas analysis	Investigation of aqueous solutions, and single crystal
Unique Information in glass structure	Stretching and bending modes of (-Si-O-Si-) bond	Structural environment around SiO_4 tetrahedra

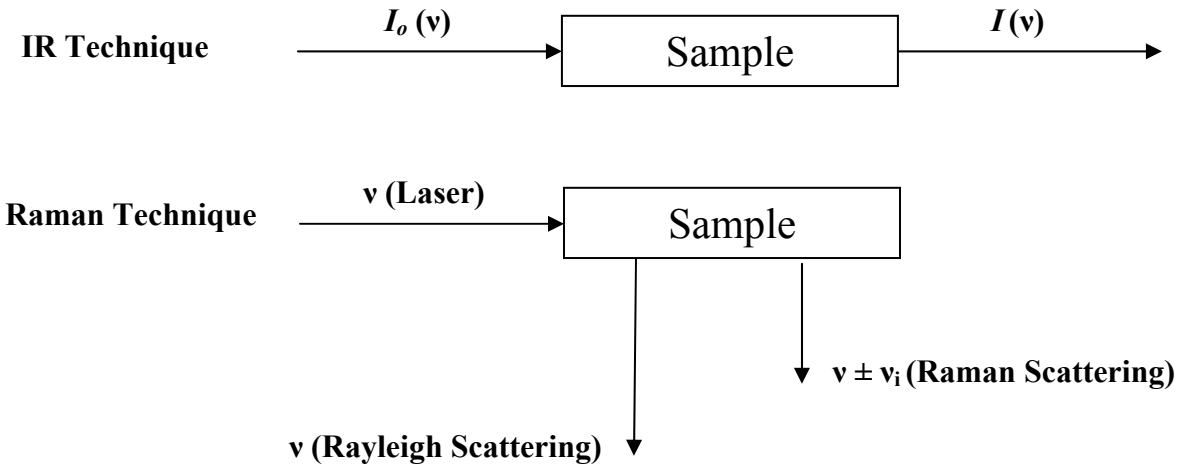

Figure 4.5: Mechanisms of Infrared absorption and Raman scattering.

the last several decades to investigate the structure of glass. Infrared spectroscopy, in particular has proven useful because it provides a means to determine local structure which constitutes of the glass network, some of the properties of the sites hosting the modifying cations and the interactions between charge carriers and network segments[162].

Absorption of light in the ultraviolet and visible regions of the spectrum is due mainly to electronic transitions. While there are some lower energy electronic transitions in the infrared region of the spectrum, most absorption in the infrared region in glasses are due to vibrational transitions[163].

The infrared spectra region can be subdivided to three regions:

1- Near infrared region (12500-4000 cm^{-1}).

2- Medium infrared region (4000-650 cm^{-1}).

3- Far infrared region (650- about 100 cm^{-1}).

a.2 The Origins of the infrared spectrum

In the most basic terms, the infrared spectrum is formed as a consequence of the absorption of electromagnetic radiation at frequencies that correlate to the vibration of specific sets of chemical bonds from within a molecule. First, it is important to reflect on the distribution of energy possessed by a molecule at any given moment, defined as the sum of the contributing energy terms (Equation 4.2)[161]:

$$\mathbf{E_{total} = E_{electronic} + E_{vibrational} + E_{rotational} + E_{translational}} \qquad \mathbf{(4.2)}$$

The translational energy relates to the displacement of molecules in space as a function of the normal thermal motions of matter (not quantized). Rotational energy, which gives rise to its own form of spectroscopy, is observed as the tumbling motion of a molecule, which

is the result of the absorption of energy within the microwave region. The vibrational energy component is a higher energy term and corresponds to the absorption of energy by a molecule as the component atoms vibrate about the mean center of their chemical bonds. The electronic component is linked to the energy transitions of electrons as they are distributed throughout the molecule, either localized within specific bonds, or delocalized over structures, such as an aromatic ring[164].

When a molecule absorbs radiation, its energy increases in proportion to the energy of the photon as expressed by Equation 4.3[161].

$$\Delta E = h \nu = h (C/\lambda) \qquad (4.3)$$

where h is Planck's constant, ν = frequency of the radiation and C is the speed of light. This increase in energy could be in the electronic, vibrational, or rotational energy of the molecule as discussed earlier. Changes in the electronic energy involve relatively large quanta while changes in the vibrational energy involve smaller quanta. The changes in the rotational energy involve quanta even smaller than those in vibrational energy. If the molecule absorbs radiation in the microwave or far infrared region, a major change in the rotational energy will happen relative to the vibrational and electronic energies of the molecule. If the radiation is in the medium infrared region, both the vibrational and rotational energies of the molecule will change. If the energy of the radiation is much greater, as in the case of ultraviolet light, there will be a change in the electronic, vibrational and rotational energies of the molecule. Thus, the infrared absorption spectra of molecules results from transitions between the vibrational and rotational energy levels[165].

The fundamental requirement for infrared activity, leading to absorption of

infrared radiation, is that there must be a net change in dipole moment during the vibration for the molecule or the functional group under study. However, in the case of Raman spectroscopy, which is complementary to infrared spectroscopy, the selection rules are different from those for infrared spectroscopy, and in this case a net change in bond polarizability must be observed for a transition to be Raman active[166].

For the most part, the basic model of the simple harmonic oscillator and its modification to account for anharmonicity suffice to explain the origin of many of the characteristic frequencies that can be assigned to particular combinations of atoms within a molecule. From a statement of Hooke's law, the fundamental vibrational frequency of a molecular ensemble can be expressed according to Equation 4.4[166]:

$$\nu = (1/2\pi)\,(k/\mu)^{1/2} \qquad (4.4)$$

where ν = fundamental vibration frequency, k = force constant, and m = reduced mass as in Equation 4.5[166]

$$m = (m1m2)/(m1+m2) \qquad (4.5)$$

where m1 and m2 are the masses of the 2 atoms forming the molecule. This Equation 4.4 provides a link between the strength (or springiness) of the covalent bond (k) between two atoms (or molecular fragments), the mass of the interacting atoms (molecular fragments), and the frequency of vibration. Although simple in concept, there is a reasonably good fit between the bond stretching vibrations predicted and the values observed[167].

This simple model does not account for repulsion and attraction of the electron cloud at the extremes of the vibration, and does not accommodate the concept of bond dissociation at high levels of absorbed energy. A model incorporating anharmonicity

terms is commonly used to interpret the deviations from ideality and the overall energy–spatial relationship during the vibration of a bond between two atomic centers. The energy transition between the ground state and the first vibrational quantum level is essentially unaffected by the anharmonicity terms. However, transitions that extend beyond the first quantum level (to the second, third, fourth, etc.), which give rise to weaker absorptions, known as overtones, are influenced by anharmonicity, which must be taken into account when assessing the frequency of these higher frequency vibrations.

It is necessary also to look at the molecule as a whole. It is very easy to imagine that there are an infinite number of vibrations, which in reality would lead to a totally disorganized model for interpretation. Instead, the model is described in terms of a minimum set of fundamental vibrations, based on a threefold set of coordinate axes, which are known as the normal modes of vibration. All the possible variants of the vibrational motions of the molecule can be reduced to this minimum set by projection onto the three fold axes. It can be shown that the number of normal modes of vibration for a given molecule can be determined from Equations 4.6 and 4.7:

$$\textbf{Number of normal modes} = 3N - 6 \text{ (nonlinear)} \quad (4.6)$$

$$= 3N - 5 \text{ (linear)} \quad (4.7)$$

where N is the number of component atoms in the molecule. In practice, apart from the simplest of compounds, most molecules have nonlinear structures, except where a specific functional group or groups generate a predominant linear arrangement to the component atoms.

b. Raman spectroscopy

Raman spectroscopy has become an important analytical and research tool in

materials science. It can be used for applications as wide ranging as pharmaceuticals, glass and ceramics, thin films, semiconductors, and even for the analysis of carbon nano-materials[168-170].

The Raman scattering technique is a vibrational molecular spectroscopy which derives from a light scattering process. With Raman spectroscopy, a laser photon is scattered by a sample molecule and loses (or gains) energy during the process. The amount of energy lost is seen as a change in energy (wavelength) of the irradiating photon. This energy loss is characteristic for a particular bond in the molecule. Raman can best be thought of as producing a precise spectral fingerprint, unique to a molecule or indeed and individual molecular structure. Raman spectroscopy can yield extremely rich information such as chemical identification, characterization of molecular structures, effects of bonding, and finally environment and stress on a sample[171]. Raman measurements were recorded with a Raman spectrometer model LabRAM-HR 800 (JOBIN YVON HORIBA) using a 514 nm green Argon laser set for 50 mW output combined with an Olympus BX 41 microscope. A 40X microscope objective was used to obtain the Raman spectra of the LS_2 glass, partially crystallized LS_2 glass and the LS_2 glass-ceramics crystallized by microwave heating or by conventional heating.

Raman spectra are used to study the structural change and the neighboring environment around SiO_4 tetrahedra (referred to as Q) in the LS_2 glass as well as LS_2 glass-ceramic samples that has been crystallized by conventional and by VFM heat treatment. In Q^{a}, the superscript (a) in Q denotes the type of central Q species. That unique information from Raman and FTIR spectra are necessary to understand the crystallization mechanism of lithium disilicate in the VFM process. Raman spectra will

provide a full picture about the structure of LS_2 glass and glass-ceramics in conjunction with the information from the FTIRRS spectra.

4.5.5. Dielectric constant measurement

The cavity perturbation technique was used to measure the complex dielectric constant of LS_2 glass, nucleated glass and glass-ceramic between room temperature and 600°C at 2.46 GHz in air. This measurement technique is based on knowing the difference in the cavity response between an empty sample holder and a sample holder with sample at each temperature. Samples were prepared by diamond core-drilling then cut by diamond saw. Handling and inserting the samples into the sample holder was always done with tweezers, so as not to contaminate the samples with finger oil. The initial dimensions and the initial mass of each sample were determined immediately before each run. Each run consisted of increasing the sample temperature up in steps of ~50°C, and holding after each step for ~ 6 minutes to allow the temperature in the sample to stabilize and become uniform. After reaching 600°C, the sample temperature was reduced in 100°C steps to 100°C. The measurements were performed at Chalk River Nuclear Labs of Atomic Energy of Canada Limited (AECL labs) by Dr. Ron Hutcheon.

4.5.6 Density measurement

The true density of the glass and glass-ceramic samples was measured by means of a pycnometer (Micromeritics -AccuPye TM 1330 model) using helium gas that produced the structural (true) density using Equation 4.8. The apparent density, ρ_a, (i.e. includes closed pores) of the same samples was measured by the Archimedes method[172], using water as a fluid from the Equation 4.9.

$$\rho_T = \frac{\text{Wt. of the powder}}{\text{Volume of the powder}} \quad (4.8)$$

$$\rho_a = \frac{a}{a - b} \times \rho_e \quad (4.9)$$

Where,

ρ_a: The apparent density of the sample (g/cm^3).

a: The weight of sample in air(g).

b: The weight of sample suspended in distilled water(g).

ρ_e: The density of distilled water at the test temperature (g/cm^3).

The density values quoted in this dissertation are the average of three measurements.

4.5.7. Molecular orbital model for microwave material interaction

a. The coupled oscillator theory

Under the influence of microwave energy, dipole polarization and rotation is effective especially in dielectric materials, as these dipoles are believed to couple well with the microwave frequency range. Most of the molecular vibrations and rotation frequencies in the infrared range are orders of magnitude higher than the microwave frequency[173], so how microwave energy interact with and heat materials is still a matter for investigation. A molecular orbital theory developed by West and Clark[70, 71] assumes that if there are two nearby connected oscillators with a known degenerate primary vibration frequency ((w_1) in the infrared range), the interaction between those oscillators could result in a coupled oscillator state between them. The coupled oscillator state could generate another secondary (or beat) frequency ((w_2) in the microwave range) that has a frequency much lower than the primary oscillators[70, 71]. Coupled oscillators can be formed between two adjacent molecules, between two nearby defect structures on the surface of a material, or at the grain boundaries and interfaces of materials. Figure 4.6

shows a schematic of a coupled oscillator whereas w_1 represents the primary frequency of the mass and w_2 represent the coupled frequency (coupled frequency for energy transfer between the two masses). The solution of the two simultaneous second order Equations will yield two modes (w^+) and (w^-) as follows:

$$(w^+)^2 = (w_1)^2 + (w_2/2)^2 \quad (4.10)$$

$$(w^-)^2 = (w_1)^2 - (w_2/2)^2 \quad (4.11)$$

By approximating using the binomial theorem and assuming $w_1 >> w_2$ then:

$$w^+ = w_1 + w_2 \quad (4.12)$$

$$w^- = w_1 - w_2 \quad (4.13)$$

So the beat (secondary) frequency that may allow direct microwave absorption w_2 can be expressed as:

$$w_2 = (w^+ - w^-)/2 \quad (4.14)$$

b. The microwave operator

The formal expression of the microwave operator, Φ_{MW} , is based on the classical coupled oscillator[174], and can be derived from Schrodinger's Equation,

$$H_{vib}\,\psi = E_{vib}\,\psi \quad (4.15)$$

where H_{vib} is the vibrational Hamiltonian, ψ is the wavefunction and E_{vib}, is the vibrational eigenvalue matrix. The Schrodinger Equation plays the role of Newton's laws and conservation of energy in classical mechanics, i.e. it predicts the future behavior of a dynamic system. It is a wave Equation in terms of the wavefunction which predicts analytically and precisely the probability of events or outcome. The Schrodinger Equation will predict the distribution of results. Each particle is represented by a wavefunction ψ (position and time). The kinetic and potential energies are transformed

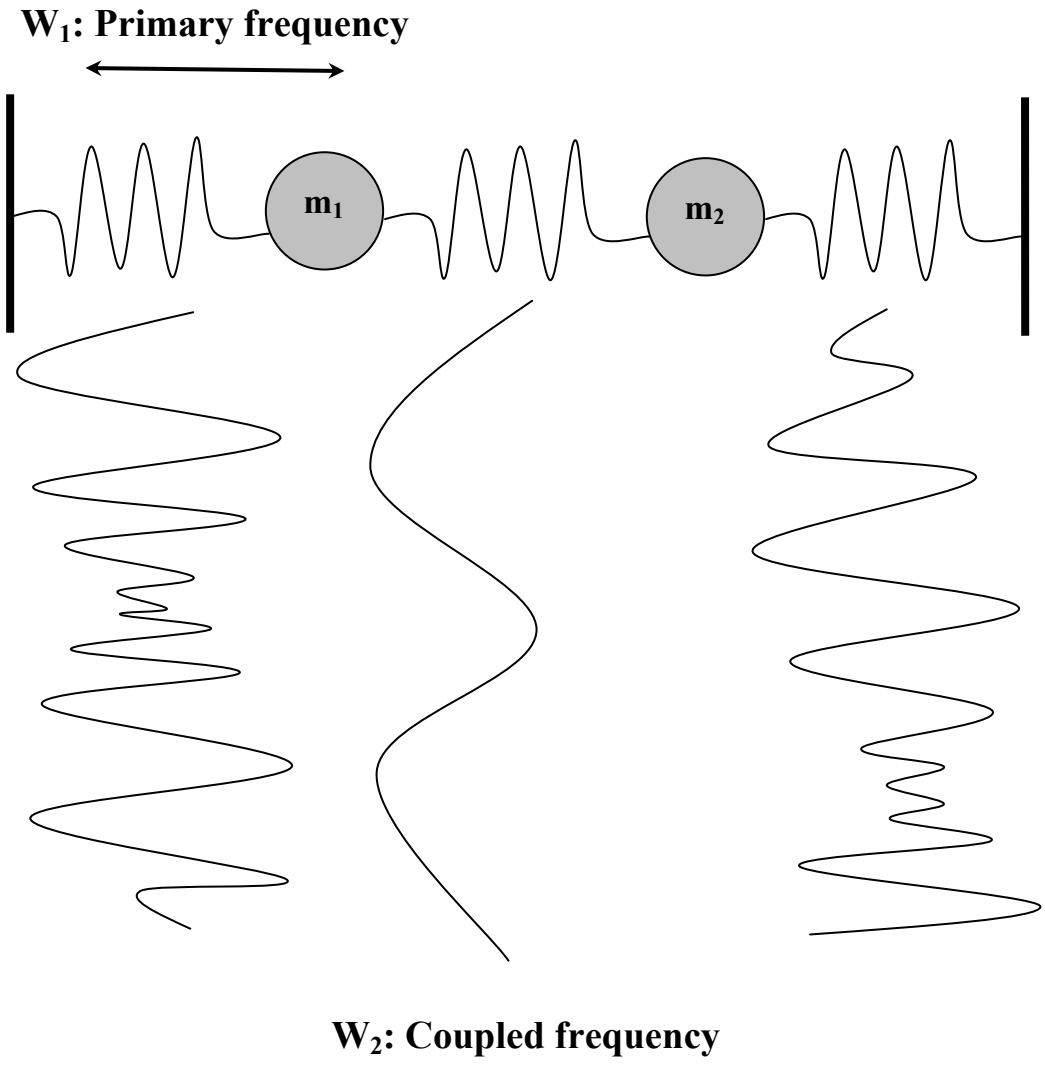

Figure 4.6: Schematic diagram of a classical coupled oscillator. Adapted from[70].
Reprinted with permission of John Wiley & Sons, Inc [copyright 2000]

into the Hamiltonian which acts upon the wavefunction to generate the evolution of the wavefunction in time and space. The Schrodinger Equation gives the quantized energies of the system and gives the form of the wavefunction so that other properties may be calculated. It is proposed by the model that

$$\Phi_{MW} H_{vib} \psi = \Phi_{MW} E_{vib} \psi \quad (4.16)$$

then

$$= E_{MW} \psi \quad (4.17)$$

where E_{MW} is the eigenvalue matrix for microwave absorption by a material. E_{MW} has the form:

$$E_{(j)MW} = \Sigma [E_{(j+1)vib} - E_{(j)vib}] \quad (4.18)$$

and the oscillator strengths, $X_{(j)}$, are estimated using:

$$X_{(j)MW} = X_{(j)vib} \quad (4.19)$$

for identical oscillators of equal masses being weakly coupled through the bulk of a material or via hydrogen bonding like interactions.

Based on the above model, the theoretical IR spectra of the LS_2 glass and the LS_2 glass-ceramic crystals (orthorhombic Ccc2) were calculated using computer-aided chemistry (CAChe) software. Those theoretical IR spectra have been compared with the actual measured experimental IR patterns. As explained in detail later, the theoretical IR patterns (calculated by CAChe) have been used to predict the microwave absorption spectra of the LS_2 glass and the glass-ceramic material by the proposed model.

c. Introduction to computer-aided chemistry (CAChe).

CAChe for Windows is a computer-aided molecular design (CAMD) modeling tool for the Microsoft® Windows® operating systems. CAChe has the capability to draw and model molecules and perform calculations on a molecule to discover molecular

properties and energy values. CAChe for Windows uses computational chemistry as an essential part of computer-aided chemistry. By applying computational molecular models derived from mathematical Equations to a chemical sample, calculation of molecular properties could be done. The computational chemistry tools that CAChe uses are derived from classical mechanics and quantum mechanics, and are applied to the chemical compound by a number of computational applications

Classical mechanics and CAChe.

Using Equations from classical Newtonian physics, classical mechanics models a molecule as if its atoms and bonds are interacting balls and springs. Empirically derived force fields describe bond stretching, bond angle bending, and non-bonded interactions such as van der Waals and hydrogen bond interactions. The sum of all these interactions is the amount of strain in the molecule—the potential energy of the molecule. CAChe applies classical molecular mechanics to a chemical sample by using the computational application mechanics. Mechanics optimizes the molecule by applying classical mechanical theories and systematically moving all the atoms in the molecule, until the net force acting on each atom is minimized.

Quantum mechanics and CAChe.

CAChe quantum mechanical methods can also optimize molecular geometries, and in addition can determine electronic properties of molecules. Semiempirical quantum mechanical methods use experimental data to simplify Schrödinger's Equation so it can be solved more quickly. Many methods for this simplification have been developed, such as PM3. CAChe for Windows applies PM3 and other methods (AM1 and PM5) are part of MOPAC (Molecular Orbital PACkage). Each semiempirical method can use one or

more parameter sets based on experimental measurements for numerous compounds. The desired type of molecule and the type of data determines which method and parameter sets to use. Comparing CAChe for Windows results with experimental laboratory data is a good way to determine which settings give the best data.

IR spectra

CAChe calculates the vibrational spectra of a given molecule by exposing the molecule to electromagnetic radiation in the infrared (IR) region (i.e. heat the molecule at different temperatures) and then measures the motions of the atoms in that molecule in the three (3) directions (X, Y and Z) around its equilibrium positions in order to predict the IR spectra. Absorption bands observed in the infrared are associated with the bending and stretching of particular types of bonds, so viewing these infrared transitions aids the analysis of molecular structure. CAChe uses quantum mechanics to compute the force necessary to distort the molecule from its equilibrium geometry and predict the frequency of vibrational transitions.

Computational applications

CAChe for Windows uses a number of computational applications which use classical and quantum mechanical methods to perform experiments on the chemical sample. This section gives an overview of each computational application.

Mechanics optimizes molecular geometry using classical molecular mechanics. Mechanics finds an optimum geometry by systematically moving all atoms in a chemical sample until the net force acting on each atom approaches zero. Mechanics generates a log data file and an output file containing experimental details, and alters the structure of the molecule in the chemical sample file to correspond to the calculated optimum

geometry.

MOPAC is a semiempirical quantum mechanical computational tool that provides optimization and wavefunction (electron distribution) data to search for optimized geometry, transition state geometry and molecular properties. MOPAC includes two sets of parameters: PM3 and AM1. MOPAC generates a log data file and an output file containing experimental details, and alters the structure of the molecule in the chemical sample file to correspond to the calculated optimum geometry.

5. Results and Discussions

5.1. Thermal analysis

The crystallization of glass is controlled by two factors: the nucleation rate (i.e. the number of nuclei formed per unit volume per unit time), and the rate of crystal growth, (i.e. the shift rate of the crystalline phase boundary in the liquid). The higher the cooling rate of the molten glass across the temperatures ranges of maximum nucleation and crystal growth rates, the greater the possibility of glass formation. Nucleation and crystallization can take place in a controlled manner throughout the bulk of the sample with a particular microstructure by holding the temperature of glass sample in the maximum nucleation and crystallization temperature ranges for sufficient time[175].

Thermal analysis is a powerful tool used in detecting and analyzing the thermal effects produced during the crystallization of glass. Figure 5.1 shows the differential scanning calorimetry (DSC) of the annealed bulk LS_2 glass. The data showed a glass transition temperature (T_g) detected at 475°C with a delta C_p value (heat capacity at constant pressure) of 0.48 J/g. T_g can be defined as an approximate temperature where the super-cooled liquid coverts to a solid on cooling or, where the solid begins to behave as viscoelastic solid on heating[155]. Since the glass transition temperature is a function of both the heating rate and the experimental method used for that measurement (thermal analysis or thermal expansion measurement)[155], it can not be considered as a true defined property of the glass. An endothermic peak that is characteristic of the nucleation process (heat absorbed in the nucleation reaction) in the LS_2 glass was detected at 488°C with an enthalpy of (+15.4) J/g. Also, the crystallization exothermic temperature was detected at 683^{o}C with an enthalpy of (-379) J/g that represents the heat released due to

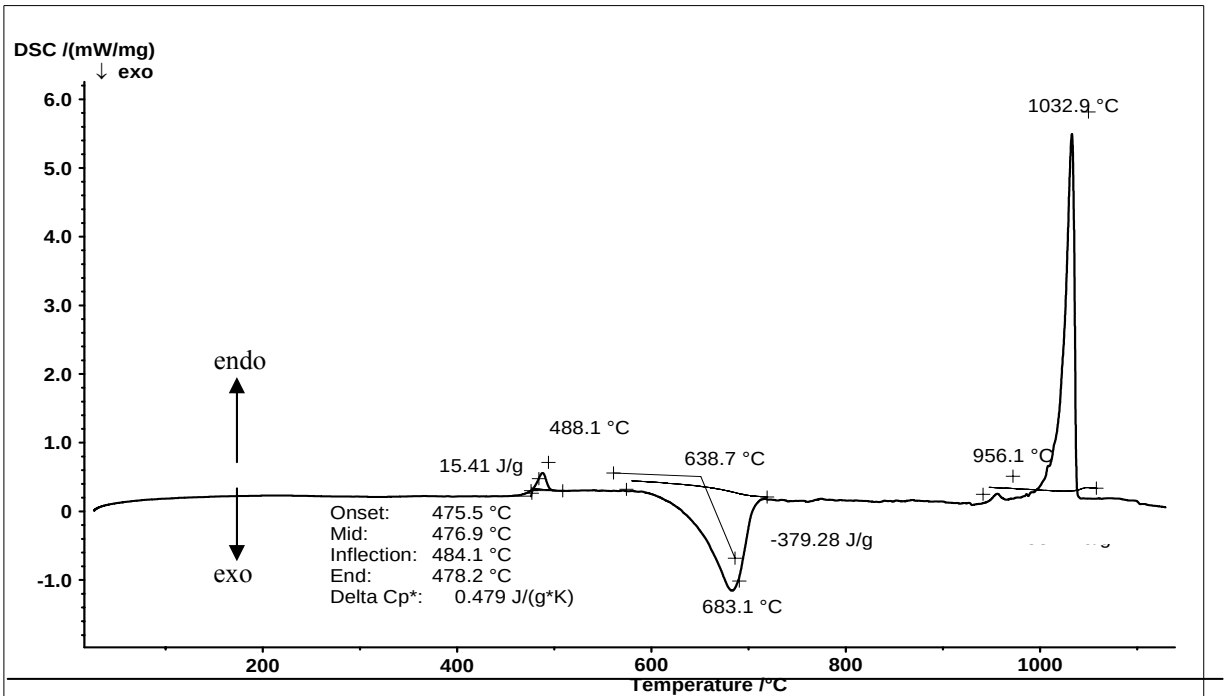

Figure 5.1: DSC curve for annealed bulk LS_2 glass.

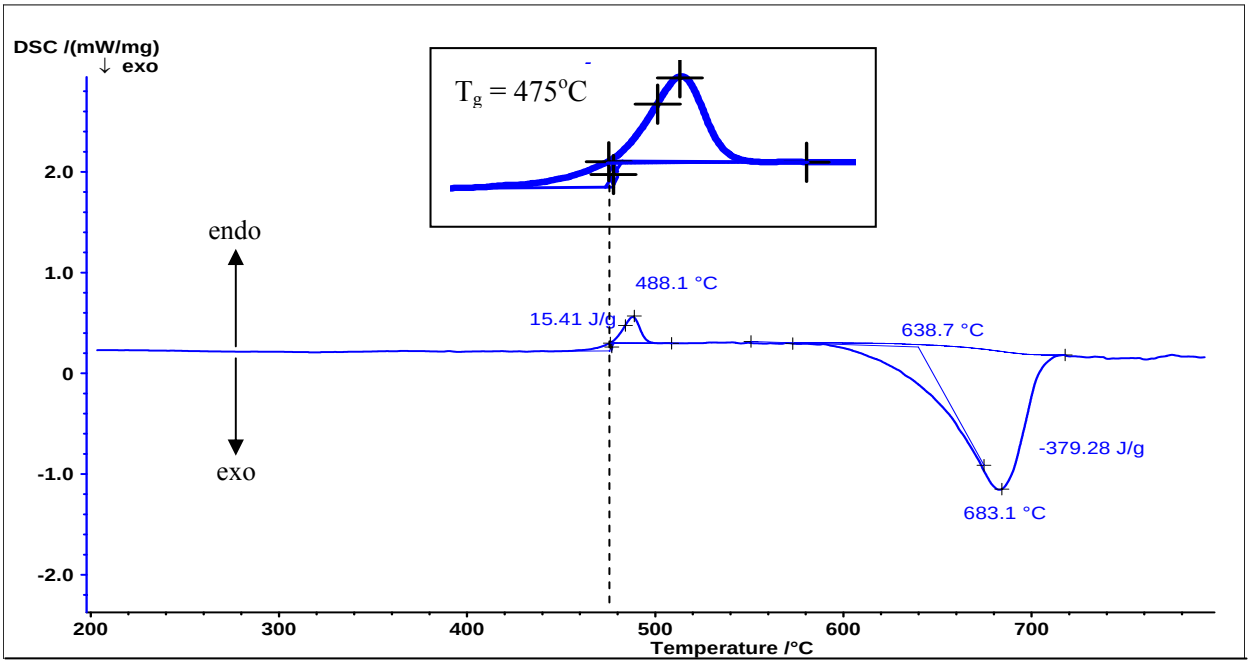

Figure 5.2: Enlarged DSC curve for annealed bulk LS_2 glass.

the crystallization reaction. The same value of crystallization temperature has also been reported by Soares, et al[16] for the bulk stoichiometric composition of LS_2 bulk glass samples. Two endothermic DSC peaks were detected at 956°C and 1033°C. These two endothermic peaks are characteristics for the polymorphous transformation (i.e. different crystal structure with the same chemical composition) of the stoichiometric LS_2 crystal phase at 956°C and for the congruent melting at 1033°C of the same crystalline phase[17]. The polymorphous transformation of LS_2 crystal phase occurs from the low temperature orthorhombic phase to the high temperature orthorhombic phase[152]. Both phases have different unit cell parameters. Figure 5.2 shows an enlarged area of the nucleation and crystallization temperature regions of the same bulk annealed glass sample.

Figures 5.3 and 5.4 show the DSC data for the same stoichiometric LS_2 glass sample but in the powder form as a frit (325 mesh). It is obvious that the crystallization peak was shifted to a lower temperature (614°C) while the nucleation temperature, glass transition temperature, polymorphous transformation temperature and the congruent melting temperature were almost the same as the bulk sample. Because the LS_2 glass frit has a much higher surface area than the bulk, the surface crystallization for the powder is higher and dominates in the frit more so than in the bulk sample. It was reported that the crystallization temperature peak of LS_2 glass is also a function of the particle size of the analyzed powder[18, 176].

Table 5.1 summarizes the following temperatures: glass transition, nucleation, crystallization, polymorphous transformation and melting of LS_2 bulk glass and the glass frit. Figure 5.3 also shows the thermogravimetric analysis (TGA) data for the frit sample.

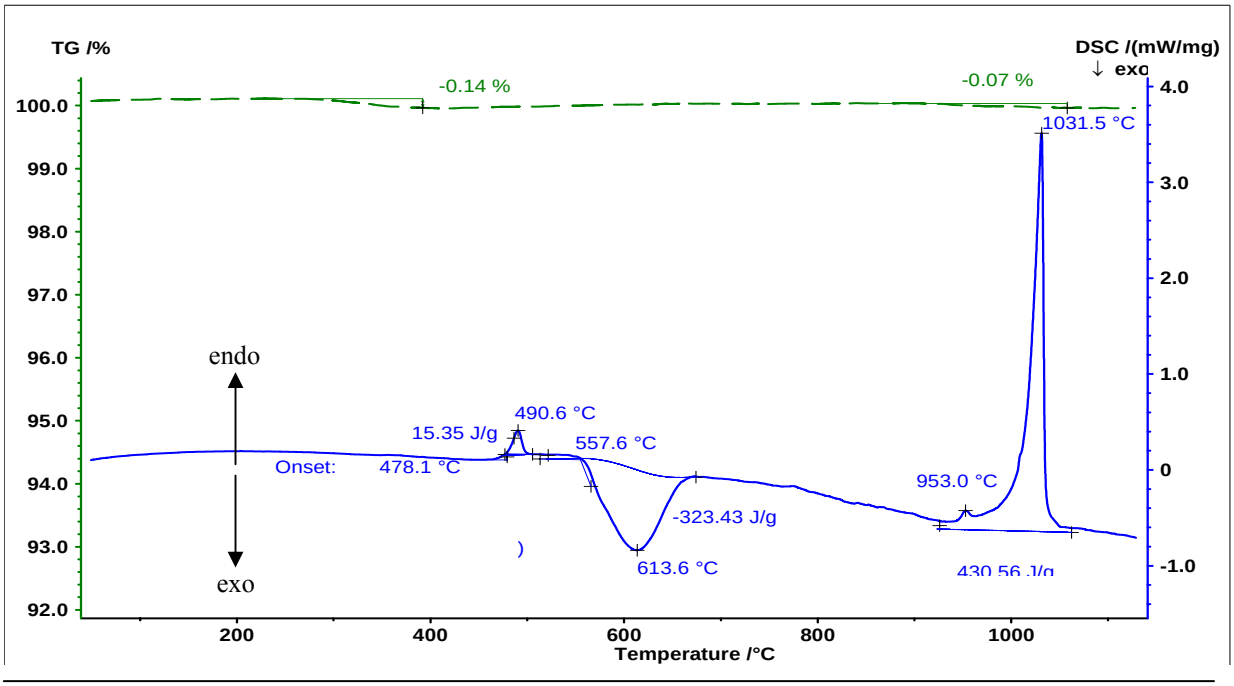

Figure 5.3: DSC curve for annealed powder LS_2 glass frit.

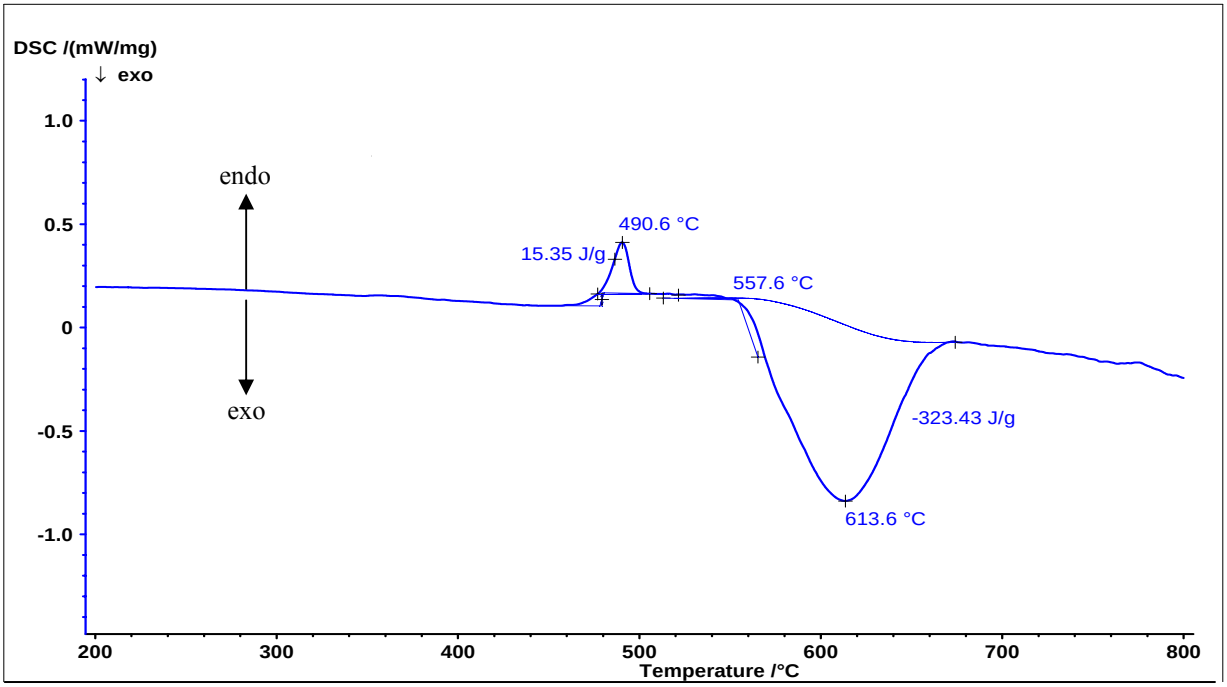

Figure 5.4: Enlarged DSC curve for annealed powder LS_2 glass frit.

Table 5.1: Nucleation and crystallization temperatures of the investigated bulk and powder LS_2 glass as deduced from the DSC curves.

Temperature (C o)	Bulk glass	Powder glass frit
Glass transition temperature (T_g)	475	478
Nucleation temperature (T_n)	488	491
Crystallization temperature (T_c)	683	614
Polymorphous transformation temperature	956	953
Congruent melting temperature	1033	1032

Two small mass loss steps with 0.14 and 0.07 wt% were observed—probably due to the loss of water and carbonate, which is an indication of the thermal stability of LS_2 glass composition. In the present study, the DSC data was used to design the nucleation process as well as the crystallization process of LS_2 glass. Bulk LS_2 glass was nucleated at the maximum nucleation temperature (T_n= 485^{o}C, 2 hours) to ensure a sufficient number of nucleation sites. The nucleated samples were then crystallized either by conventional heating at different temperatures (567^{o}C, 583^{o}C, 595^{o}C and 680^{o}C) or by VFM heating using the thermal analysis information of LS_2 glass.

5.2. FTIRRS data

Infrared spectroscopy, in general, is a very useful characterization technique that has been used successfully and routinely to study the structure of glass[162, 177-184]. In Fourier transform infrared reflection spectroscopy (FTIRRS), also known as specular reflectance, light is reflected from a smooth, mirror-like sample to record its spectrum. It is a non-destructive, non-contact technique.

Infrared reflection spectra, in particular, may look different from the transmission spectra in many ways. The variation in the sample thickness is not a factor as in transmittance or absorbance technique. In addition, bands may be shifted to higher wavenumbers, and the spectra may follow the dispersion in the refractive index. Furthermore, infrared reflection spectroscopy offers ease of sample preparation[166].

Because penetration depth (D_p) of the infrared radiation depends on the angle of incidence, the penetration depths at 45^o (the angle of incidence and reflection of FTIR beam) have been calculated in this study for LS_2 glass and glass-ceramic samples. The actual infrared penetration depth of LS_2 glass was calculated as 0.53μm - 5.3μm in the

range from 4000 cm^{-1}- 400cm^{-1} wavenumbers (corresponding to wavelengths of. 2.5μm - 25μm), using the total internal reflection Equation 5.1[185]. The penetration depth for the LS_2 glass-ceramic was calculated as 0.56 μm – 5.6 μm in the same range using the same Equation.

$$D_P = \frac{\lambda_1}{2\pi} \left(\mathrm{Sin}^2\theta - (n_{21})^2\right)^{-1/2} \qquad \textbf{(5.1)}$$

where λ_1 is the wavelength of the infrared radiation over the refractive index of the sample (λ/n_{sample}), n_{21} is the ratio between the refractive index of the sample and the crystal used in the equipment ($n_{sample}/n_{crystal}$), and Θ is the angle of incidence. Zinc selenium (ZnSe) crystal with a refractive index of 2.4 was used in this calculation. The refractive index of LS_2 glass and glass-ceramic were 1.5197 and 1.5410 respectively at 1550 nm(6452 cm^{-1})[186].

In the present study, all the IR spectra of LS_2 glass and glass-ceramics samples are displayed in the range from 1400 cm^{-1}-400 cm^{-1} wavenumbers due to the special interest in the vibration modes in this range. At 1400 cm^{-1} wavenumber, the penetration depths of LS_2 glass and glass-ceramics samples were calculated as 1.7 um and 1.8 um respectively using the total internal reflection Equation 5.1.

The FTIRRS spectra of the annealed LS_2 glass and the nucleated glass samples (T_n = 485^oC, 2 hours) are shown in Figure 5.5. The assignment of the IR bands is given in Table 5.2. As can be seen from both Figures that the IR spectra and the peak intensity (% Reflectance) of both samples are almost identical which means that the change in the structure of the LS_2 glass after nucleation can not be detected by the FTIRRS technique.

The strong band at 1085 cm^{-1} in the spectra of silicates glass is known to be caused by the highest frequency component of the asymmetric stretching mode of the

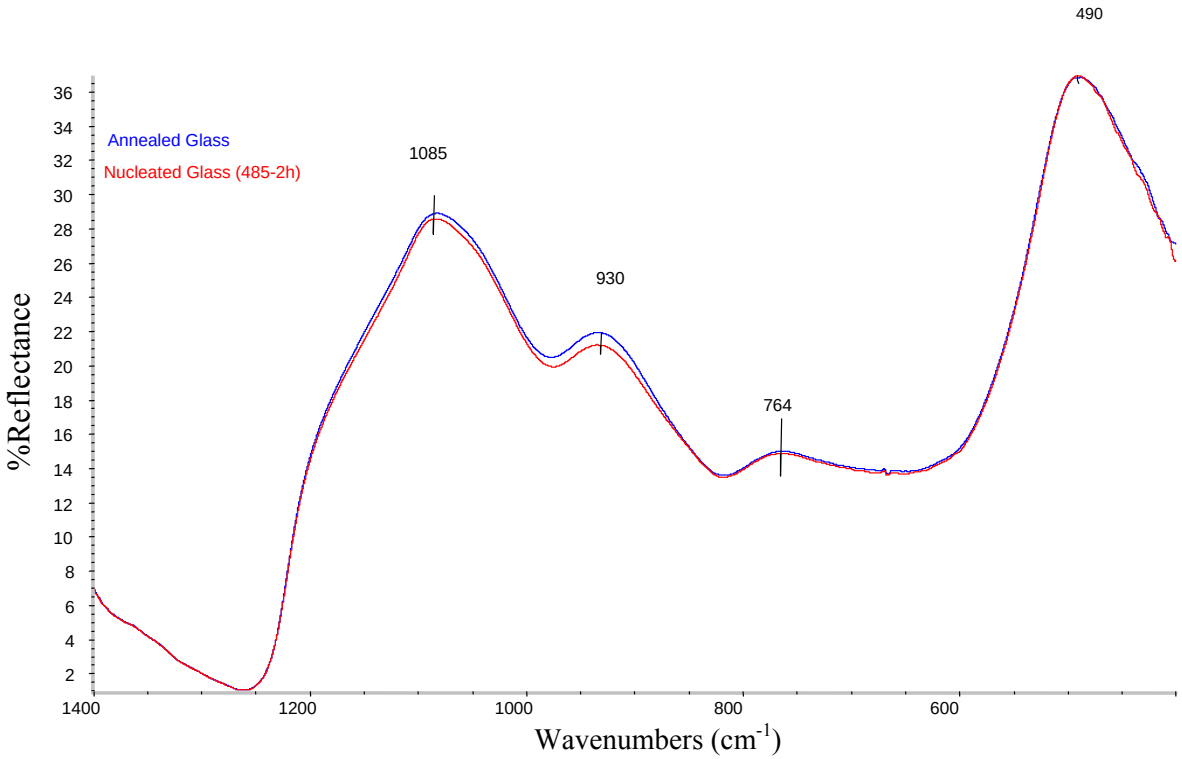

Figure 5.5: Infrared reflection spectra of LS_2 annealed glass and LS_2 nucleated glass at 485^{o}C for 2hours.

Table 5.2: FTIRRS peak assignment of LS_2 glass and nucleated glass.

Peak Number	Peak Position (cm^{-1})	Peak assignment[183]
1	1085	(Si-O-Si) asymmetric stretching
2	930	($Si-O^{-}$) NB stretching
3	764	(Si-O-Si) symmetric stretching
4	490	(O-Si-O) Bending mode

Si-O-Si[184, 187, 188]. The band at 930 cm^{-1} is known to be caused by the non-bridging oxygen stretching mode of the $Si\text{-}O^{-}$[29, 189]. The band at 764 cm^{-1} is due to the symmetric stretching of Si-O-Si bond, while the band at 490 cm^{-1} can be assigned to the bending vibration of the O-Si-O bond[183].

Figure 5.6 shows the IR spectra of glass-ceramics crystallized conventionally at 680°C for 100 hours (control crystal) and by VFM processing at ~ 600°C for 2 minutes. Both samples have almost identical spectra (the same peaks positions and intensities); the spectra has been identified as lithium disilicate crystal phase (Orthorhombic Ccc2) when compared to the literature[161]. The assignment of the IR bands is given in Table 5.3. Based on Figure 5.6, it is concluded that in significantly shorter time and lower temperature, the VFM crystallized sample has been fully crystallized and has developed the same crystal phase as the LS_2 control crystal sample. That significant reduction in time and temperature in the VFM crystallized sample is believed to be related to the non-thermal effects of microwave energy (microwave effect). In the VFM process, this fast crystallization behavior of LS_2 glass was repeatable. Around 20 samples were crystallized similarly by VFM processing. These VFM crystallized samples were characterized and used in the present study to support the concept of a microwave effect.

In order to provide an experimental evidence for the microwave effect in LS_2 glass, two (2) nucleated LS_2 glass samples (485^{o}C, 2 hours) were heat-treated conventionally at the maximum crystallization temperature (680^{o}C) for 2 minutes and 6 minutes, respectively. The spectra for these samples are provided in Figures 5.7 as compared to the control crystal sample. These samples are pictured in Figure 5.8 and compared to both the VFM crystallized sample and the control crystal sample. It is

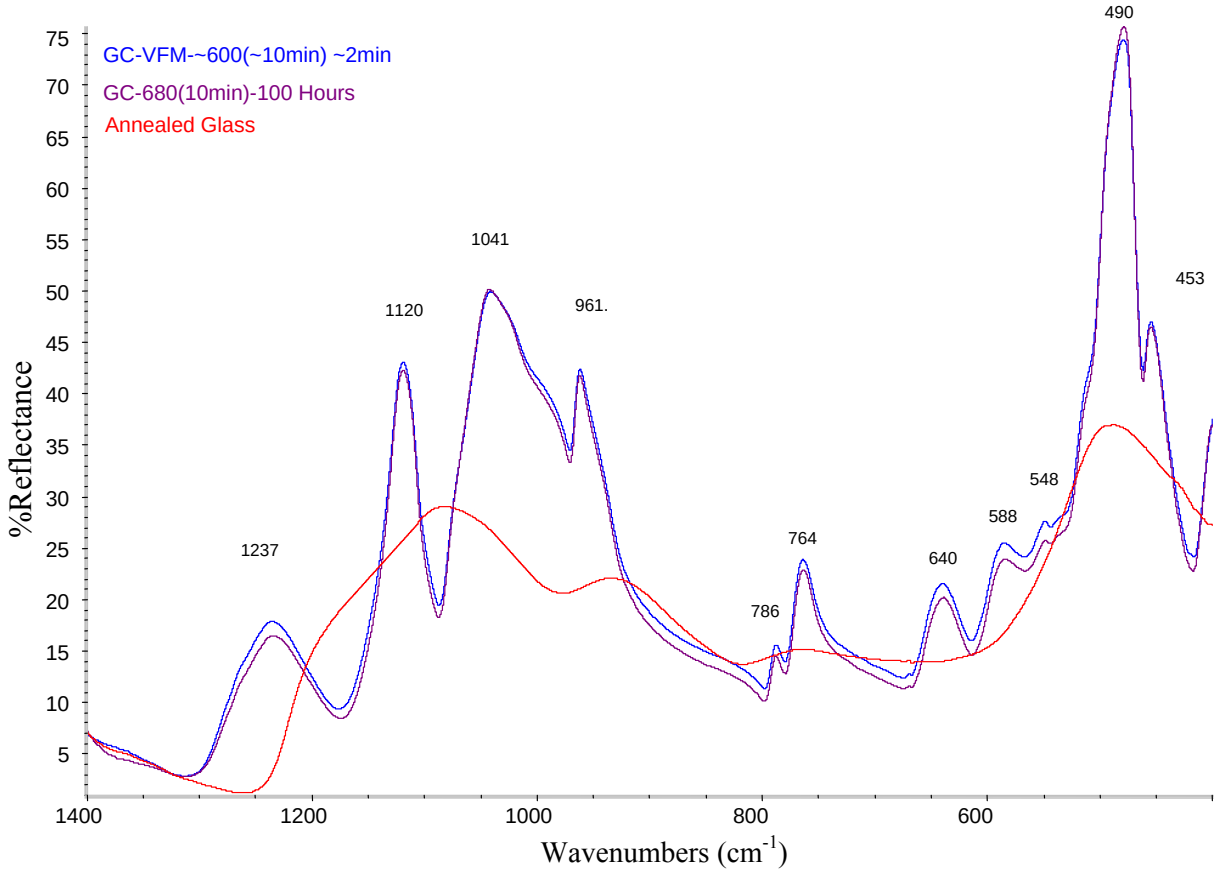

Figure 5.6: IR spectra of LS_2 glass-ceramics crystallized by VFM (~ 600°C-2min.) and conventionally (680°C-100 h). The base glass spectrum is shown for comparison.

Table 5.3: IR bands for LS_2 glass-ceramics.

IR bands (cm^{-1})	Assignment of the IR bands
1237	(Si-O-Si) asymmetric stretching
1120	(Si-O-Si) asymmetric stretching
1041	(Si-O-Si) asymmetric stretching
961	(Si-O-Si) asymmetric stretching
786	(Si-O-Si) sym. stretching
764	(Si-O-Si) sym. stretching
640	(Si-O-Si) sym. stretching
588	(Si-O-Si) sym. stretching
548	(O-Si-O) Bending mode
490	(O-Si-O) Bending mode
453	(O-Si-O) Bending mode

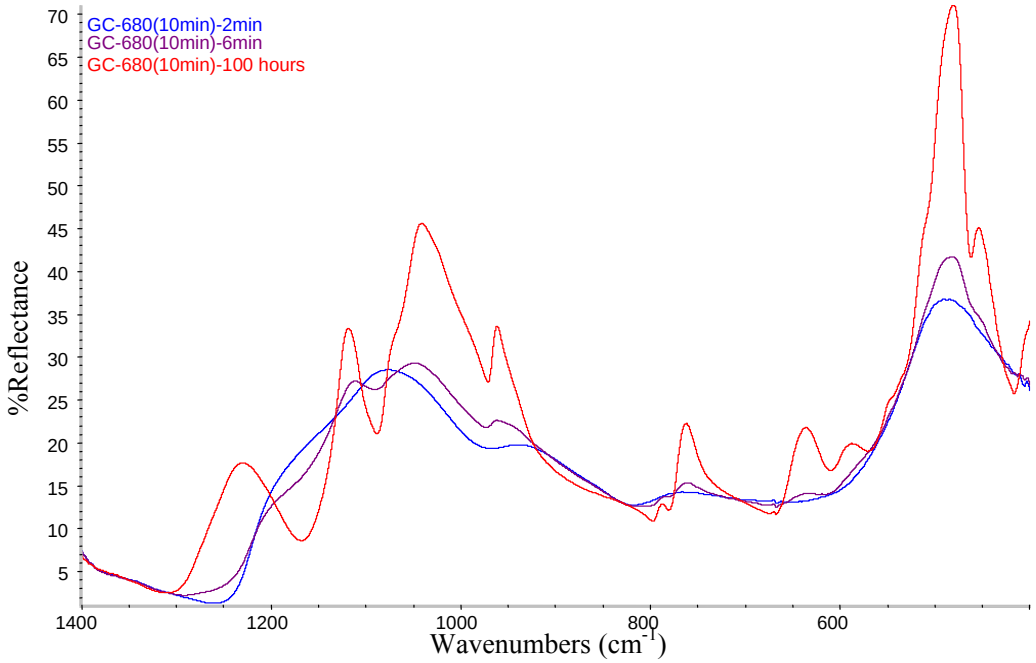

Figure 5.7: IR spectra of two LS_2 glass heat-treated conventionally at 680°C for 2 min. and 6 min. respectively. The base control crystal spectrum (680°C-100 hours) is shown for comparison.

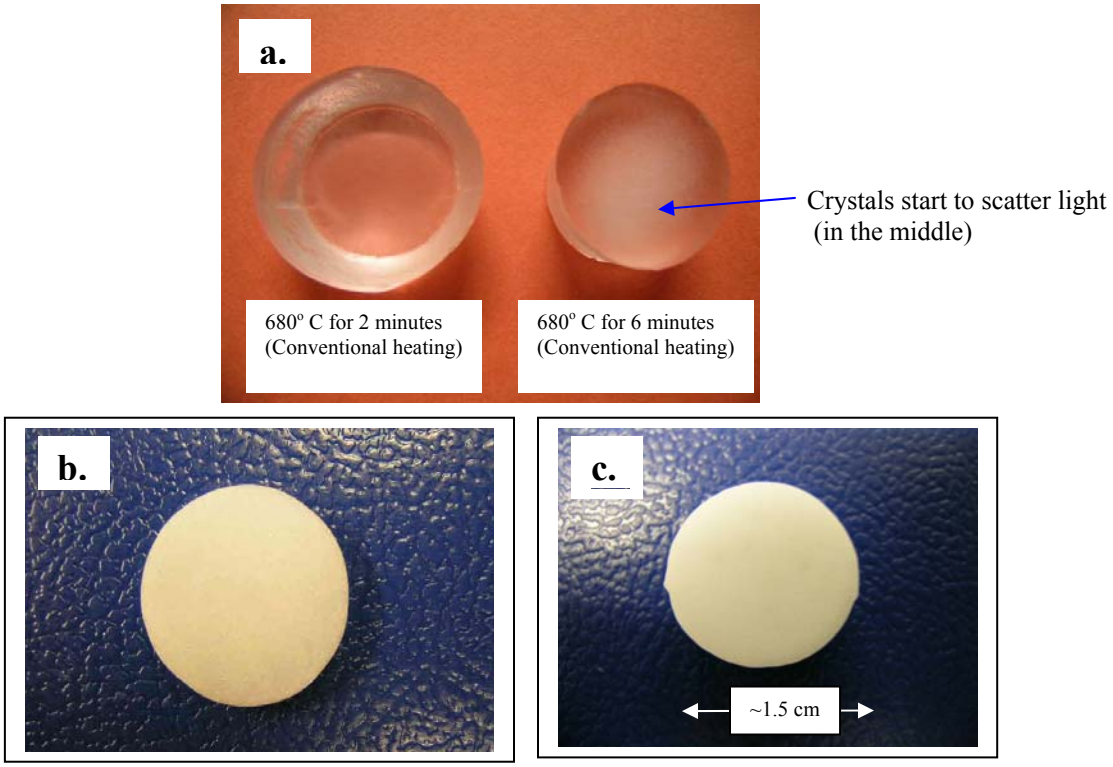

Figure 5.8: LS_2 glass-ceramic sample heat-treated:
a).Conventionally at 680°C- for 2 minutes and 6 minutes respectively.
b.) Conventionally at 680°C-for 100 Hours (control crystal).
c.) VFM heating (~600°C-2 minutes).

apparent from the FTIR spectra and the pictures as well that neither of the conventionally crystallized samples (680^{o}C, 2 and 6 minutes) were crystallized completely. That experimental observation implies that the crystallization kinetics in LS_2 glass under the influence of the VFM field is different and faster than the one experienced in conventional heat treatment. This observation is believed to be a result of the microwave effect. Because kinetics are controlled by thermally activated processes, one can argue that the microwave effect claim is not true because the temperature in the VFM process was perhaps higher than the one applied in the conventional process or was inaccurately measured.

Although temperature measurement in the VFM process was not an easy task as discussed earlier and is a well known problem in the microwave processing community [32, 35], the microwave effect in the crystallization process of LS_2 glass using VFM processing does appear to exist regardless of the temperature issue. As discussed earlier, the kinetic theory of glass formation with a special emphasis on the crystal growth rate curve (Figure 2.5), the crystal growth rate is controlled by Equation 2.8 as follows:

$$\mathbf{U= (f\,kT/\,(3(a_o)^2\,\pi\,\eta))\,[1-\exp\,(-\Delta G/RT)]} \qquad \mathbf{(2.8)}$$

Based on the previous discussion, the crystal growth rate curve is a skewed bell-shape, reaching a maximum at the maximum crystallization temperature (T_c) and reaching zero at both the high and low temperature ends. The maximum crystallization temperature (T_c) in LS_2 bulk glass was observed at 680^{o}C, so at any point higher or lower than this value, the crystal growth rate should decrease, as shown in Figure 2.5. So, if the temperature in the VFM process was much higher than it was in the conventional heating process (T_c) (as the higher temperature argument claims), the crystallization rate in the

VFM process should be lower than what was observed, and an FTIRRS spectrum with less crystallization characteristics should be observed. On the other hand, if the temperature in the VFM process was lower than the one experienced in the conventional heating process (T_c), the crystal growth rate in the VFM should also be lower than the one in T_c, and the FTIR spectra and the pictures should detect that as well. Thus, the high and the low temperature assumptions could not be the reason for the observed full crystallization of LS_2 glass and the observed reduction in the crystallization time (~2 minutes), using VFM processing. Finally if the temperature in the VFM process was near or at T_c, both samples (the VFM crystallized and the conventional treated samples at 680^{o}C for 2 minutes or even 6 minutes) should look the same and should have the same FTIR spectra, which is not the case. So the crystallization of LS_2 glass using VFM processing in less time can not be explained by the well known kinetic theory and the crystal growth rate curve. It is believed that the kinetics in the VFM process is much faster and different than that observed in the conventional heating. This difference strongly supports the presence of the microwave effect in the VFM process.

As shown in Figure 5.8, the middle of the conventionally crystallized sample at 680^{o}C for 6 minutes scatters the light more than the sample edges. The optical micrographs have confirmed this observation as will be shown later in the stereology measurement and optical microscopy data section in Figures 5.65, 5.66 and 5.67. These optical micrographs show more crystal population and larger crystals in the middle as compared to the edges of the sample. This phenomenon has also been observed in other conventionally treated samples at 567^{o}C, 583^{o}C, and 595^{o}C as well as in other VFM heat-treated samples. It is believed that the nucleation regime applied in the present study

allows the center of LS_2 glass samples to experience more localized heat than the sample edges, thus resulting in more nucleation sites. The nucleation regime consisted of two hours to reach the desired nucleation temperature of 485^{o}C which was maintained for an additional two hours then followed by a five to six hour cooling time in the furnace. As a result, heat was lost more quickly from the sample surface than from the sample center in the cooling step. Eventually, the nucleation sites in the sample center would be more than those in the sample edges. Because the nuclei size could not be detected by the optical microscopy, the nucleated samples appeared homogenous and uniformly transparent. In the crystallization stage, when nuclei grow into detectable crystals, the crystals start to scatter the light and become measurable by the optical microscopy.

5.3. Raman data

The Raman spectra of the crystallized LS_2 glass and glass-ceramic samples by both VFM heating (~600^{o}C, 2 minutes) and conventional heating (680^{o}C-100 hours) are shown in Figures 5.9, 5.10, and 5.11 respectively. Raman spectra indicate that the VFM crystallized sample and the control crystal sample, which crystallized conventionally, developed the same lithium disilicate crystal phase (Orthorhombic Ccc2)[190]. However, there was a slight difference in the structural units of the SiO_4 tetrahedra (Q species) between the VFM crystallized sample and the control crystal sample. The lithium disilicate crystalline phase consists of these SiO_4 tetrahedral structural units. An illustration of the Q species structure is shown in Figure 5.12. Tables 5.4 and 5.5 show the assignment of the Raman peaks of LS_2 glass and glass-ceramic samples respectively. According to the Raman data, the VFM crystallized sample was fully crystallized as was the control crystal. Thus, the observed reduction in the crystallization time and

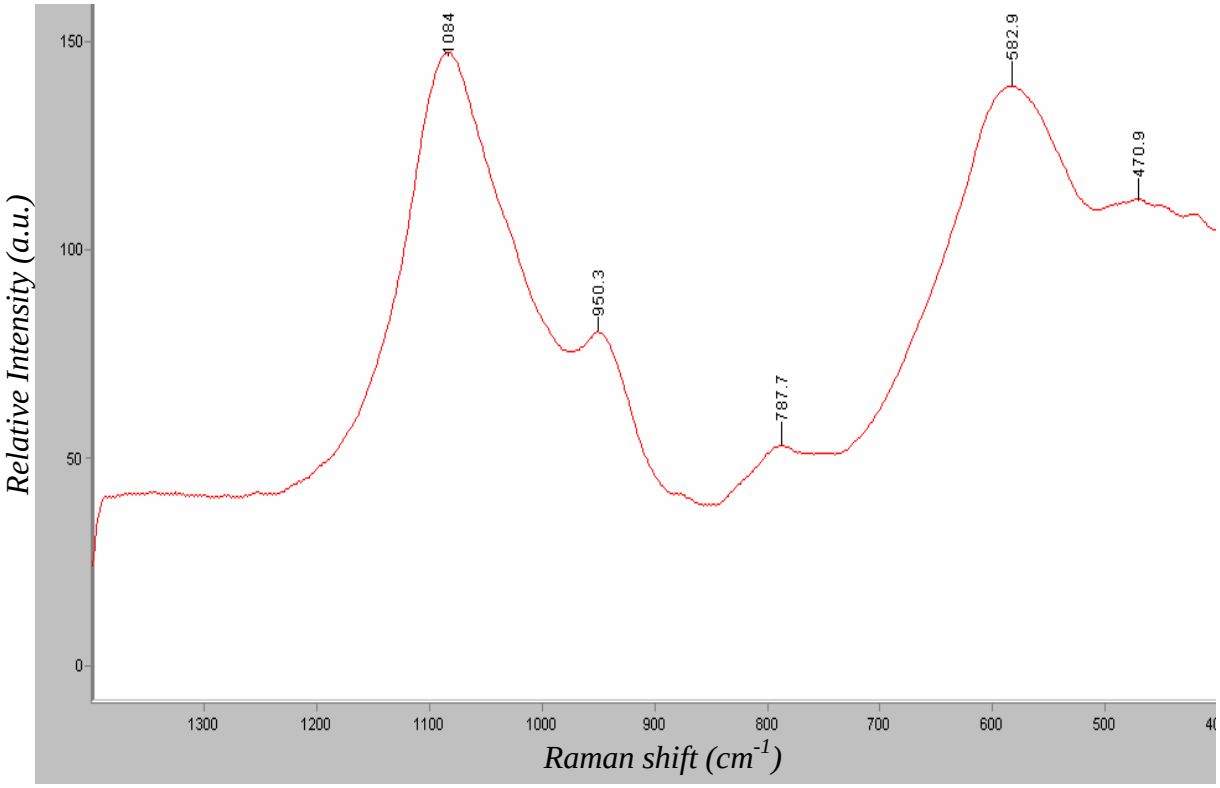

Figure 5.9: Raman spectrum of LS_2 glass.

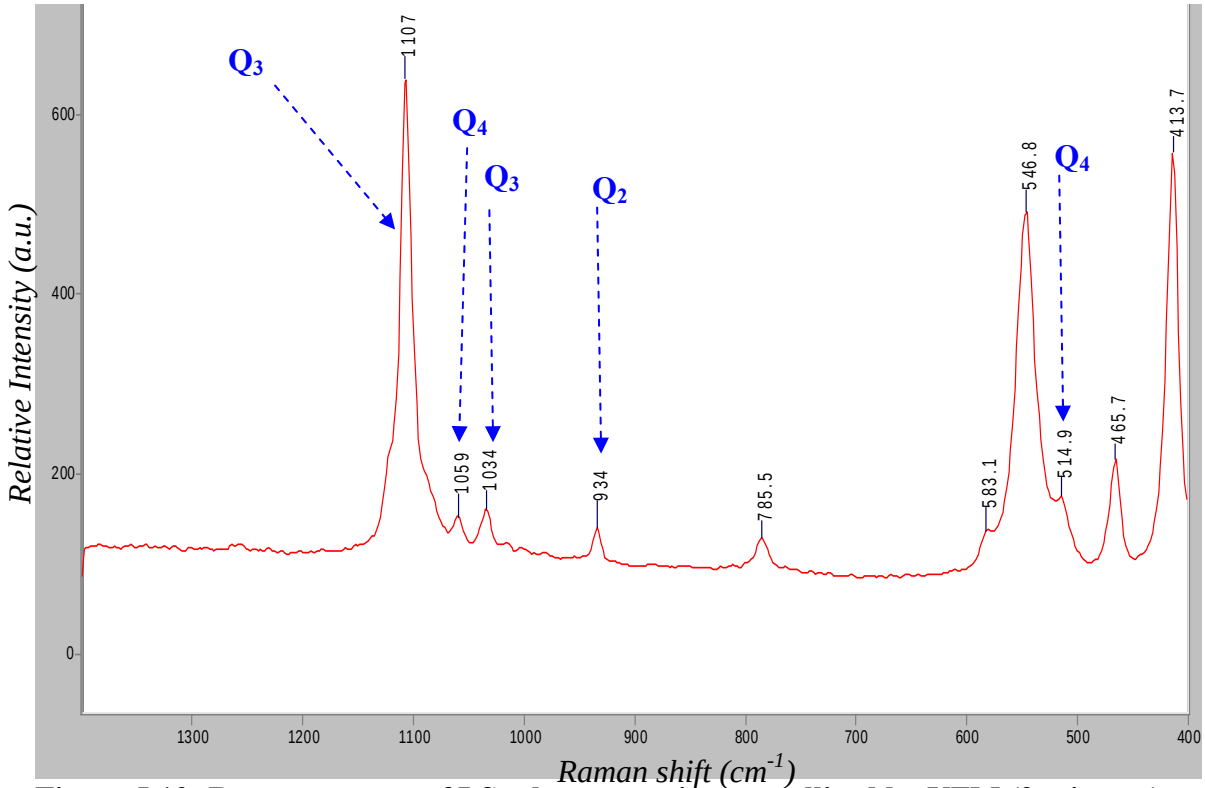

Figure 5.10: Raman spectra of LS_2 glass-ceramics crystallized by VFM (2 minutes)

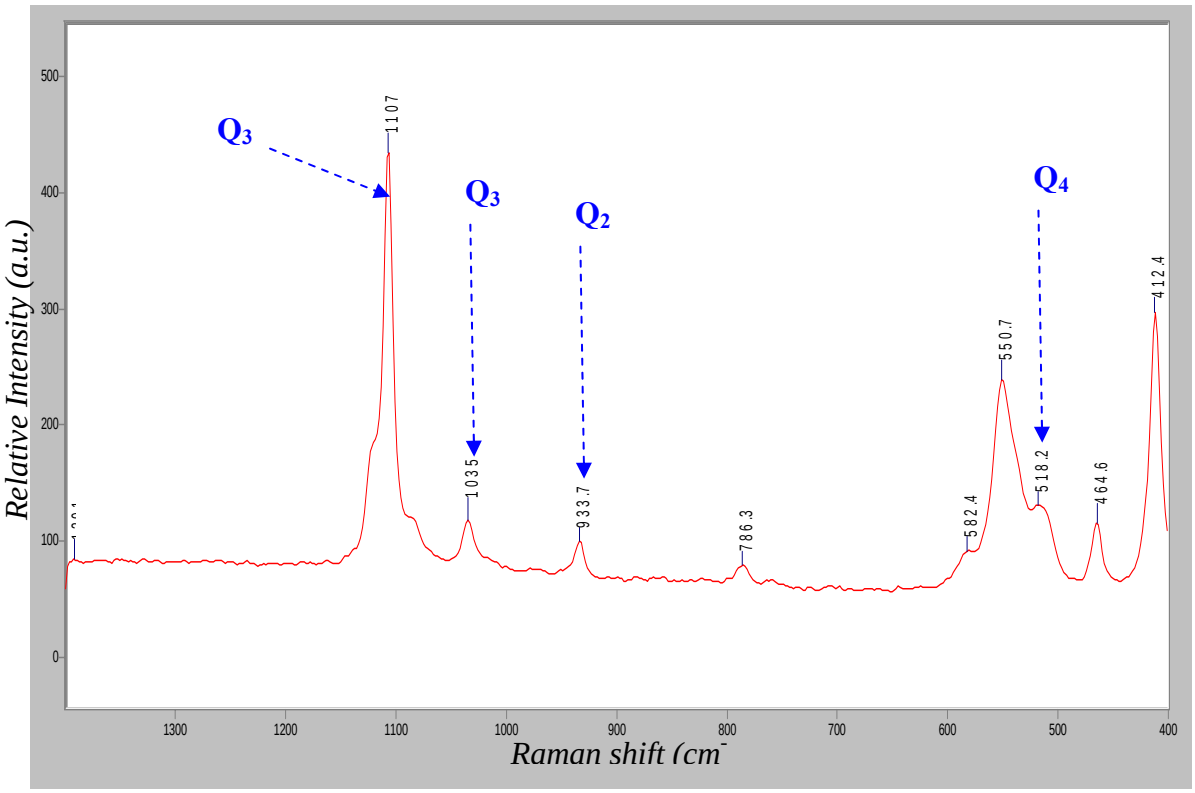

Figure 5.11: Raman spectra of LS_2 glass-ceramics crystallized conventionally (680°C-100 hours)

Table 5.4: Assignment of LS_2 glass Raman peaks

Assignment of Raman Bands	Raman Band (cm^{-1})
Q^4	461
Si-O-Si bending	583
Motion of Si in Td	788
Si-O stretching in Q^2	950
Si-O stretching in Q^3	1084

Table 5.5: Assignment of LS_2 glass–ceramics Raman peaks

Assignment of the Raman Bands Q [a*]	Raman Band (cm-1)
Q^4	515 shoulder
Si-O-Si bending	550
Q^2	934
Q^3	1035
Q^3	1107
Bands are assigned to Si-O stretching vibrations in SiO_4 tetrahedra. In Q [a*] the superscript (a) in Q denotes the type of central Q species	

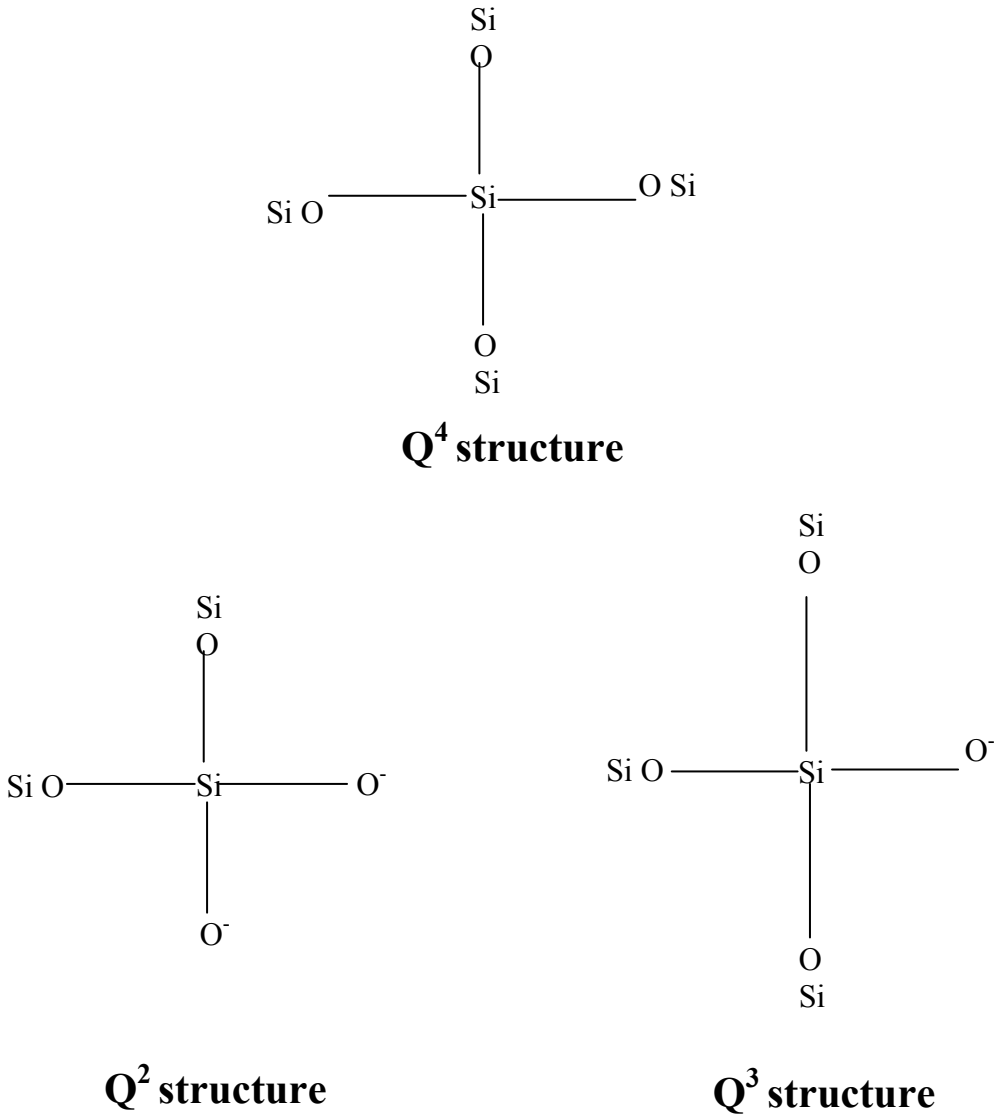

Figure 5.12: Illustration of the Q species in the SiO_4 tetrahedra.

temperature in the VFM crystallized sample, in addition to the observed difference in the Q species of LS_2 crystalline phase in the same sample, indicates the existence of the microwave effect in the VFM process.

The Raman patterns for both glass-ceramic samples were almost identical except the unique new peak at 1060 cm^{-1} that was observed in the VFM crystallized sample. That unique peak in the VFM crystallized LS_2 sample was not observed in the conventional crystallized control crystal sample and is believed to be due to the Q^4 species. A similar Q^4 peak, located at 1059 cm^{-1}, was reported in the sodium disilicate glass system[161, 164, 166, 168, 171, 191, 192]. The Raman spectra of LS_2 glass and glass-ceramics show that the Q^3 units are the major structural units (as detected at 1084 cm^{-1} and 1107 cm^{-1} respectively). It was reported in the literature that the high content of Q^3 units in LS_2 glass and glass-ceramic is due to the uniform distribution of the Li^+ ion as well as the non-bridging oxygen (NBO)[164, 166, 171, 190].

Furthermore, Q^2 and Q^4 units were reported in the literature for LS_2 glass and glass-ceramics[162, 165] and also were observed in the studied LS_2 glass and glass-ceramics as shown in the spectra. The Q^2 species were observed at 950 cm^{-1} and at 934 cm^{-1} for LS_2 glass and glass-ceramics samples respectively, while the Q^4 species were observed at 461 cm^{-1} and 515 cm^{-1} for LS_2 glass and glass- ceramics respectively. The partial decomposition of Q^3 units into Q^4 and Q^2 units is believed to occur in LS_2 glass and glass-ceramics as shown in the following reaction below[171]:

$$\mathbf{2Q^3 \longrightarrow Q^4 + Q^2}$$

Because the peak at 1060 cm^{-1} was not observed in the conventionally processed LS_2 glass-ceramics, it is believed that the microwave energy increased the rate of the Q^3 decomposition reaction and consequently the amount of Q^4 units was increased in the VFM crystallized sample as compared to the conventionally crystallized sample. It is believed that the crystallization mechanism in the VFM process is different than the one observed in the conventional heating process. In conclusion, the enhanced kinetics observed in the VFM crystallized sample, in addition to the observed difference in the crystallization mechanism between the VFM crystallized sample and the conventionally crystallized sample, is believed to be due to the presence of the microwave effect of the microwave energy in the VFM process.

5.4. Density measurements

The true density values of LS_2 glass frit, bulk glass and glass-ceramic samples are shown in Table 5.6. It was observed that the densities of the glass-ceramics were higher than the corresponding glass. This increase may be attributed to the fact that, in most cases, the crystals' densities (due to higher atomic-structural compaction) are higher than those of the glass with the same composition[193]. The true density of the glass-ceramic sample crystallized by VFM (~ 600^{o}C, 2 minutes) was almost similar to the corresponding conventionally crystallized glass-ceramic sample (680^{o}C, 120 minutes). In addition, the true density of the VFM crystallized sample was very close to the theoretical density of lithium disilicate crystals. Meanwhile, the true density of the LS_2 control crystal sample (conventionally crystallized at 680^{o}C for 100 hours) was similar to the VFM crystallized sample and close to the theoretical true density value of LS_2 crystal as well. This implies that in a significantly shorter time and lower temperature, VFM

Table 5.6: Structural (true) density measurements of LS_2 glass frit, bulk glass and glass-ceramic samples measured by Helium Pycnometry.

Material	Average true density (g/cm^3)	Standard deviation
Glass frit (Powder)	2.3401	0.0004
Bulk glass	2.3481	0.0001
Glass-ceramic (Conventional heating) 680°C-2 hr	2.4281	0.0005
Glass-ceramic (Conventional heating) 680°C-100 hr	2.4370	0.0017
Glass-ceramic (VFM heating) ~600°C-2 min.	2.4383	0.0010
Theoretical density of $Li_2Si_2O_5$ crystals[149]	2.439	

Table 5.7: Apparent density measurements of LS_2 glass and glass-ceramic samples measured by Archimedes

Material	Density (g/cm^3)	Standard deviation
Glass	2.35	0.005
Glass-ceramic (conventional heating at 680°C, 2 hr)	2.41	0.00
Glass-ceramic (conventional heating at 680°C, 100 hr)	2.42	0.00
Glass-ceramic (VFM heating at ~600 °C, 2 min.)	2.42	0.00

processing fully crystallized LS_2 glass, resulting in a dense microstructure as compared to a glass-ceramic produced using conventional heating. In conclusion, the true density measurements imply and further support the microwave effect in the crystallization process of LS_2 glass by VFM processing.

Table 5.7 shows the apparent density values for LS_2 glass and glass-ceramic samples crystallized by conventional and VFM heating. The apparent density of the conventionally and the VFM treated glass-ceramic samples are lower than the true density values of these samples. This indicates that there are still some voids (closed pores) in the microstructure. Optical microscopy and SEM have shown that some voids exist in both samples. The difference in density between the LS_2 glassy phase and its crystalline phase is believed to be the main reason for these voids as well as for the observed microcracks in LS_2 glass-ceramics samples, as will be shown later in the SEM micrographs (Figures 5.19 and 5.22). Furthermore, the thermal expansion coefficient of LS_2 glass and glass-ceramic samples was measured by dilatometry (Figure 5.23) and indicated that the thermal expansion coefficient of LS_2 glass was higher than the corresponding glass-ceramic sample. This could also contribute to the observed microcracks. Thus, similar apparent densities were observed for both types of processing but in a much shorter time and lower temperature for the microwave-processed sample.

5.5. Complex dielectric measurements

Using the cavity perturbation technique, the real part of the dielectric constant (ε') and the imaginary or absorptive part of the dielectric constant (ε'') were measured for LS_2 glass and glass-ceramics samples. The dielectric measurements performed on these samples were carried out from room temperature to 600^{o}C at 2.46 GHz. The dielectric

constant (έ) measurement at different temperatures of LS_2 glass and glass-ceramics samples at 2.46 GHz is shown in Figure 5.13. As can be seen from this Figure, έ increases with rising temperature in both LS_2 glass and LS_2 glass-ceramic. LS_2 glass has higher έ than its corresponding glass-ceramic within the measured temperature range. In the LS_2 glass sample, έ increases first as the temperature rises then it starts to decrease when the crystallization of LS_2 glass into glass-ceramic takes place. It is obvious that LS_2 glassy phase has a larger έ than the LS_2 crystalline phase. Figure 5.14 shows ε″ of LS_2 glass and its corresponding glass-ceramic in the 2.46 GHz range at different temperatures. It is obvious that the ε″ of LS_2 glass increases with rising temperature. At room temperature, the dielectric loss factor (ε″) for the LS_2 glass (0.149) is approximately eight times higher than that of the corresponding glass-ceramic material (0.019). Thus the microwave power absorption, P_a, at room temperature in the glassy phase is higher than that in the crystalline phase based on Equation 3.1:

$$\mathbf{P_a = \omega\, \varepsilon_o\, \varepsilon''_{eff}\, E^2_{rms}} \qquad \mathbf{(3.1)}$$

This trend in the dielectric measurement data (έ and ε″) of LS_2 glass and glass-ceramics at 2.46 GHz corresponds with the current observations in the VFM crystallization experiments at 6.425 GHz. In the VFM process, the power absorbed by the sample, resulting in a rise of the temperature, was higher than the power absorbed by the same sample after it was crystallized, as deduced from Figure 5.15. The existence of LS_2 glassy phase at the beginning of the crystallization experiment followed by the formation of LS_2 crystalline phase is responsible for that variation in the absorbed power observation. After crystallization, the sample temperature did not rise even when higher forward power was applied (Figure 5.15). The considerable change in the dielectric properties of

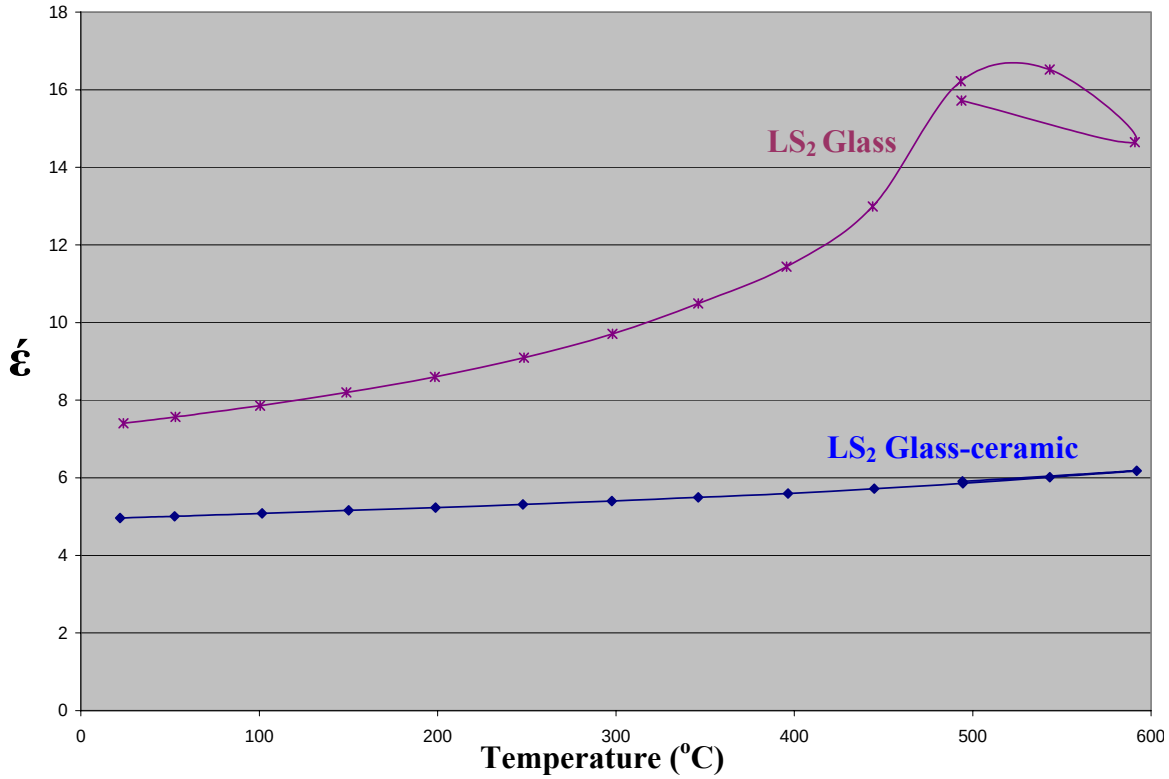

Figure 5.13: Dielectric constant (έ) measurement of LS_2 glass and glass-ceramic at 2.46 GHz at different temperatures.

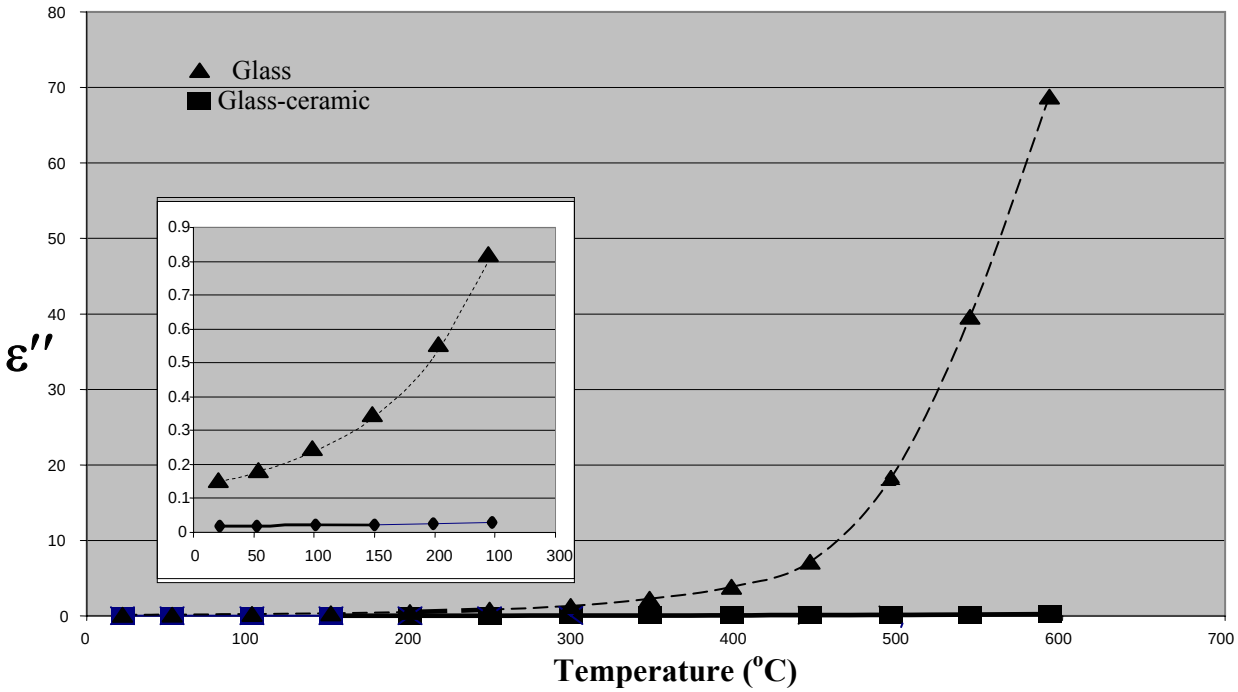

Figure 5.14: Dielectric loss measurements of LS_2 glass and glass-ceramic at 2.46 GHz at different temperatures.

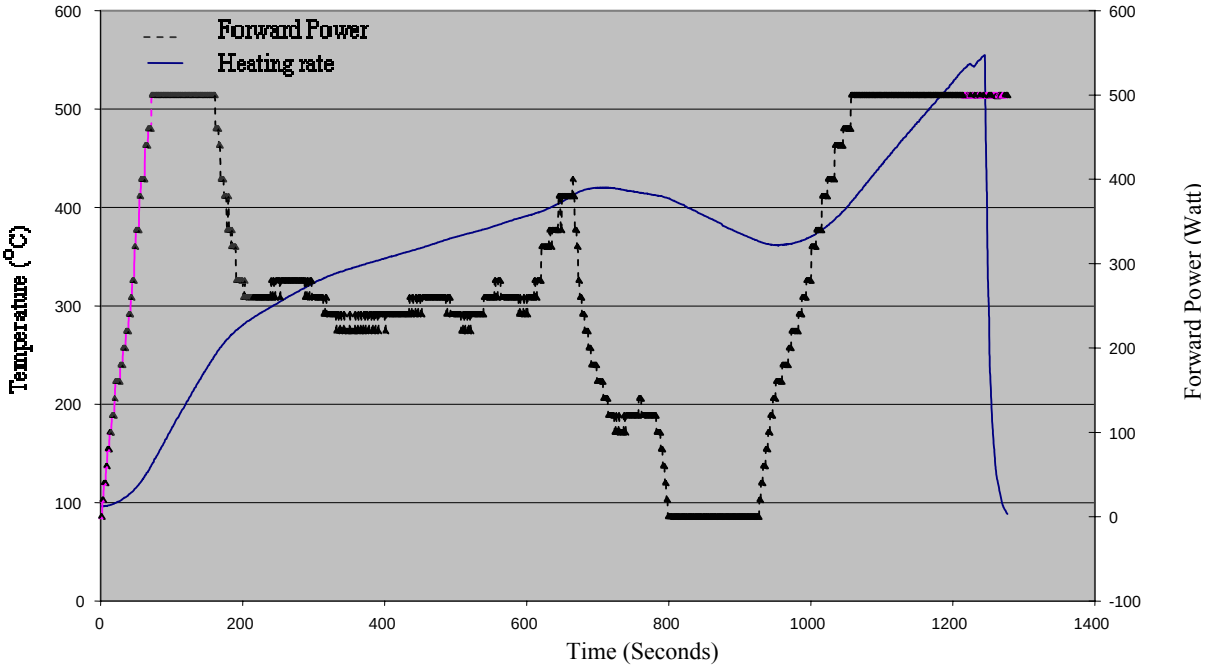

Figure 5.15: Heating rate and forward power during VFM crystallization of the glass at 6.425 GHz.

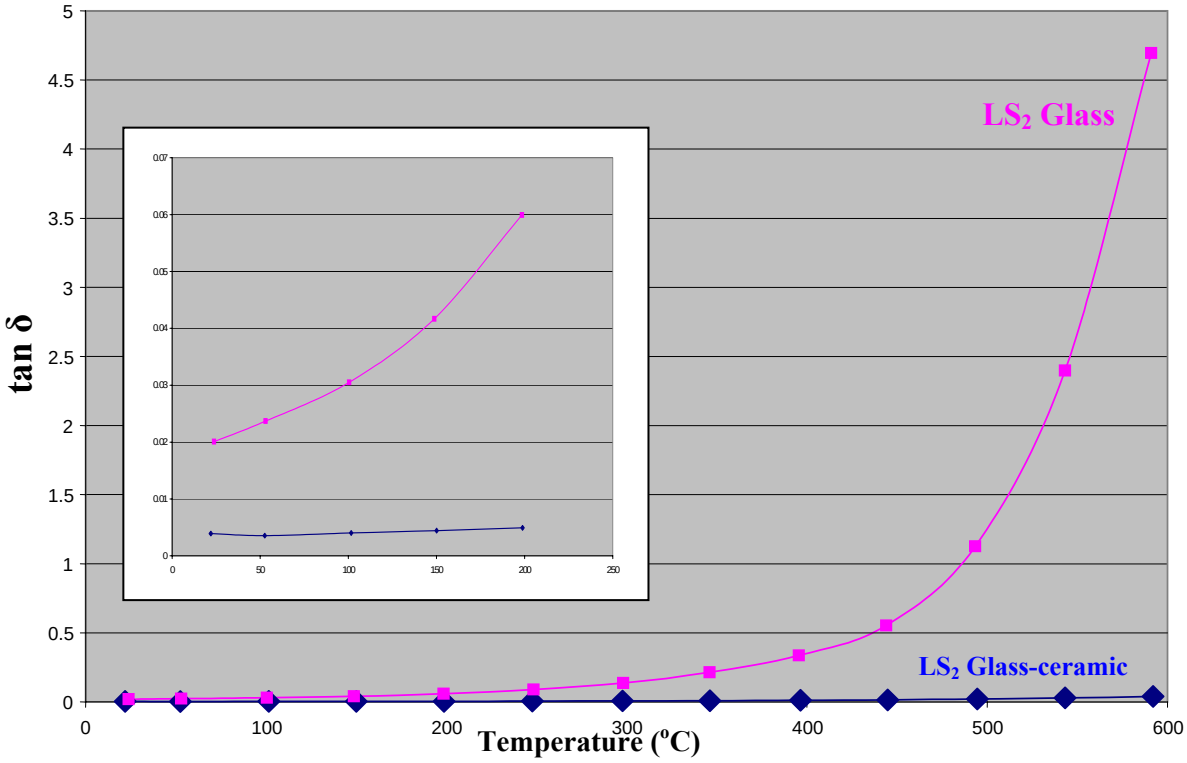

Figure 5.16: Dielectric loss (tan δ) measurement of LS_2 glass and glass-ceramic at 2.46 GHz at different temperatures.

LS_2 glass after crystallization can be used as a signal or a sensor for the completion of the microwave crystallization process if the VFM technology is used in the crystallization process of LS_2 glass. The change in the dielectric properties can be attributed to the change from the amorphous (open) structure of the glassy phase (higher dielectric loss), which is heated more easily by microwave energy, to the well ordered (compact) structure of the corresponding glass-ceramic phase (low dielectric loss) that is harder to heat with microwave energy under normal conditions[31, 68].

The έ and ε″data were used to calculate the loss tangent, tan δ (ε″/έ), of LS_2 glass and glass-ceramic samples as a function of temperatures at 2.46 GHz, as shown in Figure 5.16. As illustrated in the Figure, the loss tangent of LS_2 glass increases with rising temperature. At 2.46 GHz, the critical temperature of LS_2 glass (T_{cri}), the temperature at which the material will self heat by microwave energy, was predicted as 480^{o}C, as shown in Figure 5.17. This implies that LS_2 glass has limited microwave absorption at room temperature at 2.46 GHz and can only be crystallized by hybrid heating at this frequency. This trend in the dielectric properties at 2.46 GHz was in good agreement with what was observed in the present study, experimentally (VFM cavity characterization and the 2.45 GHz heating rate experiment), theoretically (molecular orbital model calculation) and in the literature as well[30, 31].

The microwave penetration depths (D_p) of LS_2 glass and glass-ceramic samples as a function of temperature at 2.46 GHz are shown in Figure 5.18. Tables 5.8 and 5.9 show the microwave depth of penetration calculations of LS_2 glass-ceramic and glass respectively at 2.46 GHz at different temperatures (room temperature to 600^{o}C) utilizing Equation 3.6:

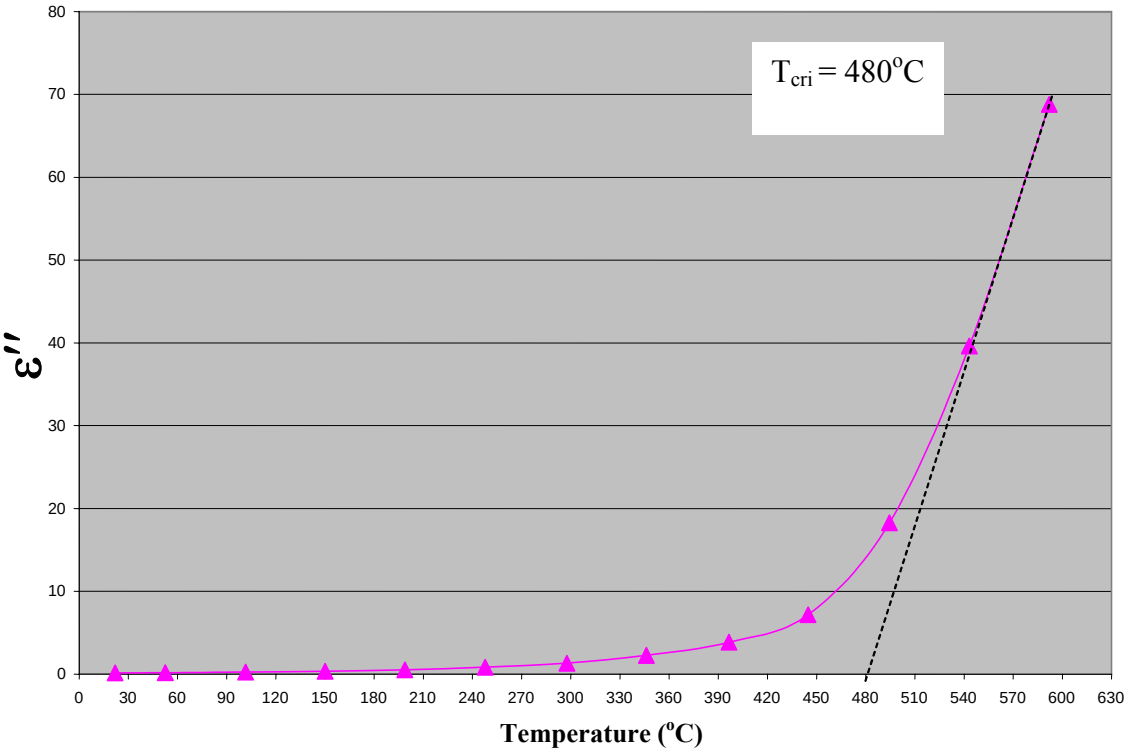

Figure 5.17: Critical temperature (T_{cri}) determination of LS_2 glass at 2.46 GHz.

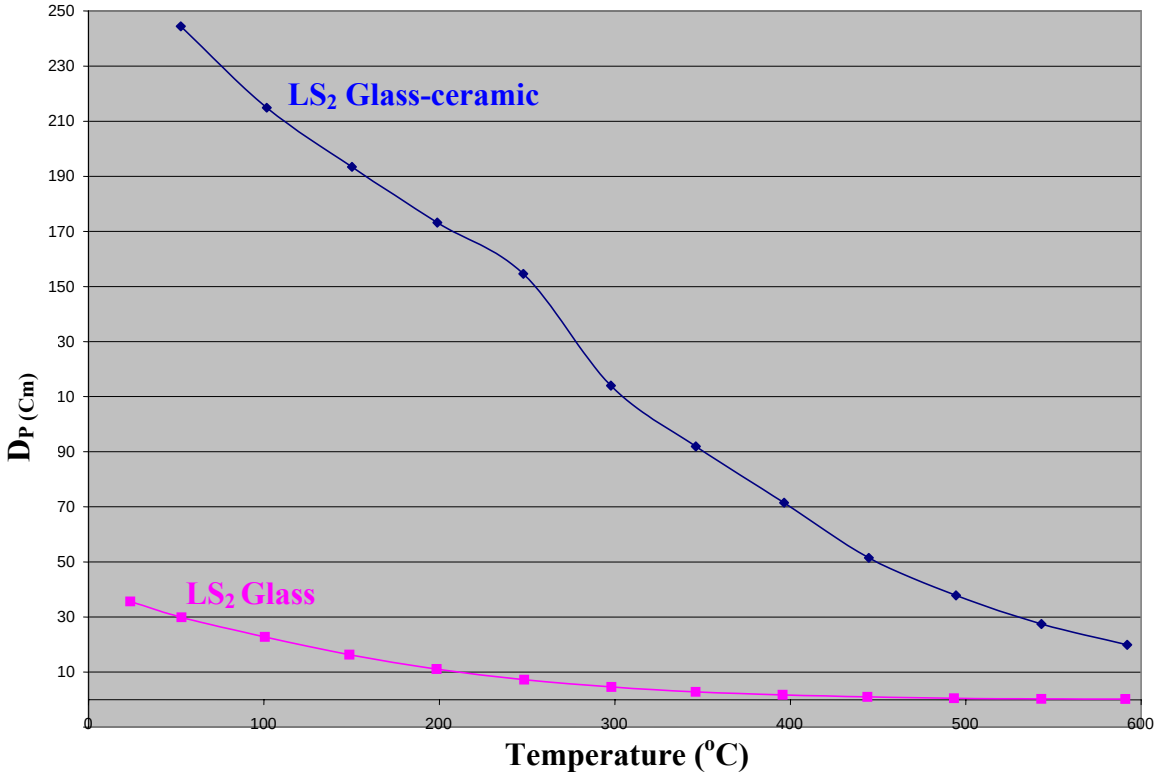

Figure 5.18: Penetration depth (Dp) calculation for LS_2 glass and glass-ceramic samples at 2.46 GHz as a function of temperature.

Table 5.8: Depth of penetration (D_p) calculation of LS_2 glass-ceramic at 2.46 GHz.

Temperature (^oC)	ε′	ε′′	tan δ	D_p(Cm)	λ_o =C/f	Speed of Light C(cm/s)
21.98	4.961	0.01946	0.003923	223.015	12.23633	29979000000
52.57	5.01	0.01784	0.003561	244.4647	12.23633	
101.6	5.082	0.02044	0.004022	214.8962	12.23633	
150.1	5.16	0.02288	0.004434	193.4467	12.23633	
198.8	5.234	0.02574	0.004918	173.1813	12.23633	
247.8	5.314	0.02906	0.005469	154.5639	12.23633	
297.7	5.403	0.03973	0.007353	113.997	12.23633	
346.2	5.496	0.04969	0.009041	91.92851	12.23633	
396.5	5.596	0.06445	0.011517	71.51787	12.23633	
444.8	5.719	0.09053	0.01583	51.47218	12.23633	
494.5	5.857	0.1246	0.021274	37.84736	12.23633	
543.2	6.019	0.1741	0.028925	27.45998	12.23633	
592	6.183	0.2439	0.039447	19.86844	12.23633	
494.3	5.906	0.1242	0.021029	38.12769	12.23633	
394.8	5.684	0.0665	0.0117	69.85608	12.23633	
297.7	5.488	0.04111	0.007491	111.0335	12.23633	
198.2	5.294	0.02724	0.005145	164.5802	12.23633	
99.45	1.238	0.02053	0.016583	105.6034	12.23633	

Table 5.9: Depth of penetration (D_p) calculation for LS_2 glass at 2.46 GHz.

Temperature (^oC).	ε′	ε′′	tan δ	D_p(Cm)	λ_o =c/f	Speed of Light C(cm/s)
23.83	7.406	0.1487	0.020078	35.6610545	12.236327	29979000000
53.05	7.571	0.1794	0.023696	29.8865699	12.236327	
100.5	7.86	0.2398	0.030509	22.7826386	12.236327	
148.8	8.197	0.3416	0.041674	16.3341011	12.236327	
198.5	8.597	0.5153	0.05994	11.0917357	12.236327	
248.4	9.093	0.8186	0.090025	7.18475409	12.236327	
298.1	9.707	1.328	0.136808	4.5818921	12.236327	
346.1	10.49	2.259	0.215348	2.80955655	12.236327	
395.6	11.44	3.858	0.337238	1.73168295	12.236327	
444	12.99	7.174	0.552271	1.01313331	12.236327	
493.3	16.22	18.26	1.125771	0.48102997	12.236327	
543.2	16.52	39.61	2.3977	0.26816355	12.236327	
591	14.65	68.79	4.695563	0.18463598	12.236327	
493.7	15.72	16.83	1.070611	0.50959657	12.236327	
396.3	11.37	3.946	0.347054	1.68918104	12.236327	
297.8	9.583	1.32	0.137744	4.58026894	12.236327	
200.3	8.534	0.5222	0.061191	10.9052053	12.236327	
100.8	7.71	0.2339	0.030337	23.1333392	12.236327	

$$D_P = \frac{\lambda_o}{2\pi(2\varepsilon')^{1/2}}\left[\left(1+\left(\varepsilon''_{eff}/\varepsilon'\right)^2\right)^{\frac{1}{2}}-1\right]^{-1/2} \quad \textbf{(3.6)}$$

As shown in Figure 5.18, the penetration depth in LS_2 glass and glass-ceramic samples decreases (increase in the microwave absorption) with increasing temperature at 2.46 GHz. From tables 5.8 and 5.9, the penetration depths of LS_2 glass and glass-ceramic samples at 2.46 GHz are 35.7cm and 223cm, respectively at room temperature. This implies that the microwave absorption of LS_2 glass at this frequency, at room temperature, will be very small, and as a result it will be difficult to heat LS_2 glass by itself without the aid of hybrid heating. Because the D_p value of LS_2 glass-ceramics is large, very small microwave absorption is expected. Hence, it will be very difficult to heat by microwave energy at this frequency at room temperature, as confirmed by our experiments. In the VFM crystallization process, LS_2 glass was crystallized successfully by stand alone heating without the aid of hybrid heating. At 6.425 GHz central frequency in the VFM process, it is expected that the penetration depth in LS_2 glass will decrease and approach the sample dimensions so that LS_2 glass will self heat and crystallize by VFM processing (based on equation 3.6). The depth of penetration at 2.46 GHz in LS_2 glass at 493^{o}C was calculated as 0.5 cm (within the sample dimension) which indicates that the microwave absorption increases in that temperature range. This is in agreement with the calculated critical temperature (480^{o}C) of LS_2 glass at this frequency. Meanwhile, the penetration depth of the LS_2 glass-ceramic sample at 592^{o}C was calculated as 19.9 cm at 2.46 GHz, which indicates that the microwave absorption in the glass-ceramic sample will be very small at this frequency, even at higher temperatures. These observations correspond with what has been observed experimentally in the VFM

process, as shown in Figure 5.15.

5.6. Scanning electron microscopy (SEM)

Figures 5.19 and 5.20 show the typical ellipsoidal LS_2 crystal shape of the apparent agglomerate of small needle like crystallites (spheralite) in partially crystallized LS_2 glass samples by conventional heating at two different temperatures. These samples were polished then etched by 2% HF acid for 2 minutes. Figure 20 shows a perpendicular view of an ellipsoidal LS_2 crystal that has been cut from the middle. Figure 5.21 shows the typical ellipsoidal shape of the LS_2 crystals in partially crystallized LS_2 samples by VFM heating. Both samples crystallized either by conventional or VFM heating developed the typical characteristic ellipsoidal shape of LS_2 crystals with a maximum crystal aspect ratio of 1.6, as shown in Figures 5.19 and 5.21[5,10,12]. These Figures show microcracks developed inside these crystals in both types of samples. When these crystals grow as a function of temperature or time, the microcracks increase and travel into the glassy phase (Figures 5.21 and 5.22). As discussed earlier, because of the difference between the true density of LS_2 crystal phase and its corresponding glassy phase, in addition to the difference between the thermal expansion coefficients of both phases, these cracks might be expected. Figure 5.23 shows the thermal expansion coefficient measurements of LS_2 glass and glass-ceramic samples. The coefficient of thermal expansion of LS_2 glass and glass-ceramic samples were calculated as $3.40*10^{-5}$ and $1.23*10^{-5}$ in./in./^{o}C respectively, in the range from 40^{o}C-450^{o}C. The thermal expansion curve shows a glass transition temperature (T_g) at 430^{o}C and a softening temperature (T_d: The temperature at which the glass will deform under the influence of it own weight) at 470^{o}C. As indicated earlier, the T_g value obtained from the DSC data was

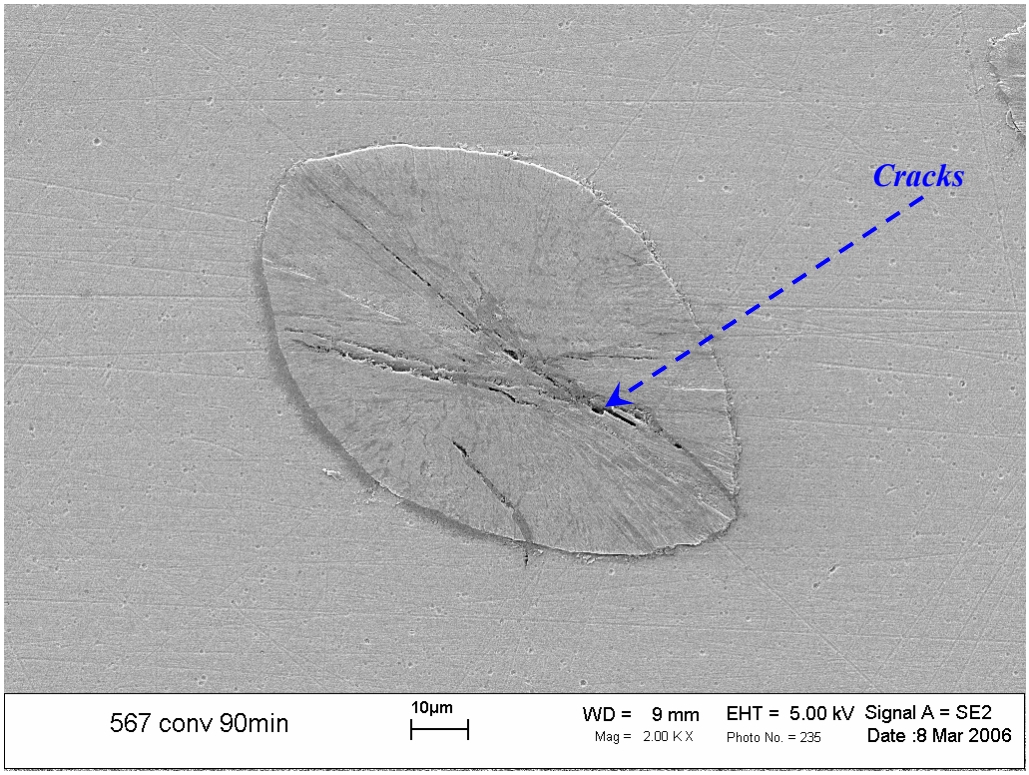

Figure 5.19: LS_2 crystal of conventionally crystallized sample (567°C, 90 minutes)

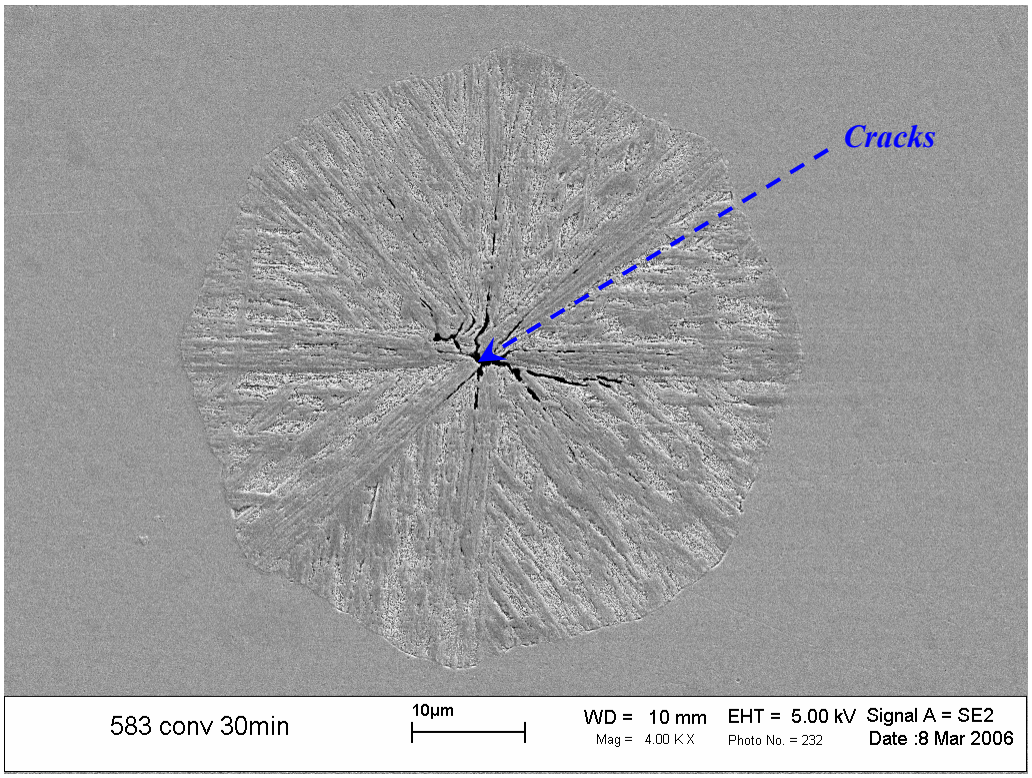

Figure 5.20: LS_2 crystal of conventionally crystallized sample (583°C, 30 minutes)

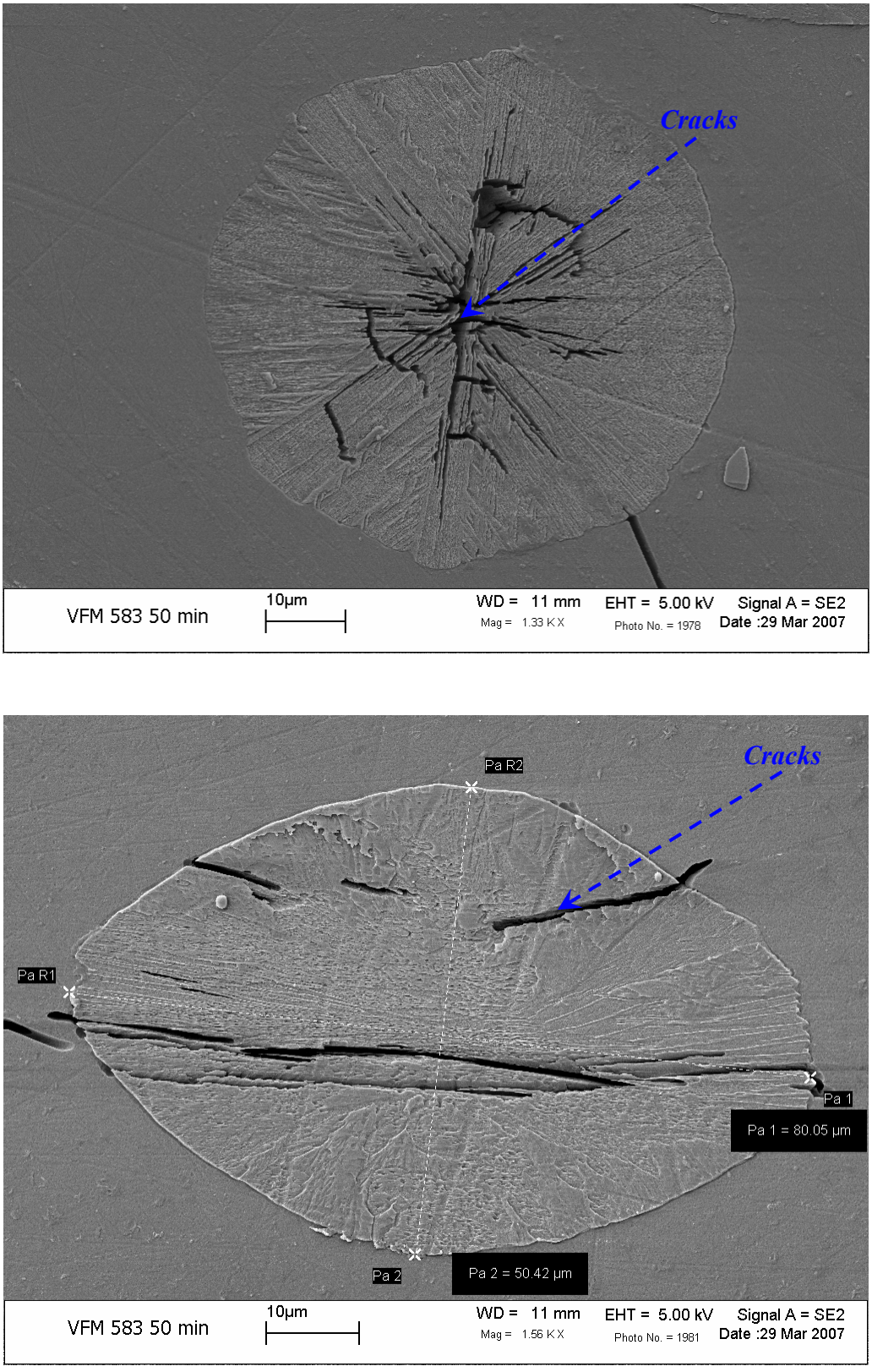

Figure 5.21: LS_2 crystals of VFM crystallized sample (583^{o}C, 50 minutes)

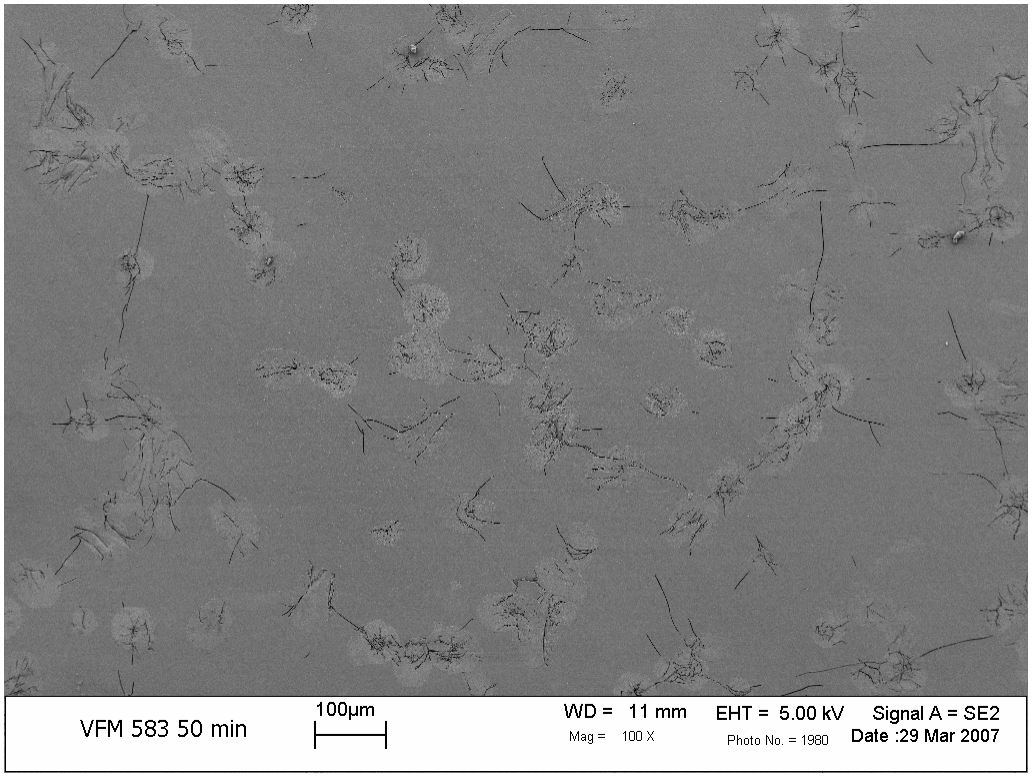

Figure 5.22: Partially crystallized LS_2 glass by VFM heating (583°C, 50 minutes)

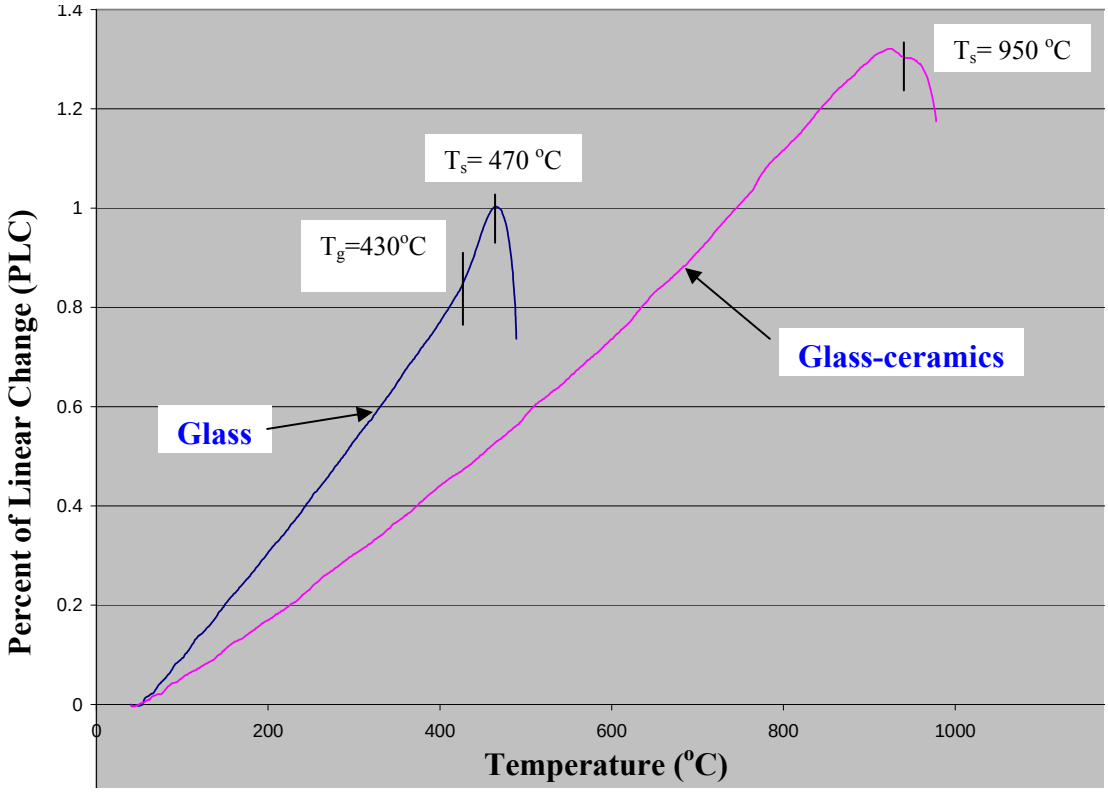

Figure 5.23: Thermal expansion coefficient curves of LS_2 glass and glass-ceramics

475°C, which is different from the one obtained from the thermal analysis data (430°C). This difference is believed to happen because the T_g value is a function of the heating rate and the method used for measurements as well. A heating rate of 20°C/min was used in the thermal expansion coefficient measurements while 10°C/min was used in the DSC measurements.

SEM micrographs of a polished etched surface (2%HF, 2 minutes) of a glass-ceramic sample fully crystallized by VFM (~600°C, 2min) are shown in Figure 5.24. Figure 5.25 shows SEM micrographs of the LS_2 control crystal's polished etched surface (conventionally crystallized at 680°C, 100 hours). Both glass-ceramic samples exhibit the tightly interlocking crystal form that is characteristic of the corrugated sheets or layers of LS_2 glass-ceramics. As a result of this microstructure, good isotropic mechanical properties are achieved[17, 194]. Thus, the higher the degree of interlocking between crystals (high crystalline content), the higher the mechanical strength and toughness of the LS_2 glass-ceramic[17]. As a result, a new generation of dental crowns containing mainly LS_2 crystalline phase is now available in the market.

Both, the fully crystallized VFM sample and the control crystal sample developed the same characteristic microstructural features as confirmed by SEM. Furthermore, the partially crystallized samples, by either VFM or conventional heating, developed the same characteristic microstructural features. Finally, the SEM micrographs of the crystallized VFM sample, fully crystallized in a significantly short crystallization time and lower temperature, provide further evidence to support the existence of a microwave effect in the crystallization process of LS_2 glass by VFM processing.

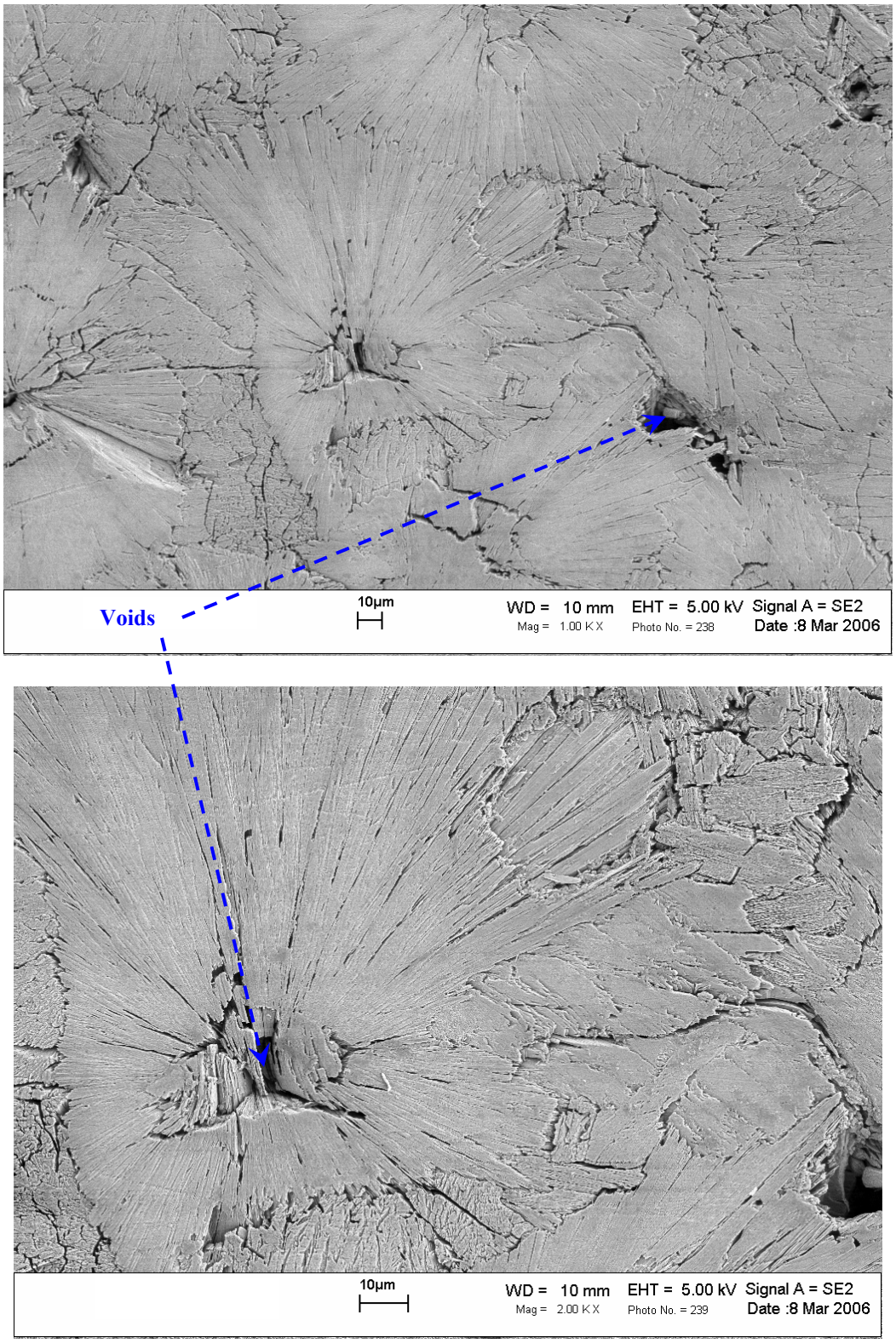

Figure 5.24: SEM micrographs of fully crystallized LS_2 by VFM heating (~600 ^oC for 2 minutes)

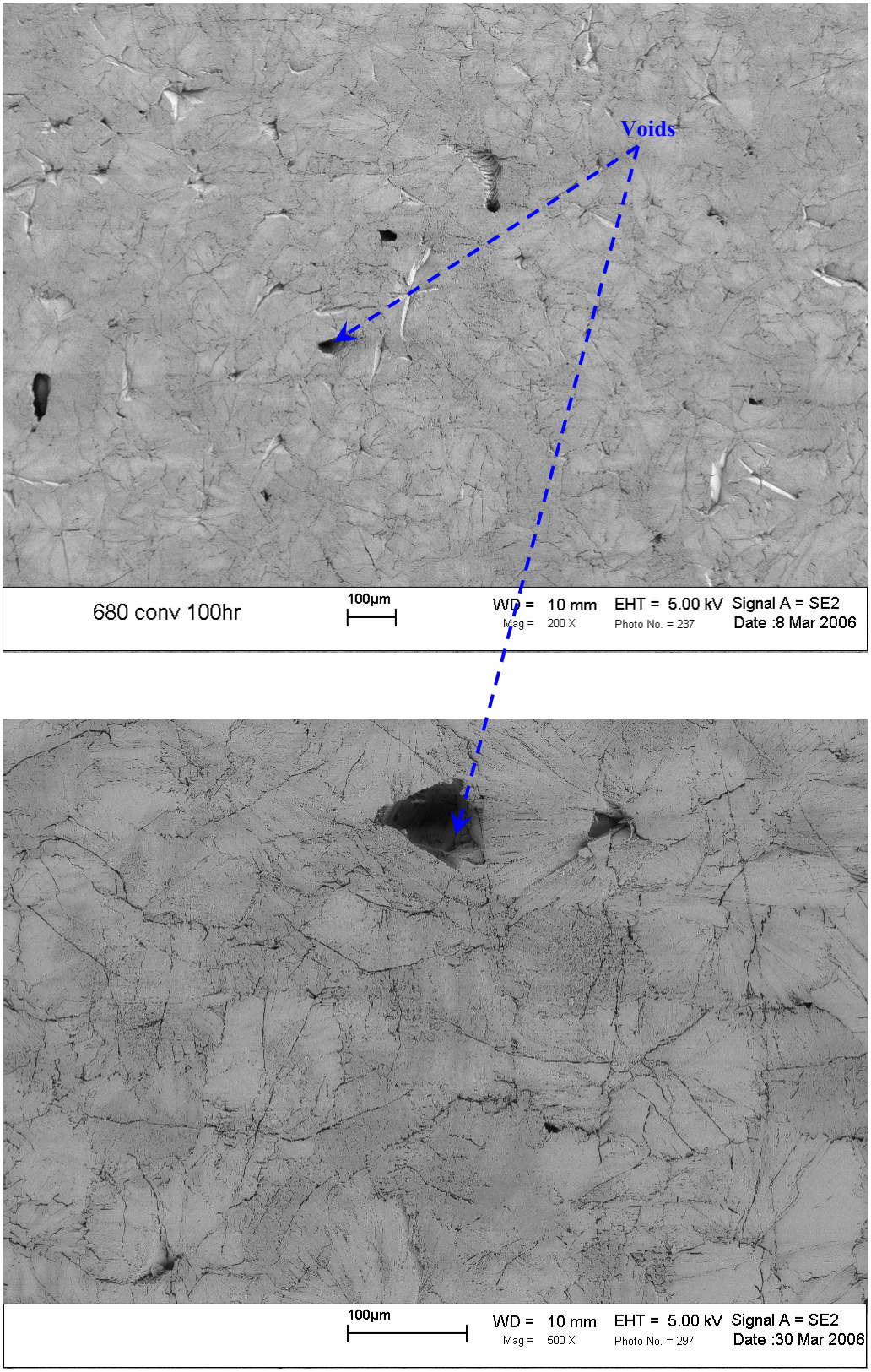

Figure 5.25: SEM micrographs of fully crystallized LS_2 by conventional heating (680 ^{o}C for 100 hours)

5.7. X-ray diffraction (XRD)

Figures 5.26 and 5.27 show the x-ray patterns of annealed LS_2 glass and VFM crystallized glass-ceramic samples, respectively. Figure 5.26 indicates that the prepared glass was quenched successfully and an amorphous structure was achieved with the characteristic short range order pattern. Figure 5.27 shows that the VFM heat-treated sample (~600^{o}C, 2 minutes) was successfully crystallized into LS_2 glass-ceramic with its characteristic XRD peaks. The crystal phase in this glass-ceramic sample was identified as orthorhombic (Ccc2) lithium disilicate crystal phase, whose features include corrugated sheets of $(Si_2O_5)^{-2}$ on the (010) plane[17]. Crystal phase identification and the crystallographic planes corresponding to the 2θ values for all the peaks was performed using the ASTM x-ray diffraction file index and from several other publications[18, 149-157].

The XRD pattern of the LS_2 glass-ceramic sample that has been crystallized conventionally at the maximum crystallization temperature 680^{o}C for 100 hours (control crystal sample) is shown in Figure 5.28. The control LS_2 crystal sample and the VFM crystallized sample developed the same lithium disilicate (Orthorhombic Ccc2) crystal structure but with the latter occurring in a significantly shorter time and temperature. Thus, the XRD patterns provide further evidence to support the microwave effect claim in the crystallization process of LS_2 glass by VFM heating.

As explained earlier, in the VFM process, a special casket containing LS_2 glass frit was developed to prevent cracking in the bulk LS_2 glass sample, contamination and to reduce the number of external factors in the VFM process so that microwave-material interaction can be studied. The glass frit used in the VFM heating setup was examined

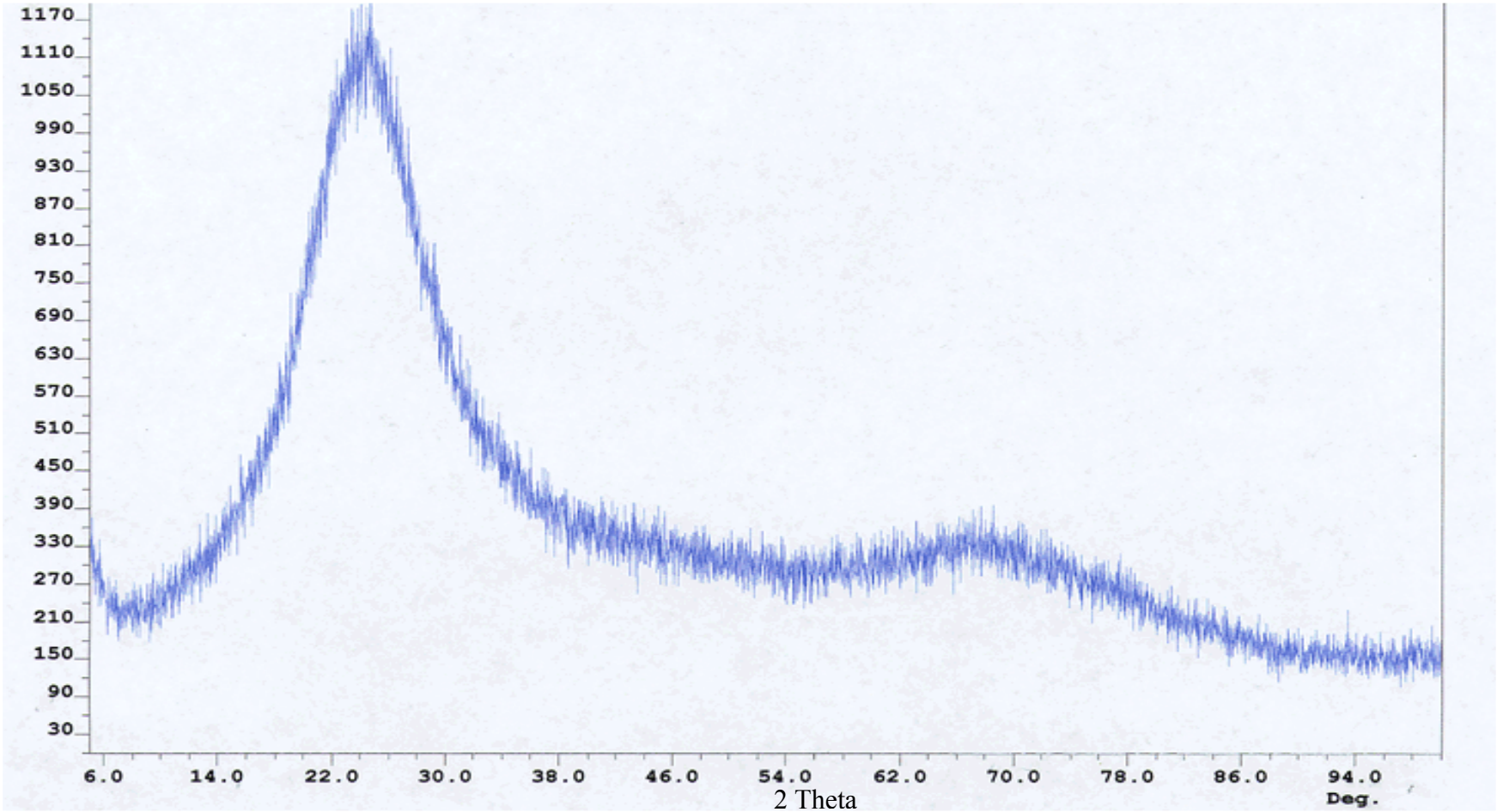

Figure 5.26: X-ray pattern of quenched and annealed LS_2 glass.

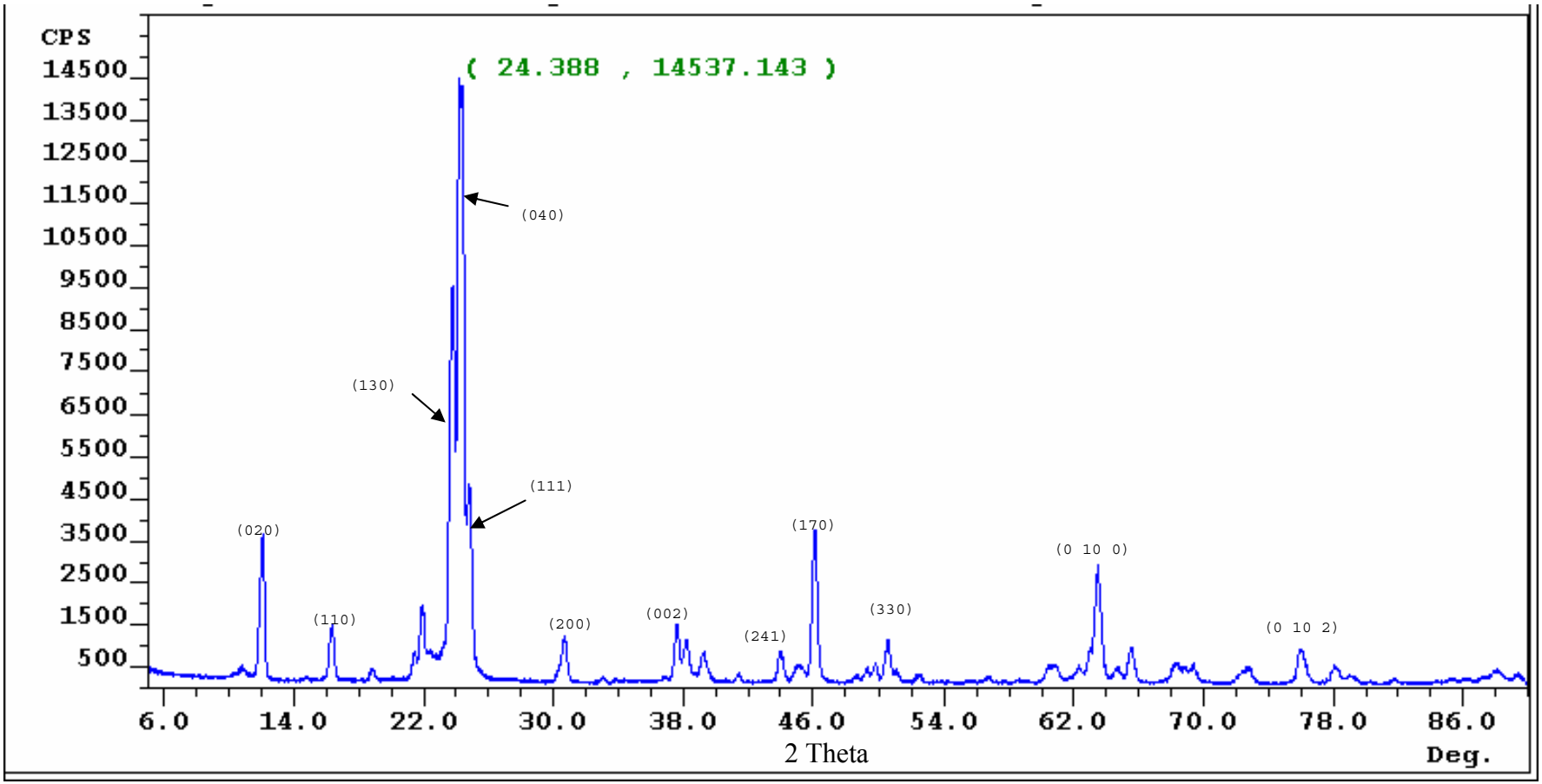

Figure 5.27: X-ray pattern of LS_2 glass-ceramic crystallized by VFM (~ 600^{o}C, 2 minutes).

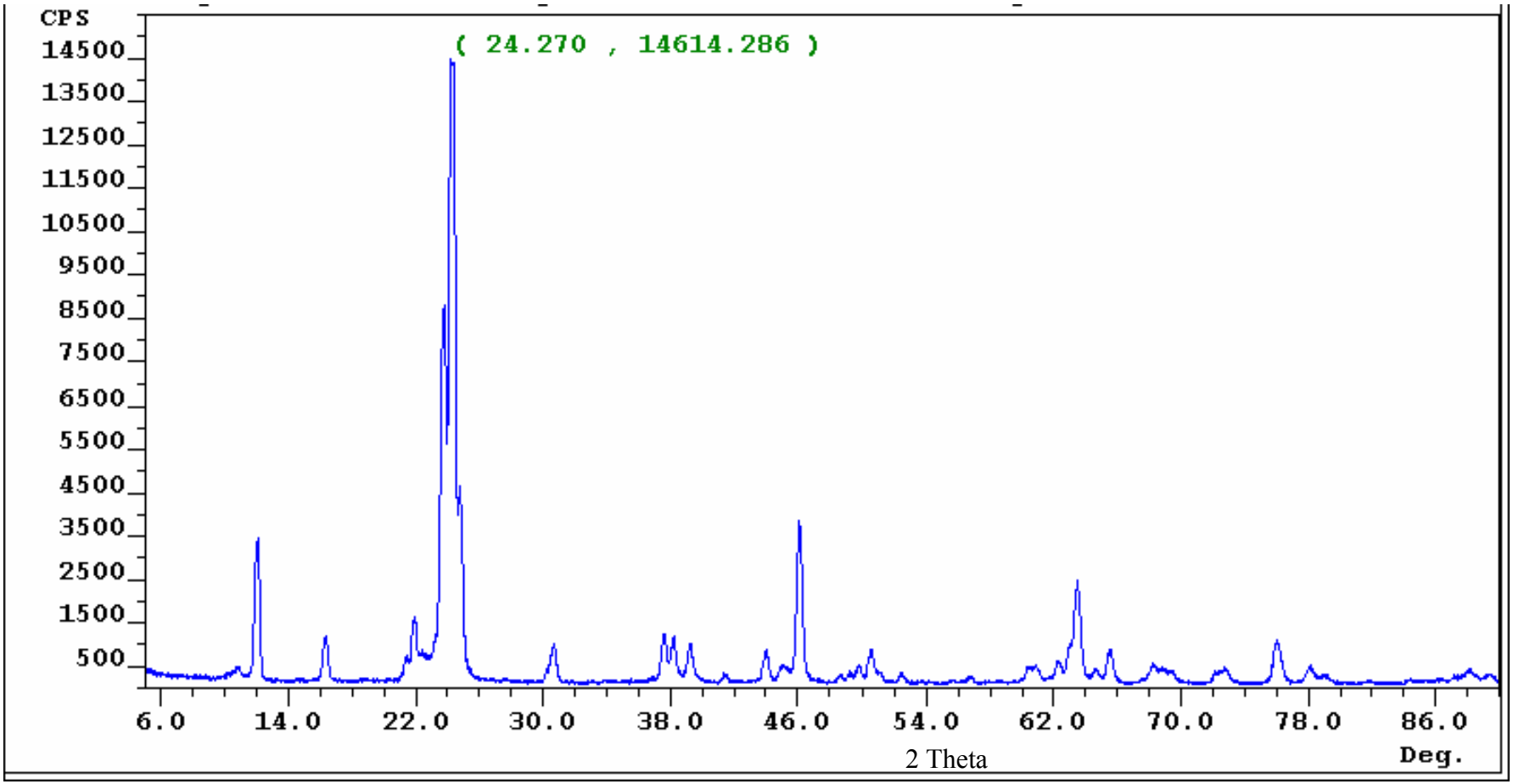

Figure 5.28: X-ray patterns of LS_2 glass-ceramic crystallized by conventional heating at 680°C for 100 hours (control crystal).

with XRD (Figure 5.29a). Another LS_2 glass frit sample heat-treated conventionally at 680^{o}C for 30 minutes was examined with XRD, as shown in Figure 5.29b. These Figures show that the LS_2 glass frit used in the VFM setup is still relatively amorphous (slightly crystalline) as compared with the glass frit that was heat-treated conventionally. This comparison implies that the bulk LS_2 glass sample in the VFM setup was crystallized mainly by the microwave field. So the full crystallization observed in this sample results mainly from the interaction between the microwave energy and the bulk glass sample in the VFM process rather than from the conventional radiant heating that could result from the heated frit. Thus, the glass frit in the VFM setup was not acting as a "heating element" (conventional radiant heating) to the bulk glass sample. This fact not only provides evidence that the full crystallization of the bulk LS_2 glass observed in the VFM process is mainly due to microwave heating; it also provides a strong basis for the existence of the microwave effect in the VFM process. Furthermore, a unique casket containing LS_2 glass frit was successfully developed in the VFM crystallization process.

In order to investigate and to establish the microwave effect phenomena, three (3) experiments were performed to provide the basic fundamental knowledge necessary to establish the microwave effect in the VFM crystallization process. In the first experiment, three (3) nucleated LS_2 glass samples were heat-treated conventionally at 600^{o}C, 680^{o}C and 730^{o}C for 25 minutes, respectively. The effect of the temperature on the major XRD peak intensity (2θ=24) of the LS_2 crystalline phase is shown in Figure 5.30. The selection of these temperature values is based upon the crystal growth peak obtained from the DSC measurement. As indicated before, the maximum crystal growth temperature is located at 680^{o}C. As expected from the DSC data, the heat-treated sample at 680^{o}C had the

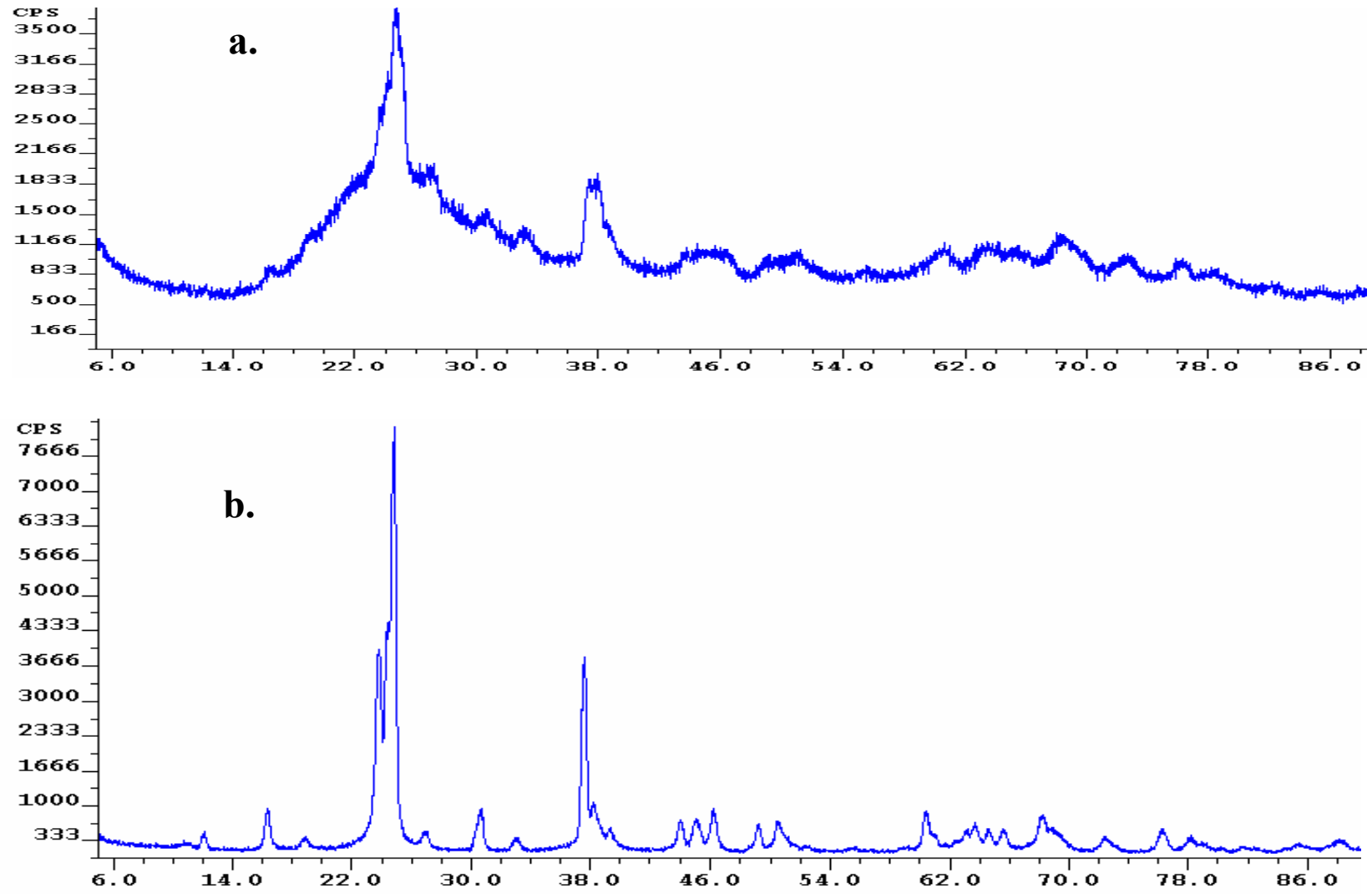

Figure 5.29: X-ray patterns of LS_2 glass frit heated in (a) VFM crystallization setup and (b) conventionally at 680^{o}C for 30 minutes

highest major XRD peak intensity. The sample at 730^{o}C had a slightly higher XRD peak intensity than the sample at 600^{o}C. This observation is in agreement with the kinetic theory (Equation 2.8), where the crystal growth rate is at its maximum value at the maximum crystal growth temperature (680^{o}C). This experiment is in agreement with the well-known fact: at any temperature higher or lower than the maximum crystal growth temperature, the crystal growth rate should decrease and be lower than the rate at the maximum crystal growth temperature.

In the second experiment, three (3) LS_2 glass samples were heat-treated conventionally at 600^{o}C, 680^{o}C and 730^{o}C for 7 minutes respectively (Figure 5.31). The heat-treated sample at 680^{o}C had a higher volume fraction of crystals (scattering light, white color) than the other two samples. On the other hand, the heat-treated sample at 730^{o}C scatters the light in the middle of the sample more than the one heat-treated at 600^{o}C. Again, this observation is in good agreement with the DSC data of the bulk LS_2 glass and the kinetic theory of glass formation. The results of this experiment clearly imply that the crystal growth rate is only maximized at the maximum crystal growth temperature (680^{o}C). This fact is very important in order to provide the scientific background necessary for the discourse about the reality of the microwave effect in the crystallization process of LS_2 glass by VFM.

Finally, Figure 5.32 shows conventionally heat-treated samples at 680^{o}C for 2, 3, 4, and 5 minutes, respectively, as the third experiment. As shown in the picture, none of these samples was fully crystallized as compared to the VFM heat-treated sample (Figure5.8). Furthermore, the VFM crystallized sample at 2 minutes is very different from the one conventionally treated at the same time and temperature. This difference in

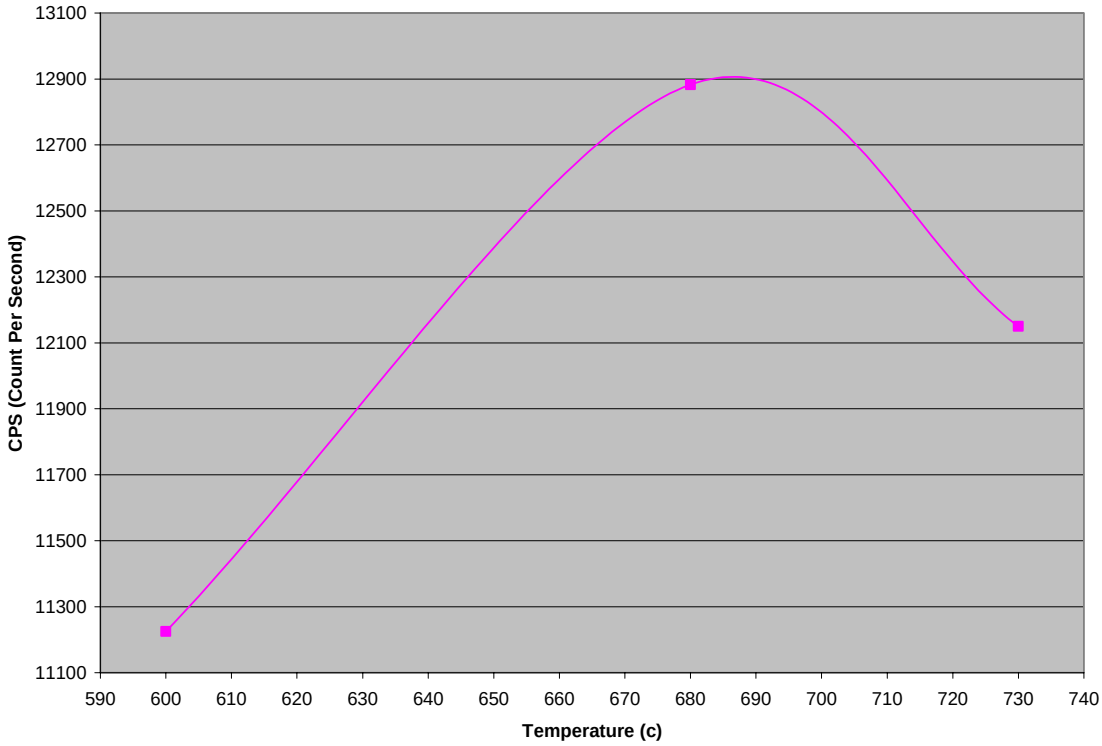

Figure 5.30: Effect of temperature on the XRD major peak (2θ = 24) intensity of LS_2 glass-ceramics samples heat-treated conventionally at 600, 680, and 730 ^{o}C for 25 minutes.

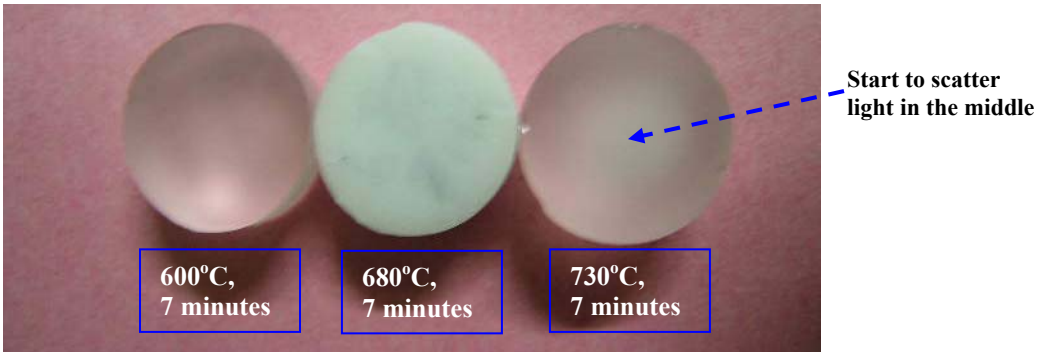

Figure 5.31: LS_2 glass samples heat-treated conventionally at 600^{o}C, 680^{o}C, and 730^{o}C for 7 minutes respectively.

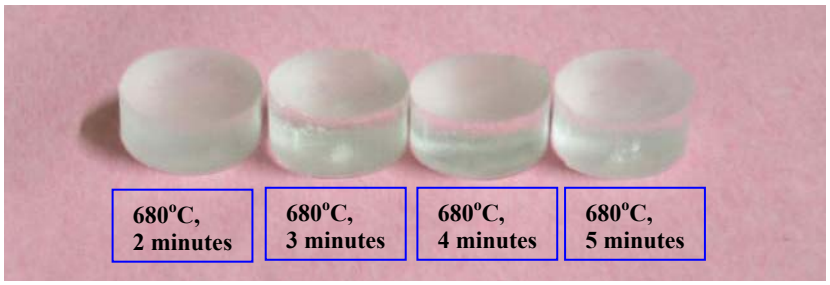

Figure 5.32: LS_2 glass samples heat-treated conventionally at 680^{o}C for 2, 3, 4, and 5 minutes, respectively.

the crystallization behavior of LS_2 glass under the influence of the VFM heating is an indication of different and enhanced kinetics in the VFM process compared to the conventional process.

In conclusion, the observed full crystallization of the VFM heat-treated sample, as confirmed by XRD, in a significantly short time and temperature can not be explained by the well known kinetic theory of glass formation, the DSC data of the bulk glass and finally by the results of the later three experiments. This unusual crystallization behavior is considered to be due to the microwave effect.

5.8. Molecular orbital theory for microwave absorption calculation

CAChe Worksystem (Computer Aided Chemistry) software was used to build the unit cell of LS_2 crystal (Orthorhombic crystal system with space group: Ccc2, $\alpha=\beta=\gamma=90^oC$, a=5.807, b=14.582, c=4.773 according to the x-ray diffraction data) and also to build a short range order glassy network of LS_2 glass. Table 5.10 shows the positional parameters of the 36 atoms in the LS_2 crystal unit cell. Figure 5.33 shows the unit cell and the short range order of LS_2 glass-ceramic and glass respectively. MOPAC (Molecular Orbital PACkage) was used to calculate the IR spectra for both the LS_2 glassy network and the LS_2 crystal unit cell. The calculated IR data was used according to the molecular orbital theory to calculate the microwave absorption for the LS_2 glass and crystal unit cell.

The experimentally measured IR spectra of LS_2 glass is shown in Figure 5.34 in transmittance mode after it was converted from the reflectance mode by the available IR software (OMINC 7). Figure 5.35 shows the calculated IR spectra of LS_2 glass in transmittance mode obtained using MOPAC, which is provided by the CAChe software.

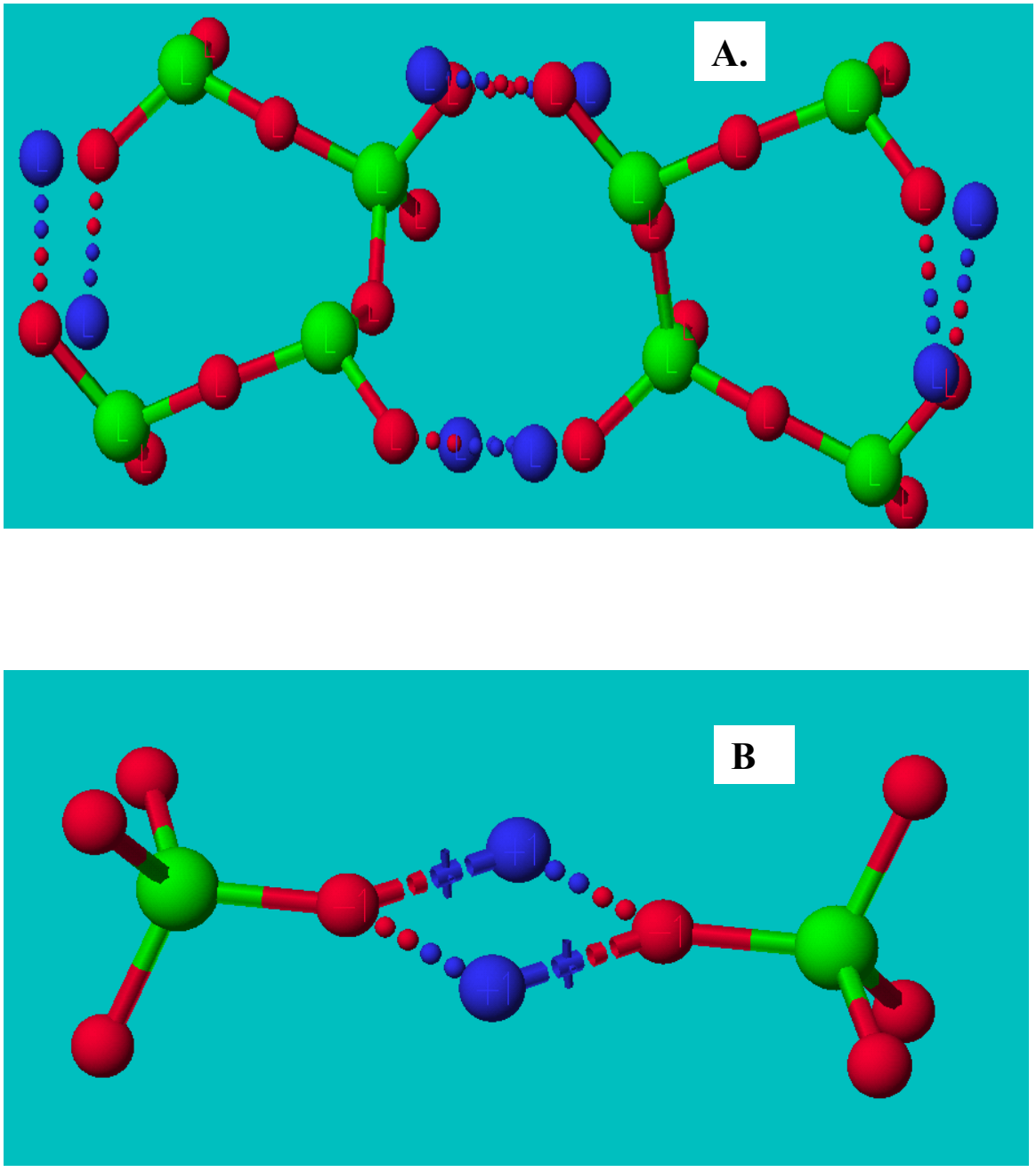

Figure 5.33: (A).Lithium disilicate crystal unit cell. (B) Short range order of lithium disilicate glass
(Green: Silicon atom, Red: Oxygen atom and Blue: Lithium atom)

Table 5.10: Positional parameters of the 36 atoms of the LS_2 crystal unit cell.

Atom	X	Y	Z
Si1	0.1552	0.14836	0.1352
O1	0.3295	0.0718	0.0491
O2	0.0932	0.1377	0.4785
O3	0.25	0.25	0.0781
Li1	0.346	0.0584	0.625
Si1	0.8448	0.85164	0.1352
O1	0.6705	0.9282	0.0491
O2	0.9068	0.8623	0.4785
O3	0.75	0.75	0.0781
Li1	0.654	0.9416	0.625
Si1	0.1552	0.85164	0.6352
O1	0.3295	0.9282	0.5491
O2	0.0932	0.8623	0.9785
O3	0.25	0.75	0.5781
Li1	0.346	0.9416	0.125
Si1	0.8448	0.14836	0.6352
O1	0.6705	0.0718	0.5491
O2	0.9068	0.1377	0.9785
O3	0.75	0.25	0.5781
Li1	0.654	0.0584	0.125
Si1	0.6552	0.64836	0.1352
O1	0.8295	0.5718	0.0491
O2	0.5932	0.6377	0.4785
Li1	0.846	0.5584	0.625
Si1	0.3448	0.35164	0.1352
O1	0.1705	0.4282	0.0491
O2	0.4068	0.3623	0.4785
Li1	0.154	0.4416	0.625
Si1	0.6552	0.35164	0.6352
O1	0.8295	0.4282	0.5491
O2	0.5932	0.3623	0.9785
Li1	0.846	0.4416	0.125
Si1	0.3448	0.64836	0.6352
O1	0.1705	0.5718	0.5491
O2	0.4068	0.6377	0.9785
Li1	0.154	0.5584	0.125

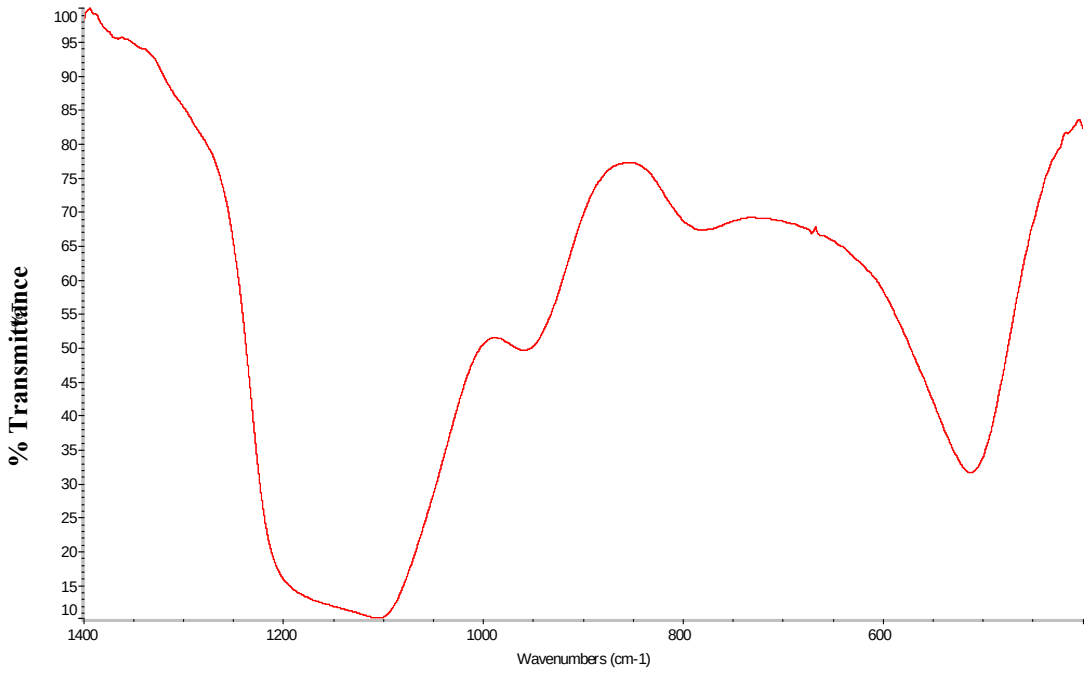

Figure 5.34: IR experimentally measured spectra of LS_2 polished glass sample.

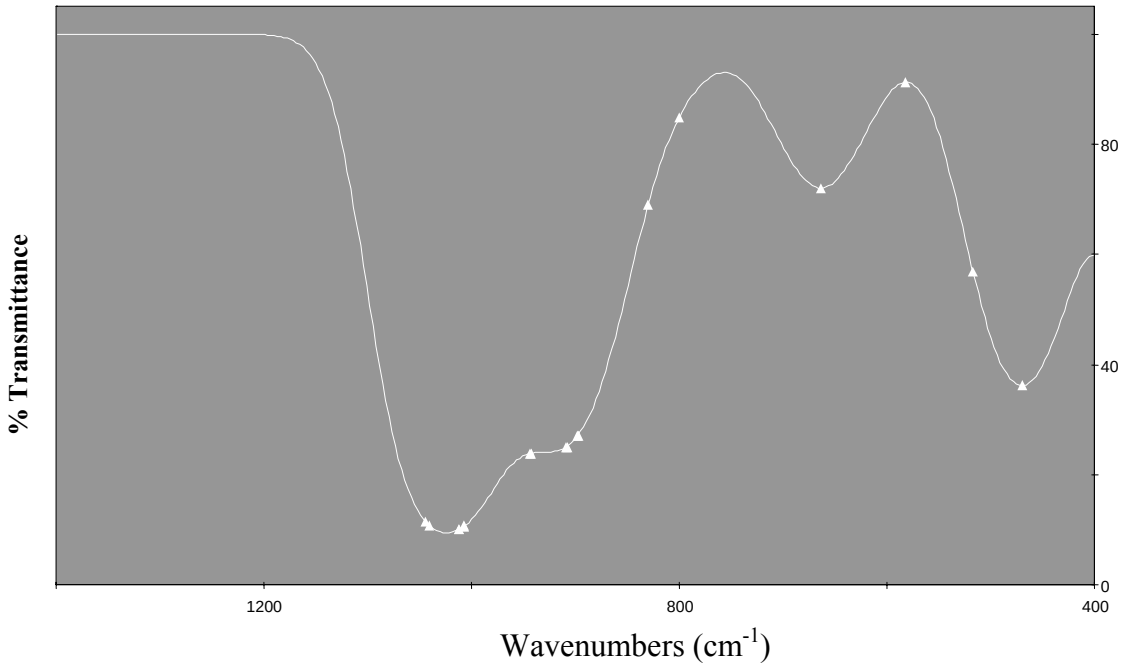

Figure 5.35: IR Calculated (Cache program) pattern of LS_2 glass.

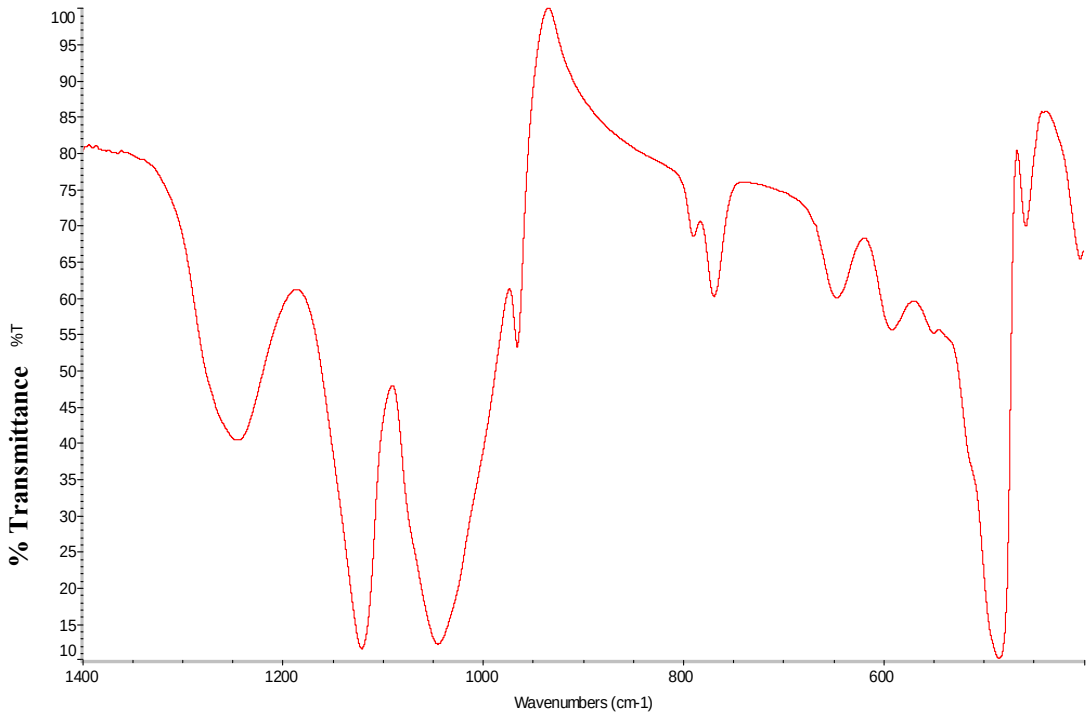

Figure 5.36: IR experimentally measured spectra of LS_2 polished glass-ceramic sample heat-treated at 680°C for 100 hours (control crystal).

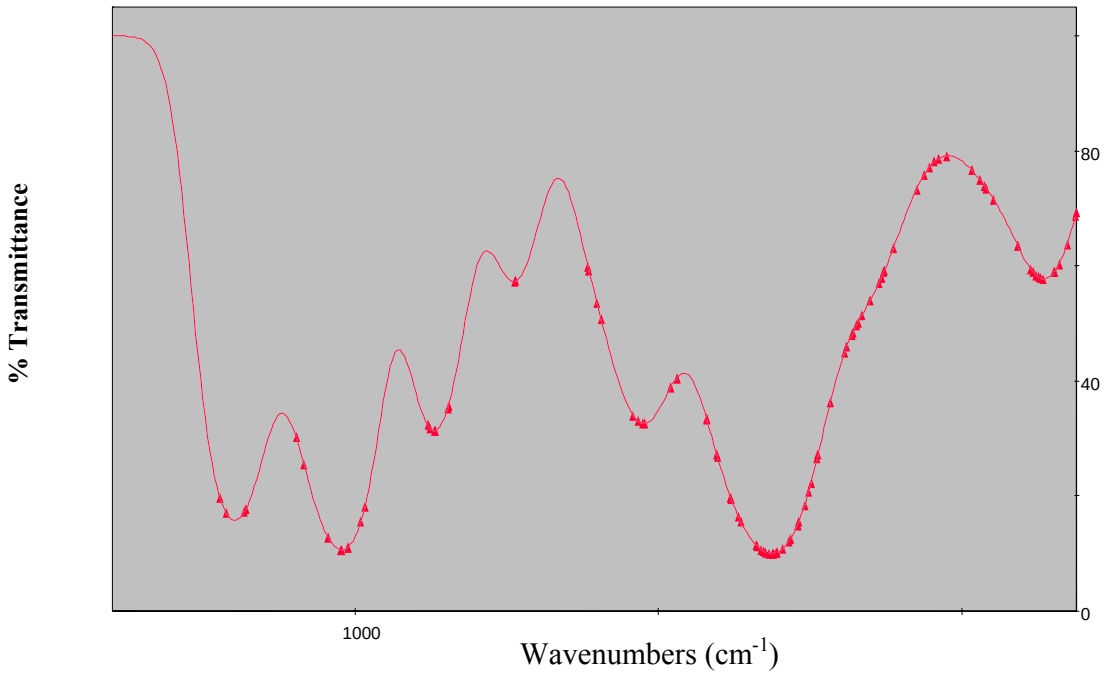

Figure 5.37: IR Calculated (Cache program) pattern of LS_2 glass-ceramic unit cell (36 atoms)

Figures 5.36 and 5.37 show both the experimentally measured (related to control crystal sample) and the calculated IR spectra of the 36 atoms unit cell of LS_2 glass-ceramic, respectively. It is understandable that the calculated and the experimentally measured IR spectra of both LS_2 glass and glass-ceramic are not exactly identical. The difference observed in these spectra is believed to result from the fact that this calculation is actually an approximation of the real case and is limited because of the small number of atoms (36) used to obtain the calculated spectra. On the other hand, this calculation still gives useful information about the real case.

The calculated IR spectra data for both LS_2 glass and glass-ceramic samples was manipulated, as explained in Appendix 1, to calculate the microwave absorption curves based on the hypothesis of the molecular orbital theory for microwave absorption in materials. Figure 5.38 shows the calculated microwave absorption calculation for LS_2 glass. Based on this calculation, the absence of strong oscillators at 2.45 GHz is obvious. On the other hand, the existence of strong oscillators capable of absorbing microwave energy at 7 GHz and 18 GHz is noticeable. Other strong oscillators exist at higher frequency ranges such as 33 GHz and 59 GHz. Figure 5.39 shows the molecular orbital theory calculation for the 36 atoms unit cell of LS_2 glass-ceramic. The absence of strong oscillators capable of absorbing microwave energy below 20 GHz is obvious.

The molecular orbital model of microwave absorption calculations of LS_2 glass and glass-ceramics are in good agreement with the following:

- The dielectric properties measurement performed in the present study for LS_2 glass and glass-ceramics at 2.46 GHz.
- What was reported in the literature[30, 31] about the possibility of crystallizing

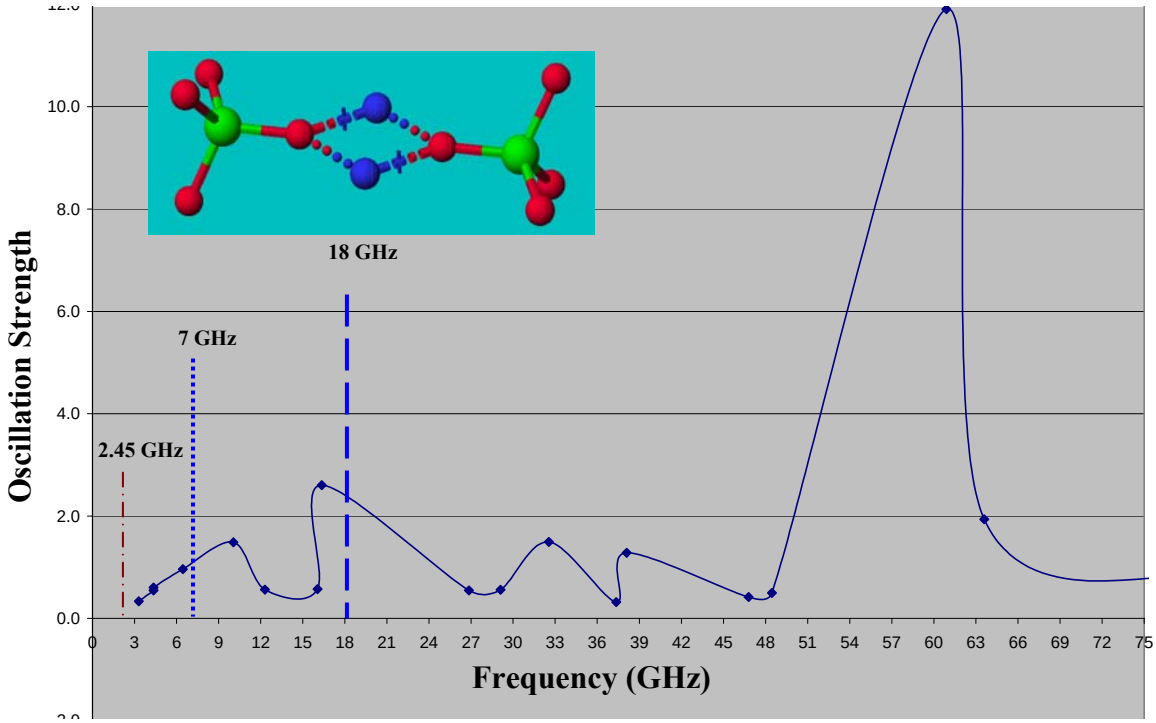

Figure 5.38: Molecular orbital theory calculation for LS_2 glass.
Note the presence of strong oscillators capable of absorbing microwave energy at 7 and 18GHz and the absence of these oscillators at 2.45 GHz.

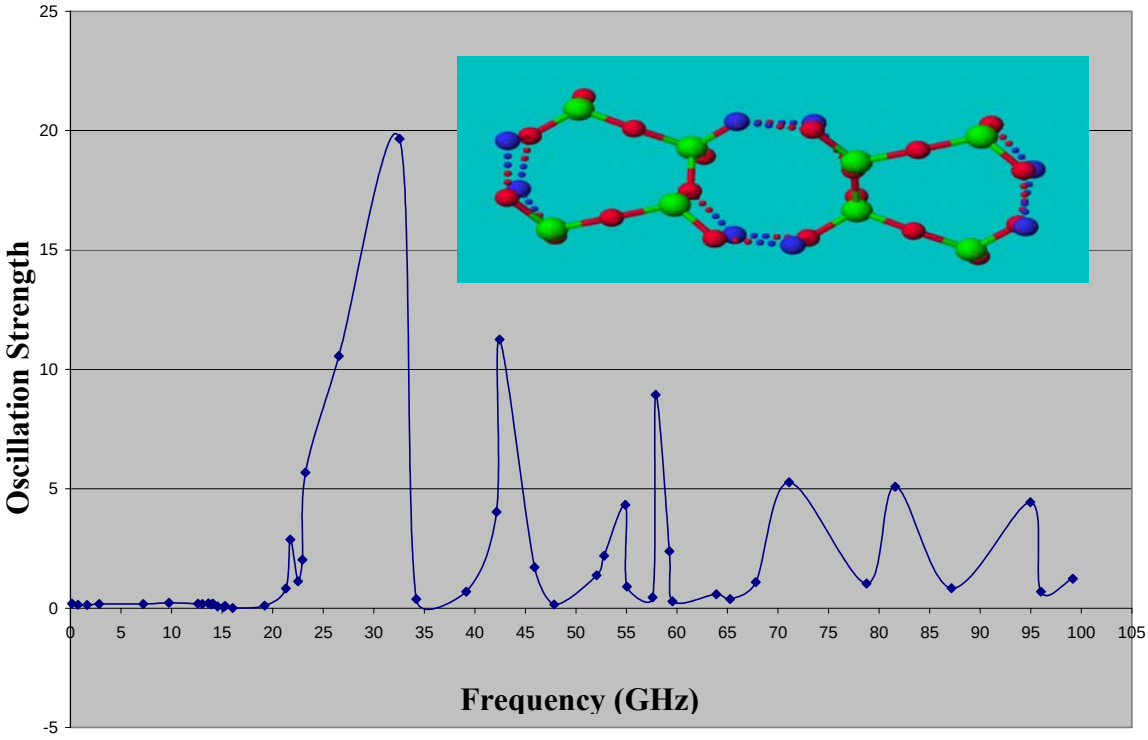

Figure 5.39: Molecular orbital theory calculation for LS_2 glass-ceramics
Note the absence of oscillators capable of absorbing microwave energy below 20 GHz.

LS_2 glass using hybrid heating at 2.45 GHz.

- The heating rate measurements for LS_2 glass and glass-ceramics at 2.45 GHz, 7 GHz and 18 GHz as shown in Figures 5.40 and 5.41.
- The reflected power measurement of LS_2 glass in the VFM cavity (cavity characterization) as shown in Figure 5.42
- The crystallization experiments of LS_2 glass in the VFM process at 6.425 GHz with 1 GHz band width (Figure 5.15)

As discussed earlier, using the dielectric measurement data at 2.46 GHz at room temperature, the D_p calculated values of LS_2 glass and glass-ceramic samples are much larger than the LS_2 samples' dimensions. As a result, the microwave absorption of the LS_2 glass sample under this condition will be very small; hence, LS_2 glass can only be crystallized by hybrid heating as demonstrated by other workers[30, 31].

The reflected microwave power in the cavity characterization experiment (Figure 5.42) of LS_2 glass in the VFM cavity was large (low microwave absorption) at 2.45 GHz (high intensity reflected power region) and started to decrease at 6 GHz (low intensity reflected power region). This is in agreement with the VFM crystallization experiment setup used to crystallize LS_2 glass.

The heating rate of LS_2 glass samples at 2.45 GHz (absence of strong oscillators) was slower than the heating rate of these samples at 7 GHz and 18 GHz, respectively, as shown in Figures 5.40 and 5.41. However, the heating rate of LS_2 glass at 18 GHz was faster than the one at 7GHz. The heating rate of LS_2 glass-ceramics samples was much slower than the heating rate of LS_2 glass samples over the tested frequencies. These heating rate observations were in agreement with the molecular orbital model calculations.

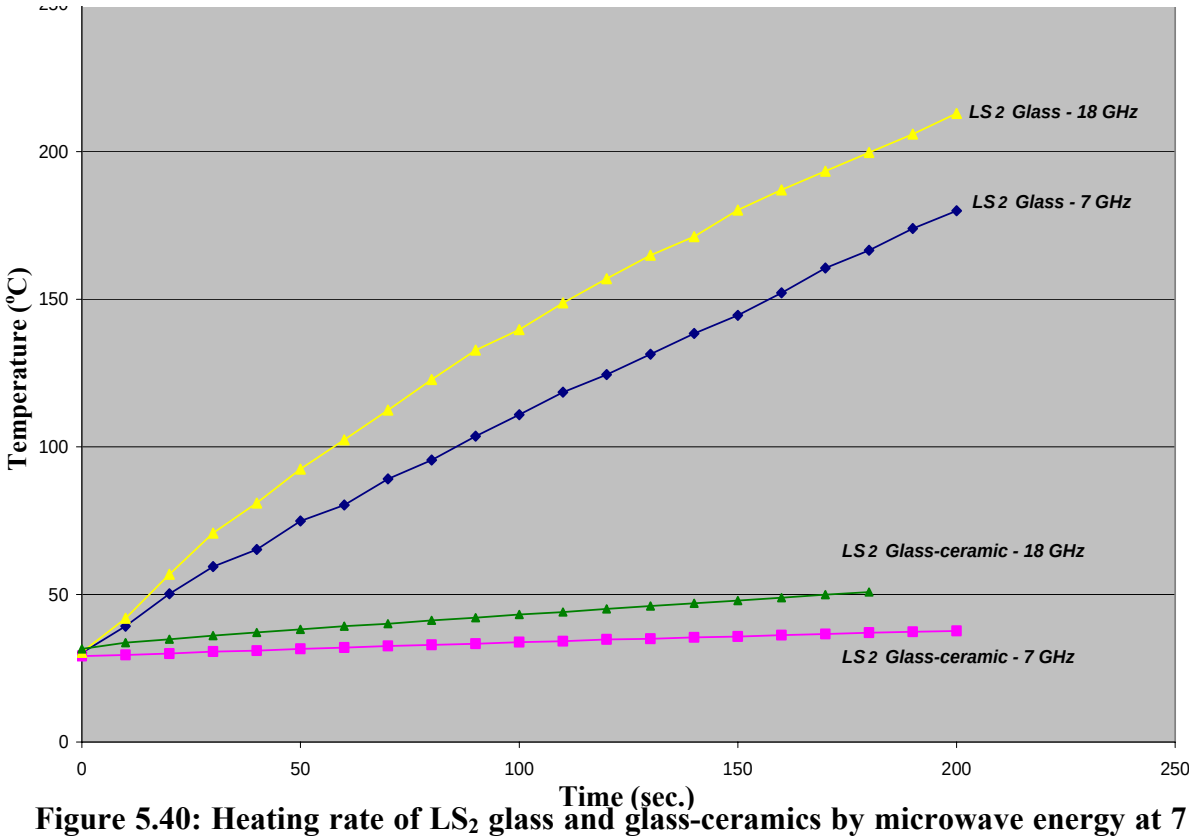

Figure 5.40: Heating rate of LS_2 glass and glass-ceramics by microwave energy at 7 and 18 GHz.

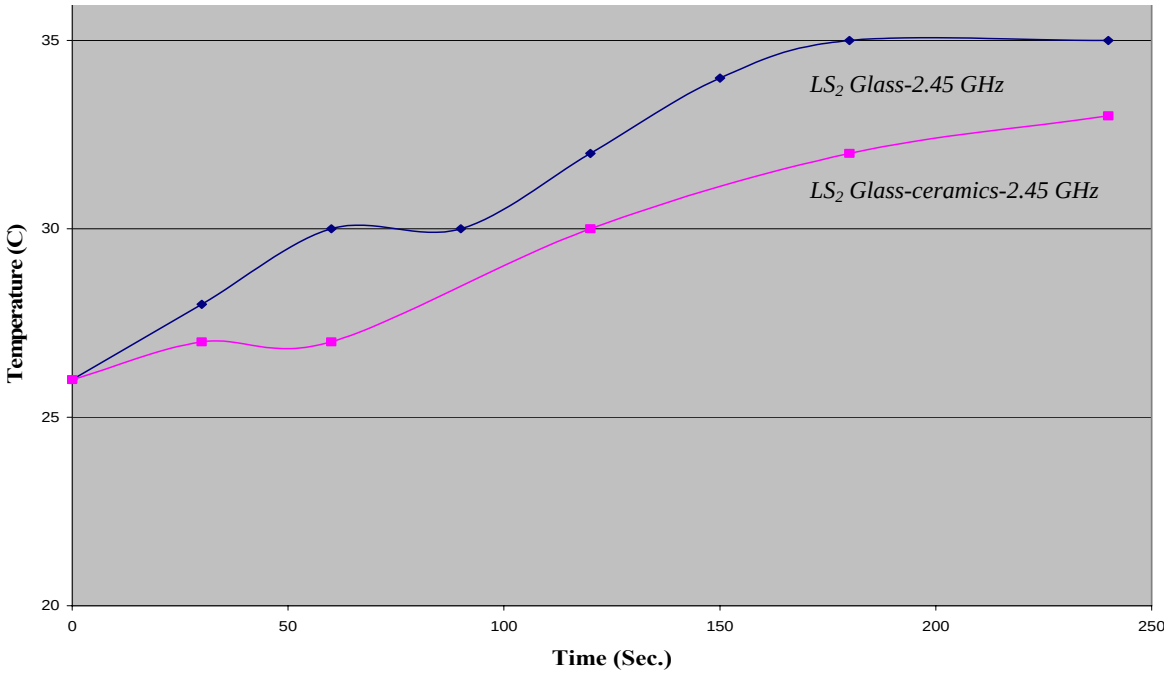

Figure 5.41: Heating rate of LS_2 glass and glass-ceramics by microwave energy at 2.45 GHz.

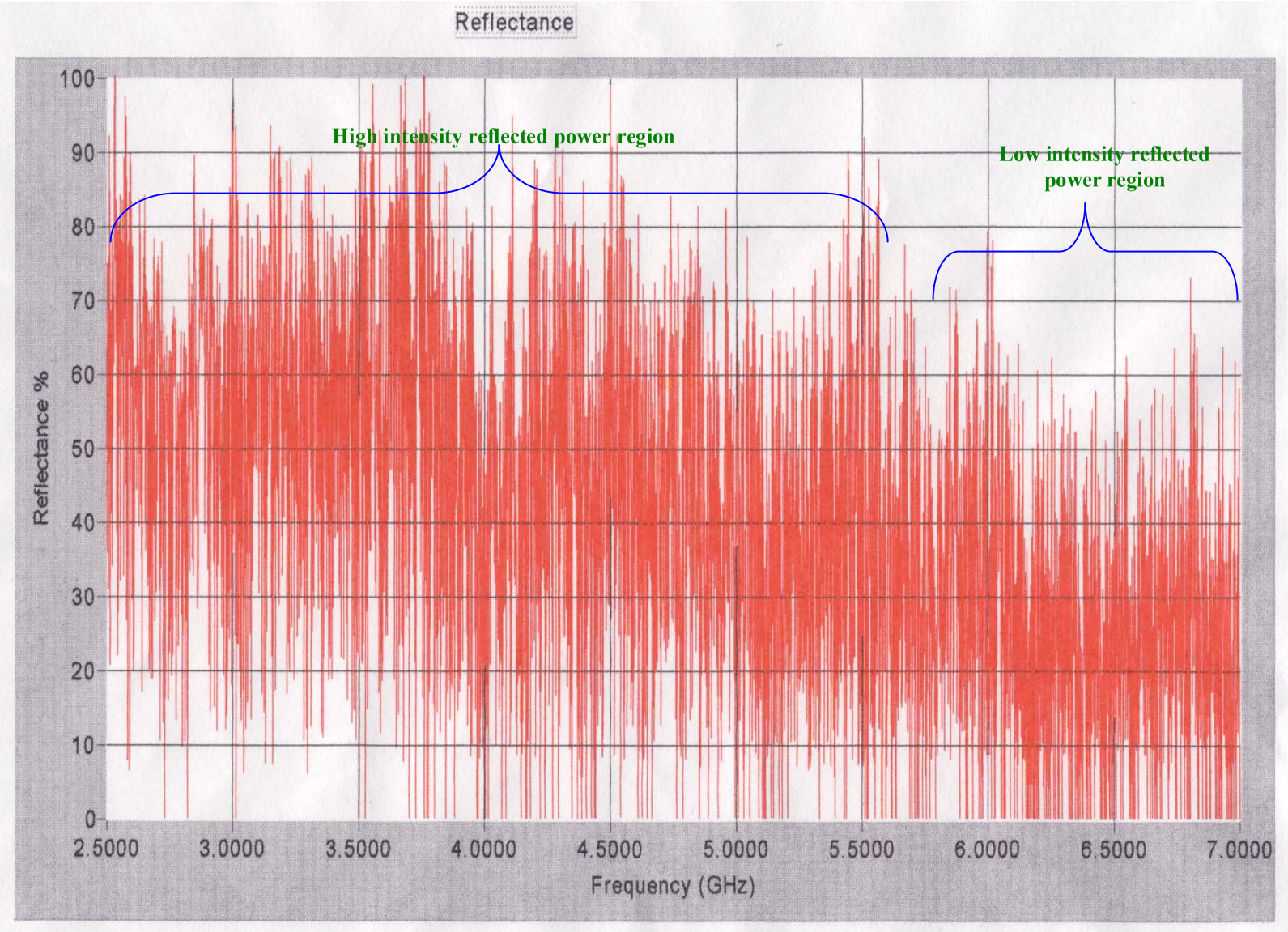

Figure 5.42: Reflected power characterization of LS_2 glass in VFM cavity. (Cavity characterization)

Finally, the heating rate in the VFM crystallization experiments (6.425 GHz, 1 GHz band width) of LS_2 glass, as shown in Figure 5.15, was in good agreement with the molecular orbital model. The treated LS_2 glass sample continued to absorb microwave energy (strong oscillators exist at this condition) until it crystallized and transformed into glass-ceramic (absence of strong oscillators at this condition). Consequently, there was a sudden drop in the heating rate and the microwave absorption even with full forwarded microwave power (The maximum power of the VFM instrument used- 250W).

5.9. FTIRRS of partially conventionally crystallized LS_2 glass.

As mentioned before, the nucleated LS_2 glass was heated at three different temperatures (567^{o}C, 583^{o}C and 595^{o}C) at different times. These temperatures were selected based on the DSC data of the annealed LS_2 bulk glass sample, as shown in Figure 5.1. These temperatures are just slightly below the onset of the crystal growth peak region (~600^{o}C) of the bulk glass. At these temperatures, the crystal growth rate is very slow compared to the crystal growth peak region. These temperatures' selection allows more control over the crystal growth rate and the ability to freeze and follow the crystallization advancement in LS_2 glass. The crystallization behavior of the LS_2 glass samples heat-treated conventionally at these selected temperatures will be presented and studied by the FTIRRS spectra in the following section.

a. FTIRRS of conventionally heat-treated LS_2 glass at 567^{o}C.

Figure 5.43 shows the FTIR spectra of LS_2 glass heat-treated conventionally at 567^{o}C for different times (15, 20, 30, 40, 50, 60, and 70 minutes) in comparison with the annealed and nucleated LS_2 glass. As can be seen from this Figure, the FTIR spectra of the heat-treated samples ranging from 15 to 60 minutes appear to have the same spectrum

as the annealed glass with a slight difference in the peak intensities located at 490 cm^{-1} and 760 cm^{-1}. The optical microscopy patterns for these glass samples are not the same, and they have different crystal sizes, as shown in the optical micrographs later (Section 5.10). It is concluded that the structural change that occurred in these heat-treated samples (small crystals size, ~100 μm) was detected by the FTIR peak intensity. The heat-treated sample at 567^{o}C for 70 minutes starts to have a slightly different FTIR pattern than the other treated samples and the annealed glass. The size and the numbers of the growing crystals in the 70 minute heat-treated sample start to affect the FTIR pattern. The IR band that was contributing to ($Si\text{-}O^{-}$) NB stretching at 930 cm^{-1} in the annealed glass sample was shifted to a higher wavelength (957 cm^{-1}) in the 70 minute heat-treated sample. In addition, the band at 1085 cm^{-1} (Si-O-Si asymmetric stretching) split into 2 bands (1055 cm^{-1} and 1111 cm^{-1}) in the same sample. Moreover, the intensity of the two bands at 764 cm^{-1} (Si-O-Si stretching) and at 490 cm^{-1} (O-Si-O Bending mode) increased by a significant amount. The evolution of a small band at 635 cm^{-1} was first seen at 70 minutes.

Figure 5.44 shows the FTIR spectra of conventionally heat-treated LS_2 glass at 567^{o}C for 70, 80, 90 and 100 minutes. As shown from the FTIR patterns, the crystallization of the LS_2 glass at 567^{o}C increases with increasing the heat treatment time from 70 minutes to 100 minutes. The assignment of the IR bands can be found in Table 5.11. In the 100-minute sample, the bands had not only increased in intensity and become more defined, but also a small shift in the 1055 cm^{-1} (as in 70 minutes sample) to a lower frequency (1041 cm^{-1}) was observed. A new weak band (589 cm^{-1}) corresponding to Si-O-Si symmetric stretching was observed in the sample that was treated for 100 minutes.

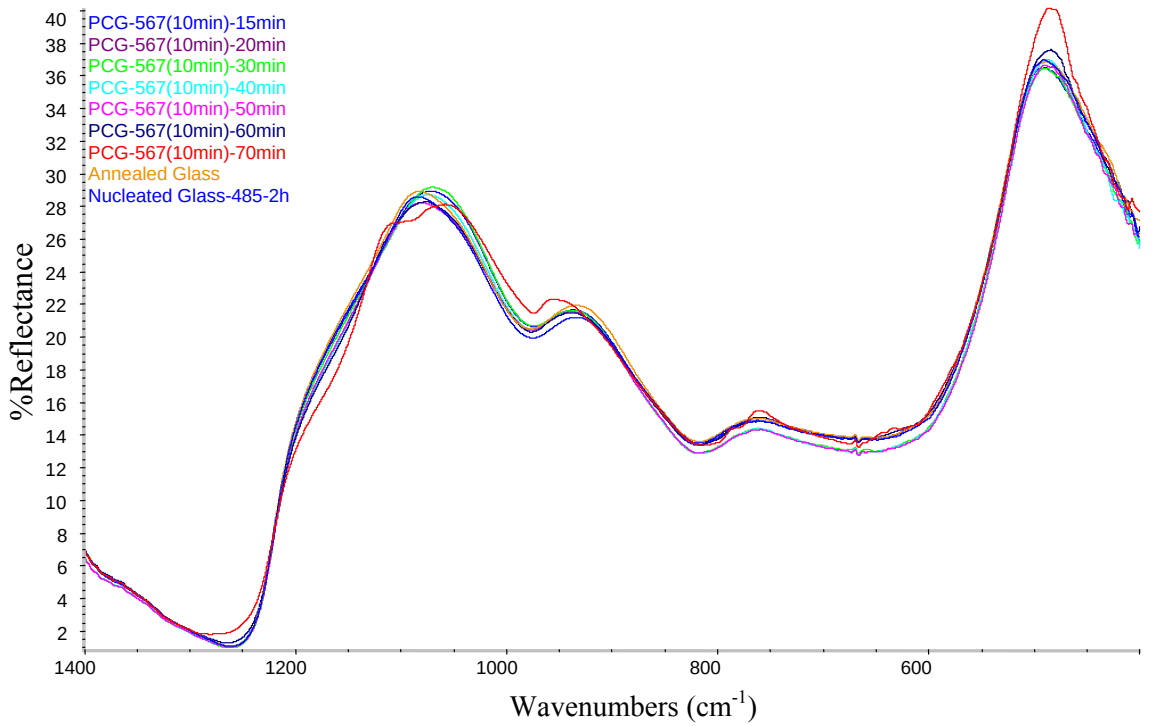

Figure 5.43: IR spectra of LS_2 glass heat-treated conventionally at 567°C at 15, 20, 30, 40, 50, 60 and 70 minutes. The base glass and the nucleated glass spectra are shown for comparison.

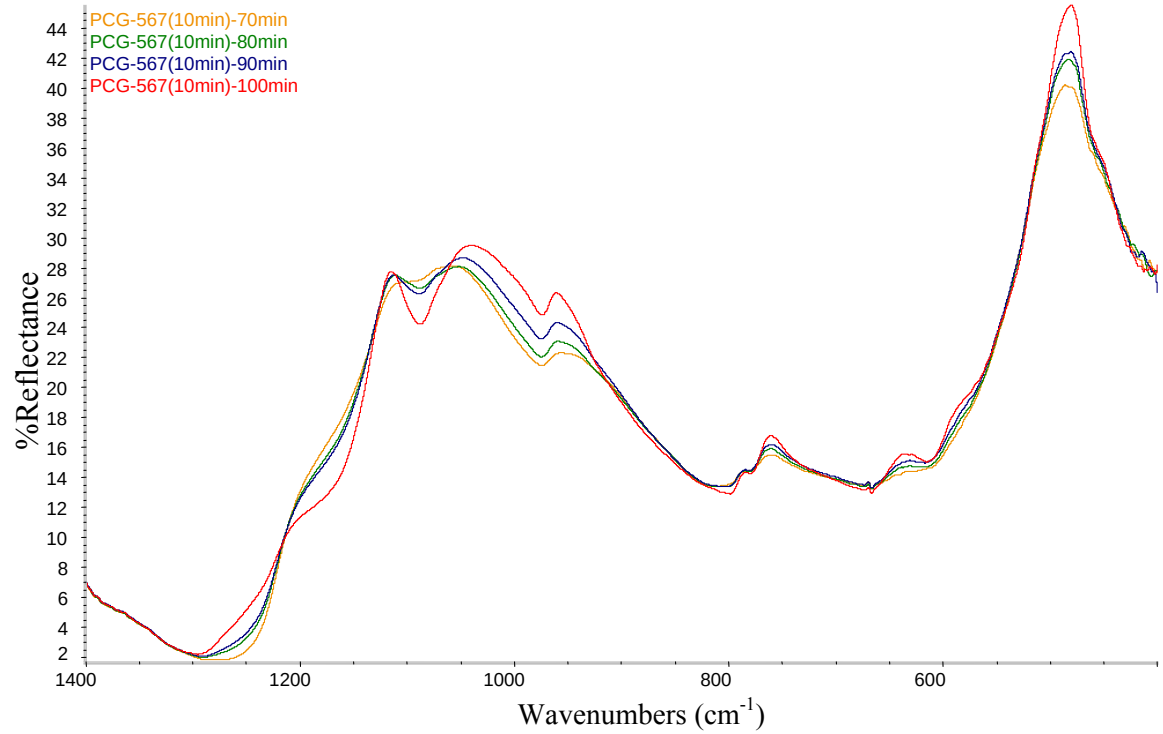

Figure 5.44: IR spectra of LS_2 glass heat-treated conventionally at 567°C at 70, 80, 90 and 100 minutes.

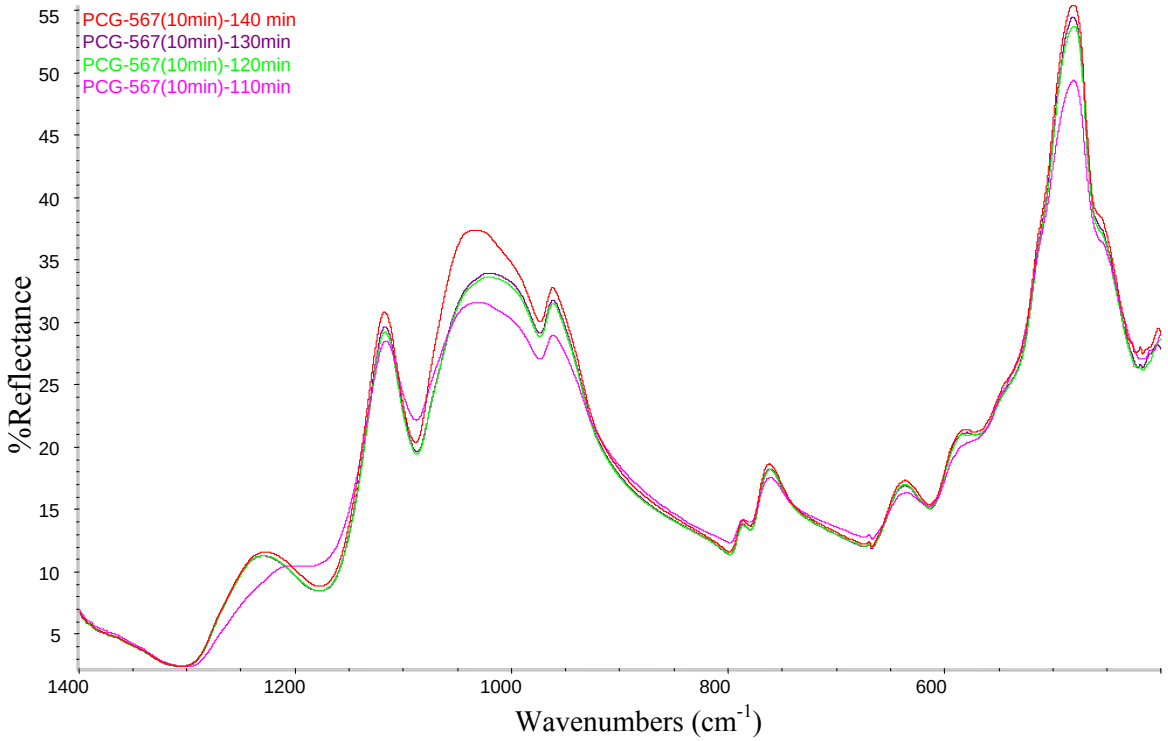

Figure 5.45: IR spectra of LS_2 glass heat-treated conventionally at 567°C at 110, 120, 130 and 140 minutes.

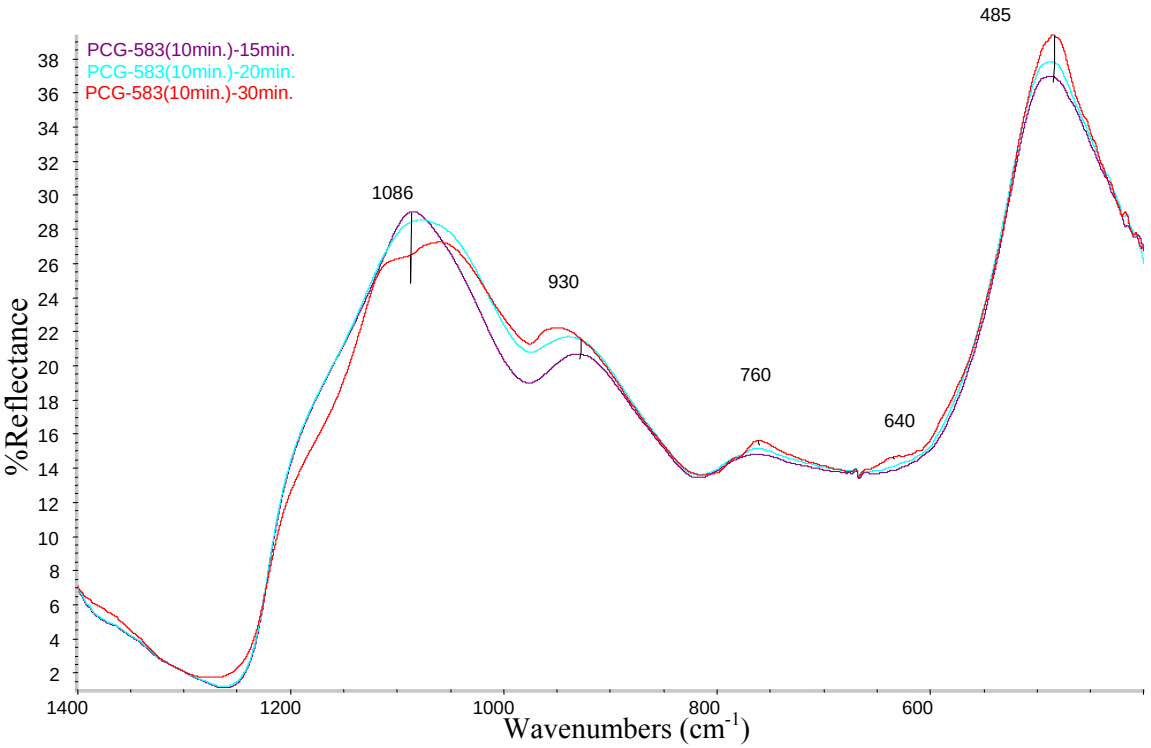

Figure 5.46: IR spectra of LS_2 glass heat-treated conventionally at 583°C at 15, 20 and 30 minutes.

Figure 5.45 shows the FTIR spectra of conventionally crystallized LS_2 glass samples at 567^{o}C for 110, 120, 130 and 140 minutes. The evolution of the two new bands at 1234 cm^{-1} and at 587 cm^{-1} that contribute to the $Si\text{-}O^{-}$ and Si-O-Si asymmetric stretching and to Si-O-Si symmetric stretching, respectively, was the main difference from the last set of samples. The intensities of the remaining bands continued to increase as the crystallization time increased, as seen before.

It is concluded that the peak positions and intensities of the FTIR spectra of LS_2 glass-ceramic samples are a function of the crystal size, volume fraction of crystals, heat treatment time and finally heat treatment temperature. This relation will be used for the correlation found in the present study between the peak intensities and the volume fraction of crystals of LS_2 glass-ceramics, as shown later in the stereology section.

b. FTIRRS of conventionally heat-treated LS_2 glass at 583^{o}C.

Figure 5.46 shows the FTIR spectra of conventionally heat-treated samples at 583^{o}C for 15, 20 and 30 minutes, respectively. The FTIR patterns of the heat-treated samples at 15 and 20 minutes look similar to the annealed LS_2 glass pattern. A slight difference in the peak intensities of these FTIR patterns was observed especially at 490 cm^{-1} and 760 cm^{-1} peak regions. Figure 5.47 shows the FTIR spectra of conventionally heat-treated samples for 35 and 40 minutes, respectively. The FTIR spectra of these two samples indicated that a major structural change occurred compared to the previously heat-treated samples for 15 to 30 minutes. As shown in Figure 5.63b, the picture of the 35 minute treated sample starts to scatter light more than the 30 minute treated sample, which still looks transparent. So this major structural change that occurred in this sample was detected by the FTIR spectra and observed visually as well. As shown in Figure 5.47,

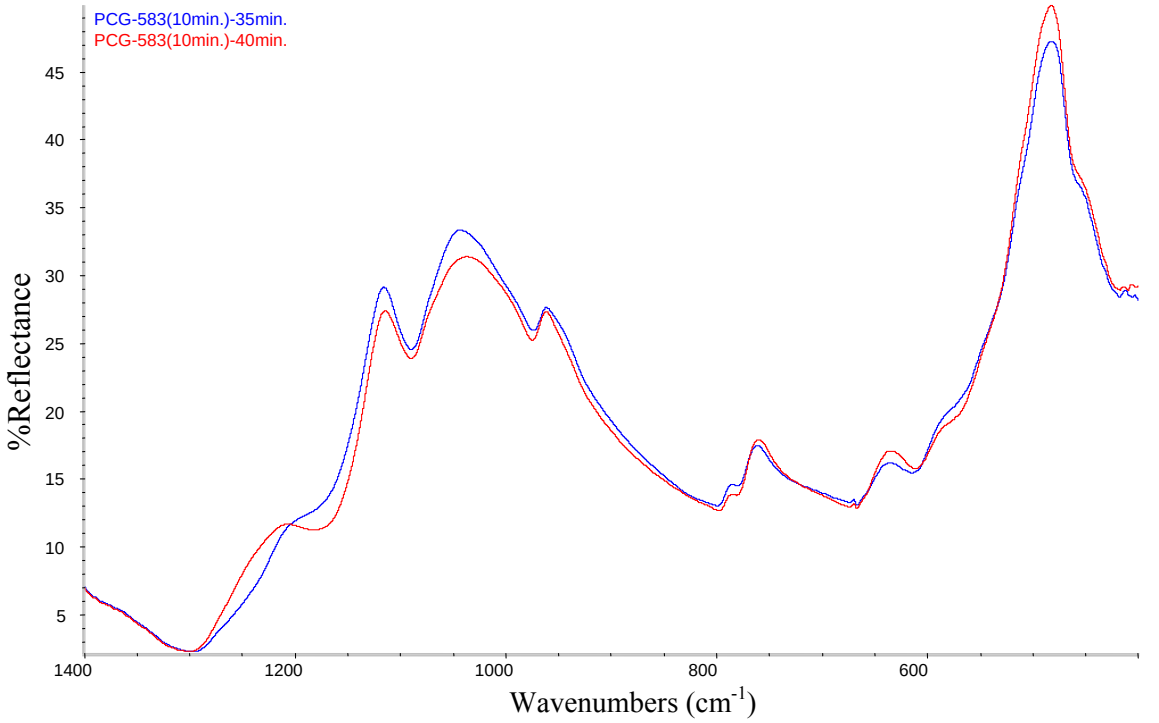

Figure 5.47: IR spectra of LS_2 glass heat-treated conventionally at 583°C at 30 and 40 minutes.

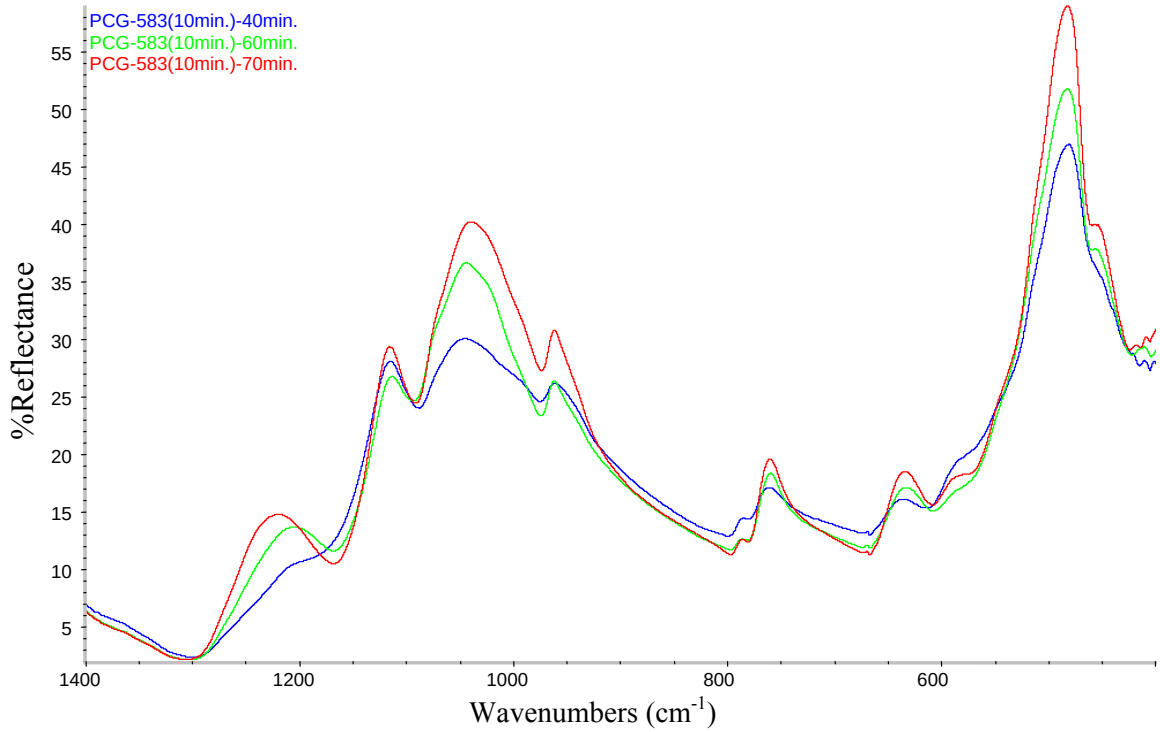

Figure 5.48: IR spectra of LS_2 glass heat-treated conventionally at 583°C at 40, 60 and 70 minutes.

the peak intensities of the FTIR spectra are a function of heat treatment time. Figure 5.48 shows the FTIR spectra of conventionally heat-treated samples for 40, 60 and 70 minutes respectively. The FTIR peak intensities increased as the heat treatment time increased.

In conclusion, the FTIR is very sensitive to the structural change that occurred in the crystallization process of LS_2 glass. As concluded before with the 567^oC treated samples and confirmed at the 583^oC treated samples, the FTIR peak intensities and positions are a function of the heat treatment time, heat treatment temperature, crystal size and volume fraction of crystals. Figures 5.49 and 5.50 show the effect of the heat treatment time on the FTIR peak intensity, measured at 490cm^{-1} and 760cm^{-1} respectively, of LS_2 glass samples heat treated at 583^oC. Both peak regions show the same trend as the heat treatment time increased.

c. FTIRRS of conventionally heat-treated LS_2 glass at 595^oC.

Figures 5.51 shows the FTIR spectra of LS_2 glass samples heat-treated conventionally at 595^oC for 10, 15, 20, and 30 minutes as compared with the base glass spectrum. Figure 5.52 shows the FTIR spectra of LS_2 conventionally heat-treated samples for 30, 35, and 40 minutes, while Figure 5.53 shows the FTIR spectra of the LS_2 heat-treated samples for 40 and 60 minutes. As shown in Figure 5.51, the FTIR pattern of the 30 minute heat-treated sample is totally different from the other heat-treated samples at 10,15, and 20 minutes. This structural change observed by the FTIR spectra matches the picture of the same samples in Figure 5.63c. This 30-minute heat-treated sample starts to scatter the light more than the other heat-treated samples at 10, 15, and 20 minutes. This observation corresponds with the one found in the 583^oC heat-treated sample, but at 35 minutes. This noticeable difference in the structure of the heat-treated LS_2 samples is

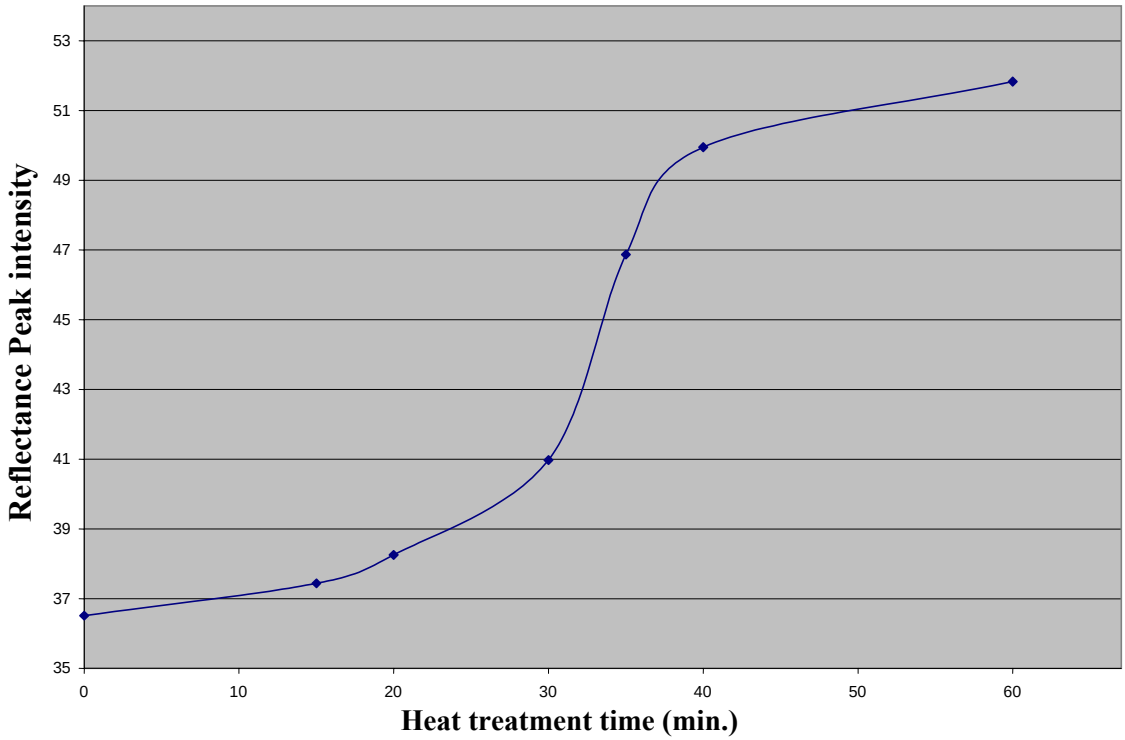

Figure 5.49: Peak intensity measurement of LS_2 glass heat-treated conventionally at 583^{o}C at different times (490 cm^{-1} peak region).

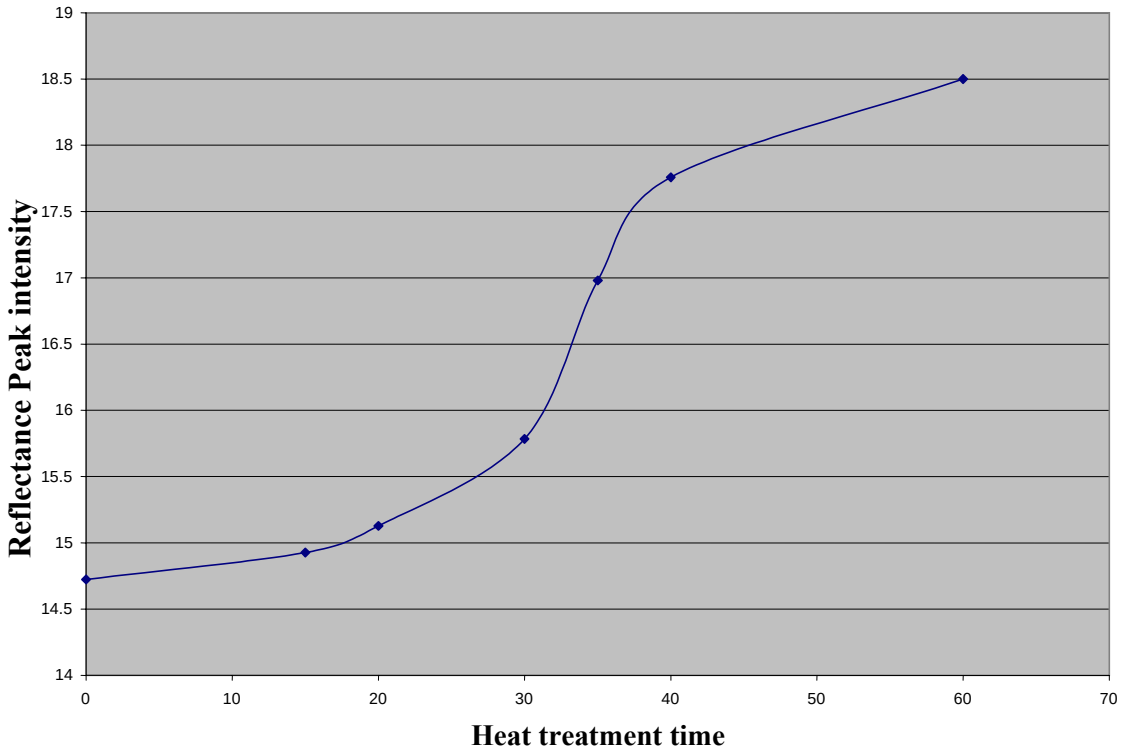

Figure 5.50: Peak intensity measurement of LS_2 glass heat-treated conventionally at 583^{o}C at different times (760 cm^{-1} peak region)

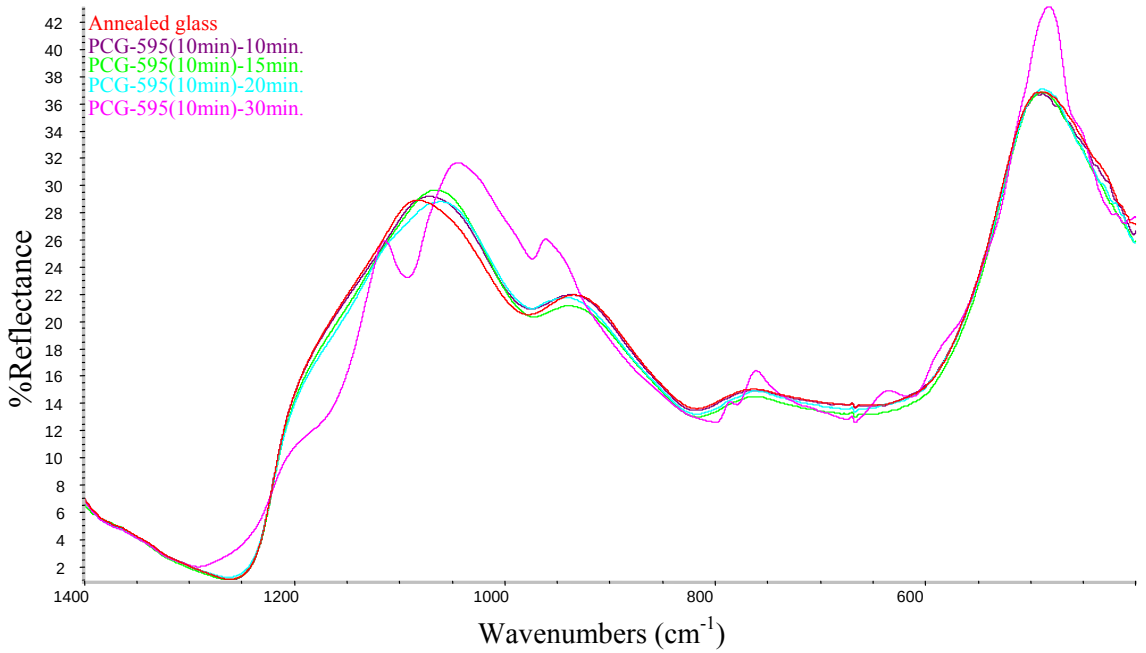

Figure 5.51: IR spectra of LS_2 glass heat-treated conventionally at 595°C at 10, 15, 20 and 30 minutes. The base glass spectrum is shown for comparison.

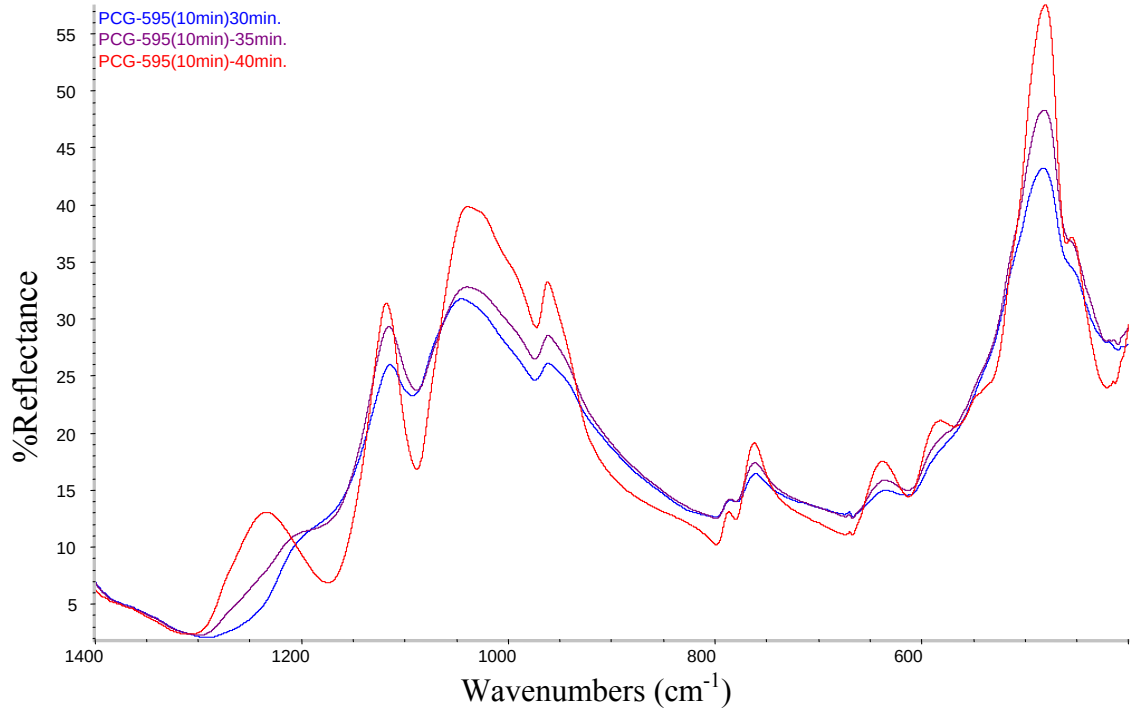

Figure 5.52: IR spectra of LS_2 glass heat-treated conventionally at 595°C at 30, 35 and 40 minutes.

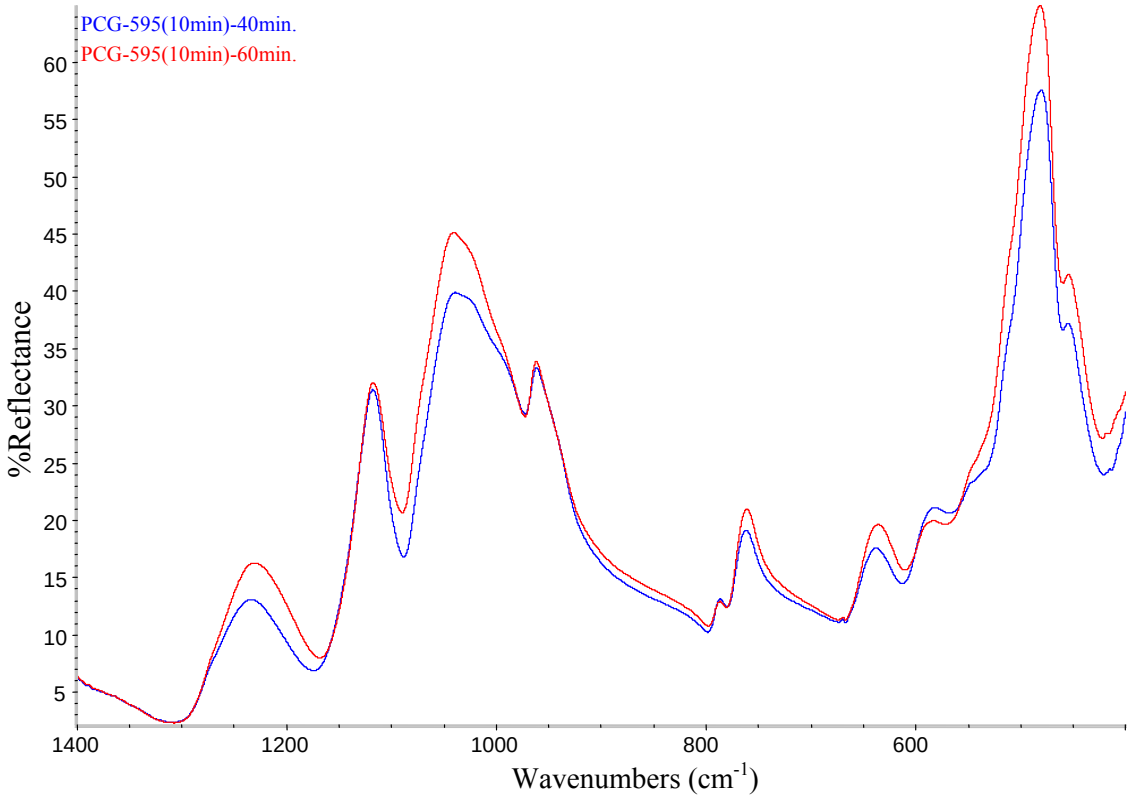

Figure 5.53: IR spectra of LS_2 glass heat-treated conventionally at 595°C at 40 and 60 minutes.

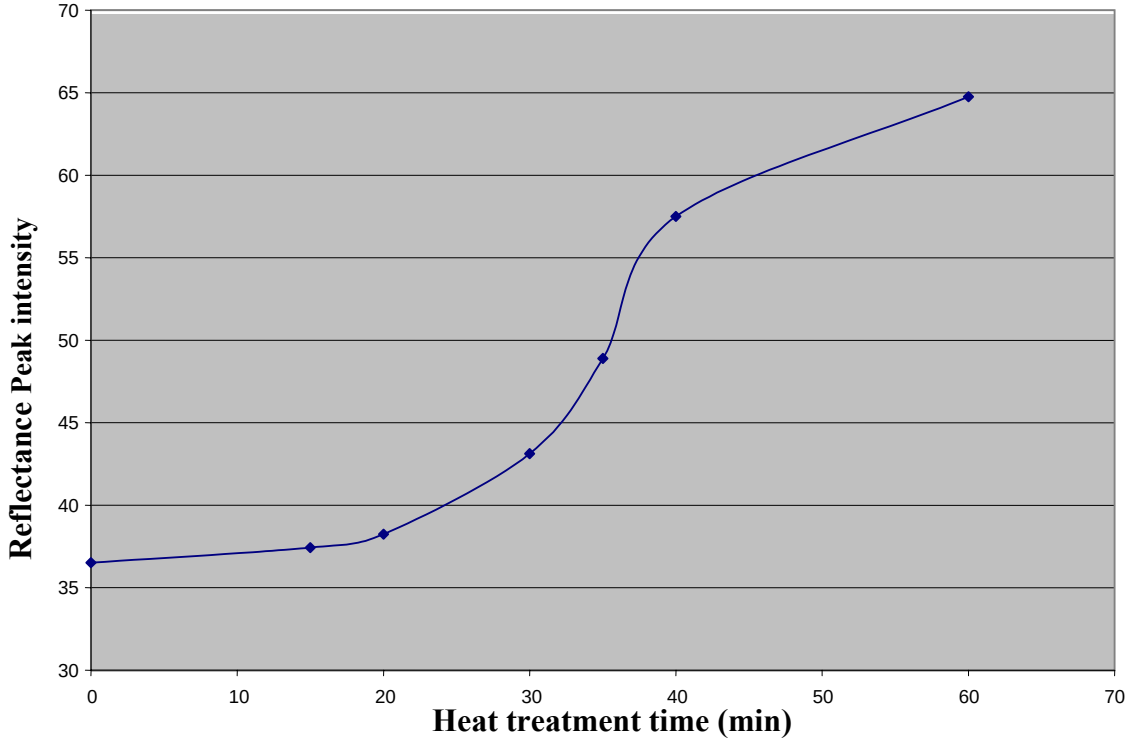

Figure 5.54: Peak intensity measurement of LS_2 glass samples heat-treated conventionally at 595°C at different times (490 cm^{-1} peak region)

observed when the volume fraction of crystals is around 49%-47%, as in Table 512 (583^{o}C, 35 min) and 5.13 (595^{o}C, 30 min) respectively. Thus, the first noticeable change in the sample color from transparent to white is an indication that the sample has approximately more than or equal to 50% volume fraction of crystals at a given temperature. On the other hand, this change in color does not mean that the sample has been fully crystallized. Therefore, the correlation between the FTIR peak intensity and the volume fraction of crystals of the LS_2 glass-ceramic samples is believed to be very important. This correlation could be vital in the quality-control process of a given glass-ceramic product. It is well known, the volume fraction of crystals of a given glass-ceramic product affects the properties and the performance of this product. Furthermore, the FTIR measurement is a non-destructive, easy to use, fast and well-established technique that can be easily performed by regular operators.

Figures 5.54 and 5.55 show the effect of the heat treatment time on the FTIR peak intensities, measured at 490 cm^{-1} and 760 cm^{-1} peak regions respectively, of LS_2 glass-ceramic samples heat-treated at 595^{o}C. It is apparent that the peak intensity increases as the heat treatment time increases.

Figures 5.56 and 5.57 show a comparison of peak intensity measurement of LS_2 glass samples heat-treated conventionally at 583^{o}C and 595^{o}C, measured at 760 cm^{-1} and at 490 cm^{-1} peak regions respectively. As shown from these Figures, a similar trend in both peak regions was observed in both temperatures. Moreover, the FTIR peak intensity is a function of heat treatment temperature and time. Below and at 20 minutes heat treatment time, the heat-treated samples at 583^{o}C and 595^{o}C had a very small peak intensity difference, as shown in Table 5.11 and 5.12 respectively. This difference starts

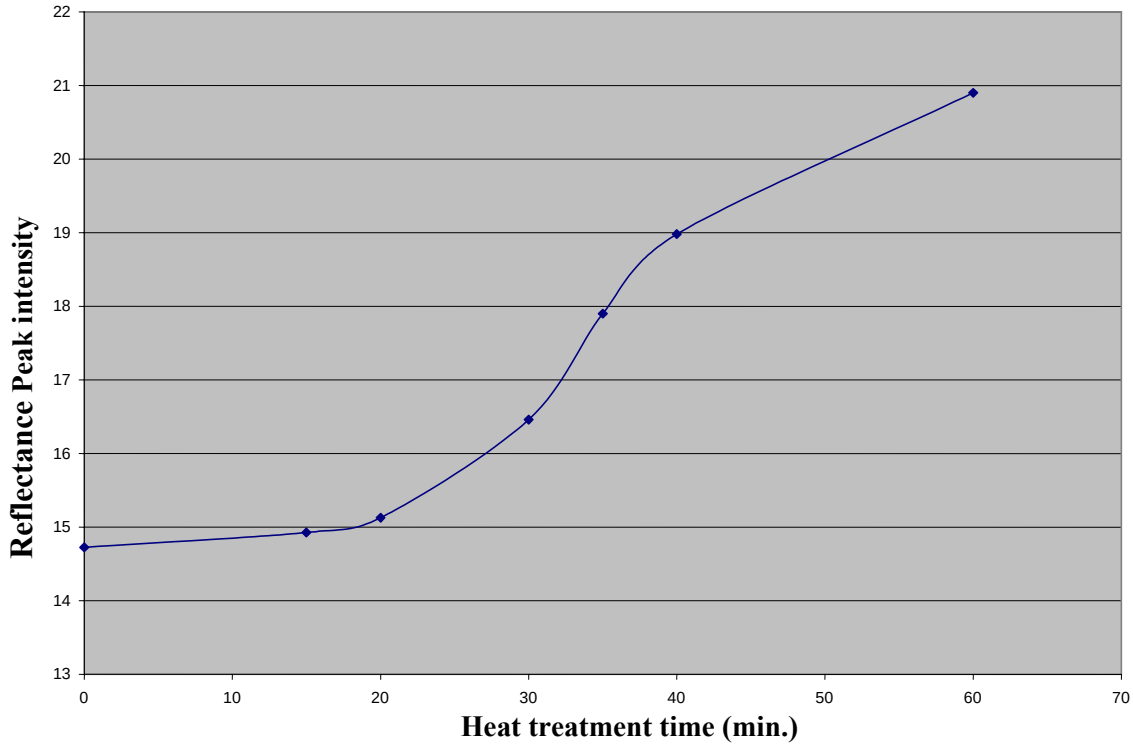

Figure 5.55: Peak intensity measurement of LS_2 glass samples heat-treated conventionally at 595^{o}C at different times (760 cm^{-1} peak region)

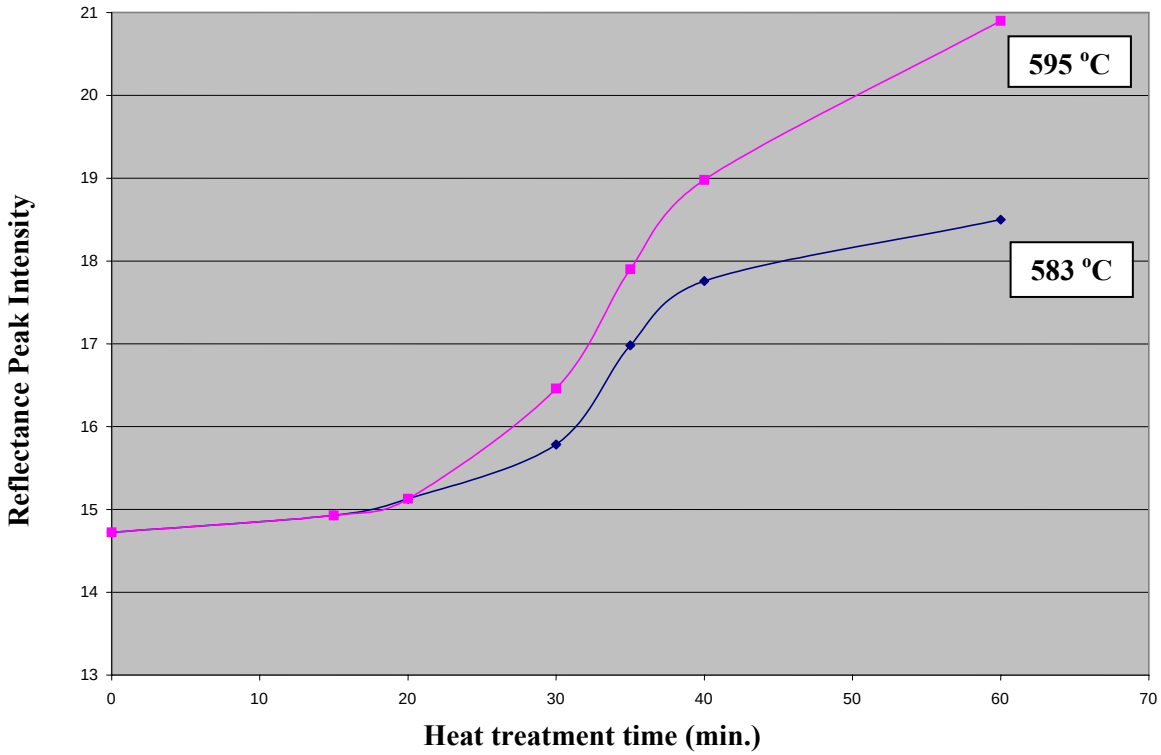

Figure 5.56: Comparison of peak intensity measurement of LS_2 glass samples heat-treated conventionally at 583^{o}C and 595^{o}C (760 cm^{-1} peak region).

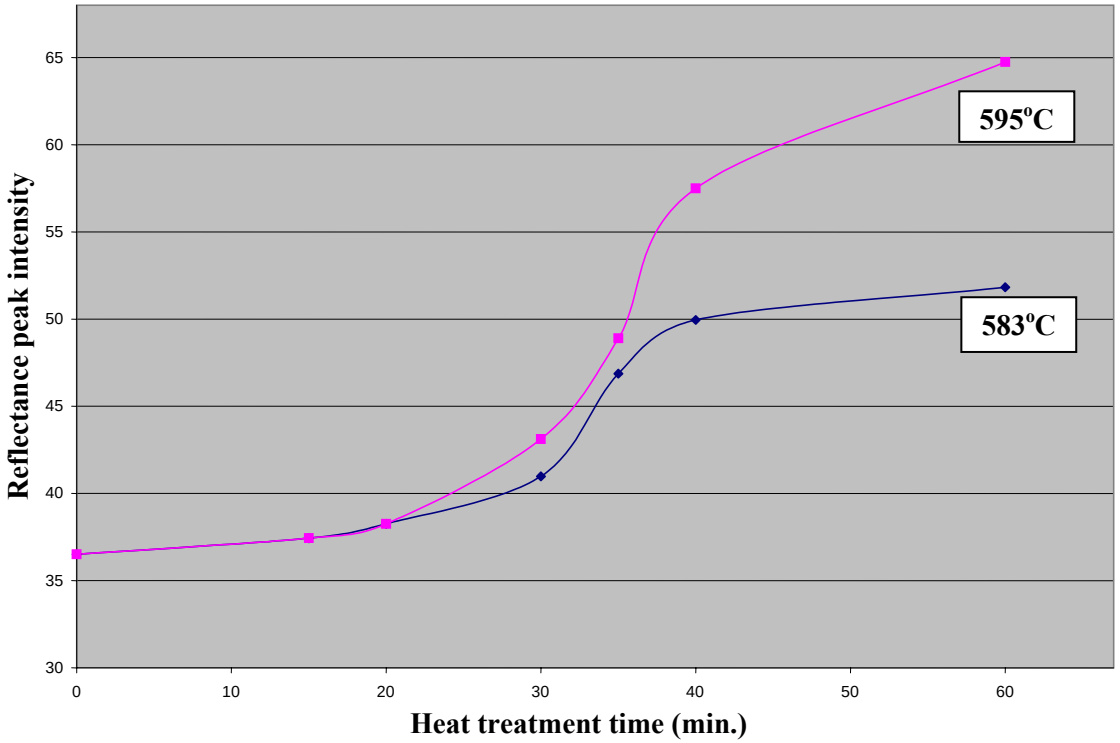

Figure 5.57: Comparison of peak intensity measurement of LS_2 glass samples heat-treated conventionally at 583°C and 595°C (490 cm^{-1} peak region).

to increase at or higher than the 30 minute heat treatment. Thus, the FTIR peak intensity is sensitive to the volume fraction of crystals change in LS_2 glass-ceramics samples.

5.10. Stereology measurement and optical microscopy data

As discussed earlier in the materials and experimental procedure section (chapter 4), the stereology measurement was used to estimate the volume faction of crystals (V_v) in the LS_2 glass-ceramics samples. A point count grid placed over a uniform, cross-sectional 2D image of this sample can estimate the volume fraction of a certain phase within a 3D sample. The number of points hitting the phase of interest was counted and divided over the total number of points in the grid, and as a result, a volume fraction of this phase was estimated.

A stereology measurement was performed on partially crystallized LS_2 glass-ceramics samples using both the VFM heating at 583^{o}C and conventional heating at 583^{o}C and 595^{o}C for different periods of time. The volume fraction of these partially crystallized LS_2 samples was calculated using a 400 point count grid stereology technique to ensure and to increase the precision of this measurement as discussed earlier (Section 4.5.3). Figure 5.58 shows the optical micrograph of a partially crystallized LS_2 sample at 583^{o}C for 30 minutes with the 400 point count grid. The volume fraction of crystals of this particular sample was calculated as 20% according to 80 points count found within the 400 point grid using the following calculation:

$$P_p = (80/400)*100 = 20 = V_v$$

As described before, for any given sample, the volume fraction of crystals was calculated at five different randomly selected micrographs of the same sample in order to represent the data statistically, as shown in Table 5.11. The standard precision is calculated using

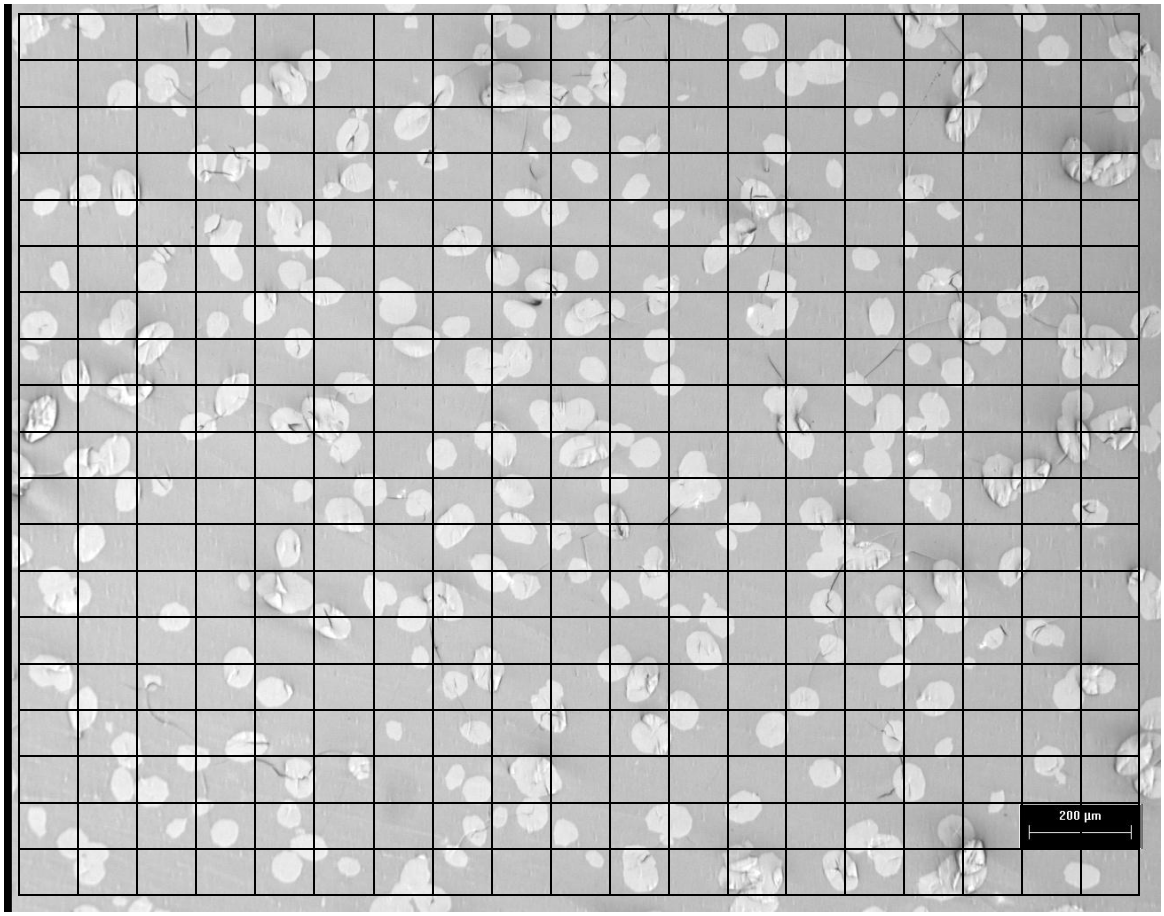

Figure 5.58: Point count micrograph of polished surface of conventionally crystallized LS_2 glass sample at 583°C-30 minutes-50x.

Table 5.11: Peak intensity, volume fraction of crystals and crystals aspect ratio of conventionally crystallized LS_2 samples at 583°C at different times.

Sample	490 cm^{-1} Peak Intensity	760 cm^{-1} Peak Intensity	Volume Fraction of Crystals	Standard Deviation	Standard Precision	Aspect Ratio	
						Min.	Max
Glass	35.9	14.7	0	0	0	0	0
583-15 min.	37.4	14.9	3	0.5	0.1	1	1.6
583-20 min.	38.3	15.1	13	1.5	0.4	1	1.6
583-30 min.	40.9	15.8	20	2.4	0.6	1	1.6
583-35 min.	47.2	17.3	49	2.6	0.7	1	1.6
583-40 min.	49.9	17.8	53	2.5	0.6	1	1.6

the following Equation[159]:

Standard Precision = (Standard deviation/ Total number of point count)*100 (5.1)

Table 5.11 shows the volume fraction of crystals measurements of LS_2 glass-ceramics samples, conventionally crystallized at 583^oC for 15, 20, 30, 35 and 40 minutes respectively, using the 400 point count technique. As shown from the table that the volume fraction of crystals increases as the heat treatment time increases at a constant given crystallization temperature. The aspect ratio of the LS_2 crystals in these samples was measured. A maximum aspect ratio value was found as 1.6, which corresponds to the typical ellipsoidal LS_2 crystal, as shown in Figures 5.19. The minimum aspect ratio value was found as one (1), which corresponds to the typical ellipsoidal LS_2 crystal that was cut in the middle and placed perpendicular to the plane of view, as shown in Figure 5.20.

The FTIR peak intensities at both 490 cm^{-1} and 760 cm^{-1} peak regions were measured of LS_2 glass-ceramics samples, conventionally crystallized at 583^oC for 15, 20, 30, 35, and 40 minutes respectively. The FTIR peak intensity measurement was performed for the annealed LS_2 glass at the same peak regions. Figure 5.59 shows the correlation between the FTIR peak intensity, at both 490 cm^{-1} and 760 cm^{-1} peak regions, respectively, and the volume fraction of crystals of the conventionally crystallized LS_2 samples at 583^oC.

This correlation can be used to estimate the crystals volume fraction of a given sample by its FTIR peak intensity. The correlation offers some advantages over other well- known techniques (such as XRD and Stereology) to estimate the volume fraction of crystals in a given glass-ceramic material by its FTIR peak intensity. For example, stereology requires qualified operators with an adequate basic knowledge of the

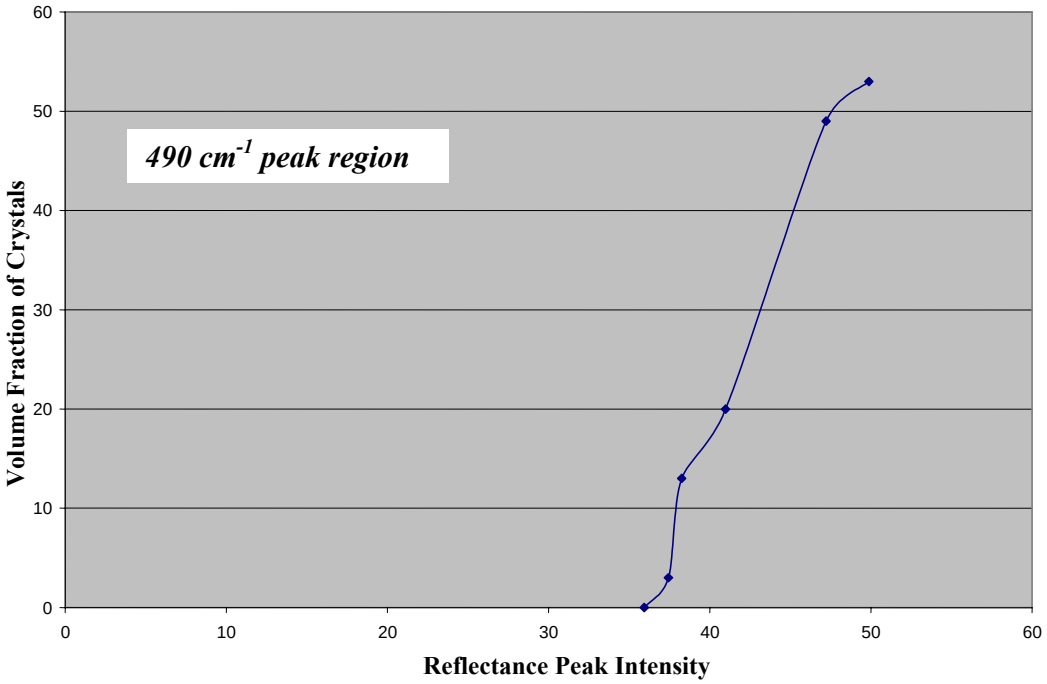

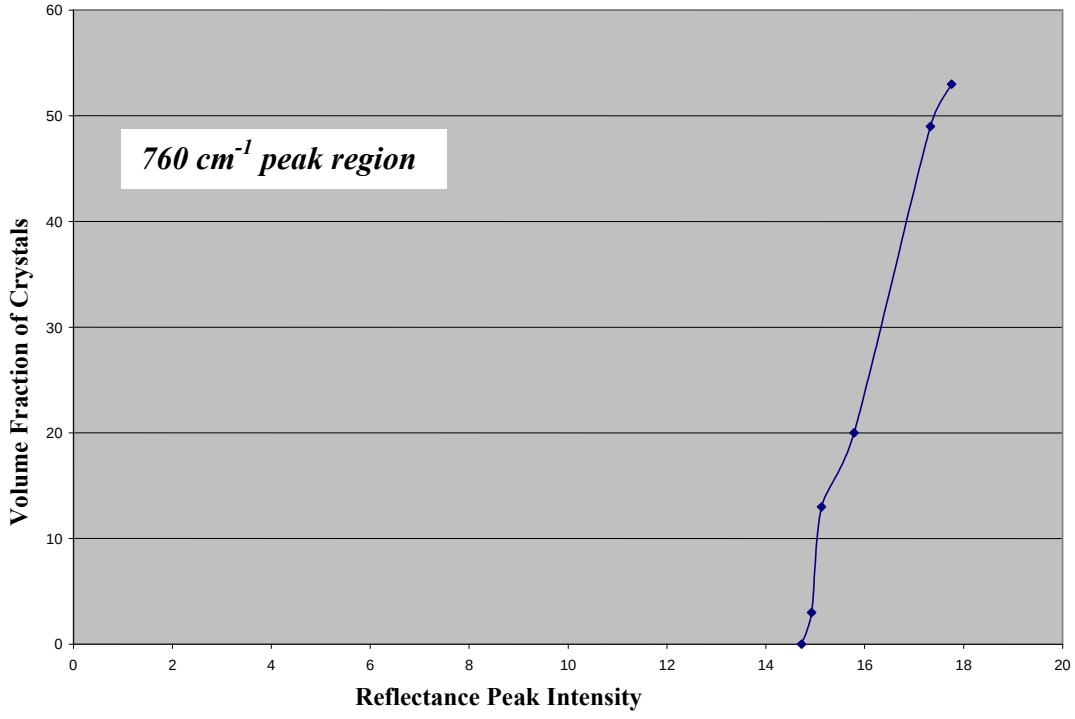

Figure 5.59: Correlation between the peak intensity and the volume fraction of crystals of conventionally crystallized LS_2 glass heat-treated at 583°C at 490 cm^{-1} and at 760 cm^{-1} peak regions.

technique in order to estimate the volume fraction of crystals in a given sample. Moreover, it is a time-consuming technique. Furthermore, XRD is a destructive technique that also needs qualified persons to operate the machine and to interpret the data. On the contrary, FTIR is a fast and easy to use technique. It is a finger print of the sample and it is a non destructive technique. FTIR is a precise measurement method requiring no external calibration, and it is well established. Finally it does not require sophisticated sample preparation. In general, this correlation could be produced by qualified persons and then used by regular workers in a given industry. Thus, the correlation could be used in quality control of the glass-ceramics industry.

Figure 5.60 shows the 400 point grid stereology measurement for LS_2 glass sample, conventionally crystallized at 595^{o}C for 15 minutes. Table 5.12 shows the volume fraction of crystals measurement by point count technique of LS_2 glass-ceramics samples, conventionally crystallized at 595^{o}C for 15, 20, 30, 35, and 40 minutes. As shown from the Figure that the heat-treated samples at 595^{o}C had a higher volume fraction of crystals than the heat-treated samples at 583^{o}C at the same period of time. This observation is in agreement with the kinetic theory of glass formation and the DSC data. The FTIR peak intensities measurements of the same samples at both the 490 cm^{-1} and 760 cm^{-1} peak regions are shown in the same Table. The maximum aspect ratio of the LS_2 crystals in the heat-treated samples, at 595^{o}C, was found as 1.6 and one (1) as a minimum value. These aspect ratio values were similar to the ones observed in the heat-treated samples at 583^{o}C. Figure 5.61 shows the correlation between the FTIR peak intensities, at 490cm^{-1} and 760 cm^{-1} peak regions respectively, and the volume fraction of crystals of the conventionally crystallized LS_2 glass-ceramics samples at 595^{o}C. Thus, the

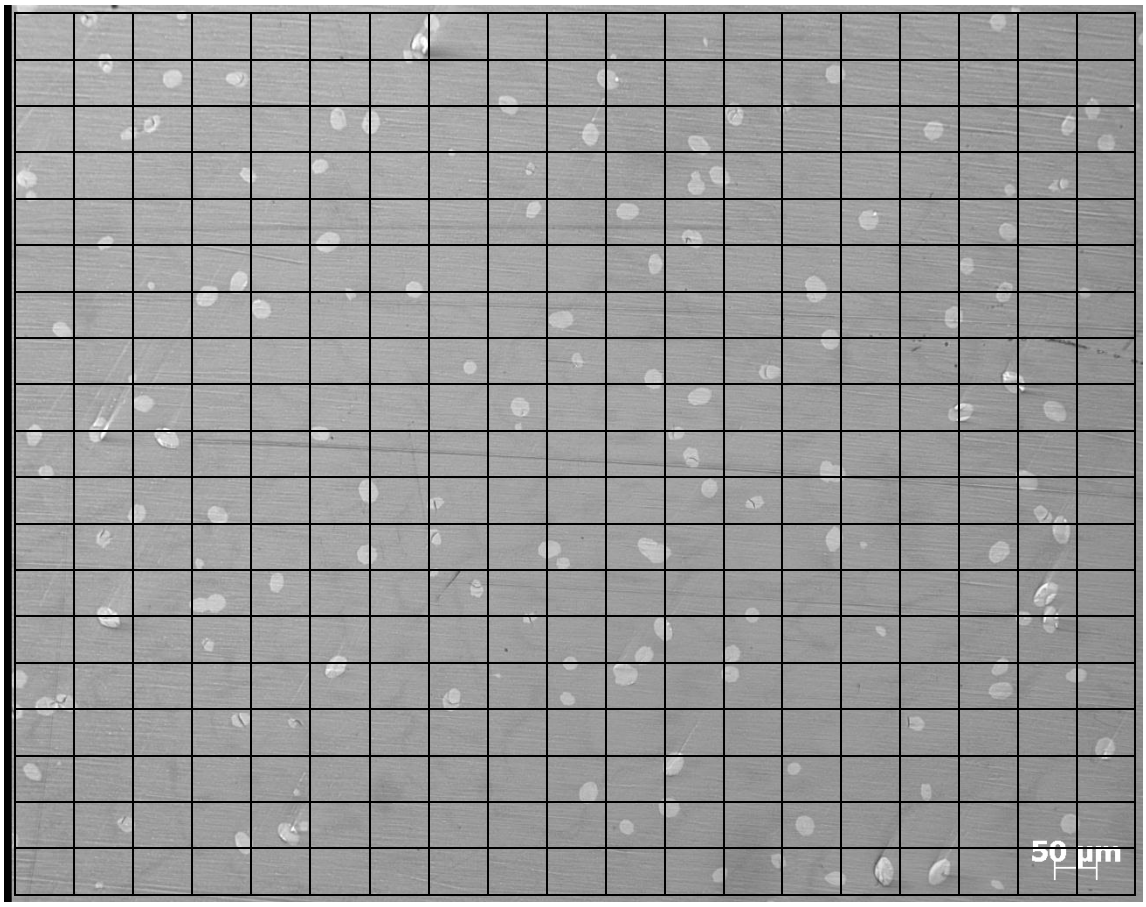

Figure 5.60: Point count micrograph of polished surface of conventionally crystallized LS_2 glass sample heat-treated at 595°C-15 minutes-50x.

Table 5.12: Peak intensity, volume fraction of crystals and crystals aspect ratio of conventionally crystallized LS_2 sample heat-treated at 595°C at different times.

Sample	490 cm^{-1} Peak Intensity	760 cm^{-1} Peak Intensity	Volume Fraction of Crystals	Standard Deviation	Standard Precision	Aspect Ratio	
						Min.	Max
Glass	35.9	14.7	0	0	0	0	0
595-15 min.	37.4	14.9	6	0.9	0.2	1	1.6
595-20 min.	38.3	15.1	23	2.3	0.6	1	1.6
595-30 min.	43.12	16.46	47	2.5	0.6	1	1.6
595-35 min.	48.9	17.9	55	2.6	0.7	1	1.6
595-40 min.	57.5	18.98	64	2.4	0.6	1	1.6

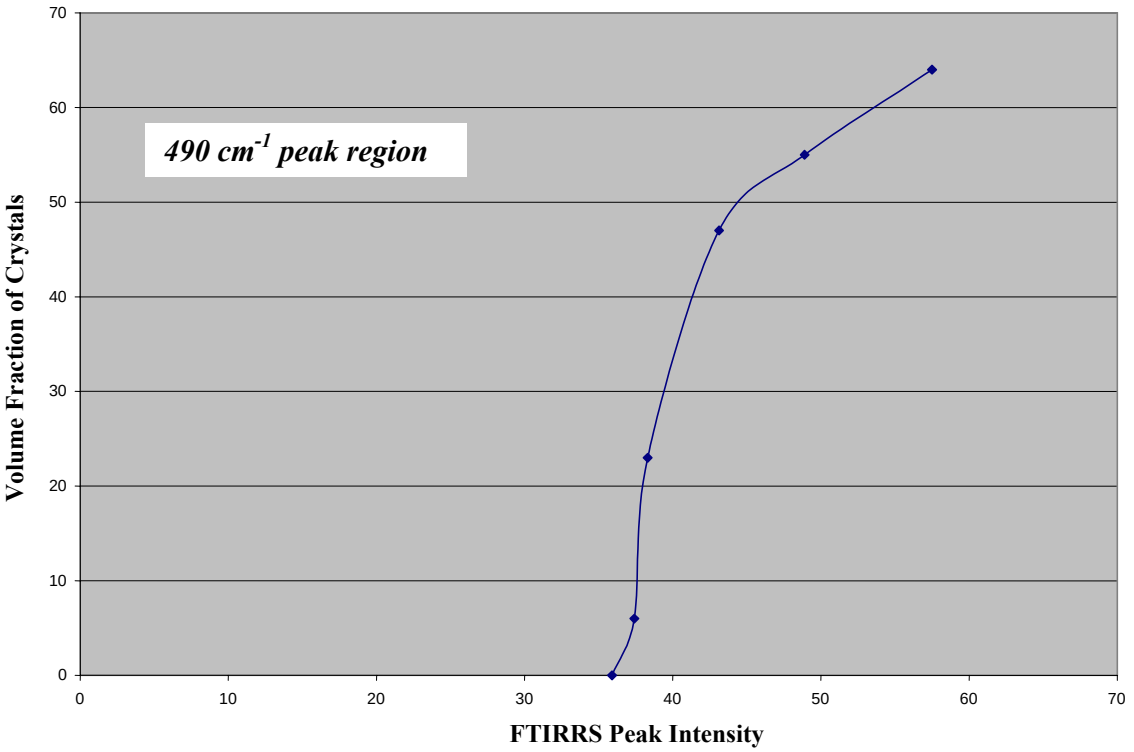

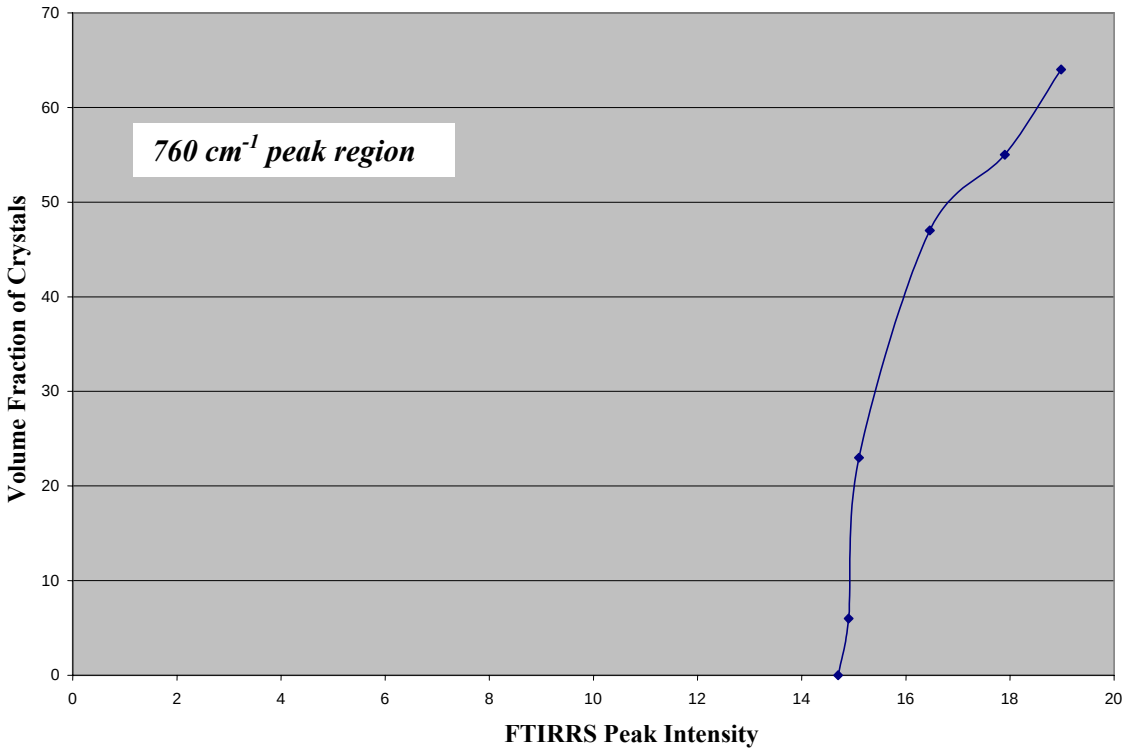

Figure 5.61: Correlation between the peak intensity and the volume fraction of crystals of conventionally crystallized LS_2 glass-ceramics sample at 595°C, at 490 cm^{-1} and at 760 cm^{-1} peak regions.

peak intensities and the volume fraction of crystals depend on both the heat treatment time and temperature.

Figure 5.62 shows pictures of LS_2 glass samples partially crystallized at different periods of time, either by conventional heating at 567^{o}C, 583^{o}C and 595^{o}C, or by VFM heating at 583^{o}C. At 567^{o}C, the heat-treated sample starts to scatter the light at 100 minutes. Meanwhile, at 583^{o}C, the heat-treated sample starts to scatter the light at 35 minutes. At 595^{o}C, scattering of the light occurs by the sample that was heat-treated at 30 minutes. The volume fraction of crystals in all these samples was estimated to be ~ 50%, based on the scattering of light observation, as discussed earlier. Furthermore, the volume fraction of crystals increases as the heat treatment temperature increases from 567^{o}C to 595^{o}C. This trend is in agreement with the kinetic theory of glass formation as well as the DSC data of the bulk LS_2 glass. As discussed earlier (Section 5.1), because these temperatures are just below the onset of the crystal growth peak (~600^{o}C), the crystal growth rate at these temperatures is very slow compared to the ones at the maximum crystal growth rate (T_c). Thus the abnormal, fast-crystallization behavior of LS_2 glass sample in the VFM process (~600^{o}C, 2 min), which can not be explained by either the kinetic theory of glass formation or the DSC data of LS_2 bulk glass, is a strong evidence for the existence of the microwave effect in the VFM crystallization process.

On the other hand, the trend observed in the picture of the VFM heat-treated samples at 583^{o}C for 20, 30, 40 and 50 minutes is not consistent with the microwave effect observation. Furthermore, this picture shows that the crystal growth rate in the VFM process at this temperature is slower than the one observed in conventional heating. The visual appearance of this set of samples indicates that the volume fraction of crystals

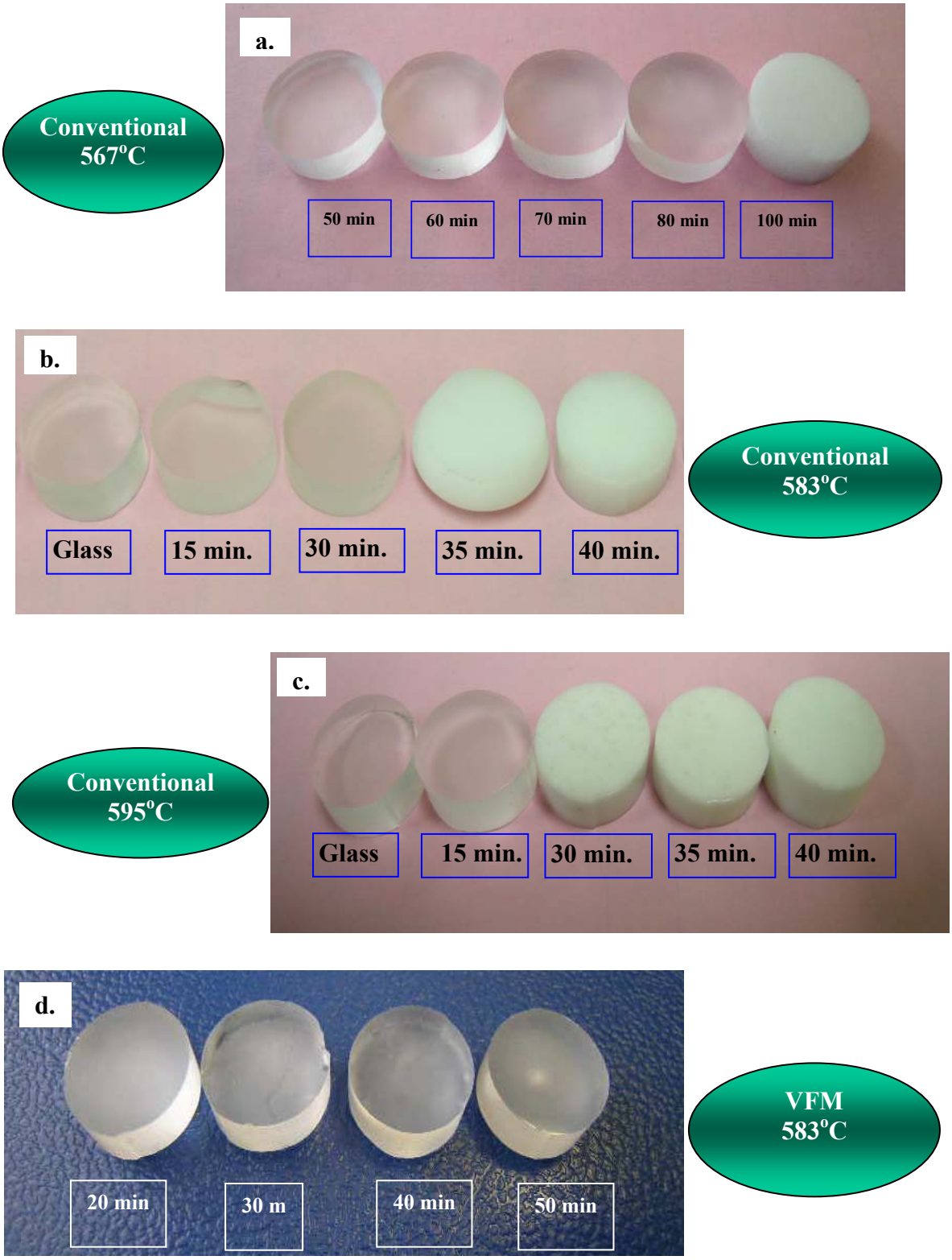

Figure 5.62: Partially crystallized LS_2 glass samples crystallized:
a, b, c: Conventionally at 567°C, 583°C and 595°C respectively for different periods of time.
d: VFM at 583°C for different periods of time.

in these samples is estimated to be below ~50%, and as a result, it does not scatter the light, even at 50 minutes heat treatment time. The volume fraction of crystals of this 50 minute sample was measured as 29% using stereology. On the other hand, the conventionally treated sample at the same temperature starts to scatters light at 35 minutes with a V_v = 49%. Figure 5.63 shows the 400 point count stereology micrograph of this VFM crystallized sample (583^{o}C, 50 minutes). The stereology measurement of this set of VFM crystallized samples is shown in Table 5.13. The volume fraction of crystals measurement of these VFM samples is in agreement with the visual appearance of the samples. The aspect ratio of the LS_2 crystals in these crystallized samples is shown in Table 5.13. The aspect ratio of the LS_2 crystals in these VFM treated samples is similar to the one observed in the conventionally heat-treated samples (with a maximum value as 1.6 and a minimum as one (1)), as confirmed by SEM (Figure 5.21). On the other hand, the volume fraction of crystals values in these VFM crystallized samples at 583^{o}C indicate that the kinetics are slower in these samples than the corresponding samples crystallized conventionally at the same temperature. The two possible explanations for this contradiction might be:

1- The microwave effect exists at a certain temperature range and does not exist below this range. If this assumption is true, the volume fraction of crystals of these VFM crystallized samples should be at least similar to the one observed in the conventionally crystallized samples at the same temperature, and not lower as was observed.

2- The VFM process retards the kinetics of LS_2 crystallization at this specific temperature (583^{o}C). Some researchers[195-200] reported that an external electric filed could retard or enhance phase separation in some glass systems based on the composition. On the

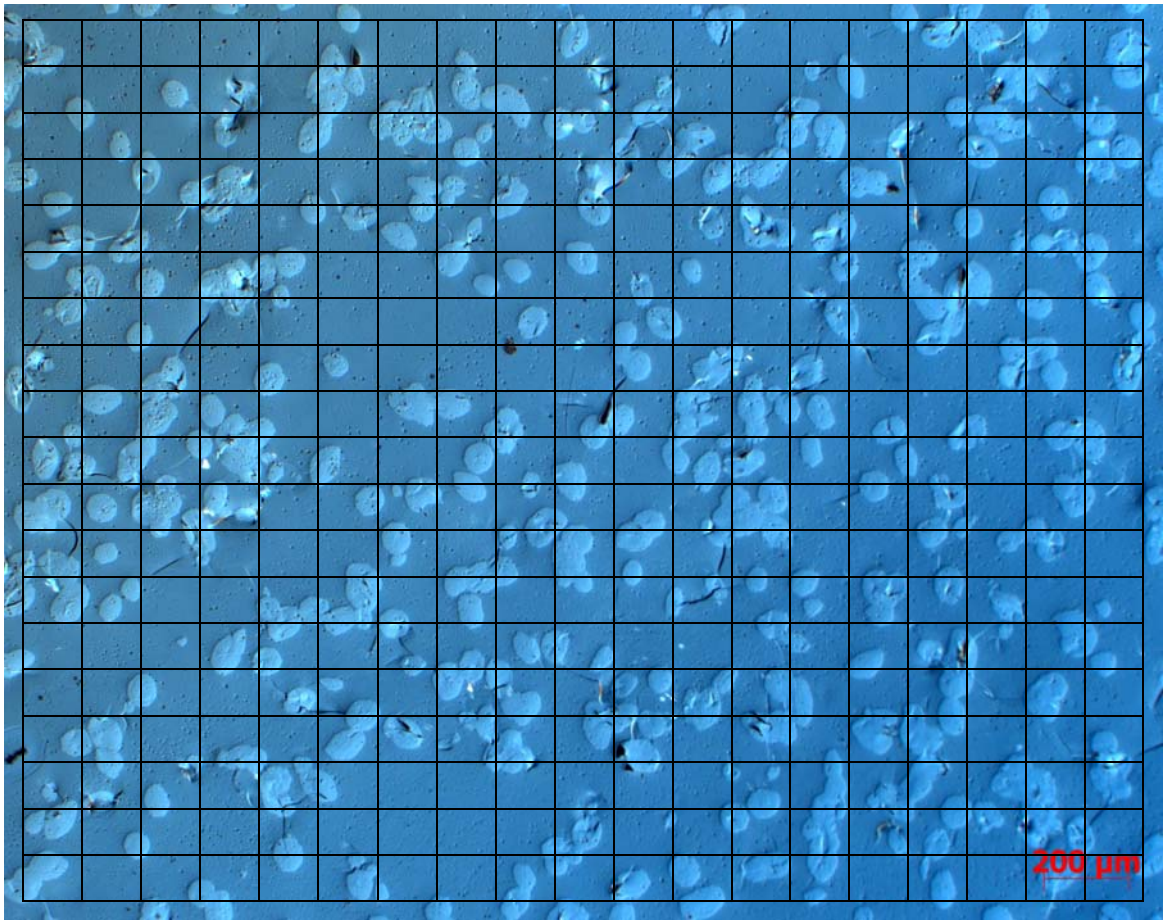

Figure 5.63: Point count micrograph of polished surface of VFM partially crystallized LS_2 glass sample heat-treated at 583°C-50 minutes-50x.

Table 5.13: Volume fraction of crystals and crystals aspect ratio of VFM partially crystallized LS_2 sample heat-treated at 583°C at different times.

Sample	Volume Fraction of Crystals (%)	Standard Deviation	Standard Precision	Aspect Ratio	
				Min.	Max.
583-30 minutes	5	0.5	0.1	1	1.6
583-50 minutes	29	3.1	0.8	1	1.6
583-60 minutes	37	2.9	0.7	1	1.6
583-80 minutes	58	2.6	0.7	1	1.6

other hand, the composition of the 583°C VFM treated samples is similar to the other ones treated at ~600°C by VFM process, which posses the highest kinetics (Figure 5.64). Furthermore, this retarding assumption is contradicting with the data published on the same glass at 2.45 GHz by Boonyapiwat (figure1.4b)[30].

3- In the VFM process, if this specific temperature (583°C) was inaccurately measured with the thermocouple (i.e.10°C-15°C higher than the sample temperature), thus could account for the lower crystallization rate in these specific VFM samples. Thus the volume fraction of crystals at any given time for these VFM samples will be lower than the one observed in the conventional heating at 583°C, as what was observed. In the VFM experimental setup (Figure 4.3), the IR temperature reading was always lower than the thermocouple temperature reading by 10°C-15°C. Because of the temperature measurement issue in the microwave cavity (well known issue in the microwave processing field), it is believed that this assumption is most likely the actual reason for the lower V_v observation in these specific VFM treated samples at 583°C.

Figure 5.64 shows the volume fraction of crystals as a function of time in conventionally heat-treated LS_2 samples at 567°C, 583°C, 595°C, 730°C and 680°C in comparison with VFM heat-treated samples at 583°C and 600°C. As shown from the Figure, the volume fraction of crystals of the conventionally crystallized LS_2 glass-ceramic samples at 583°C is lower than the ones conventionally crystallized at 595°C, 730°C and 680°C (T_c) but higher than the one at 567°C. Also, the crystal growth kinetics of the conventionally crystallized LS_2 glass-ceramics samples at 680°C (T_c) is higher than the ones conventionally crystallized at 730°C 595°C, 583°C and 567°C. Furthermore, the crystal growth kinetics at 595°C is higher than the one at 583°C and 567°C but lower than

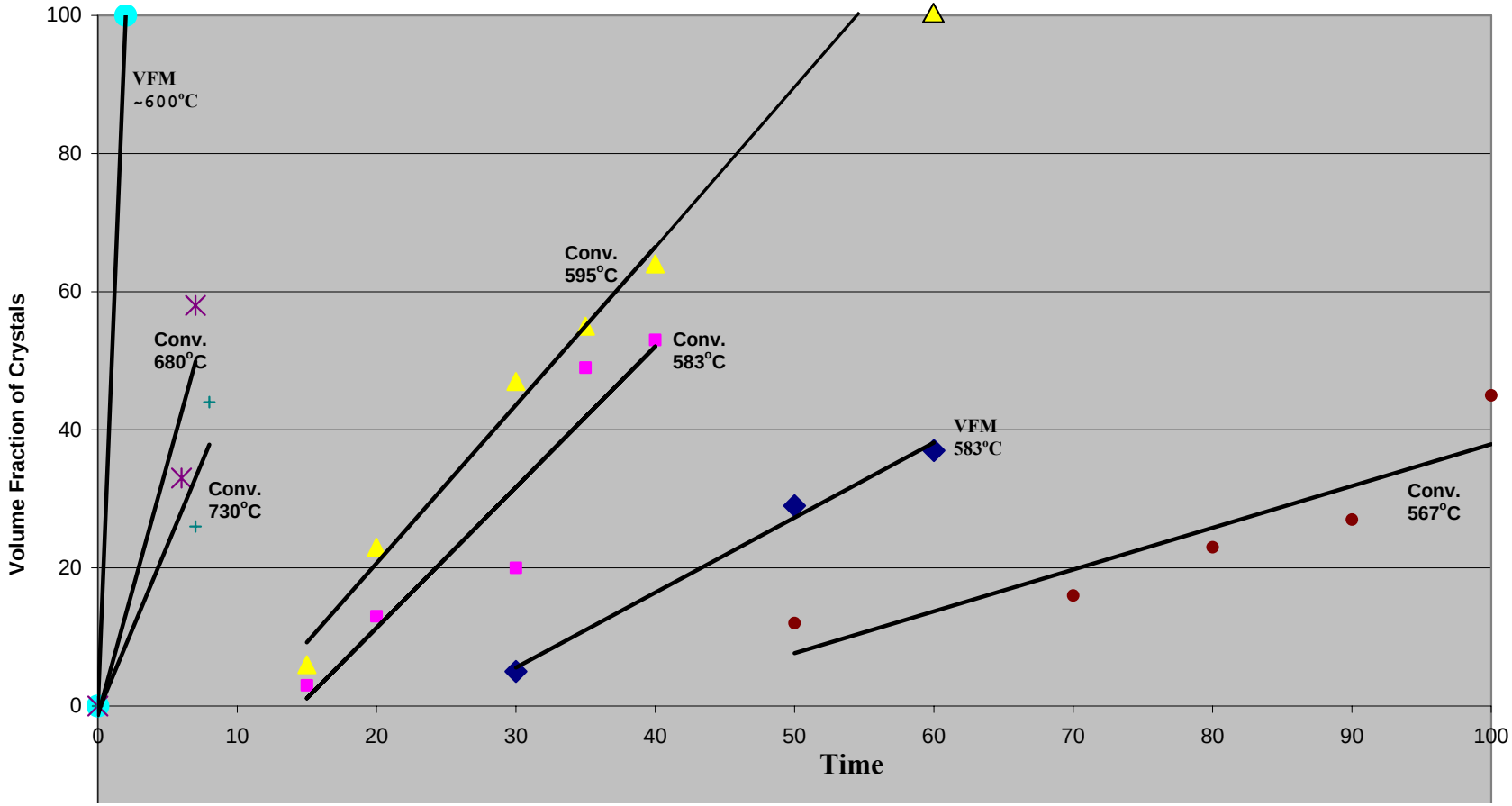

Figure 5.64: Volume fraction of crystals as a function of time of LS_2 glass samples heat-treated by conventional and VFM heating at different temperatures.

Note: All the temperature readings shown in this figure are made with a thermocouple. Temperatures for the samples processed by the VFM processing technique were also measured with an IR pyrometer and were 10°C-15°C lower than the temperature measured with the thermocouple. The IR temperatures are probably more accurate in the microwave cavity.

the one at 730°C. This trend is in agreement with the DSC data of the bulk LS_2 glass, pictures of these samples (Figure 5.62), and the kinetic theory of glass formation. As shown in Figure 5.64, the VFM crystallized samples at 583°C show unexpectedly lower kinetics even when compared with the corresponding conventionally heat-treated samples at the same temperature. This trend is believed to happen most likely due to the inaccurate temperature measurement in the VFM process. Further investigation is required to understand this trend.

On the other hand, the VFM crystallized sample at ~600°C for two (2) minutes has the fastest crystal growth rate as compared to the 730°C, 680°C, 595°C, 583°C and 567°C conventionally heat-treated samples. Furthermore, the 600°C VFM crystallized sample posses higher crystal growth kinetics than the conventionally treated sample at the maximum crystal growth temperature (T_c=680°C). So a microwave effect appears to be valid in the VFM process regardless of the temperature issue. In conclusion, this enhanced kinetics in the VFM heat-treated sample in addition to the different crystallization mechanism, as compared to the conventional heat-treated sample, appears to be due to the microwave effect.

The microstructural uniformity of LS_2 glass samples, crystallized either by conventional or VFM heating, was studied by optical microscopy. As discussed earlier, microwaves heat the materials from inside to outside, while conventional heating heats the materials in a reverse pattern (Figure 1.3). So it was expected that the conventionally crystallized samples will have larger crystals at the samples edges as compared to the middle of the samples. Unexpectedly, both samples crystallized either by conventional or VFM heating had larger crystals and more crystal population in the middle of samples as

compared to the samples edges, as shown in Figures 5.65, 5.66, and 5.67. As discussed before (Section 5.2), this observation is believed to occur due to the nucleation procedure applied in the present study. Further investigation is required to understand this behavior.

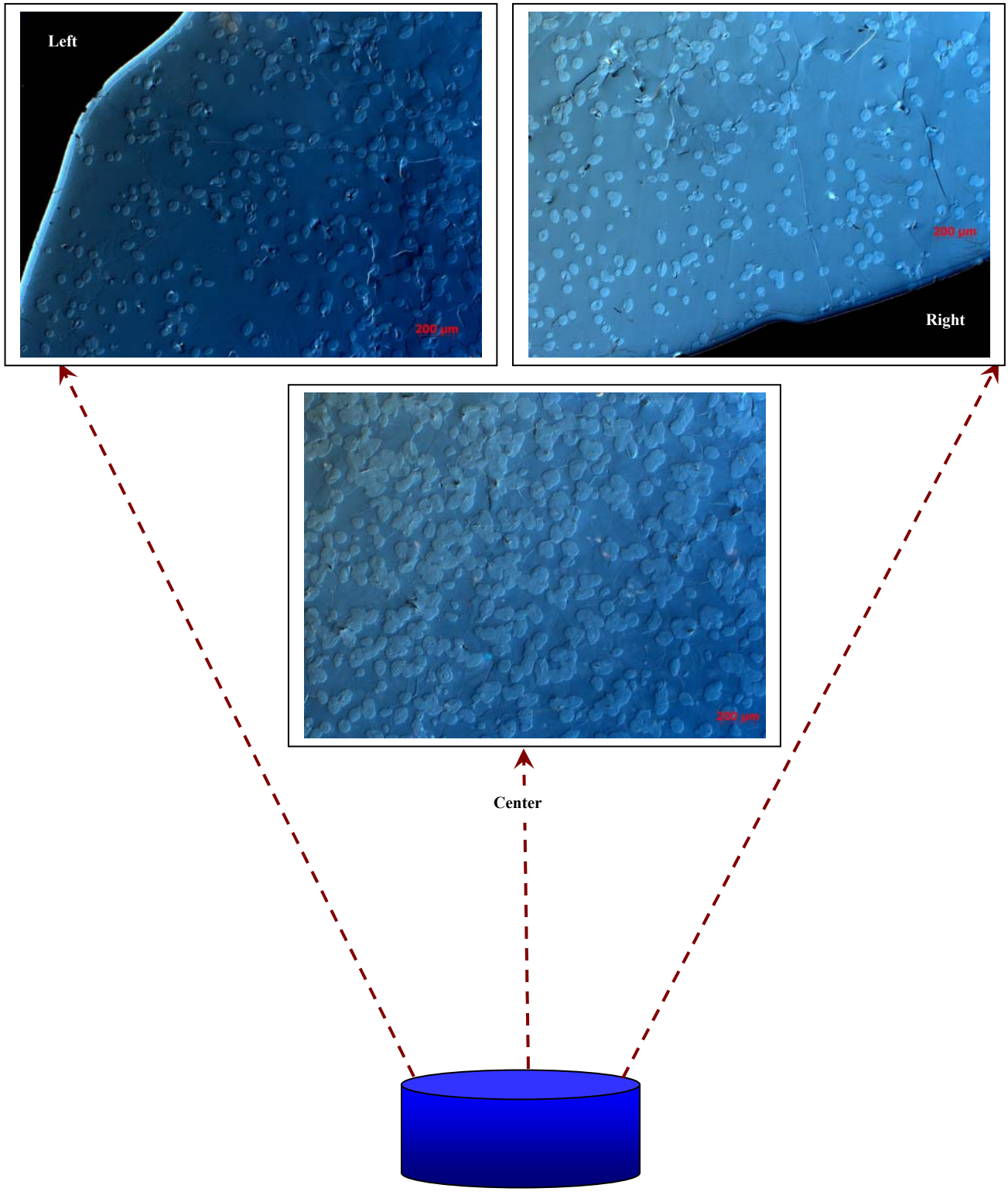

Figure 5.65: Optical micrographs of partially crystallized LS_2 glass sample heat-treated at 583^{o}C for 80 min. by VFM processing (50X).

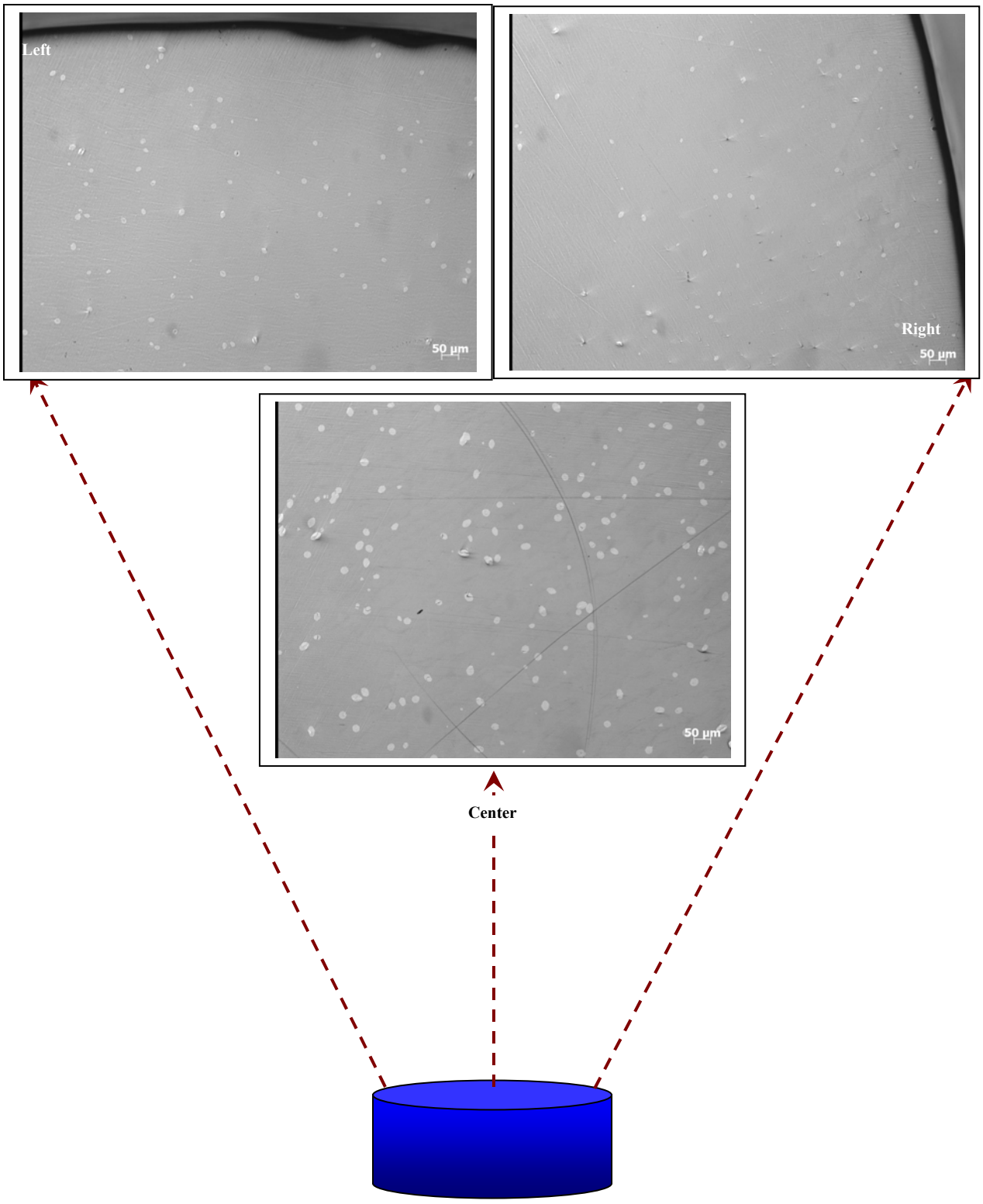

Figure 5.66: Optical micrographs of partially crystallized LS_2 glass sample heat-treated conventionally at 595^{0}C-15 min. (50X).

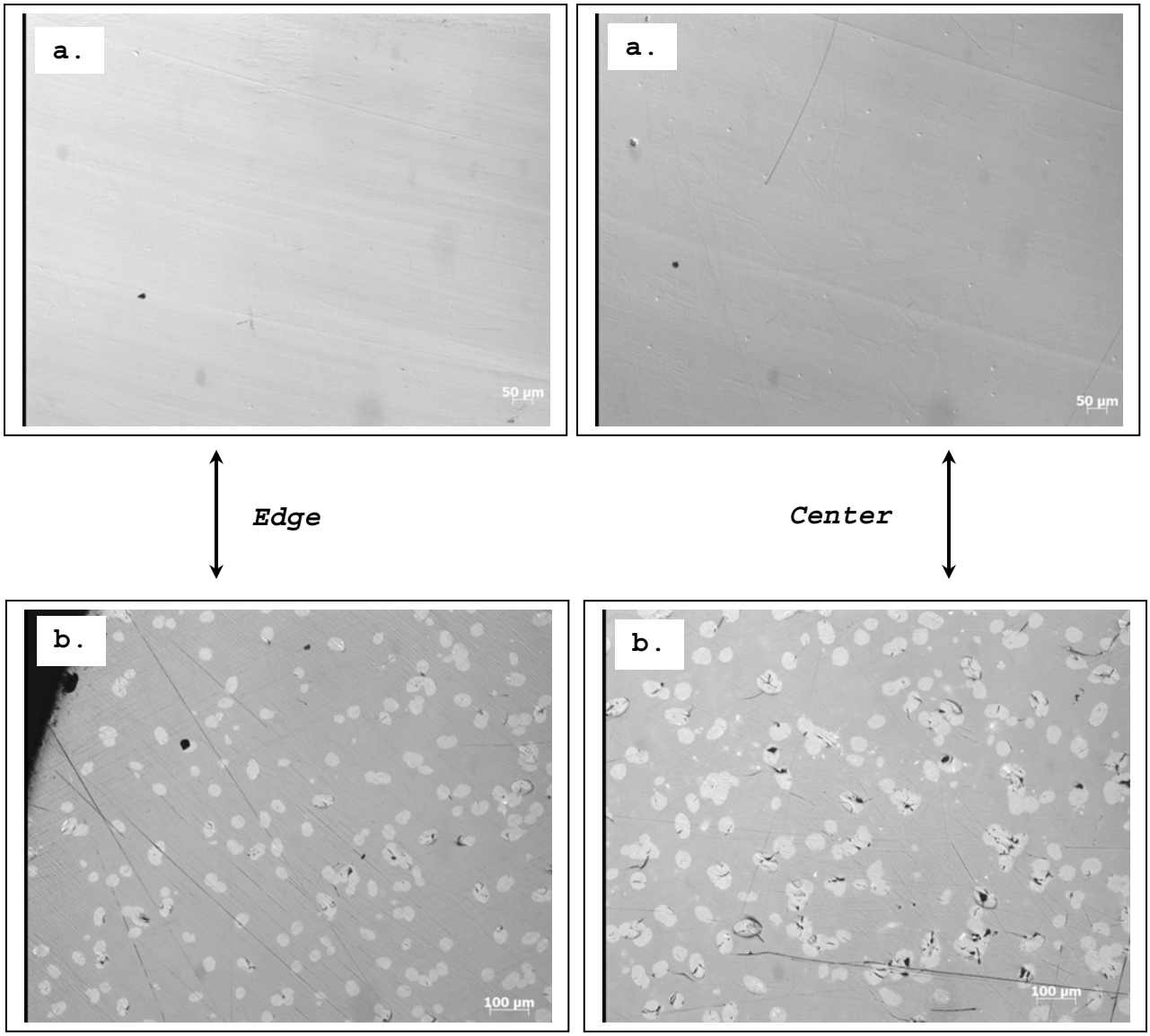

Figure 5.67: Optical micrographs of partially crystallized LS_2 glass samples heat-treated conventionally at 680°C for:

a. **2 minutes (50X*)*.**
b. **6 minutes (50X).**

5.11. Possible explanation of the observed microwave effect

As discussed earlier, the "microwave effect" was reported by numerous researchers studying different materials and processes. On the other hand, some controversy still exists regarding the interpretation of the experimental results (microwave effect). Experimental evidence to date does not provide the data necessary to substantiate this claim. Because temperature measurement in a microwave field is not an easy task, some researchers argue that the observed differences are not due to the microwave effect but rather are purely thermal and misreported.

In the present study, the enhanced kinetics and the different crystallization mechanism observed in the crystallization of LS_2 glass using VFM processing prove strong and obvious evidence for the reality of the microwave effect, regardless of the temperature issue. As discussed earlier, the enhanced kinetics in the crystallization of LS_2 glass using VFM processing might require a reduction in the activation energy as shown in the literature (Figure 1.4a)[55].

The following discussion will focus on the possible explanation for the existence of the microwave effect in the crystallization of LS_2 glass by VFM processing. The microwave energy consists of an electric field and a magnetic field perpendicular to each other. Both fields are expected to contribute to how microwaves influence a given process. In the following discussion, special attention will be given to the electric field; this does not, however, mean that the magnetic field has no effect. Meanwhile, few researchers have studied the effect of applied external magnetic field on some phase transformation processes[201]. Furthermore, Roy et al [63, 148, 202, 203] reported unexpected and abnormal behavior (microwave effect) of some ferrite materials under the

influence of a microwave magnetic field. Formation of nanocrystalline phases or decrystallization of other phases in some ferrite materials (3d materials) were reported in a significantly shorter time compared to conventional heating, using microwave magnetic field. The authors suggested alteration of the free energy (activation energy) of these processes under the influence of the microwave magnetic field, because these phase transformation processes are forbidden thermodynamically under normal conventional heating. It is suggested that the free energy value of a given process should be dependent on the electric and the magnetic field strength.

The electric field in the microwaves is believed to distort the activation energy barriers for an atom or ion in a certain lattice or network over an interatomic distance (a), as shown in Figure 5.68[81]. This distortion will decrease or increase the activation energy as shown in the same Figure. In a given glass, there is no single value of the activation energy barrier between the atom or ion positions due to the random short range order in the glass, as shown in Figure 5.69. The environment of each single atom or species in the glassy network varies considerably. There are always adjacent low energy positions with small energy barriers between them. Large energy barriers occur between occasional adjacent positions.

Most of the microwave experimental configurations have a microwave electric field strength of $\leq 10^5$ to 10^6 V/m[33]. Furthermore, recent calculations of the lattice field strength in ionic polycrystalline solids are estimated to be around $\approx 10^{11}$ V/m[33]. Hence, it has been argued that the microwave field strength can not distort the activation energy barriers in a given polycrystalline solid. So the microwave effect observed in these materials can not be explained by the activation energy barriers' distortion assumption.

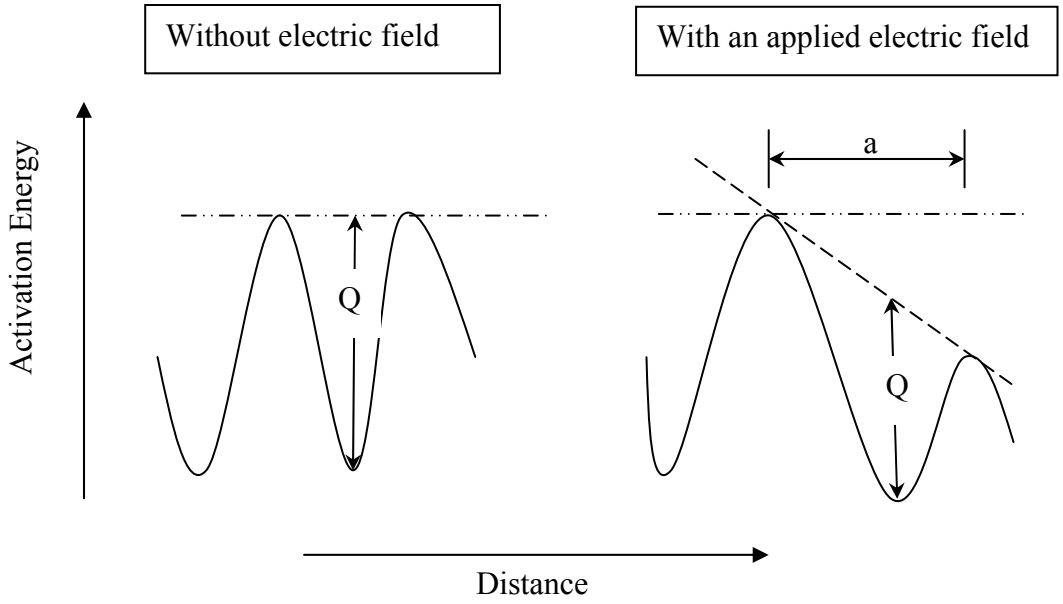

Figure 5.68: Effect of the applied electric field on the activation energy (Q) of atom motion. Adapted from[81]. Reprinted with permission of John Wiley & Sons, Inc. [copyright 1976]

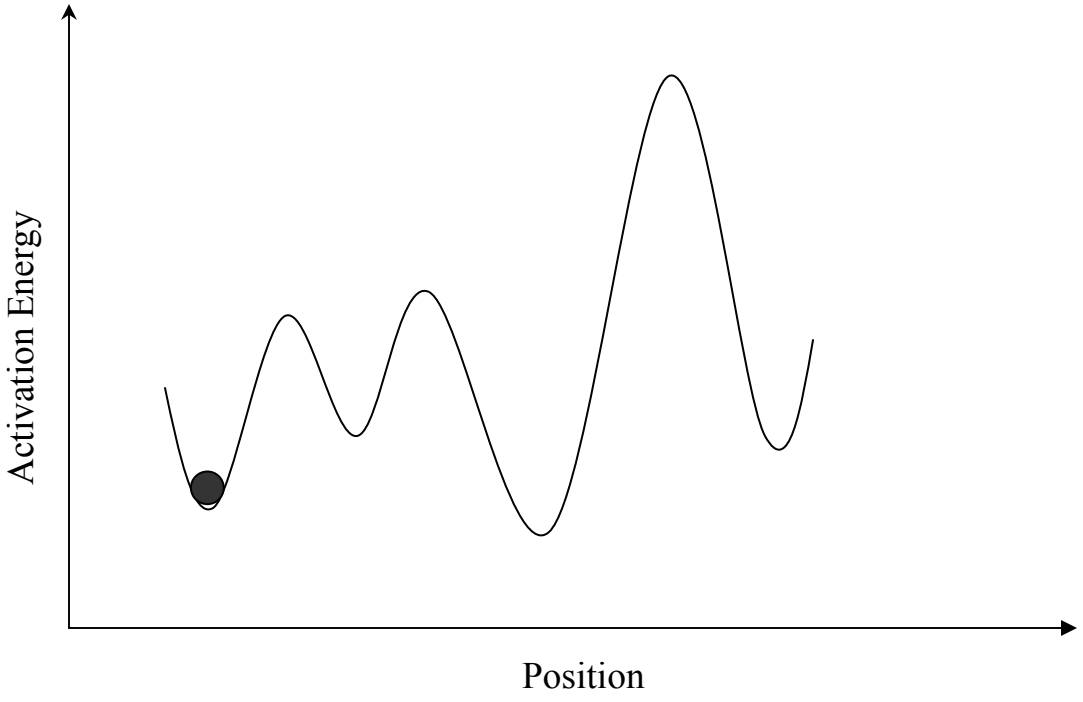

Figure 5.69: Activation energy barriers along the path of an atom in a glassy network. Adapted from[81]. Reprinted with permission of John Wiley & Sons, Inc. [copyright 1976]

On the other hand, as discussed (Figure 5.69) in a given glassy material there is no one single value of the activation energy barriers due to the random short range order within the glass network. There are always adjacent low energy positions with small energy barriers between them. In glasses, it is expected that these low energy barriers will be sufficiently reduced so that the microwave field strength can distort these activation energy barriers.

In terms of the thermodynamics that limits phase stability, the minimum Gibbs free energy (ΔG) specifies which phase is stable under particular conditions. The variables commonly applied to phase stability are temperature and pressure. However, magnetic field intensity and electric field strength can also contribute to the free energy since phases may have different magnetic susceptibilities or different dielectric constants (LS_2 glassy and crystalline phases). Thus, magnetic or electric fields can modify the activation energy, and as a result the kinetics of a given process can also be affected by the magnetic or electric fields. For example, crystallization that requires atomic transport (diffusion) can be modified by the effect of the electric fields. The growth morphology can also be controlled by the magnetic field direction in processes involving phases with different magnetic properties.

The following section will provide some literature review about the effect of the external electric field on mass transport processes, such as phase separation and crystallization of glass and amorphous metallic alloys. The effect of the electric field on the phase separation in glass, phase transformations in several materials, and crystallization of amorphous metallic alloys and ceramics was studied [148, 195, 197-201, 204-208]. It was reported that the electric field can enhance or slow a given process

based on how this field interacts with the material.

Enhanced phase separation kinetics due to an external applied electric field (1–2 kV, either AC (50 Hz) or DC) was first reported for oxide glasses by deVekey and Majumdar[33]. The system studied was $CaO–Al_2O_3–SiO_2–MgO–TiO_2$. The normal nucleation temperature range for phase separation for this glass was 725–800°C. Glasses heated at 690°C showed little evidence for phase separation without an electric field, but with the electric field, well formed nuclei due to phase separation were observed. Heating in the normal temperature range for phase separation in the presence of an electric field resulted in a coarser microstructure than without the field. Thus, the growth of the phase separated regions was faster with an applied electric field.

Subsequently, Liu et al. [195, 197-199, 205] systematically studied the effect of an external electric field on the phase separation of glasses. They studied two systems: (1) $CaO–Al_2O_3–SiO_2$ (CAS) and (2) $CaO–B_2O_3–P_2O_5$ (CBP). They found that the electric field greatly affects the phase separation. In the CAS system, the electric field treatment promotes the phase separation. However, in the CBP glass system, phase separation was inhibited by the electric field. A model was developed to explain the effect of the electric field on the phase separation of glasses. The model considered the variation of dielectric constants between the matrix and the precipitating phase. The electric field is believed to alter (distort) the activation energy barriers required for diffusion in these materials, thus an increase or decrease in the overall kinetics would take place.

Furthermore, the crystallization of amorphous metal alloys under the influence of an external electric field was studied by other authors[206, 207]. It was shown that the crystallization process was markedly enhanced by an external electric field. The

crystallization time at 600°C decreased from 1 hour to 30 minutes by using a modest external electric field (10^4 V/m). Note that this studied external electric field lies within the microwave electric field strength. This study suggested that the electric-field-enhanced crystallization might result from the enhancement in the atomic diffusion based on the following Equation 5.2, which defines the atomic diffusion coefficient, D, in the presence of an electric field.

$$D = D_o \exp\left(\frac{-Q_o - (1/2) E_o l}{RT}\right) \qquad \textbf{(5.2)}$$

where D_o is a constant, R is the gas constant, T is the temperature, Q_o is the activation energy for atomic migration in the absence of electric field, E_o is the amplitude of the electric field strength, and l is the distance between two potential wells. From this Equation, it can be seen that the presence of an electric field promotes atomic diffusion, which makes atomic mobility easier. Thus, the high atomic mobility promotes the growth of crystals during the crystallization process.

In conclusion, these reported studies show that the external electric field (within the microwave field strength) is believed to alter the activation energy barriers in glass and enhance the diffusion process in the crystallization of amorphous metal alloys. In the present study, the microwave effect observed in the VFM process is believed to be because of a possible reduction in the activation energy barriers within LS_2 glass.

In general, two possible types of dielectric losses might occur in silicate glasses: losses due to the movement of alkali ions (i.e. Li^+ ion) through the network (relaxation losses) and losses related to the vibration of these atoms or units of atoms within their positions (vibration losses)[33]. The relaxation losses are related to the dipole polarization. It was observed that the more the connectivity in the glass structure (number

of bridging oxygen - Q^4 units), the lower the dielectric loss was. So losses are a function of the glass structure and composition.

The first proposed mechanism suggests the distortion of the activation energy barriers in LS_2 glass due to the microwave electric field strength that will facilitate the movement of the Li^+ ion (relaxation losses). In the VFM process, when the microwave energy hits the LS_2 glass sample, the activation energy barriers in LS_2 glass are distorted, as in Figure 5.68, favoring the movement of the Li^+ ion in the direction of the applied electric field. Because of the alternation of the microwave electric field, the Li^+ passage over the energy barriers is favored in one half of the cycle in a certain direction, and favored in the opposite direction in the other half of the cycle (relaxation losses). Thus, the Li^+ ions will jump over these energy barriers back and forth as the electric field alternates. As a result, the Li^+ ions gain energy from the microwave electric field and lose some energy upon collision with the glassy network that causes heat. If the frequency of the applied electric field is too small or too large as compared to the jump frequency of the Li^+ ions, the glass will have small microwave absorption and hence limited heating will occur. On the other hand, if the frequency of the applied electric field is within the same range of the jump frequency of the Li^+ ions, the LS_2 glass will absorb most of the microwave energy and heat effectively, as observed in the experiments. Because of the coupling between the Li^+ ion and the frequency of the electric field, the local temperature of these ions will increase in a very short period of time before the heat is transferred and conducted to the rest of the glass network. As a result of this increase in the local temperature of the Li^+ ions, the jumps over the activation energy barriers will be easier, resulting in the enhanced kinetics observations in the overall process. The number of Li^+

ions in the studied LS_2 glass (33% mole Li_2O) is efficient enough to cause a substantial increase in the kinetics as was observed experimentally. Thus, this is a possible mechanism by which the microwave effect might occur in the crystallization process of LS_2 glass by VFM processing.

The second proposed mechanism by which the microwave effect can occur is the coupling of the glass network constituents (network formers [Si^{4+}], network modifiers [Li^{+}] and oxygen anions [O^{-}]) with the microwave frequency. This type of loss will be a resonance loss instead of a relaxation loss. These glass networks constituent will all vibrate around their equilibrium positions due to the thermal agitations. Each atom or group of atoms can be treated as harmonic oscillators. Its vibrational frequency will depend on its mass and the restoring elastic forces (force constant). As discussed before in the molecular orbital model, these atoms or group of atoms will act as the coupled oscillators. The coupled oscillators' frequency will be in the range of the microwave frequency so that coupling could happen. This will lead to strong microwave absorption, and as a result, localized heat will generate due to the resulting friction. If the number of localized heat spots is efficient to cause an increase in the crystallization rate, this localized heat is believed to lead to the microwave effect.

The third possible mechanism proposed by Zakaryae[33] can lead to the microwave effect in LS_2 glass. Macdowell[209] explained that the high temperature achieved in nephline glass-ceramic materials heated by microwave energy is because of the ability of the sodium ions, in larger nephline lattice positions, to couple with the microwave field. Zakaryae proposed a rattling mechanism of the Na^{+} ions in their cages (oxygen atom) in glass. Based on that, the rattling of the Li^{+} ions within a larger silicate

cages in LS_2 glass (rings of the silicate structure – 3, 4, 5, and 6 member rings) in response to the microwave field will generate heat. The degree of rattling will depend on the size of the ring and the looseness of the Li^+ ion. If the Li^+ ion resides in a larger cage, it will rattle violently compared to smaller cage situation. The dipole between the Li^+ ion and the coordinating oxygen ion cage will rattle in an effort to match its alignment with the microwave oscillating electric field as well. This will lead to strong microwave absorption with a localized increase in the temperature of the Li^+ ion while the bulk LS_2 glass sample is relatively unchanged. If the number of rattling Li^+ ions is sufficient to create localized heat centers within the material, a substantial increase in diffusion will occur while the bulk LS_2 glass sample is still at relatively lower temperature. This is believed to lead to the microwave effect.

The fourth proposed mechanism suggests the distortion of the activation energy barriers in LS_2 glass due to the microwave electric field strength that will facilitate the movement and the diffusion of the Li^+ ion from the highest energy barrier position (amorphous glassy structure) to the lowest energy barrier position (well ordered crystalline structure). In the VFM process, when the microwave energy hits the LS_2 glass sample, the activation energy barriers in LS_2 glass are distorted, as in Figure 5.68, favoring the movement of the Li^+ ion in the direction of lowest energy barrier position (crystalline phase).

Finally, a combination of these proposed mechanisms (explanations) for the occurrence of the microwave effect could happen at the same time or in various sequences. More work is needed in order to fully understand how microwave energy affects the kinetics of crystallization in LS_2 glass.

6. Conclusions

The following conclusions correspond with the objectives discussed earlier in the statement of the work section.

- Variable frequency microwave processing was successfully used to crystallize LS_2 glass in a significantly shorter time and lower temperature as compared to conventional heating and without the aid of hybrid heating.
- Lithium disilicate crystal phase (Orthorhombic Ccc2) was developed in both samples crystallized either by conventional or VFM heating. The Q^4 species of the SiO_4 tetrahedra in the VFM crystallized samples were slightly higher than the ones in conventionally crystallized samples, so the mechanism of crystallization might be slightly different.
- Both observations, the enhanced kinetics in the crystallization process as well as the different crystallization mechanism that occurred in the VFM crystallized sample, provide evidence for the existence of the microwave effect in the VFM crystallization process.
- Microwave materials interaction was highly dependent on the structure of the material when the temperature and the frequency are the same. The structure was affected by the formation of crystals and by the phase boundaries between the glassy and the crystalline phase. LS_2 glass system was selected so that the chemical composition of the glass and the crystals are the same.
- Microwave material interaction with LS_2 glass and glass-ceramic was highly dependent on frequency as proposed by the molecular orbital model and confirmed by experiments.

- The molecular orbital model was successfully used to predict the microwave absorption of this material system.
- A correlation to estimate the volume fraction of crystals in LS_2 glass-ceramics by FTIRRS peak intensities of the same materials was established.

7. Future work

Microwave processing of materials provides several advantages over conventional processing in some materials. It is still an open area for investigations and further efforts to understand how microwaves energy interacts with materials. As a follow up to this study, some areas of interest are presented.

1- As shown before, large crystals' size and population were developed in the middle of both LS_2 glass-ceramics samples, crystallized either by VFM or conventional heating. On the other hand, smaller crystals' size and population were developed on the samples' edges. Because of the heating profile for a given material by microwave energy (Figure 1.3), this observation was expected to exist in the VFM crystallized samples and not in the conventional crystallized samples. It is believed that the experimental conditions applied to promote the homogenous nucleation regime in the studied LS_2 glass samples cause this observation. Due to the unexpected similar microstructural uniformity of both LS_2 glass-ceramics samples, crystallized either by microwave or conventional heating, a heterogeneous nucleation regime is proposed to investigate this matter. Introducing nucleating agents, such as TiO_2, to promote the heterogeneous nucleation in LS_2 glass will allow more control of the nucleation stage.

2- Perform microwave crystallization of LS_2 glass with a 5.8 GHz single mode microwave apparatus that is equipped with a power meter to monitor the absorbed and the reflected power. At this frequency, there were strong microwave oscillators in the LS_2 glass, as shown earlier by the molecular orbital theory model results; hence, self heating is expected to occur in LS_2 glass. The effect of the microwave power on the crystallization behavior of LS_2 glass at this frequency will be studied. Furthermore, the

crystallization behavior of LS_2 glass under the influence of single mode and multimode microwaves will be studied and compared. This is expected to provide a better fundamental understanding of microwave-material interactions.

3- Magic-angle-spinning nuclear magnetic resonance (MAS-NMR) investigation of LS_2 glass and glass-ceramics samples crystallized either by conventional or microwave heating (VFM or/and 5.8 GHz single mode) is proposed. This will help to study the difference in the structural environment around the Li^{+}, Si^{4+} and O^{-} atoms in these samples. This will help to understand the difference in the crystallization mechanisms observed between these two types of samples. As a result, microwave-material interaction can be further understood.

4- Find a better way to monitor the temperature in the crystallization process of LS_2 glass by microwave energy. It is proposed to measure the emissivity of LS_2 glass under normal conditions and without the microwave field over a certain temperature range ($25^{o}C$-$680^{o}C$). Afterward, using these emissivity data to calibrate the pyrometer, a two color pyrometer will be used to monitor the temperature in the crystallization process (using the microwave field).

References

1. Berezhnoi, A.I., *Glass-ceramic and photositalls*. 1970, New York Plenum press,P.2.
2. Mc Millan, P.W., *Glass-ceramics*. 1979, London: Academic press,2nd edition,P.1.
3. Stooky, S.D., *Catalyzed crystallization of glass in theory and practice.* Ind. Eng. chem, 1959. **51**: p. 805-808.
4. Cherneva, E.F. and V.A. Florinskaya, *Crystallization of the composition lithium disilicate glass over a wide temperature range.* Zhurnal Fizicheskoi Khimii, 1965. **39**(2): p. 500-8.
5. Glasser, F.P., *Crystallization of lithium disilicate from lithium oxide-silicon dioxide glasses.* Physics and Chemistry of Glasses, 1967. **8**(6): p. 224-32.
6. Filipovich, V.N. and A.M. Kalinina, *Kinetics of the crystallization of lithium disilicate from simple and complex glasses.* Izvestiya Akademii Nauk SSSR, Neorganicheskie Materialy, 1970. **6**(2): p. 351-6.
7. Doremus, R.H. and A.M. Turkalo, *Crystallization of lithium disilicate in lithium silicate glasses.* Physics and Chemistry of Glasses, 1972. **13**(1): p. 14-14D.
8. Borom, M.P.T.A.M. and R.H. Doremus, *Strength and microstructure in lithium disilicate glass-ceramics.* Journal of the American Ceramic Society. Vol. 58, 1975: p. no. 9-10.
9. James, P.F., et al., *Positron lifetimes in lithium disilicate glass with different degrees of crystallization.* Journal of Physics C: Solid State Physics, 1975. **8**(4): p. 393-8.
10. James, P.F., *Kinetics of crystal nucleation in lithium disilicate glass. A comparison between melts prepared in platinum and silica crucibles and between melts prepared from ordinary and high purity starting materials.* Phys. Chem. Glasses. , 1978. **19**: p. no. 2.
11. McCracken, W.J., D.E. Clark, and L.L. Hench, *Aqueous durability of lithium disilicate glass-ceramics.* American Ceramic Society Bulletin, 1982. **61**(11): p. 1218-23.
12. Zanotto, E.D. and P.F. James, *Experimental tests of the classical nucleation theory for glasses.* Journal of Non Crystalline Solids, 1985. **74**: p. 2-3.
13. Joseph, I., *Nucleation and related phenomena in lithium disilicate glass*. 1985. p. 152 pp.
14. Hannon, A.C., B. Vessal, and J.M. Parker, *The structure of alkali silicate glasses.* Journal of Non-Crystalline Solids, 1992. **150**(1-3): p. 97-102.
15. Zanotto, E.D., *Metastable phases in lithium disilicate glasses.* Journal of Non Crystalline Solids, 1997. **219**: p. 42-48.
16. Soares Jr, P.C., et al., *TEM and XRD study of early crystallization of lithium disilicate glasses.* Journal of Non Crystalline Solids, 2003. **331**: p. 1-3.
17. Holand, W. and G. Beall, *Glass-ceramic technology*. 2002: The American Ceramic Society.
18. Ray, C.S., X. Fang, and D.E. Day, *New method for determining the nucleation and crystal-growth rates in glasses.* Journal of the American Ceramic Society, 2000. **83**: p. 865-872.

19. Burgner, L.L. and M.C. Weinberg, *Assessment of crystal growth behavior in lithium disilicate glass.* Journal of Non Crystalline Solids, 2001. **279**: p. 28-43.
20. James, P.F., *Kinetics of crystal nucleation in silicate glasses.* Journal of Non-Crystalline Solids, 1985. **73**(1-3): p. 517.
21. Gonzalez-Oliver, C.J.R., P.S. Johnson, and P.F. James, *Influence of water content on the rates of crystal nucleation and growth in lithia-silica and soda-lime-silica glasses.* Journal of Materials Science, 1979. **14**(5): p. 1159.
22. Ranasinghe, K.S., C.S. Ray, and D.E. Day, *A generalized method for determining the crystal nucleation and growth rates in glasses by differential thermal analysis.* Journal of Materials Science, 2002. **37**(3): p. 547.
23. Ray, C.S., K.S. Ranasinghe, and D.E. Day, *Determining crystal growth rate-type of curves in glasses by differential thermal analysis.* Solid State Sciences, 2001. **3**(6): p. 727-732.
24. Ray, C.S. and D.E. Day, *Nucleation and crystallization in glasses as determined by DTA.* Ceramic Transactions, Nucleation and Crystallization in Liquids and Glasses, 1993. **30**: p. 207.
25. Ray, C.S., et al., *Surface and internal crystallization in glasses as determined by differential thermal analysis.* Journal of the American Ceramic Society, 1996. **79**: p. 3155-3160.
26. Holand, W., V. Rheinberger, and E. Apel, *Glass crystallisation in dental materials.* Glass Technology, 2004. **45**: p. 74-77.
27. Soares Jnr, P.C., P.A.P. Nascente, and E.D. Zanotto, *XPS study of lithium disilicate glass crystallization.* Physics and Chemistry of Glasses, 2002. **43**(3): p. 143-146.
28. Iqbal, Y., et al., *Metastable phase formation in the early stage crystallization of lithium disilicate glass.* Journal of Non Crystalline Solids, 1998. **224**: p. 1-16.
29. Fuss, T., *Effect of pressure on crystallization in lithium disilicate glass*, in *Ceramic Engineering*. 2004, University of Missouri-Rolla. p. 84.
30. Boonyapiwat, A., D.C. Folz, and D.E. Clark, *Microwave crystallization of glass.* Ceramic Transactions, 2000. **101**(Surface-Active Processes in Materials): p. 87-96.
31. A.D.Cozzi, et al. *Nucleation and crystallization of Li2O-2SiO2 in a 2.45 GHz microwave field*. in *17th Annual Conference on Composite and Advanced ceramic Materials*. 1993.
32. Clark, E.D., et al., *Microwave Soultions for Ceramics Engineers*. 2005, Westerville,Ohio: The American Ceramic Society. 494.
33. Fathi, Z., *Surface modification of sodium aluminosilicate glasses using microwave energy*, in *Materials Science and Engineering*. 1994, University of Florida: Florida. p. 293.
34. Metaxas, A.C., *Applicators for industrial microwave processing.* 1993.
35. National Materials Advisory Board, N.R.C., *Microwave Processing Of Materials*. Committee on Microwave Processing Of Materials: An Emerging Industrial Technology, Commission On Engineering And Technical Systems. 1994, Washington, D.C.: National Academy Press.
36. Sutton, W.H., *Microwave Processing of Ceramic Materials.* American Ceramic Society Bulletin, 1989. **68**(2): p. 376-386.

37. Freeman, S.A., J.H. Booske, and R.F. Cooper, *Novel method for measuring intense microwave radiation effects on ionic transport in ceramic materials.* Review of Scientific Instruments, 1995. **66**(6): p. 3606-3609.
38. Surapanani, S., M.E. Mullins, and B.C. Cornilsen, *Microwave drying of borosilicate gels.* 1991.
39. Clark, D.E. and W.H. Sutton, *Microwave processing of materials.* Annual Review of Materials Science, 1996. **26**: p. 299-331.
40. Clark, D.E., I. Ahmad, and R.C. Dalton, *Microwave Ignition and Combustion Synthesis Of Composites.* Materials science & engineering. A, 1991. **144** p. 91-97.
41. Clark, D.E., et al., *Microwaves: Theory and Application in Materials Processing III. (Proceedings of the Microwaves: Theory and Application in Materials Processing III Symposium, presented at the 97th Annual Meeting of the American Ceramic Society, held in Cincinnati, May 1-3, 1995.) [In: Ceram. Trans, 1995; 59]*. 1995. 592 pp.
42. Fathi, Z., et al. *Processing and Characterisation of a Polymer Matrix Composite Using Variable Frequency Microwave Heating* in *Ceram.Trans.* . 1995.
43. Clark, D.E., D.C. Folz, and S.J. Oda, *Ceramic Transactions, Volume 59: Theory and Application in Materials Processing III*. 1995.
44. Clark, D.E., et al., *Recent developments in the microwave processing of ceramics.* MRS Bulletin, 1993. **18**(11): p. 41-6.
45. Ahmad, I. and D.E. Clark, *Effect of microwave heating on the mass transport in ceramics.* Ceramic Transactions, 1993. **36**(Microwaves: Theory and Application in Materials Processing II): p. 287-95.
46. Tinga, W.R. and W.H. Sutton, *Key issues in microwave processing, research, and commercialization--an open forum.* 1993.
47. Sutton, W.H., *MICROWAVE PROCESSING OF MATERIALS.* MRS Bulletin. Vol. 18, 1993: p. no. 11.
48. Clark, D.E., *Microwave processing: present status and future promise.* Ceramic Engineering and Science Proceedings. Vol. 14, 1993: p. no. 7-8.
49. Al-Assafi, S. and D.E. Clark, *Microwave joining of ceramics: a study on joining alumina both directly and with alumina gel.* Materials Research Society Symposium Proceedings, 1992. **269**(Microwave Processing of Materials III): p. 335-40.
50. Clark, D.E., F.D. Gac, and W.H. Sutton, *Ceramic Transactions, Volume 21: Microwave: Theory and Applications in Materials Processing*. 1992.
51. De, A., et al., *Microwave (hybrid) heating of alumina at 2.45 GHz: II. Effect of processing variables, heating rates and particle size.* Ceramic Transactions, 1991. **21**(Microwaves: Theory Appl. Mater. Process.): p. 329-39.
52. De, A., et al., *Effect of green microstructure and processing variables on the microwave sintering of alumina.* Materials Research Society Symposium Proceedings, 1991. **189**(Microwave Process. Mater. 2): p. 283-8.
53. Copson, D., *Microwave Heating: In Freeze Drying, Electronic Ovens and Other Applications*. Avi Publishing Company. 1962, Westport, CN.
54. Anderson, B., et al. *Rapid Processing and Properties Evaluation of Flip-Chip Underfills*. in *Proc., Technical Program NEPCON West '98 Conference,*. 1998. Anaheim, CA.

55. Janney, M.A. and H.D. Kimrey. *Diffusion-controlled processes in microwave-fired oxide ceramics*. in *Scientific Basis for Nuclear Waste Management XVI* 1991. San Francisco, CA (United States): (Mater. Res. Soc. Symp. Proc) Spring meeting of the Materials Research Society (MRS)
56. Janney, M.A., H.D. Kimrey, and J.O. Kiggans, *Microwave processing of ceramics: guidelines used at the Oak Ridge National Laboratory.* Materials Research Society Symposium Proceedings, 1992. **269**(Microwave Processing of Materials III): p. 173-85.
57. Folz, D.C., et al., *Microwave and Radio Frequency Applications: Bridging Science, Technology, and Applications. (Proceedings of the Third World Congress held in Sydney, Australia September 2002.)*. 2003. 519 pp.
58. Mahmoud, M., et al. *Variable Frequency Microwave (VFM) Processing: A New Tool to Crystallize Lithium Disilicate Glass*. in *Proceedings of the 30th International Conference on Advanced Ceramics and Composites* 2006. Cocoa Beach, Florida: Ceramic Engineering and Science Proceedings.
59. Mahmoud, M., et al. *Microwave crystallization of lithium disilicate glass*. in *AIChE Annual Meeting, Conference Proceedings*. 2004. Austin, TX.
60. Sivakumaran, K. and C.K.S. Nair, *Rapid synthesis of chalcogenide glasses of Se-Te-Sb system by microwave irradiation.* Journal of Physics D: Applied Physics, 2005. **38**(14): p. 2476-2479.
61. Sung, T., S.A. Bidstrup Allen, and P.A. Kohl, *Low temperature rapid curing of polymer dielectrics on metallized organic laminates by variable frequency microwave processing.* Journal of Microelectronics and Electronic Packaging, 2005. **2**(2): p. 142-154.
62. Matsutani, H., et al., *Low temperature curing of polyimide precursors by variable frequency microwave.* Journal of Photopolymer Science and Technology, 2005. **18**(2): p. 327-332.
63. Roy, R., et al., *Decrystallizing Solid Crystalline Titania, Without Melting, Using Microwave Magnetic Fields.* Journal of the American Ceramic Society, 2005. **88**(6): p. 1640-1642.
64. Baldassari, S., et al., *Rapid Microwave-Hydrothermal Synthesis of Anatase Form of Titanium Dioxide.* Journal of the American Ceramic Society, 2005. **88**(11): p. 3238-3240.
65. Mitsudo, S., et al., *Non-thermal effects on B4C ceramics sintering.* IRMMW-THz 2005, Joint 30th International Conference on Infrared and Millimeter Waves & 13th International Conference on Terahertz Electronics, Williamsburg, VA, United States, Sept. 19-23, 2005, 2005. **1**: p. 225-226.
66. Minay, E.J., et al., *Processing of novel glass matrix composites by microwave heating.* Journal of Materials Processing Technology, 2004. **155-156**: p. 1749-1755.
67. Ghussn, L. and J.R. Martinelli, *A novel method to produce niobium phosphate glasses by microwave heating.* Journal of Materials Science, 2004. **39**(4): p. 1371-1376.
68. Clark, D. and D. Folz, *Microwave processing of materials.* Advances in Science and Technology (Faenza, Italy), 2003. **31**(10th International Ceramics Congress, 2002, Part B): p. 367-380.

69. Newnham, R.E., S. J. Jang. M. Xu, and a.F. Jones, eds. *Fundamental Interaction Mechanisms Between Microwaves and Matter*. Ceramic Transactions, Microwaves: Theory and Application in Materials Processing, ed. D. E. Clark, F. D. Gac, and a.W.H. Sutton. Vol. 21. 1991, American Ceramic Society: Westerville, Ohio.
70. West, J.K. and D.E. Clark, *Microwave absorption by materials: Theory and application.* Ceramic Transactions, 2000. **101**(Surface-Active Processes in Materials): p. 53-73.
71. West, J.K. and D.E. Clark, *A Molecular Orbital Model for Absorption of Microwave Energy by Materials.* Proceedings, 2nd World Congress on Microwave and Radio Frequency Processing, Orlando, Florida, Ceramic Transactions, 2000. **111**: p. 43-56.
72. Barsoum, M.W., *Fundamentals of ceramics*. 1997: McGraw-Hill International editions,p. 322.
73. Shackelford, J.F., *Introduction to materials science for engineers*. 1992, New York: Mac- Millan publishing company,3rd edition,P. 387.
74. Askeland, D.R., *The science and engineering of materials*. 1990, London: Chapman & Hall,2nd edition,P.501.
75. James, P.F.J., R.W, *Glass-ceramics in "High performance glasses"*, ed. M. Cable and J.M. Parker. 1992, New York: Chapman & Hall,P.102.
76. Mahmoud, M.M., *The Use of Copper Slag For Making Glass-ceramics*, in *Materials Science* 1999, Alexandria University: Alexandria,Egypt. p. 118.
77. Volf, B.M., *Technical approach to glass*. 1990, New York: Elsevier science publishing.
78. Zachariasen, W.J., *Atomic arrangement in glass.* J. Am. Chem. Soc, 1932. **54**(10): p. 3841-51.
79. Lewis, M.H., *Glass and glass-ceramics*. 1989, London: Chapman & Hall.
80. Tammann, G., *Glass as supercooled liquids.* J. Soc. Glass Tech, 1925. **9**: p. 166.
81. Kingery, W.D., H.K. Bowen, and D.R. Uhlmann, *Introduction to Ceramics*. 2nd ed. 1976, New York: John Wiley and Sons.
82. Uhlmann, D.R., *The energetic of nucleation.* Ind. Eng. Chem, 1965. **57**: p. 19-31.
83. Weyl, W.A., *Nucleation, crystallization and glass formation.* Sprechsaal, 1960. **95**(6): p. 128-36.
84. Stewart, D.R., et al., *Introduction to glass science*. 1973, N.Y: Plenum Press,237-71.
85. Hench, L.L., S.w.Frieman, and D.L.Kinser, *The early stages of crystallization in a Li2O-SiO2 glass.* Phys. chem. Glasses, 1971. **12**(2): p. 58-63.
86. Holland, D., et al., *Early stages of crystallisation of lithium disilicate glasses containing P2O5 - An NMR study.* Journal of Non-Crystalline Solids, 1998. **232-234**: p. 140-146.
87. Rabinovich, E.M., *Influence of crystal chemical similarity on heterogeneous crystallization of glass*. The structure of glass, v.3. "Catalyzed crystallization of glass". 1964, N.Y: consultant Bureau. 21.
88. Roy, R., *Metastable liquid immiscibility and subsolidus nucleation.* J.Am. ceram. soc, 1960. **43**: p. 670-71.
89. Roy, R., *Symposium on nucleation and crystallization in glasses and melts.* J. Am.

Ceram. Soc., 1962. **73**: p. 39-45.
90. Ohlberg, H.R., H.R. Golob, and D.W. Stricker. *Crystal nucleation by glass-in-glass separation"*. in *Symposium on nucleation and crystallization in glass*. 1962. Ohio: Am. ceram. Soc. Inc.
91. Vogel, W. and K. Gerth. *Symposium on nucleation and crystallization in glasses and melts*. 1962. Columbus, Ohio: Am. ceram. Soc. Inc.
92. Maurer, R.D. *Crystallization of a titania-nucleated glass*. in *symposium on nucleation and crystallization in glasses and melts*. 1962. Ohio,USA: Am. ceram. soc.
93. Kitaigorodskii, I.I.a.K., R.Ya., *The precrystallization period in glass and its significance*. structure of glass, v.3.,. 1964, N.Y: consultants Bureau, . 27-33.
94. Tashiro, M. *Nucleation and crystal growth in glasses*. in *proc. 8th Int. Cong. on glass*. 1968: Soc. Glass Techn,Sheffield.
95. Beall, G.H. and H.L. Rittler, *Process for forming a basaltic glass-ceramic products*. 1971: U.S. patent.
96. Dietzel, A., *Reaction and adhesion between glass and metal sealings.* Glastech. Ber., 1951. **24**: p. 263-8.
97. Levin, E.M. and S. Block, *Structural interpretation of immiscibility in oxid systems.* J.Am. ceram. Soc., 1957. **40**: p. 95-113.
98. Glasser, F.P., I. Warshaw, and R. Roy, *Liquid immiscibility in silicate systems.* phys. chem. Glasses, 1960. **1**: p. 39.
99. Hench, L.H. *Structure and properties of glass-ceramics*. in *4th space congr., Cocoa Beach Florida*. 1967.
100. Hillig, W.B. *A thearetical and experimental investigation of nucleation leading to uniform crystallization of glass*. in *Symposium on nucleation and crystallization in glasses and melts*. 1962. Columbus, Ohio: Am. ceram. soc. Inc.
101. Doherty, P.E., D.W. Lee, and R.S. Davis, *Direct observation of the crystallization of Li2O3-Al2O3-SiO2 glasses containing TiO2.* J. Am. Ceram. Soc., 1967. **50**(2): p. 77-81.
102. Neilson, G.f., *Nucleation and crystallization in Zro2 nucleated glass-ceramic systems.* Dis. Faraday soc., 1970. **50**: p. 145-54. .
103. Neilson, G.F. *Introduction to glass science*. in *Pittsburgh diffraction conference*. 1966: Plenum pub. corp., N.Y.
104. Blinov, V.A., *Mechanism of nucleated crystallization of glass in lithia-alumina-silica cordierite system.* J.Mater. Sci., 1969. **4**(5): p. 461-68.
105. Nakagawa, K. and T. Izumitani, *Relationship between phase separation and crystallization in Li2O.2.5. SiO2 glass and a Lithium silicate containing a large amount of titanium oxide.* phy. chem. Glasses, 1969. **10**(5): p. 179-84.
106. Bell, G.H. and J.f. Mac Dowell, *Fine ceramics from glass.* CHEMTCH, 1988. **18**: p. 673-679.
107. El-Shennawi, A.W.A., A.A. Omar, and A.M. Morsy, *The role of titania and titania mixtures in the nucleation and crystallization of spodunene-willemite-diopside glasses.* Thermochimica Acta, 1982. **58**: p. 125-53.
108. Omar, A.A., A.W.A. El-Shennawi, and A.R. El-Ghannam, *Crystallization of some spodumene-Lithium Zinc ortho silicate glasses.* J. Mater. Sci., 1991. **26**: p. 3366-73.

109. K.Varshneya, A., *Fundamentals of Inorganic Glasses*. 1994: Academic Press. 570.
110. Rogers, P.s., *The initian of crystal growth in glasses.* Min. Mag., 1970. **37**: p. 741.
111. Williamson, J., *The kinetics of crystal growth in an aluminosilicate glass containing small amounts of transition metal ions.* Min. Mag., 1970. **37**(291): p. 759-69.
112. Uhlmann, D.R. and E.V. Uhlmann, *Crystal growth and melting in glass-forming systems, a view from 1992.* Ceramic Transactions, Nucleation and Crystallization in Liquids and Glasses, 1993. **30**: p. 109.
113. Uhlmann, D.R., J.F. Hays, and D. Turnbull, *The effect of high pressure on crystallization kinetics with special reference to fused silica.* Physics and Chemistry of Glasses, 1966. **7**(5): p. 159.
114. Omar, A.A., *The use of natural rocks for the production of glass-ceramics materials*, in *project No. 202/188/2,second Report*. 1991, Academy of scientific Research and Technology: Cairo,Egypt.
115. Omar, A.A. and A.W.A. El-Shennawi, *Crystallization of some molten Egyptian basaltic rocks and corresponding glasses.* U.A.R.J. Geol., 1971. **15**: p. 65-73.
116. Omar, A.A., *Viscosity of basic silicate melts in relation to their structure.* Egypt. J.chem, 1972. **15**(2): p. 103-9.
117. Omar, A.A., S.M. Salman, and Youssef.M., *Catalyzed crystallization of various glasses based on sedimentary rock mixtures.* Ceramurgia, 1985. **xv**(2): p. 57-66.
118. Omar, A.A., S.M. Salman, and M.Y. Mahmoud, *phase relation in the diopside-anorthite-Akermanite system.* ceramic International, 1986. **12**: p. 53-59.
119. Beall, G.H. and H.L. Rittler, *Basalt glass-ceramics.* Am. ceram. soc. Bull. , 1976. **55**: p. 579-82.
120. El-Shennawi, A.W.A., A.A. Omar, and G.A. Khater, *Crystallization of celsian polymorphous in some alkaline earth aluminosilicate glasses.* Glass Technology, 1991. **32**(4): p. 131.
121. Clark, D.E., Sutton W. H., and Lewis D.A. *Microwave Processing of Materials*. in *Microwaves:Theroy and Application in Materials Processing IV*. 1997. Westerville,OH: Ceramic Transactions,American Ceramic Society.
122. Clark, D.E. and D.C. Folz. *Developments in microwave processing technologies*. in *Ceramic Engineering and Science Proceedings (USA). Vol. 18, no. 4, pp. 531-541.* 1997.
123. Clark, D.E., et al., *Applications of microwave processing in ceramics and waste remediation.* Ceramic Transactions, 1997. **80**(Microwaves: Theory and Application in Materials Processing IV): p. 507-514.
124. Leiser, K.S. and D.E. Clark, *Microwave behavior of silicon carbide/high alumina cement composites.* Ceramic Transactions, 2001. **111**(Microwaves: Theory and Application in Materials Processing V): p. 267-275.
125. Metaxas A.C. and R.J. Meredith, *Industrial Microwave Heating*. 1983, London,UK: Peregrinus.
126. Ku, H.S., et al., *Applications of fixed and variable frequency microwave (VFM) facilities in polymeric materials processing and joining.* Journal of Materials Processing Technology, 2001. **113**(1-3): p. 184-188.
127. Garard, R.S., Z. Fathi, and J.B. Wei, *Materials processing via variable frequency*

microwave irradiation. Ceramic Transactions, 1995. **59**: p. 117-24.
128. Lane, G.M., Jr., *The use of variable frequency microwave (VFM) to thermally enhance soil vapor extraction (SVE) remediation.* Book of Abstracts, 214th ACS National Meeting, Las Vegas, NV, September 7-11, 1997: p. ENVR-013.
129. Johnson, A., *Development of a variable frequency microwave processing system for post-curing of thermoset polymer matrix composite materials*. 1995, Lambda Technologies Acquisition Corp.,Raleigh,NC,USA. p. 14 pp.
130. Garard R. S. , Fathi Z. , and Wei B. *Materials Processing Via Variable Frequency Microwave Irradiation*. in *Microwaves: Theory and Application in Materials Processing III*. 1995. Cincinnate,USA: Ceramic Transactions,The American Ceramic Society.
131. Tanikella, R.V., *Variable frequency microwave processing of materials for microelectronic applications*. 2003. p. 285 pp.
132. Fathi, Z., et al., *Industrial applications of variable frequency microwave energy in materials processing.* Materials Research Society Symposium Proceedings, 1996. **430**(Microwave Processing of Materials V): p. 21-28.
133. Moon, K.-S., et al., *Lead-free interconnect technique by using variable frequency microwave.* Journal of Electronic Materials, 2005. **34**(7): p. 1081-1088.
134. Ku, H.S., et al., *Variable frequency microwave (VFM) processing facilities and application in processing thermoplastic matrix composites.* Journal of Materials Processing Technology, 2003. **139**(1-3): p. 291-295.
135. Fathi, Z., et al., *Rapid cure of liquid encapsulants and structural adhesives for electronics packaging using variable frequency microwave (VFM) energy.* Materials Research Society Symposium Proceedings, 1997. **445**(Electronic Packaging Materials Science IX): p. 125-130.
136. Wei, J.B., et al., *Materials characterization and diagnosis using variable frequency microwaves.* Materials Research Society Symposium Proceedings, 1996. **430**(Microwave Processing of Materials V): p. 73-78.
137. McMillan, A.D., et al., *Variable frequency microwave curing in polymer systems.* Polymeric Materials Science and Engineering, 1995. **72**: p. 72-3.
138. Fathi, Z., et al., *Processing and characterization of a polymer matrix composite using variable frequency microwave heating.* Ceramic Transactions, 1995. **59**: p. 441-8.
139. Demeuse, M.T. and A.C. Johnson, *Variable frequency microwave processing of thermoset polymer matrix composites.* Materials Research Society Symposium Proceedings, 1994. **347**(Microwave Processing of Materials IV): p. 723-8.
140. Lauf, R.J., et al., *Materials processing using a variable frequency microwave furnace.* Ceramic Transactions, 1993. **36**(Microwaves: Theroy Application in Materails Processing II): p. 571-9.
141. http://www.microcure.com/. [cited.
142. David, J.B. and E.D. Richard, *Microwave-induced plasma reactor based on a domestic microwave oven for bulk solid state chemistry.* Review of Scientific Instruments, 2004. **75**(12): p. 5277-5279.
143. Kataoka S, et al., *Photocatalytic oxidation in the presence of microwave irradiation: observations with ethylene and water.* Journal of Photochemistry and Photobiology A: Chemistry, 2002. **148**(1): p. 323-330(8).

144. Levinson, L.M., H.A. Comanzo, and W.N. Schultz, *Microwave sintering of ZnO varistor ceramics.* 1992.
145. Sutton, W.H., M.H. Brooks, and I.J. Chabinsky, *Materials Research Society Symposium Proceedings, Vol. 124: Microwave Processing of Materials. Symposium Held in Reno, Nev*. 1988. 399.
146. West, L.L.H.a.J.K., *Principles of Electronic Ceramics*. 1990, New York: Wiley Interscience.
147. Metaxas, A.C. and J.G.P. Binner, *Microwave processing of ceramics.* Adv. Ceram. Process. Technol., 1990. **1**: p. 285-367.
148. Agrawal, D., J. Cheng, and R. Roy, *Microwave processing of ceramics and metallic materials in single mode E field and H field.* Advances in Science and Technology (Faenza, Italy), 2003. **31**(10th International Ceramics Congress, 2002, Part B): p. 381-388.
149. De Jong, B.H.W.S., *2000 JCPDS International Diffraction Data;file 82-2396.* Journal of Non-Crystalline Solids, 1994. **176**: p. 164.
150. Smith, R.I., *JCPDS-International Center for Diffraction Data, file 80-1470.* Powder Diffraction, 1990. **5**(137).
151. Smith, R.I., *JCPDS-International Center for Diffraction Data, file 79-1899.* Acta Crystallographica, 1990. **46**(Section C): p. 363.
152. Kalinina, A., *JCPDS-International Center for Diffraction Data, file 24-0651.* Inorg. Mat. er. (Engl. Transl.), 1970. **6**: p. 389.
153. Liebau, F., *JCPDS-International Center for Diffraction Data, file 40-0376.* Acta Crystallographica, 1961. **14**: p. 389.
154. West, A.J., *JCPDS-International Center for Diffraction Data, file 30-0767.* Journal of American Ceramic Society, 1976. **59**: p. 124.
155. Maksinov, B.A., *JCPDS-International Center for Diffraction Data, file 74-2145.* Dokl. Akad. Nauk. SSSR, 1968. **178**: p. 1309.
156. Voellenkle, H., *JCPDS-International Center for Diffraction Data, file 63-1517.* Z. Kristallogr, 1981. **77**: p. 154.
157. Hesse, K., *JCPDS-International Center for Diffraction Data, file 29-0829.* Acta Crystallographica, 1977. **33**(Structural Science,Section B): p. 901.
158. Donnay, G., *JCPDS-International Center for Diffraction Data, file 17-0447.* Am.Mineral., 1953. **38**: p. 163.
159. John, C.R. and R. T.Dehoff, *Practical Stereology*. Second edition ed. 2000: Kluwer Academic/Plenum Publishers. 381.
160. Alois F. and Frank, M., *Vibrational spectroscopy, methods and applications*. 1989: Ellis Horwood Limited, Halsted Press: a division of John Wiley & Sons, New York.
161. Nakamoto, K., *Infrared and Raman Spectra of Inorganic and Coordination Compounds, Part A : Theory and Applications in Inorganic Chemistry.* 5 th ed. 1997, New York: John Wiley & Sons, Inc. 387.
162. E.I.Kamitsos, Y.D.Y., C.P.Varsamis and H.Jain, *Structure property correlation in glasses by infrared reflectance spectroscopy.* Journal of non crystalline solids, 1997. **222**: p. 59-68.
163. James E, S., *Introduction to glass science and technology*. RSC Paperbacks. 1997: The Royal Society of Chemistry. 244.

164. Gans, P., *Vibrating Molecules: an Introduction to the Interpretation of Infrared and Raman Spectra*. 1975: Chapman & Hall,London.
165. C.N.R.Rao, *Chemical applications of infrared spectroscopy*. 1963: Academic press, New York and London.
166. N.B. Colthrup, L.H.D., S.E. Wiberley, *Introduction to Infrared and Raman Spectroscopy*. 1990: Academic Press, San Diego, CA.
167. Hollas, J.M., *Modern Spectroscopy*. 3rd edition ed. 1996: John Wiley & Sons, New York.
168. Yano, T., T. Maehara, and S. Shibata. *High-temperature Raman spectroscopy of alkali silicate glass melts*. in *Ceramic Transactions*. 2005. Indianapolis, IN.
169. Maehara, T., et al., *Structure and phase transformation of alkali silicate melts analysed by Raman spectroscopy.* Philosophical Magazine, 2004. **84**(29): p. 3085-3099.
170. Mysen, B.O. and J.D. Frantz, *Raman spectroscopy of silicate melts at magmatic temperatures: sodium oxide-silica, potassium oxide-silica, and lithium oxide-silica binary compositions in the temperature range 25-1475 Deg C.* Chemical Geology, 1992. **96**(3-4): p. 321-32.
171. McMillan, P.F., G.H. Wolf, and B.T. Poe, *Vibrational spectroscopy of silicate liquids and glasses.* Chemical Geology, 1992. **96**(3-4): p. 351-366.
172. Marghussian, V.K. and M.H. Dayi Niaki, *Effects of composition changes on the crystallization behavior and properties of SiO2-Al2O3-CaO-MgO (Fe2O3-Na2O-K2O) glass-ceramics.* Journal of the European Ceramic Society, 1995. **15**: p. 343-48.
173. Bykov, Y.V., K.I. Rybakov, and V.E. Semenov, *High-temperature microwave processing of materials.* Journal of Physics D: Applied Physics, 2001. **34**(13): p. R55-R75.
174. Symon, K.R., *Mechanics*. 2nd ed. Addison-Wesley series in physics. 1960: Reading, Mass., Addison-Wesley Publishing.Co..Inc. 557.
175. Pelino, M., et al., *Crystallization of glasses obtained by recycling goethite industrial wastes to produce glass-ceramic materials.* J. Mater. Sci., 1994. **29**: p. 2087-94.
176. Ray, C.S., et al., *Non-isothermal calorimetric studies of the crystallization of lithium disilicate glass.* Journal of Non-Crystalline Solids, 1996. **204**(1): p. 1-12.
177. Noshiro, M. and Y. Jitsugiri, *Infrared determination of percent crystallinity of lithium metasilicate and lithium disilicate devitrified from glass.* Asahi Garasu Kenkyu Hokoku, 1968. **18**(2): p. 59-70.
178. John, R.F., H.M. Murli, and J.B. Louis, *Infrared absorption spectra of lithium and potassium silicate glasses at high pressure.* Journal of Applied Physics, 1973. **44**(12): p. 5391-5396.
179. Abe, Y. and D.E. Clark, *Determination of combined water in glasses by infrared spectroscopy.* Journal of Materials Science Letters, 1990. **9**(2): p. 244-5.
180. Efimov, A.M., *Model of the IR spectra of silicate glasses.* Soviet Journal of Glass Physics & Chemistry, 1990. **15**: p. 195-203.
181. Prokhorenko, O.A., et al., *Distribution of components in leached layer in the segregating lithium silicate glasses according to data of infrared spectra of disturbed total internal reflection.* Fizika i Khimiya Stekla, 1994. **20**: p. 616-626.

182. El-Batal, H.A., et al., *Infrared spectra and crystallization of some Li2O-SiO2 glasses and the effect of CaO, Al2O3, and K2O additives.* Applied Mineralogy: In Research, Economy, Technology, Ecology and Culture, Proceedings of the International Congress on Applied Mineralogy, 6th, Goettingen, Germany, July 17-19, 2000, 2000. **1**: p. 127-129.
183. El-Alaily, N.A., *Study of some properties of lithium silicate glass and glass ceramics containing blast furnace slag.* Glass Technology, 2003. **44**: p. 30-35.
184. Efimov, A.M., et al., *Infrared reflection spectra,optical constants and band parameters of binary silicate and borate glasses obtained from water free polished sample surface.* Glass Technology, 2005. **46**(1): p. 20-27.
185. McCracken, W.J., *Corrosion of glass-ceramics.* Corros. Glass, Ceram. Ceram. Supercond., 1992: p. 432-54.
186. Ding, Y., et al., *Lithium Disilicate Crystalline Slab Waveguides from Surface Crystallised Glass.* Electronics Letters, 1999. **35**(6): p. 504-505.
187. Fuxi, G., *Optical and Spectroscopic properties of glass*. 1992: Springer-Verlag. 283.
188. Hench, L.L., D.E. Clark, and E.L. Yen-Bower, *Corrosion of glasses and glass-ceramics.* Nuclear and Chemical Waste Management, 1980. **1**(1): p. 59-75.
189. Efimov, A.M., *Vibrational spectra, related properties and structure of inorganic glasses.* Journal of Non Crystalline Solids, 1999. **253**: p. 95-118.
190. Brawer, S.A. and W.B. White, *Raman spectroscopic investigation of the structure of silicate glasses. I. The binary alkali silicates.* The Journal of Chemical Physics, 1975. **63**(6): p. 2421-2432.
191. Furukawa, T., K.E. Fox, and W.B. White, *Raman spectroscopic investigation of the structure of silicate glasses. III. Raman intensities and structural units in sodium silicate glasses.* J. Chem. Phys., 1981. **75**(7): p. 3226-3237.
192. Soltay, L.G. and G.S. Henderson, *Structural differences between lithium silicate and lithium germanate glasses by Raman spectroscopy.* Physics and Chemistry of Glasses, 2005. **46**: p. 381-384.
193. Cumpston, B., F. Shadman, and S. Risbud, *Utilization of coal-ash minerals for technological ceramics.* J. Mater. Sci., 1992. **27**: p. 1781-84.
194. Krishnaswami, S., et al., *Connection between the microwave and far infrared conductivity of oxide glasses.* Journal of Non Crystalline Solids, 2000. **274**: p. 307-312.
195. Wang, G., et al., *The effect of an electric field on the phase separation of Ag-doped glass.* Materials Science and Engineering A, 2004. **367**(1-2): p. 272-276.
196. Alvarez, M.A. and L.C. Klein, *Study of glass/metal interfaces under an electric field: Low temperature/high voltage.* Ceramic Transactions, 2002. **127**(Materials for Electrochemical Energy Conversion and Storage): p. 177-185.
197. Liu, W., et al., *Controlled phase separation by an electric field in glasses.* Materials Science and Engineering A, 1999. **265**(1-2): p. 25-28.
198. Gu, X.M., W. Liu, and K.M. Liang, *The effect of electric field on phase separation in glasses: a model and experimental testing.* Materials Science and Engineering A, 1999. **278**(1-2): p. 22-26.
199. Liu, W., et al., *The effect of an electric field on the phase separation of glasses.* Journal of Physics D: Applied Physics, 1997. **30**: p. 3366–3370.

200. De Vekey, R.C. and A.J. Majumdar, *Effect of Electric Field on Phase Separation of Glass.* Nature, 1970. **225**(5228): p. 172-173.
201. Koch, C.C., *Experimental evidence for magnetic or electric field effects on phase transformations.* Materials Science and Engineering A, 2000. **287**(2): p. 213-218.
202. Agrawal, D., J. Cheng, and R. Roy. *Microwave Processing of Ceramics and Metallic Materials in Single Mode E field and H field*. in *Adv.Sci.Technol.* 2003.
203. Roy, R., et al., *Definitive experimental evidence for microwave effects: radically new effects of separated E and H fields, such as decrystallization of oxides in seconds.* Materials Research Innovations, 2002. **6**(3): p. 128-140.
204. Li, S., et al., *Crystallization behavior and magnetic properties of amorphous B-rich NdFeB alloy in presence of an external electric field.* Materials Science and Engineering: A, 2005. **405**(1-2): p. 321-324.
205. Wang, G.L., et al., *An experimental and theoretical investigation on the nucleation mechanism of copper-containing glass in an electric field.* Applied Physics A: Materials Science & Processing, 2005. **81**(2): p. 413-417.
206. Liu, W., et al., *Electric-field-enhanced crystallization of amorphous Fe86Zr7B6Cu1 alloy.* Journal of Alloys and Compounds, 2006. **420**(1-2): p. 171-174.
207. Jiancheng Tang, et al., *Effect of electric field on the crystallization process of amorphous Fe86Zr7B6Cu1 alloy* Journal of Physics D: Applied Physics, 2005. **38**: p. 729-732.
208. K. V. Saban, J.T.P.A.V.G.V., *Thermodynamics of Crystal Nucleation in an External Electric Field.* Crystal Research and Technology, 2002. **37**(11): p. 1188-1199.
209. MacDowell, J.F. and G.H. Beall. *Low K Glass-Ceramics For Microelectronic Packaging*. in *Ceram.Trans.* 1989.

Appendix 1

Detailed calculation of molecular orbital theory of microwave absorption in LS_2 glass

Step 1

a) Get the IR data from Cache output file.

b) Find "Transition dipole and the strength values in that file"

Oscillator	*Transition Dipole*	*Strength*
1	4.16	0.0355
2	14.29	0.1059
3	36.98	0.4073
4	45.6	0.1579
5	83.23	0.5359
6	89.85	0.3016
7	130	0.4196
8	133.12	0.322
9	135.61	0.9274
10	146.39	0.4963
11	149.62	0.8934
12	183.59	0.4082
13	195.98	0.7641
14	201.95	1.9376
15	206.19	0.8191
16	211.48	1.1167
17	217.38	0.6414
18	231.99	0.4496
19	266.65	1.4724
20	282.72	8.0224
21	298.77	1.2837
22	301.31	1.1614
23	313.48	0.4695
24	332.11	6.499
25	470.03	8.972
26	517.32	0.3018
27	583.98	0.1513
28	664.52	2.8754
29	799.51	0.2223
30	829.86	0.7563
31	898.66	1.4887
32	899.33	3.3476
33	906.01	0.965
34	906.44	3.7485
35	941.7	2.6063
36	942.79	0.6052
37	1008.85	0.5476
38	1009.14	1.4946
39	1011.31	0.3363
40	1011.53	3.1036
41	1040.45	11.9066
42	1044.51	1.6088
43	3928.92	0.604
44	3929.21	0.5478
45	3931	0.5655
46	3931.82	0.561
47	3933.76	0.5731
48	3934.83	0.5605

Step 2

a) Calculate differences between Oscillators n and n+1 = delta w.

b) Convert delta w to beat MW frequency = (delta w "GHz"/2) cm^{-1}.(To convert cm^{-1} to Hz multiply by the speed of light $3*10^{10}$ cm/sec Note Hz=cm^{-1} GHz=10^9 Hz)

Oscillator	*Transition Dipole*	*Strength*	*delta w "1/cm"*	*w" "GHz"*
1	4.16	0.03550	10.13000	151.950
2	14.29	0.10590	22.69000	340.350
3	36.98	0.40730	8.62000	129.300
4	45.6	0.15790	37.63000	564.450
5	83.23	0.53590	6.62000	99.300
6	89.85	0.30160	40.15000	602.250
7	130	0.41960	3.12000	46.800
8	133.12	0.32200	2.49000	37.350
9	135.61	0.92740	10.78000	161.700
10	146.39	0.49630	3.23000	48.450
11	149.62	0.89340	33.97000	509.550
12	183.59	0.40820	12.39000	185.850
13	195.98	0.76410	5.97000	89.550
14	201.95	1.93760	4.24000	63.600
15	206.19	0.81910	5.29000	79.350
16	211.48	1.11670	5.90000	88.500
17	217.38	0.64140	14.61000	219.150
18	231.99	0.44960	34.66000	519.900
19	266.65	1.47240	16.07000	241.050
20	282.72	8.02240	16.05000	240.750
21	298.77	1.28370	2.54000	38.100
22	301.31	1.16140	12.17000	182.550
23	313.48	0.46950	18.63000	279.450
24	332.11	6.49900	137.92000	2068.800
25	470.03	8.97200	47.29000	709.350
26	517.32	0.30180	66.66000	999.900
27	583.98	0.15130	80.54000	1208.100
28	664.52	2.87540	134.99000	2024.850
29	799.51	0.22230	30.35000	455.250
30	829.86	0.75630	68.80000	1032.000
31	898.66	1.48870	0.67000	10.050
32	899.33	3.34760	6.68000	100.200
33	906.01	0.96500	0.43000	6.450
34	906.44	3.74850	35.26000	528.900
35	941.7	2.60630	1.09000	16.350
36	942.79	0.60520	66.06000	990.900
37	1008.85	0.54760	0.29000	4.350
38	1009.14	1.49460	2.17000	32.550
39	1011.31	0.33630	0.22000	3.300
40	1011.53	3.10360	28.92000	433.800
41	1040.45	11.90660	4.06000	60.900
42	1044.51	1.60880	2884.41000	43266.150
43	3928.92	0.60400	0.29000	4.350
44	3929.21	0.54780	1.79000	26.850
45	3931	0.56550	0.82000	12.300
46	3931.82	0.56100	1.94000	29.100
47	3933.76	0.57310	1.07000	16.050
48	3934.83	0.56050	-3934.83000	-59022.450

Step 3

a) Arrange the beat frequency (w^-) with the oscillator strength.

b) Sort array by w^-, this is the MW Spectra.

Oscillator	*w^- "GHz"*	*Strength*
48	-59022.450	0.56050
39	3.300	0.33630
37	4.350	0.54760
43	4.350	0.60400
33	6.450	0.96500
31	10.050	1.48870
45	12.300	0.56550
47	16.050	0.57310
35	16.350	2.60630
44	26.850	0.54780
46	29.100	0.56100
38	32.550	1.49460
8	37.350	0.32200
21	38.100	1.28370
7	46.800	0.41960
10	48.450	0.49630
41	60.900	11.90660
14	63.600	1.93760
15	79.350	0.81910
16	88.500	1.11670
13	89.550	0.76410
5	99.300	0.53590
32	100.200	3.34760
3	129.300	0.40730
1	151.950	0.03550
9	161.700	0.92740
22	182.550	1.16140
12	185.850	0.40820
17	219.150	0.64140
20	240.750	8.02240
19	241.050	1.47240
23	279.450	0.46950
2	340.350	0.10590
40	433.800	3.10360
29	455.250	0.22230
11	509.550	0.89340
18	519.900	0.44960
34	528.900	3.74850
4	564.450	0.15790
6	602.250	0.30160
25	709.350	8.97200
36	990.900	0.60520
26	999.900	0.30180
30	1032.000	0.75630
27	1208.100	0.15130
28	2024.850	2.87540
24	2068.800	6.49900
42	43266.150	1.60880

Detailed calculation of molecular orbital theory of microwave absorption in LS_2 glass-ceramics

Step 1

a) Get the IR data from Cache output file.

b) Find "Transition dipole and the strength values in that file"

Oscillator	*Transition Dipole*	*Strength*
1	-189.05	0.1057
2	-187.77	1.6607
3	-173.56	0.7363
4	-160.83	2.7562
5	-153.4	0.00520
6	-152.33	1.2682
7	-134.33	1.0246
8	-129.08	1.7175
9	-126.02	2.3838
10	-122.07	1.0846
11	-117.55	0.3798
12	-113.2	0.7829
13	-92.48	0.1709
14	-92.29	3.1859
15	-52.76	0.5324
16	-40.5	0.6886
17	-37.89	2.2695
18	-30.12	0.7862
19	-16.64	1.6321
20	25.28	0.3709
21	38.21	1.268
22	45.14	0.8413
23	53.44	0.708
24	61.91	0.4662
25	74.73	1.3759
26	113.01	1.9412
27	127	2.8693
28	128.45	0.5768
29	132.71	0.9006
30	136.38	2.4394
31	150.7	1.2556
32	164.54	1.2287
33	171.15	0.3785
34	173.43	0.6867
35	179.83	2.0232
36	181.36	1.4871
37	189.33	1.373
38	192.8	2.1044
39	216.88	3.9451
40	237.03	0.8263
41	238.45	0.1083
42	248.53	0.2859
43	252.5	4.4347
44	258.83	4.8027
45	268.09	4.0305
46	270.9	0.18884
47	270.91	1.4421
48	282.22	0.1522

49	285.41	6.9431
50	295.71	2.9768
51	304.78	0.17829
52	305.65	5.277
53	310.39	0.18627
54	311.33	3.2028
55	318.08	5.0913
56	323.52	0.4507
57	327.36	8.9331
58	331.22	0.8334
59	337.03	5.6756
60	338.58	1.0632
61	364.45	4.3258
62	368.11	5.0038
63	380.41	0.227
64	381.06	7.7966
65	403.12	0.1842
66	403.96	1.5059
67	420.63	0.13418
68	420.74	1.2387
69	470.1	0.14393
70	470.15	5.1963
71	479.34	0.04738
72	480.35	0.4278
73	523.59	10.5578
74	525.36	3.602
75	534.04	8.0696
76	541.57	3.9277
77	594.77	0.8203
78	601.8	9.4269
79	614.55	1.1193
80	616.05	0.7756
81	734.84	11.2542
82	737.67	4.9014
83	846.21	0.08851
84	847.23	0.4214
85	867.82	0.19605
86	868.73	10.359
87	876.8	2.1956
88	880.32	8.587
89	983.85	0.477
90	990.74	15.773
91	1011.55	0.17063
92	1012.03	6.9701
93	1022.58	0.0722
94	1023.55	18.7505
95	1044.03	0.1609
96	1044.96	4.9863
97	1084.67	1.2291
98	1097.28	16.3015
99	1180.23	19.6575
100	1182.4	4.4718
101	1213.34	31.1278
102	1223.13	3.5082

Step 2

c) Calculate differences between Oscillators n and n+1 = delta w.

d) Convert delta w to beat MW frequency = (delta w "GHz"/2) cm^{-1}.(To convert cm^{-1} to Hz multiply by the speed of light $3*10^{10}$ cm/sec Note Hz=cm^{-1} GHz=10^9 Hz)

Oscillator	***Transition Dipole***	***Strength***	***delta w "1/cm"***	***w- "GHz"***
1	-189.05	0.1057	1.28000	19.200
2	-187.77	1.6607	14.21000	213.150
3	-173.56	0.7363	12.73000	190.950
4	-160.83	2.7562	7.43000	111.450
5	-153.4	0.0052	1.07000	16.050
6	-152.33	1.2682	18.00000	270.000
7	-134.33	1.0246	5.25000	78.750
8	-129.08	1.7175	3.06000	45.900
9	-126.02	2.3838	3.95000	59.250
10	-122.07	1.0846	4.52000	67.800
11	-117.55	0.3798	4.35000	65.250
12	-113.2	0.7829	20.72000	310.800
13	-92.48	0.1709	0.19000	2.850
14	-92.29	3.1859	39.53000	592.950
15	-52.76	0.5324	12.26000	183.900
16	-40.5	0.6886	2.61000	39.150
17	-37.89	2.2695	7.77000	116.550
18	-30.12	0.7862	13.48000	202.200
19	-16.64	1.6321	41.92000	628.800
20	25.28	0.3709	12.93000	193.950
21	38.21	1.268	6.93000	103.950
22	45.14	0.8413	8.30000	124.500
23	53.44	0.708	8.47000	127.050
24	61.91	0.4662	12.82000	192.300
25	74.73	1.3759	38.28000	574.200
26	113.01	1.9412	13.99000	209.850
27	127	2.8693	1.45000	21.750
28	128.45	0.5768	4.26000	63.900
29	132.71	0.9006	3.67000	55.050
30	136.38	2.4394	14.32000	214.800
31	150.7	1.2556	13.84000	207.600
32	164.54	1.2287	6.61000	99.150
33	171.15	0.3785	2.28000	34.200
34	173.43	0.6867	6.40000	96.000
35	179.83	2.0232	1.53000	22.950
36	181.36	1.4871	7.97000	119.550
37	189.33	1.373	3.47000	52.050
38	192.8	2.1044	24.08000	361.200
39	216.88	3.9451	20.15000	302.250
40	237.03	0.8263	1.42000	21.300
41	238.45	0.1083	10.08000	151.200
42	248.53	0.2859	3.97000	59.550
43	252.5	4.4347	6.33000	94.950
44	258.83	4.8027	9.26000	138.900
45	268.09	4.0305	2.81000	42.150
46	270.9	0.18884	0.01000	0.150
47	270.91	1.4421	11.31000	169.650
48	282.22	0.1522	3.19000	47.850

49	285.41	6.9431	10.30000	154.500
50	295.71	2.9768	9.07000	136.050
51	304.78	0.17829	0.87000	13.050
52	305.65	5.277	4.74000	71.100
53	310.39	0.18627	0.94000	14.100
54	311.33	3.2028	6.75000	101.250
55	318.08	5.0913	5.44000	81.600
56	323.52	0.4507	3.84000	57.600
57	327.36	8.9331	3.86000	57.900
58	331.22	0.8334	5.81000	87.150
59	337.03	5.6756	1.55000	23.250
60	338.58	1.0632	25.87000	388.050
61	364.45	4.3258	3.66000	54.900
62	368.11	5.0038	12.30000	184.500
63	380.41	0.227	0.65000	9.750
64	381.06	7.7966	22.06000	330.900
65	403.12	0.1842	0.84000	12.600
66	403.96	1.5059	16.67000	250.050
67	420.63	0.13418	0.11000	1.650
68	420.74	1.2387	49.36000	740.400
69	470.1	0.14393	0.05000	0.750
70	470.15	5.1963	9.19000	137.850
71	479.34	0.04738	1.01000	15.150
72	480.35	0.4278	43.24000	648.600
73	523.59	10.5578	1.77000	26.550
74	525.36	3.602	8.68000	130.200
75	534.04	8.0696	7.53000	112.950
76	541.57	3.9277	53.20000	798.000
77	594.77	0.8203	7.03000	105.450
78	601.8	9.4269	12.75000	191.250
79	614.55	1.1193	1.50000	22.500
80	616.05	0.7756	118.79000	1781.850
81	734.84	11.2542	2.83000	42.450
82	737.67	4.9014	108.54000	1628.100
83	846.21	0.08851	1.02000	15.300
84	847.23	0.4214	20.59000	308.850
85	867.82	0.19605	0.91000	13.650
86	868.73	10.359	8.07000	121.050
87	876.8	2.1956	3.52000	52.800
88	880.32	8.587	103.53000	1552.950
89	983.85	0.477	6.89000	103.350
90	990.74	15.773	20.81000	312.150
91	1011.55	0.17063	0.48000	7.200
92	1012.03	6.9701	10.55000	158.250
93	1022.58	0.0722	0.97000	14.550
94	1023.55	18.7505	20.48000	307.200
95	1044.03	0.1609	0.93000	13.950
96	1044.96	4.9863	39.71000	595.650
97	1084.67	1.2291	12.61000	189.150
98	1097.28	16.3015	82.95000	1244.250
99	1180.23	19.6575	2.17000	32.550
100	1182.4	4.4718	30.94000	464.100
101	1213.34	31.1278	9.79000	146.850
102	1223.13	3.5082	-1223.13000	-18346.950

Step 3

c) Arrange the beat frequency (w^-) with the oscillator strength.

d) Sort array by w^-, this is the MW Spectra.

Oscillator	*w^- "GHz"*	*Strength*
102	-18346.95	3.5082
46	0.150	0.18884
69	0.75	0.14393
67	1.65	0.13418
13	2.85	0.1709
91	7.2	0.17063
63	9.750	0.22700
65	12.6	0.1842
51	13.050	0.17829
85	13.650	0.19605
95	13.95	0.1609
53	14.1	0.18627
93	14.55	0.0722
71	15.150	0.04738
83	15.3	0.08851
5	16.05	0.0052
1	19.200	0.10570
40	21.3	0.8263
27	21.75	2.8693
79	22.5	1.1193
35	22.950	2.02320
59	23.25	5.6756
73	26.55	10.5578
99	32.550	19.65750
33	34.200	0.37850
16	39.150	0.68860
45	42.15	4.0305
81	42.45	11.2542
8	45.9	1.7175
48	47.850	0.15220
37	52.050	1.37300
87	52.8	2.1956
61	54.9	4.3258
29	55.05	0.9006
56	57.6	0.4507
57	57.900	8.93310
9	59.25	2.3838
42	59.55	0.2859
28	63.9	0.5768
11	65.25	0.3798
10	67.8	1.0846
52	71.1	5.277
7	78.75	1.0246
55	81.6	5.0913
58	87.15	0.8334
43	94.95	4.4347
34	96.000	0.68670
32	99.15	1.2287

Vita

Morsi Mohamed Mahmoud will be awarded his Ph.D. degree in spring 2007 in materials science and engineering from materials science and engineering department, Virginia Tech, USA. He joined the department in January 2002. He got a M.ENG degree from the same department in materials science and engineering, Virginia Tech, USA in December 2006. He received his B.Sc. in chemistry from Alexandria University, Alexandria, Egypt in 1991 and his M.Sc degree in materials science in November 1999, department of materials science, Institute of Graduate Studies and Research at Alexandria University.

He got a full scholarship from the Egyptian government to study his PhD in the USA in 2002. His major research interests include production of glass-ceramic materials from industrial waste, ceramic materials properties and applications and, most recently, microwave processing of materials with special emphasis on crystallization of glass.

Mr. Mahmoud got Virginia Tech Citizen Scholar Award, November 2005, an Honor Scholarship from Virginia Tech Graduate School. He also won the 2nd place in the student poster competition "20th Annual National Educators Workshop-Student Poster Competition-Nano/Bio Science and Technology Education for the 21st Century", October 16-19, 2005, National Institute of Standards and Technology (NIST), Gaithersburg, MD. Mr. Mahmoud had won the 2nd place in the academic poster competition in The 4th World Congress on Microwave and Radio Frequency Applications", from 7-12 November 2004, Austin, Texas, USA.

Mr. Mahmoud was one of the editors of a book in the microwave processing field entitled "Microwave Solutions for Ceramic Engineers" published by the American Ceramic Society, Westerville, Ohio, November 2005.

He joined the National Research Center, Cairo, Egypt, as a Research Assistant in 1993, and then moved to a newly established research center as an Assistant Researcher for the Advanced Technologies and New Materials Research Institute (IATNM), Mubarak City for Scientific Research and Technology (MCSRT), Alexandria, Egypt.

He is a member in American Ceramic Society (ACerS), National Institute of Ceramics Engineer (NICE), Materials Engineering Professional Societies (MEPS) in Virginia Tech, and finally in Materials Advantage Student Program.

Mr.Mahmoud got married from his wife, Faten; in 2001.They have three children, Rowan, Nada and Abdel-Rahman.

Dr. Morsi Mohamed Mahmoud Morsi
momahmou@vt.edu
April 24, 2007